NASA CR-134606
WANL-M-FR-74-002

NASA

FINAL REPORT

PROCESS DEVELOPMENT OF TWO HIGH STRENGTH TANTALUM BASE ALLOYS (ASTAR-1211C AND ASTAR-1511C)

By
R. L. Ammon

WESTINGHOUSE ASTRONUCLEAR LABORATORY

Prepared for
National Aeronautics and Space Administration
NASA-Lewis Research Center
Contract NAS 3-12971

WESTINGHOUSE ELECTRIC CORPORATION - P. O. BOX 10864 - PITTSBURGH, PENNSYLVANIA 15236

1. Report No.	2. Government Accession No.	3. Recipient's Catalog No
NASA CR-134606		

4. Title and Subtitle	5. Report Date
PROCESS DEVELOPMENT OF TWO HIGH STRENGTH TANTALUM BASE ALLOYS (ASTAR-1211C AND ASTAR-1511C)	November, 1974
	6. Performing Organization Code

7. Author(s)	8. Performing Organization Report No.
R. L. Ammon	WANL-M-FR-74-002
	10. Work Unit No.

9. Performing Organization Name and Address	11. Contract or Grant No.
Westinghouse Astronuclear Laboratory P. O. Box 10864 Pittsburgh, PA 15236	NAS 3-12971
	13. Type of Report and Period Covered
12. Sponsoring Agency Name and Address	Contractor (6/69 - 2/72)
National Aeronautics and Space Administration Washington, DC 20546	14. Sponsoring Agency Code

15. Supplementary Notes

P. E. Moorhead, NASA Project Manager, Materials and Structures Division, NASA-Lewis Research Center, Cleveland, Ohio

16 Abstract

Two tantalum base alloys, Ta-12W-1.0Re-0.7Hf-0.025C (ASTAR-1211C)and Ta-15W-1.0Re--0.7Hf-0.025C (ASTAR-1511C), were cast as 12.5 cm (5 inch) diameter ingots and processed to swaged rod, sheet, forged plate, and tubing. Swaged rod was evaluated with respect to low temperature ductility, elevated temperature tensile properties, and elevated temperature creep behavior. A standard swaging process and final annealing schedule were determined. Elevated temperature tensile properties, low temperature impact properties, low temperature DBTT behavior, and extended elevated temperature creep properties were determined. A process for producing ASTAR-1211C and ASTAR-1511C sheet were developed. The DBTT properties of GTA and EB weld sheet given post-weld anneal and thermal aging treatments were determined using bend and tensile specimens. High and low temperature mechanical properties of forging ASTAR-1211C and ASTAR-1511C plate were determined as well as elevated temperature creep properties. Attempts to produce ASTAR-1211C tubing were partially successful while attempts to make ASTAR-1511C tubing were completely unsuccessful.

17. Key Words (Suggested by Author(s))	18. Distribution Statement
Tantalum Alloy Processing Mechanical Properties Swaged Rod, Sheet, Forging, Tubing	

19. Security Classif. (of this report)	20. Security Classif. (of this page)	21. No. of Pages	22. Price*
UNCLASSIFIED	UNCLASSIFIED	309	

* For sale by the National Technical Information Service, Springfield, Virginia 22151

NASA-C-168 (Rev. 6-71)

FOREWORD

The work described in this report was performed by Westinghouse Electric Corporation, Astronuclear Laboratory, during the period June, 1969 through February, 1972. Technical administration at the Astronuclear Laboratory was under the direction of Mr. R. W. Buckman with Mr. R. L. Ammon as principal investigator, while Mr. P. Moorhead served as the NASA Project Manager.

The author wishes to acknowledge the following people for their contribution to the success of this program:

Arc Melting	-	J. Sundin
Swaging and Rolling	-	C. Fitterer
Welding	-	R. Sprecace
Mechanical Testing	-	M. Dawida and G. Yatsko
Creep Testing	-	G. Fechko
X-ray Diffraction Analysis	-	R. Conlin
Metallography	-	K. Galbraith

In addition to those who performed the experimental work on this program, the author wishes to express gratitude to Mr. R. Davies of NASA-Lewis for guidance, to Mr. R. W. Buckman of WANL for many encouraging and constructive discussions, and to Mr. R. E. Gold of WANL who carried out the welded sheet evaluation.

TABLE OF CONTENTS

TABLE OF CONTENTS (Continued)

TABLE OF CONTENTS (Continued)

TABLE OF CONTENTS (Continued)

LIST OF ILLUSTRATIONS

LIST OF ILLUSTRATIONS (Continued)

LIST OF ILLUSTRATIONS (Continued)

LIST OF ILLUSTRATIONS (Continued)

LIST OF ILLUSTRATIONS (Continued)

LIST OF ILLUSTRATIONS (Continued)

LIST OF ILLUSTRATIONS (Continued)

LIST OF ILLUSTRATIONS (Continued)

LIST OF TABLES

LIST OF TABLES (Continued)

LIST OF TABLES (Continued)

1.0 SUMMARY

The purpose of this program was to investigate the processing and properties of two high strength tantalum base alloys. The selection of alloy composition was based on results of a prior program, NAS 3-10939. The alloy designation and composition were as follows:

ASTAR-1211C - Ta-12.0W-1.0Re-0.7Hf-0.025C*
ASTAR-1511C - Ta-15.0W-1.0Re-0.7Hf-0.025C

The ASTAR-1211C composition was selected to provide an alloy with good high temperature tensile and creep properties with sufficient low temperature ductility to permit sheet and tubing to be fabricated. The alloy was expected to possess moderate weldability. The ASTAR-1511C composition was selected to provide even better elevated temperature tensile and creep properties with some sacrifice in low temperature ductility and weldability.

1.1 PROCESSING STARTING MATERIAL

Two 12.6 cm (5.0 inch) diameter ingots of each alloy composition were produced by double vacuum arc melting. Primary ingot breakdown was accomplished by extrusion at 1649°C (3000°F) to produce 7.1 cm (2.8 inch) diameter bar stock. To evaluate the fabricability of each alloy, the extruded bar stock was recrystallized and reextruded to nominal 2.5 cm (1.0 inch) diameter bar stock, to 2.3 cm (0.9 inch) by 5 cm (2.0 inch) sheet bar, and to tube hollows. Other sections were upset forged to disc shapes for evaluation.

1.2 SWAGED ROD EVALUATION

The material extruded to nominal 2.5 cm (1.0 inch) diameter bar stock was swaged to 9.5 mm (0.375 inch) diameter rod at two processing temperatures, 1371°C (2500°F) and 1649°C (3000°F), to evaluate the effect of working temperature on material properties. The effect of final annealing temperature was also investigated. Material swaged at the two working

* Percent by weight.

temperatures were annealed at 1371°C (2500°F), 1482°C (2700°F), 1649°C (3000°F), 1815°C (3300°F), and 1982°C (3600°F). To evaluate the effect of working and fina' annealing temperatures on properties, a testing program to investigate low temperature tensile properties, 1316°C (2400°F) tensile properties, and elevated temperature creep behavior was conducted.

While both alloys exhibited room temperature elongation values on the order of 20 percent regardless of processing and final heat treatment, material annealed above 1649°C (3000°F) experienced a ductile-to-brittle transition as test temperature was reduced to sub-zero values. The 1316°C (2400°F) tensile properties of ASTAR-1211C were unaffected by processing temperature, except where wrought material was involved. Ultimate strengths ranged from 372 MN/m^2 (54 ksi) to 442 MN/m^2 (64 ksi) as a function of final annealing temperature. The tensile properties of ASTAR-1511C at 1316°C (2400°F) exhibited a degree of sensitivity to processing temperature, particularly for material final annealed at 1482°C (2700°F), 1649°C (3000°F), and 1815°C (3300°F). The material swaged at 1649°C (3000°F) had tensile strength properties which averaged 69 MN/m^2 (10 ksi) higher than material swaged at 1371°C (2500°F). Final annealing temperature appeared to have little affect on 1316°C (2400°F) tensile strength properties of ASTAR-1511C. The ultimate strength of 1371°C (2500°F) swaged material was 414 MN/m^2 (60 ksi) while the ultimate strength of 1649°C (3000°F) swaged material was 483 MN/m^2 (70 ksi).

The creep behavior of both alloys was similar. Material of both alloys processed at 1649°C (3000°F) had greater creep resistance than material processed at the lower temperature. The disparity in creep resistance was greatest for final annealing temperatures below 1649°C (3000°F). In general, the higher the final annealing temperature the better the creep properties for both alloys and both processing temperatures.

Based on the results of the low ductility behavior, 1316°C (2400°F) tensile properties, and creep properties, a standard final annealing temperature of 1 hour at 1649°C (3000°F) was selected for both alloys. This final annealing temperature provided the best compromise between low temperature ductility and elevated temperature strength properties.

Swaged rod stock of each alloy was given the standard final annealing treatment, and extensive mechanical properties were developed. They included tensile properties from room temperature to 1649°C (3000°F) at 333°C (600°F) increments; elastic properties including Young's modulus, shear modulus, and Poison ratio; impact properties; tensile DBTT; notched-unnotched strength properties; and additional creep properties. The additional three percent of tungsten in ASTAR-1511C was reflected in all of the properties evaluated.

ASTAR-1511C had higher tensile properties than ASTAR-1211C at all test temperatures. At 1649°C (3000°F), the ultimate strength of ASTAR-1211C was 204 MN/m^2 (29.5 ksi) compared to 244 MN/m^2 (35.4 ksi) for ASTAR-1511C. Young's modulus for ASTAR-1511C was slightly higher than ASTAR-1211C, 196.1 GN/m^2 (28.4 x 10^6 psi) versus 199.1 GN/m^2 (28.8 x 10^6 psi) at room temperature. A similar relationship was noted for the shear modulus, 74.7 GN/m^2 (10.8 x 10^6 psi) versus 76.8 GN/m^2 (11.13 x 10^6 psi). Poisson's ratio for ASTAR-1211C was 0.32 and 0.30 for ASTAR-1511C. Both values remained constant up to 871°C (1600°F). Under impact loading, ASTAR-1211C exhibited indications of a transition from brittle-to-ductile behavior as temperature increased to 538°C (1000°F) while ASTAR-1511C exhibited completely brittle behavior up to the same temperature. The tensile DBTT for swaged rod annealed 1 hour at 1649°C (3000°F), was < -157°C (-250°F) for ASTAR-1211C and approximately -129°C (-200°F) for ASTAR-1511C. The unnotched-notched ratio of both alloys was greater than one for temperatures as low as -196°C (-320°F). In creep, ASTAR-1511C exhibited slightly better properties. The stress required to produce 1 percent creep strain in 1000 hours at 1204°C (2000°F) was 176 MN/m^2 (25.5 ksi) for ASTAR-1511C. For ASTAR-1211C, the stress required was 155 MN/m^2 (22.5 ksi). These values were significantly higher than

those of ASTAR-811C, 124 MN/m^2 (18 ksi), and T-111, 93 MN/m^2 (13.5 ksi) for the same time and temperature requirements.

It was also demonstrated that a duplex anneal, 1 hour at 1649°C (3000°F) followed by 1 hour at 1260°C (2300°F), reduced room temperature tensile strength approximately 10 percent without adversely affecting room temperature ductility. Although elevated temperature 1316°C (2400°F) tensile properties were reduced about 10 percent by the duplex anneal, creep properties were unaffected by the heat treatment.

1.3 SHEET EVALUATION

Both ASTAR-1211C and ASTAR-1511C were successfully converted to 1.0 mm (0.040 inch) thick sheet. The sheet bars produced by the reextrusion of bar stock were forged to plate at 1316°C (2400°F), conditioned to remove the co-extruded molybdenum clad, annealed, and rolled at the rate of 10 percent reduction per pass. ASTAR-1211C was reduced 60 percent by rolling before intermediate heat treatment was required. ASTAR-1511C was reduced 40 percent prior to intermediate heat treatment. Sufficient sheet material of both alloys was produced to permit mechanical property evaluation and characterization of welded sheet.

The tensile and creep properties of ASTAR-1211C and ASTAR-1511C sheet given the standard final heat treatment, 1 hour at 1649°C (3000°F), were comparable to swaged rod properties of both alloys.

The bend DBTT for longitudinally EB and GTA welded ASTAR-1211C sheet was determined for "as-welded" and post-weld-annealed conditions. The 1t bend DBTT for "as-welded" GTA welded ASTAR-1211C sheet was 121°C (250°F) compared to 10°C (50°F) for base metal. A post-weld anneal of 1 hour at 1649°C (3000°F) reduced the weld bend DBTT to 38°C (100°F). The "as-welded" DBTT for EB welded ASTAR-1211C sheet was 24°C (75°F). A post-weld

anneal of 1 hour at 1315°C (3300°F), resulted in an increase in the DBTT to 38°C (100°F).

ASTAR-1511C, reflecting the effect of a higher tungsten content, exhibited a DBTT above 316°C (600°F) for GTA welded material in the "as-welded" condition compared to 38°C (100°F) for base metal. The most affecting PWA, 1 hour at 1815°C (3300°F), reduced the DBTT to 149°C (300°F). In the case of EB welded ASTAR-1511C, all the post-weld annealing treatments affected a reduction in the DBTT from 107°C (225°F) for "as-welded" condition to 93°C (200°F).

The DBTT of GTA welded ASTAR-1211C and ASTAR-1511C sheet was also determined in the tensile mode. "As-welded" and post-weld-annealed tensile specimens were thermally aged for 100 hours at 1149°C (2100°F), 1316°C (2400°F), and 1427°C (2600°F). The tensile DBTT for nonpost-weld-annealed ASTAR-1211C and for material given PWA of 1 hour at 1649°C (3000°F) were not affected by thermal aging. In many cases, the DBTTs for thermally aged material were below "as-welded" levels. The DBTT for thermally aged, nonpost-weld-annealed ASTAR-1211C ranged between 52°C (125°F) and 66°C (150°F) compared to 121°C (250°F) for the "as-welded" condition. A PWA of 1 hour at 1649°C (3000°F) prior to thermal aging produced DBTTs in the range 38°C (100°F) to -46°C (-50°F). The behavior of GTA welded ASTAR-1511C was quite similar to ASTAR-1211C. The DBTTs for thermally aged material, given a PWA of 1 hour at 1649°C (3000°F) fell in the range 52°C (125°F) to 93°C (200°F). These values were the lowest observed for welded ASTAR-1511C.

1.4 TUBING EVALUATION

Although ASTAR-1211C and ASTAR-1511C were not specifically designed for tubing applications, the feasibility of producing tubing of the two alloys was investigated. Tube hollows suitable for drawing to tubing with an OD of 1.9 cm (0.75 inch) and 1.0 mm (0.040 inch) wall were

successfully produced by two methods. Hollows were made by "rifle" drilling extruded round bar stock and by direct extrusion over a mandrel. The tube hollows were conditioned by machining to 2.7 cm (1.1 inch) OD by 2.3 cm (0.9 inch) ID. A process for producing ASTAR-1211C tubing of the desired size was developed. The process consisted of drawing on a mandrel at reductions of 10 to 12 percent per pass at a temperature of 204°C (400°F) to 316°C (600°F). The tube hollows were initially given a duplex anneal, 1 hour at 1649°C (3000°F) followed by 1 hour at 1316°C (2400°F). The drawn tubing was stress relieved by annealing 1 hour at 1316°C (2400°F) between drawing passes. The major problem areas encountered involved "tagging" the tube end to accommodate mandrel grip, removing the drawn tube from the mandrel, and determining the proper lubricant. Insufficient ASTAR-1211C tubing was produced to permit evaluation. ASTAR-1511C could not be "tagged" or pointed due to lack of ductility and thus no tubing was produced.

1.5 EVALUATION OF FORGED DISCS

Both alloys were successfully upset forged to flat discs which ranged from 11.5 mm (0.455 inch) to 13.9 mm (0.545 inch) in thickness. Upset ratios ranged from 2.8 to 3.7. The recrystallized forging billets were encapsulated in powder met molybdenum cans, heated to 1538°C (2800°F) and then forged in one blow in a high-energy-rate machine. The resulting forged discs of both alloys were crack free. Mechanical properties of the forged discs were comparable to the data for swaged rod and sheet of each alloy given the standard final anneal of 1 hour at 1649°C (3000°F).

2.0 INTRODUCTION

2.1 BACKGROUND

This program was the third and final of a series aimed at the development of advanced high temperature strength tantalum base alloys for use in Rankine cycle space nuclear power systems operating in the 1093°C (2000°F) - 1649°C (3000°F) temperature regime.

The initial program of the series was conducted under Contract NAS 3-2542[1] and led to the development of ASTAR-811C (Ta-8.0W-1.0Re-0.7Hf-0.025C), a highly fabricable, weldable, creep resistant alloy. During the conduct of that program a number of pertinent observations were made and conclusions drawn as to the character of tantalum base alloys. They were:

- Excessive reactive metal (Hf, Zr) additions to a tantalum matrix severely degrades creep resistance. To retain optimum creep resistance without compromising corrosion resistance to liquid alkali metals, the reactive metal addition must be maintained at nominally 0.5 to 1.0 atom percent.
- Creep behavior was significantly affected by rhenium content with maximum improvement resulting at rhenium concentrations of 0.5 to 1.5 atom percent. Improvements in creep properties were achieved without affecting short time tensile properties or low temperature ductility.
- Optimum creep properties commensurate with good "as-welded" ductility was achieved by limiting carbon concentrations within the range of 200 to 300 ppm.
- Partial or total substitution of carbon with nitrogen results in a still further improvement in creep properties by the formation of a coherent nitride precipitation reaction.

Continued studies were conducted in the second program of the series, under Contract NAS 3-10939[2] and were directed toward higher creep properties. The level of strengthening additions to the ASTAR-811C composition was limited by fabricati... and weldability considerations. It was, however, apparent during the initial investigation that relaxation of

the weldability criterion would permit development of alloys with higher elevated temperature strength that would be competitive with high strength columbium modified TZM molybdenum base alloy. Continuing studies under Contract NAS 3-10939 were directed towa.d higher creep properties by increasing, principally, the tungsten level of the ASTAR-811C composition while retaining the hafnium, rhenium, and carbon within the limits discussed. Small heats, 7.3 kg (16 pounds) maximum size, with tungsten levels ranging from 13 to 16 atom percent and rhenium levels varying from 1.0 to 2.0 atom percent were produced and evaluated. The results of the program are summarized in Figures 1 and 2. Significant improvement in creep properties of tantalum base alloys was achieved by increasing alloy solute content A comparison of the creep strength of the experimental tantalum alloys with ASTAR-811C, T-111, and columbium modified TZM alloy is shown in Figure 1. At temperature above 1204°C (2200°F), the experimental tantalum base alloys were clearly superior, even on a density compensated basis. It is apparent from Figure 2, that increasing solute content above 15 percent, results in an abrupt decrease in room temperature tensile ductility. Although the elevated temperature strength increases monotonically with increasing solute content, a trade off in elevated temperature strength must be made to retain low temperature ductility, since ductility is one of the prime requisites of tantalum base alloys.

2.2 PROGRAM OBJECTIVES

The objective in this program was to select two alloy compositions based on the results of the screening studies carried out under NAS 3-10939. In this program larger ingots 12.5 cm (5.0 inches) in diameter were produced, processed to various mill shapes, and extensively evaluated with respect to mechanical and physical properties.

The alloy compositions selected were as follows:

ASTAR-1211C - Ta-12.0W-1.0Re-0.7Hf-0.025C
ASTAR-1511C - Ta-15.0W-1.0Re-0.7Hf-0.025C

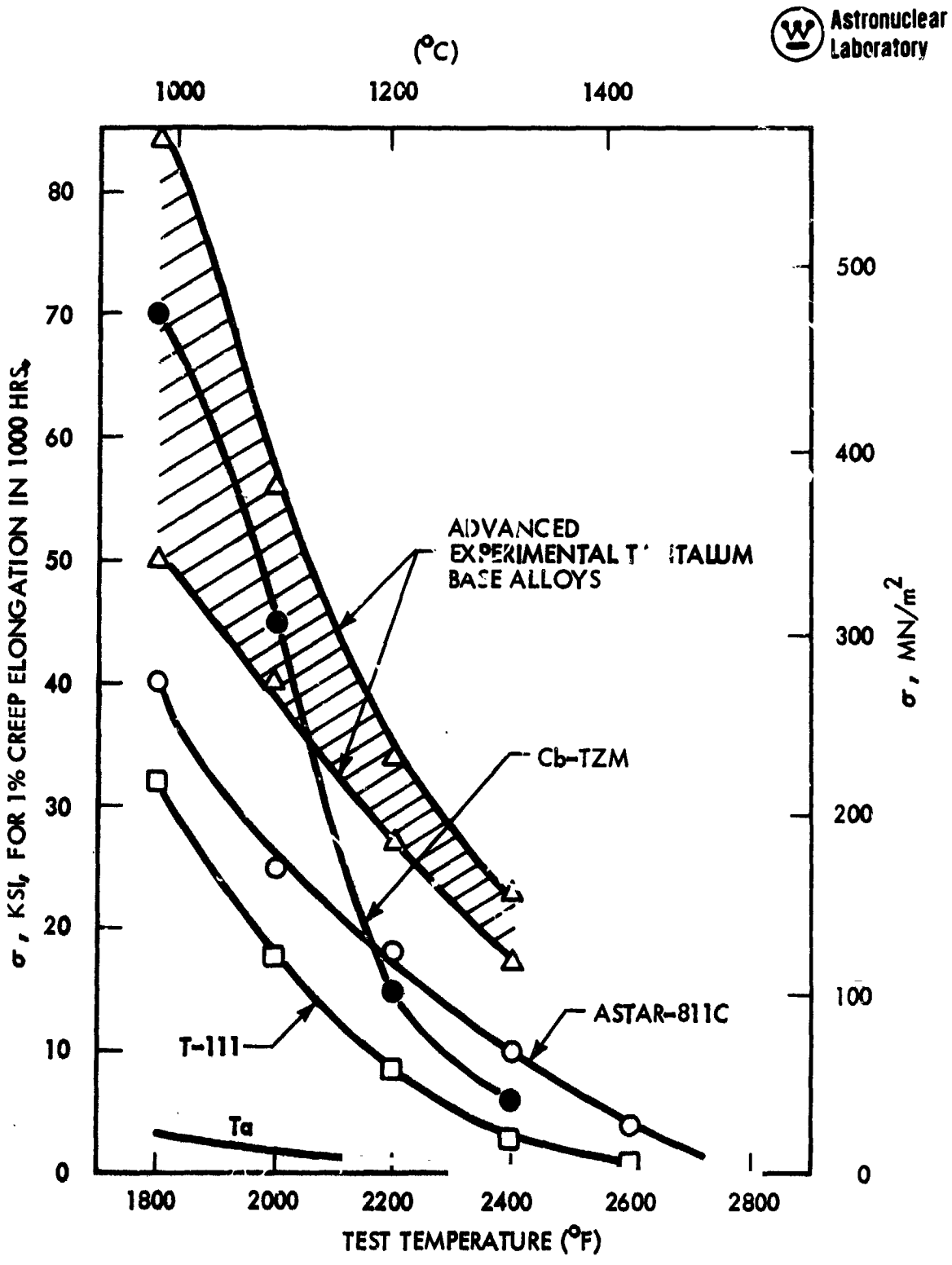

Figure 1. Creep Properties of Refractory Metal Alloys[2]

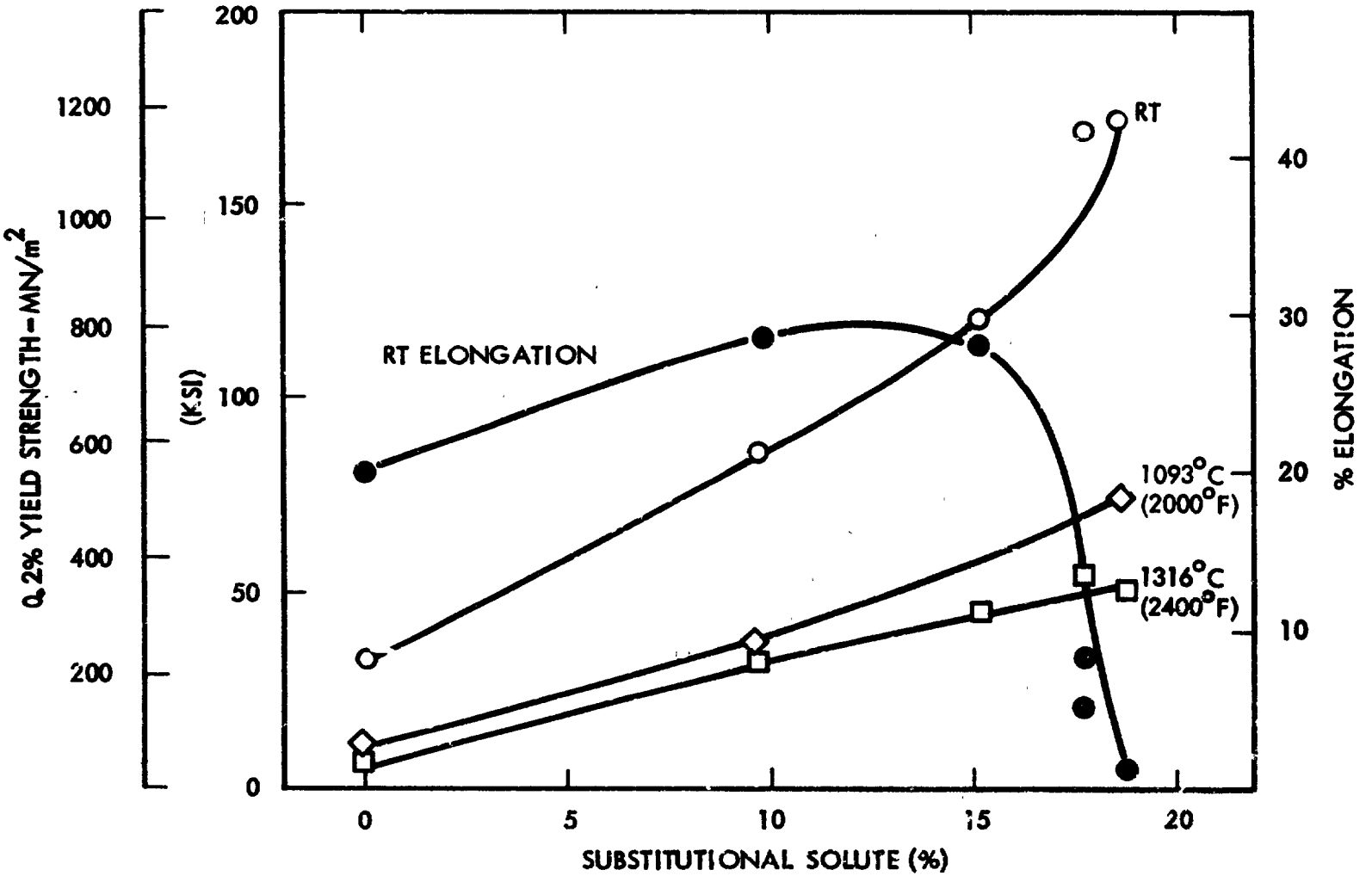

Figure 2. Effect of Substitutional Solute Level on Yield Strength and Room Temperature Elongation of TA, 8-16W, 1-2 Re, 0.7 Hf -0.025C Alloy Rod[2]

The primary selection criteria for the ASTAR-1211C composition was the attainment of high creep and yield strengths while maintaining a moderately fabricable alloy. From Figure 2, the total solute content of ASTAR-1211C, 13.7 atom percent, provides a low temperature ductility level sufficient to permit the fabrication of sheet and possibly tubing. The selection of the ASTAR-1511C composition was based on obtaining the highest possible creep and yield strengths and still provide so chance of producing most mill products. It was anticipated that the production of sheet or tubing from ASTAR-1511C would be difficult. The solute content of ASTAR-1511C, 16.7 atom percent, falls in the region where ductility is decreasing rapidly with increasing solute content.

2.3 PROGRAM PLAN

In order to meet the objectives, the program was divided into five specific areas:

- Melting and Processing of Starting Material
- Processing and Evaluation of Swaged Bar Stock
- Processing and Evaluation of Sheet
- Processing and Evaluation of Tubing
- Processing and Evaluation of Forged Discs

The purpose of the first task was to provide sound, homogeneous starting material in a suitable form for the remaining four tasks. To provide the required material, two 12.5 cm (5.0 inch) diameter ingots of each alloy were double vacuum arc melted. Prior programs were limited to a maximum diameter of 5.0 cm (2.0 inches). Possible commercial production would be demonstrated by the scale-up of ingot size.

In the second task, both alloys were processed to small diameter swaged rod. The effect of swaging and final annealing temperature on low temperature ductility, elevated temperature tensile and creep properties was determined, and a standard final annealing temperature was

selected. Extended physical and mechanical properties for standard annealed swaged rod were determined for both alloys.

For the sheet evaluation, a process for reducing both alloys to 1.0 mm (0.040 inch) thick sheet was developed. A major portion of the sheet evaluation was determining the effect of fusion welding on the ductile-to-brittle transition temperature (DBTT). The DBTT was determined in bending and tension for both electron beam (EB) and inert-gas-tungsten-arc (GTA) welded material. The effect of post weld annealing (PWA) and thermally aging the DBTT of welded material was also investigated.

The feasibility of producing tubing from both alloy compositions was also scheduled for investigation. This effort was conducted in cooperation with a commercial tubing manufacturer. Standard tubing practice and equipment were utilized.

Since there are many applications where forged parts are required in turbo-machinery for space power generation, a study involving the properties of forged discs was also included in this program.

2.4 EXPERIMENTAL PROCEDURES

The experimental procedures used on this program have been described in detail in prior reports[1-3].

3.0 MELTING AND PROCESSING OF STARTING MATERIAL

The objective of this task was to provide material for the evaluation tasks of this program. The processing schedule for achieving this objective is shown in Figure 3. Two 12 cm (5 inch) diameter ingots of each alloy composition were produced by double vacuum arc melting. The heats were identified as follows:

	Heat Designation
ASTAR-1211C (Ta-12W-1Re-0.7Hf-0.025C)	NASVF-1000A NASVF-1000B
ASTAR-1511C (Ta-15W-1Re-0.7Hf-0.0250C)	NASVF-2000A NASVF-2000B

The arc cast ingots were processed to round bar approximately 7 cm (2.6 inches) in diameter by extrusion.

3.1 FIRST MELT ELECTRODE FABRICATION AND MELTING

Four first melt electrodes of each composition were fabricated to produce two 12 cm (5 inch) diameter ingots. Two first melt electrodes were required to produce one finished ingot. Vendor analyses of the starting material are given in Table 1. Tantalum strip, 0.635 cm (0.250 inch) thick by 2.54 cm (1 inch) wide was used with tungsten, hafnium, and rhenium strips interspersed between. A typical first melt electrode cross section is shown in Figure 4. Carbon was added as carbon cord wrapped in tantalum foil. First melt electrodes averaged 32.7 kg (72 pounds). A fabricated first melt electrode is shown in Figure 5 along with a resulting first melt ingot. First melts were made using AC power, 4500 to 4800 amps at 30 volts to produce a 9 cm (3-1/2 inch) diameter ingot. The melting rates averaged 3.6 kg (8 pounds) per minute.

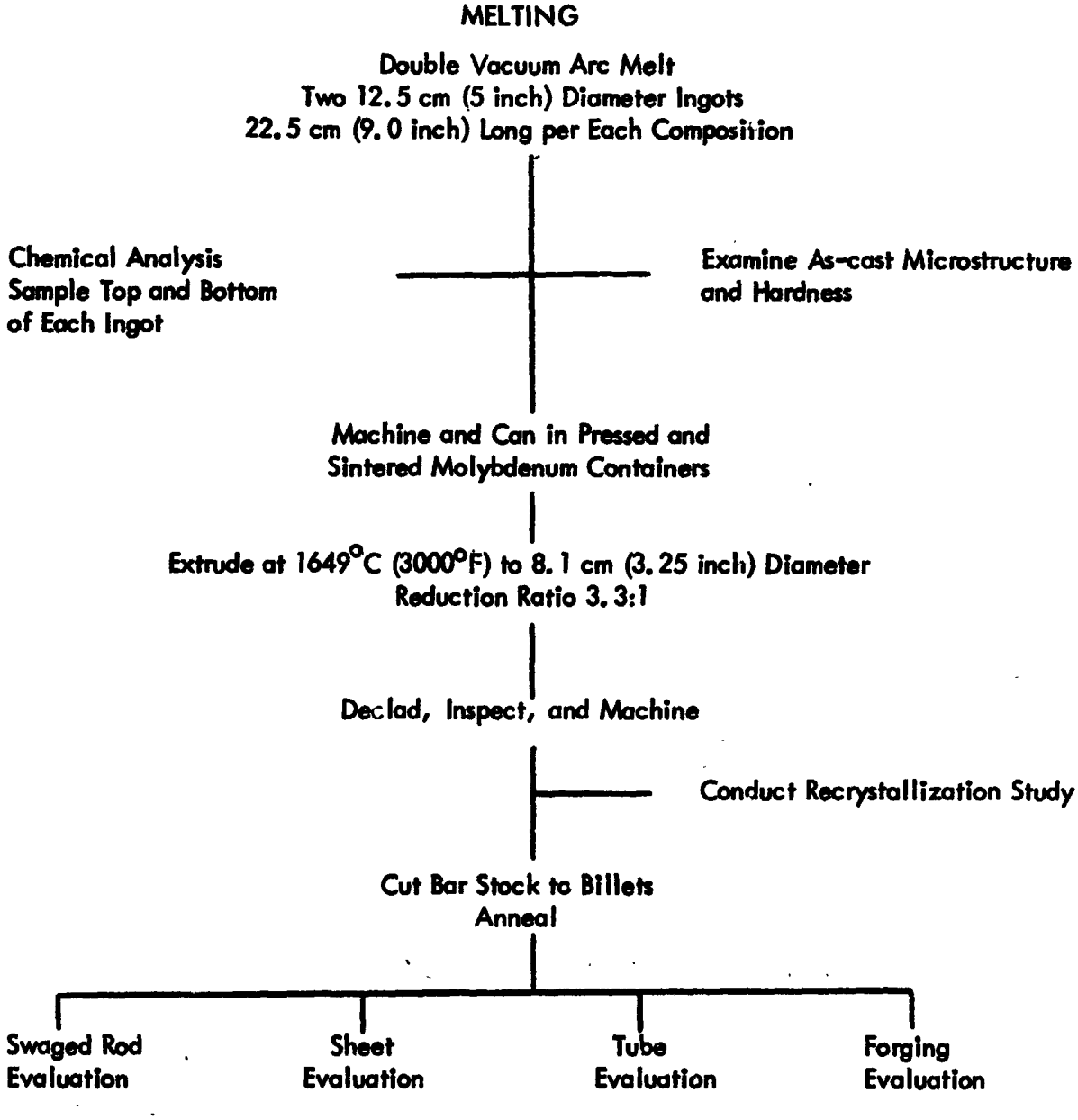

Figure 3. Schedule for Processing Starting Material

Table 1. Vendor Analyses of Starting Material

		Analyses (ppm)														
Material	Supplier	Form	C	O	N	Fe	Ni	Cr	Co	Al	Cu	Sn	Si	Ca	Zr	W
Tantalum	Fansteel	Plate	24	29	<10	<10	<10	<10	<10	<10	<10	<10	<10	<10	<10	130
Tungsten	Wah Chang	Strip	<20	<50	-	15	15	<10	<10	<10	<10	<10	<10	<10	-	Bal
Tungsten	Wah Chang	Strip	<20	<50	-	50	20	10	<10	<10	<10	<10	<10	<10	-	Bal
Hafnium	Amax	Strip	-	340	<16	185	-	-	-	<20	-	-	-	<20	3.4%	-
Rhenium	Cleveland Refractory	Strip	6	38	10	17	5	10	-	12	3	< 5	< 5	< 1	-	<100

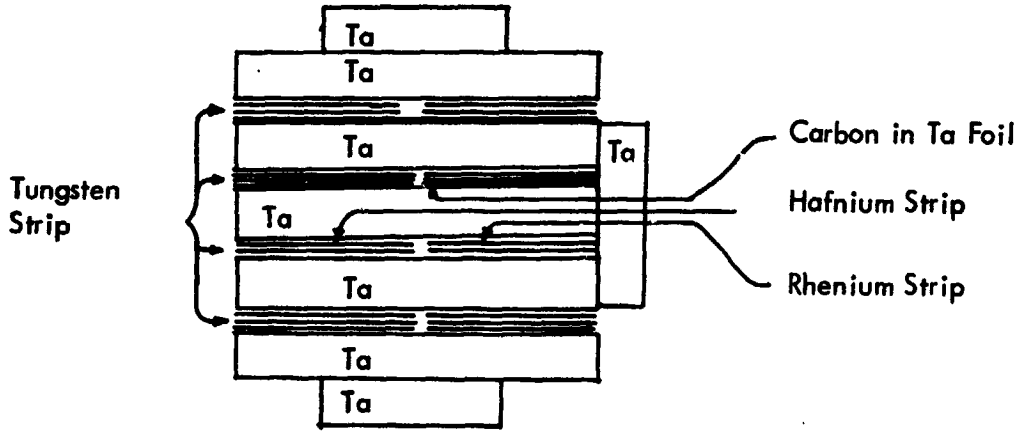

Figure 4. Typical First Melt Electrode Cross Section

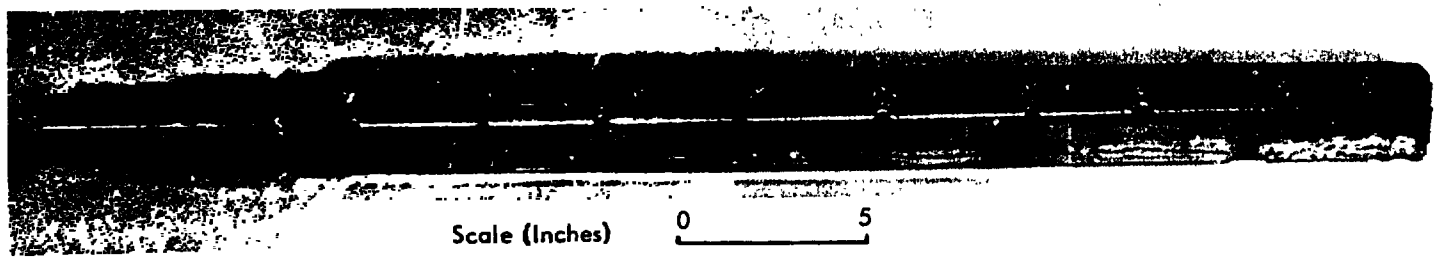

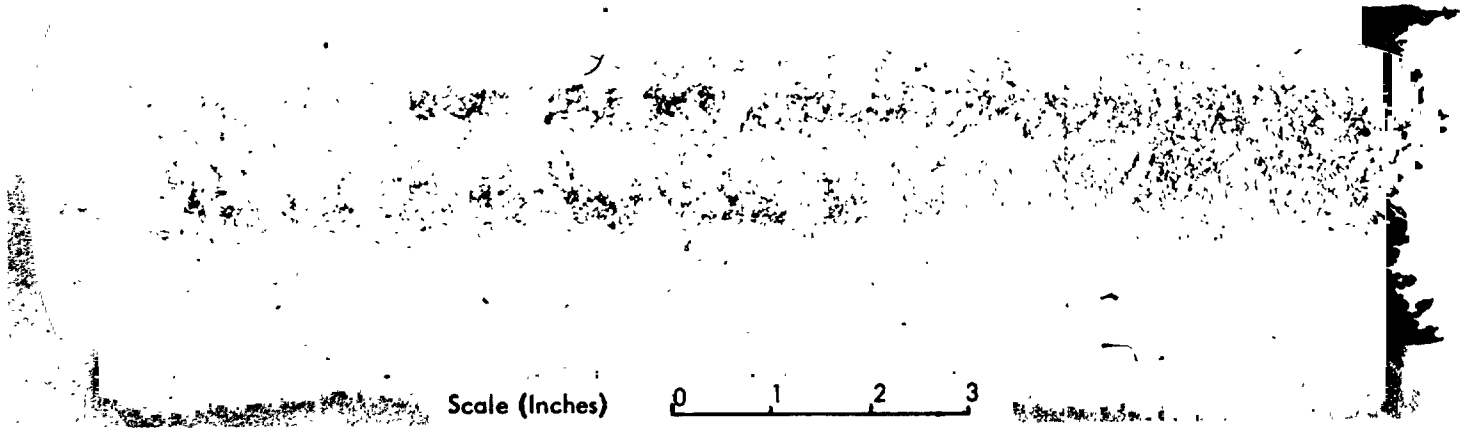

Figure 5. First Melt Electrode and a First Melt Ingot

3.2 SECOND MELT ELECTRODE FABRICATION AND MELTING

The second melt electrodes were composed of two first melt ingots joined together as shown in Figure 6. The second melt electrodes for ASTAR 1211C (heats NASVF-1000 A and B) weighed 60 kg (132 pounds) and 61.4 (135 pounds). The second melt electrodes for ASTAR 1511C (heats NASVF-2000 A and B) weighed 61.9 kg (136 pounds) and 63.2 kg (139 pounds), respectively.

Melting of the second melt electrodes into a 12 cm (5 inch) diameter mold proved to be more difficult than anticipated. The initial attempts to melt electrode NASVF-1000B using DC power with a DC stirring coil were unsuccessful due to poor electrical contact between the starting pad and the mold bottom. Thin tantalum sheet wedged between the starting pad and the mold side wall alleviated the problem. The arc was struck at 30 volts and 5500 amps and gradually increased to 8000 amps. After 3/4 of the electrode had been melted, it was noted that melting had ceased even though the arc was being maintained. It was also noted that the buss bar carrying the current back to the power supplies was overheated. Melting was halted to prevent damage to the equipment. The resulting ingot, which had excellent sidewall, and the remainder of the unmelted electrode are shown in Figure 7. Inspection of the current return path from the mold to the buss revealed several high resistance interfaces where excessive heat buildup was occurring, thus reducing power at the arc. A new mold with a heavier flange was designed which would permit direct coupling to the return buss bar with water-cooled leads, thus reducing extraneous power losses. Electrode NASVF-1000A was melted using the redesigned mold assembly. During the final minute of the NASVF-1000A melt, the rate of electrode burn-off decreased significantly indicating a loss of melting power at the arc. For this reason, no intentional hot topping operation was conducted. The resulting ingot is shown in Figure 8. Because of the reduction in melt rate during the first two melts, it was concluded that the available DC power, 8500 amps at 30 volts, was marginal for the electrode/mold diameter ratio being used. An additional 2500 amps of continuous duty cycle power was added to give a total of 10,000 amps at 40 volts.

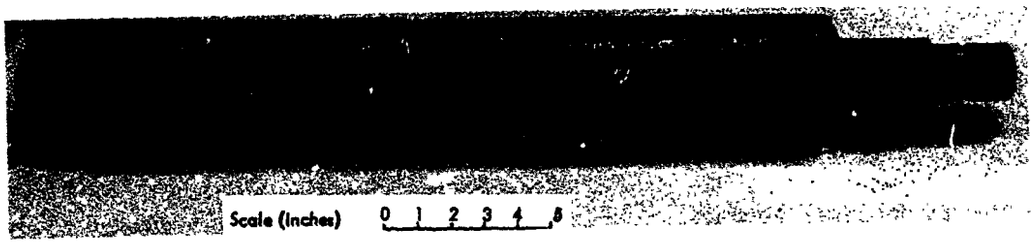

Figure 6. Second Melt Electrode

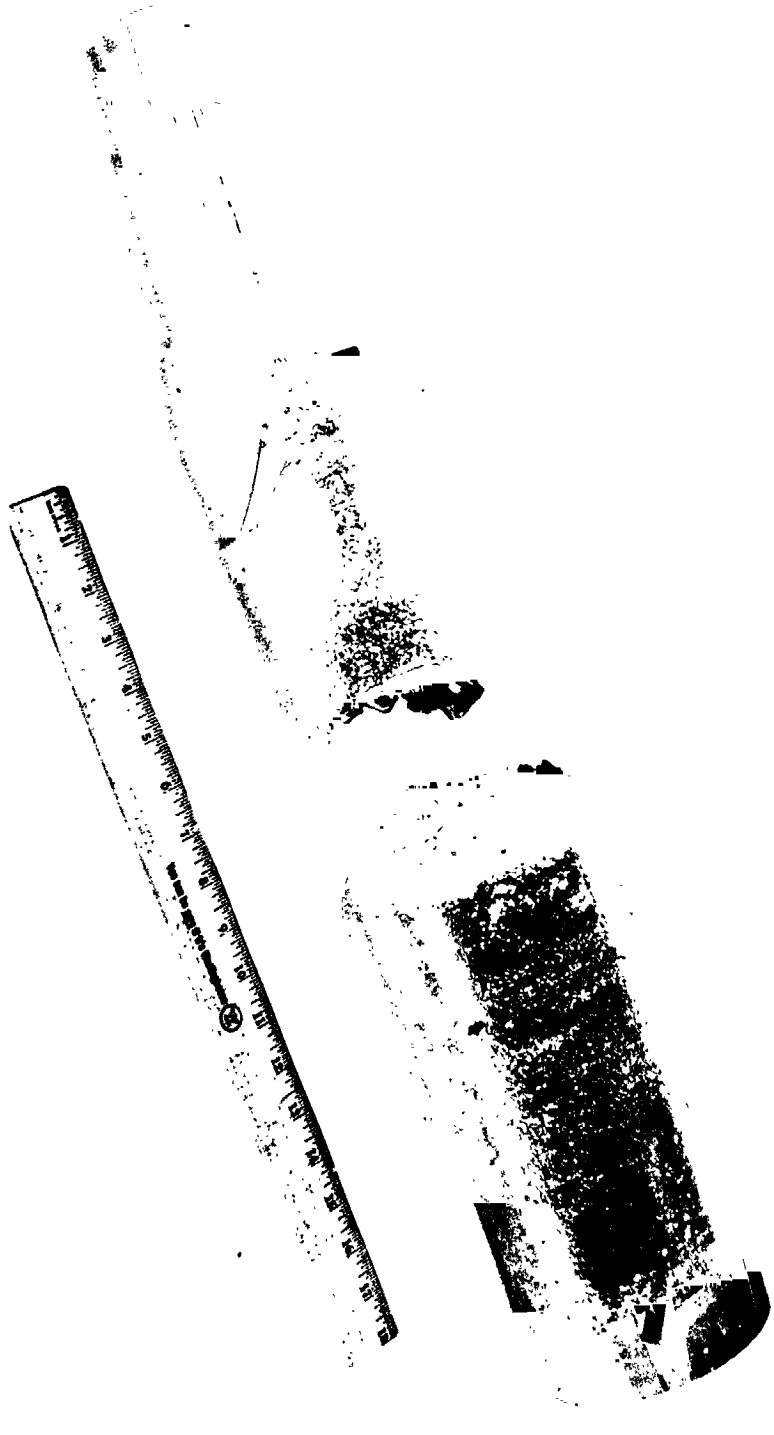

Figure 7. Five Inch Diameter Ingot of NASVF-1000-B and Remaining Electrode

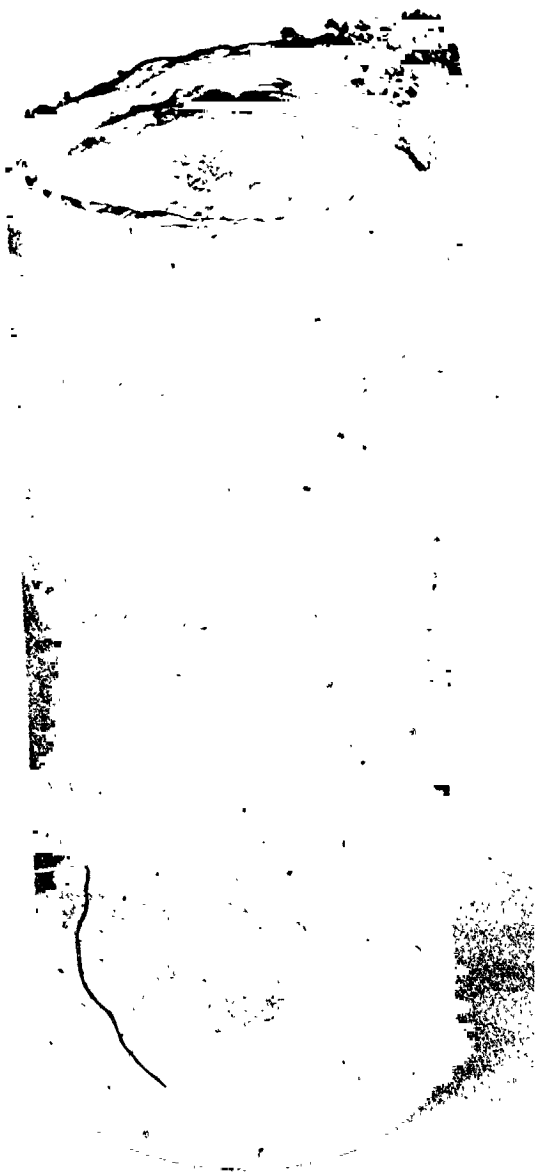

Figure 8. Five Inch Diameter Ingot of NASVF-1000A

The final two ingots of NASVF-2000 were made with the additional power. Electrode NASVF-2000A was melted at an initial DC current of 8000 amps at 30 volts. As melting progressed, power was increased to 9500 amps at 35 volts. However, melting had to be stopped after 80 percent of the electrode had been cast when the pressure in the chamber rose from 2×10^{-4} torr to the 1 to 10 torr range. The pressure retumed to the 10^{-5} torr range immediately on cessation of melting. The pressure burst was traced to the overheating of a micarta insulating ring.

Electrode NASVF-2000B was melted at an initial current of 9000 amps at 35 volts which was increased to 9500 amps at 40 volts during the melt. Again melting had to be stopped after 80 percent of the electrode had been cast due to the rupture of a water line carrying cooling water to a power lead.

Information concerning the arc casting of the four 12.7 cm (5 inch) diameter ingots is given in Table 2.

3.3 INGOT CHEMISTRY

Upon completion of the melting process and prior to encapsulation of the ingots in the molybdenum cans, chemical samples in the form of machining chips were taken from the top and bottom of each ingot. The ingot ends were divided into three zones to assess the homogeneity of the ingots. Chips from Zone 1 were taken from the center area 7.2 cm (3 inches) in diameter. Zone 2 included the area between the 7.6 cm (3 inches) and 10.2 cm (4 inches) diameters. Zone 3 consisted of the area from the 10.2 cm (4 inch) diameter out to the OD of the ingot. The zones are illustrated in Figure 9. Solid samples for interstitial analyses were taken from a slice, approximately 1.3 cm (1/2 inch) thick, cut from the top of the ingot. The results of the chemical analyses are given in Table 3 along with the specification range. The accuracy of the chemical analysis as determined through the use of standards is $\pm$ 0.2 percent for tungsten and $\pm$ 0.04 percent for the hafnium and rhenium. The tungsten and

Table 2. Melting Parameters for 12.7 cm (5 inch) Diameter Ingots[1]

Melt Identification	DC Volts	DC Amps	Melt Rate		Unconditioned	
			(g/sec)	(lbs/min)	Mass (kg)	Weight (lbs)
NASVF-1000A[2]	30	5500-8000	37.2	4.9	50.0	110
NASVF-1000B[3]	30	5800-8500	37.9	5.0	46.5	102
NASVF-2000A[4]	30-35	8000-9500	25.0	3.3	47.8	105
NASVF-2000B[5]	30-35	9000-9500	36.4	4.8	45.0	99

(1) DC stirring coil was used.
(2) No hot top attempted.
(3) Melting stopped due to overheated buss bar - no hot top.
(4) Melting stopped due to pressure rise in the chamber.
(5) Melting stopped due to an external water leak.

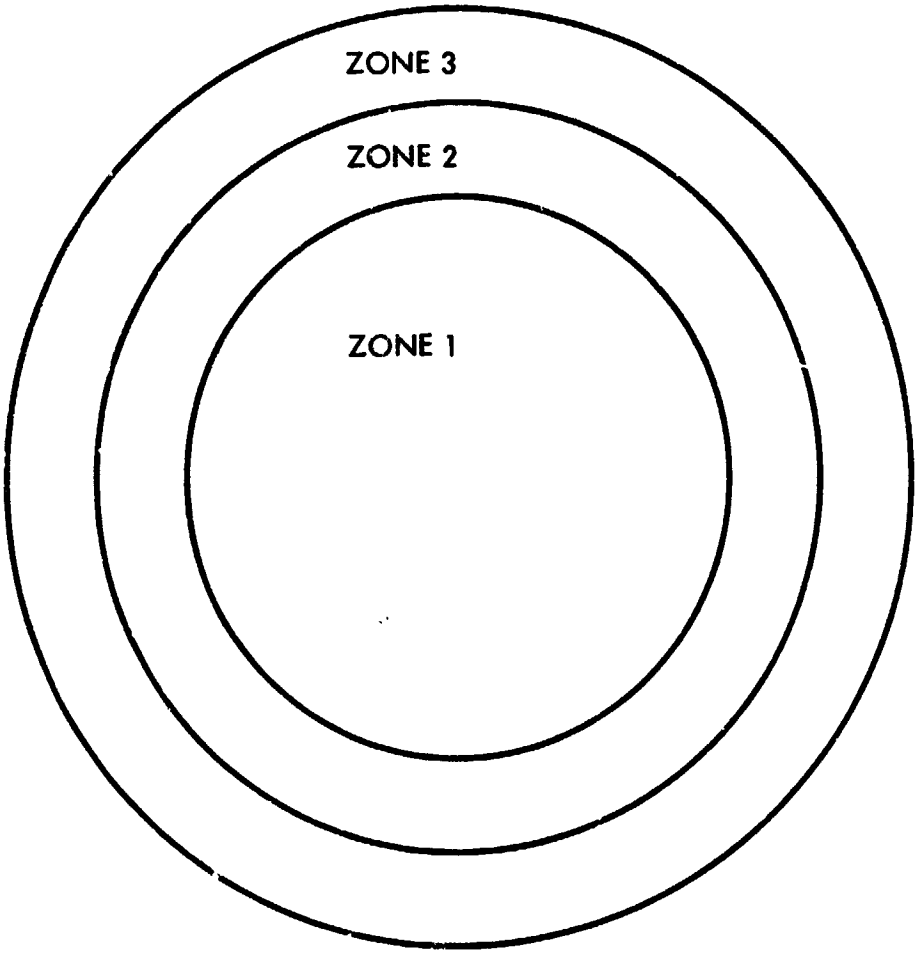

Figure 9. Locations of Chemistry Sampling Zones
(Dimensions are described in text)

Table 3. Chemical Analyses of 12.7 cm (5 inch) Diameter Ingots

Ingot Designation	Sample Location	Chemical Analyses					
		Metallics (%)			Interstitials (ppm)		
		W	Hf	Re	O	N	C
NASVF-1000A Ta-12W-1.0Re 0.7Hf-0.0250C	Zone 1 Top	11.6	0.81	1.09	3	28 15	270
	Zone 2 Top	11.8	0.79	1.08			
	Zone 3 Top	11.8	0.78	1.08			
	Zone 1 Bot	11.9	0.59	1.01			
	Zone 2 Bot	11.7	0.62	1.02			
	Zone 3 Bot	11.0	0.60	0.97			
NASVF-1000B Ta-12W-1.0Re 0.7Hf-0.0250C	Zone 1 Top	12.0	0.72	1.11	3 11*	21 19*	310 290*
	Zone 2 Top	11.8	0.70	1.09			
	Zone 3 Top	11.9	0.70	1.08			
	Zone 1 Bot	11.5	0.60	0.98			
	Zone 2 Bot	11.2	0.56	0.90			
	Zone 3 Bot	10.2	0.55	0.84			
NASVF-2000A Ta-15W-1.0Re 0.7Hf-0.0250C	Zone 1 Top	14.5	0.80	1.13	19	<10	250
	Zone 2 Top	14.5	0.82	1.13			
	Zone 3 Top	14.6	0.80	1.13			
	Zone 1 Bot	15.0	0.52	1.04			
	Zone 2 Bot	14.7	0.52	1.04			
	Zone 3 Bot	14.6	0.62	1.04			
NASVF-2000B Ta-15W-1.0Re 0.7Hf-0.0250C	Zone 1 Top	14.5	0.80	1.10	11	24	250
	Zone 2 Top	14.5	0.80	1.12			
	Zone 3 Top	14.5	0.80	1.12			
	Zone 1 Bot	15.6	0.58	1.00			
	Zone 2 Bot	15.4	0.58	1.03			
	Zone 3 Bot	15.3	0.62	1.04			
Specification Range		11.4-12.6 14.25-15.75	.63-.77	.9-1.1	<100	<50	210-290

*Check Analyses

rhenium are well within the specification range. The lower values for the bottoms of ingots NASVF-1000A and B are the result of the pure tantalum chips which were used to initiate the arc during melting. The ingots were cut from the starting pads at this interface in order to conserve material. The distribution of hafnium, however, presented a different picture. In general, the hafnium levels were slightly below specification range at the ingot bottoms and slightly higher at the ingot tops. The dilution effect of the starting chips, although evident, does not account for the consistent difference in hafnium concentration noted between the top and bottom of all four ingots. One possible explanation involves the melting point of hafnium. Considering that the melting points of tantalum, tungsten, and rhenium are relatively close to one another (3000 to 3410°C) and that the melting point of hafnium (2222°C) is significantly lower, a zone refining effect is possible where hafnium is rejected to the molten pool as solidification proceeds from bottom to top. Additional chemistry checks, which are described in detail in a following section of this report, indicated hafnium levels which were very near to target values.

3.4 METALLOGRAPHY OF AS-CAST INGOTS

Metallographic samples were taken from the slice cut from the top of each ingot. Micrographs of ingots NASVF-1000A and B are shown in Figure 10; ingots NASVF-2000A and B are shown in Figure 11. The micrographs reveal a typical cast structure with the dendritic pattern more pronounced in the ASTAR-1511C alloy. This difference is most likely due to sample location than to the difference in composition. The 1500X micrographs for both compositions show a typical secondary phase precipitate which formed during cooling of the cast ingots after melting. Prior experience on previous programs with alloys of similar composition indicates that the precipitate is most likely Ta_2C[1].

100X DPH 288 1500X

NASVF-1000-A

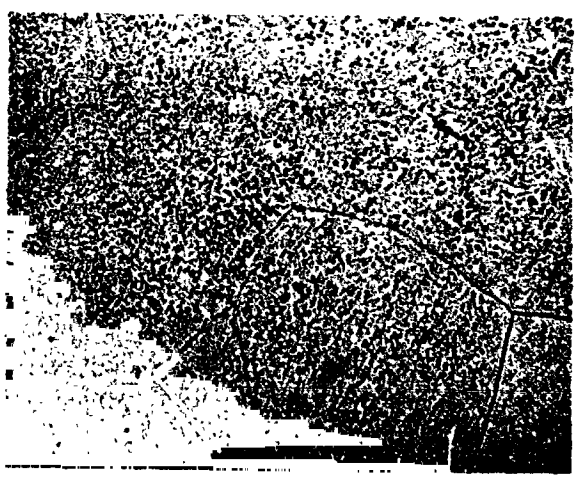

100X DPH 293 1500X

Heat NASVF-1000 B

Figure 10. Microstructures of 12.7 cm (5 inch) Diameter Ingots of ASTAR-1211C (Heats NASVF-1000 A&B)

100X DPH 335 1500X

Heat NASVF-2000 A

100X DPH 320 1500X

Heat NASVF-2000 B

Figure 11. Microstructure of 12.7 cm (5 inch) Diameter Ingots of ASTAR 1511C (Heats NASVF-2000 A&B)

3.5 INGOT PROCESSING AND EXTRUSION

The four ingots were conditioned and clad in pressed and sintered molybdenum in preparation for extrusion. A minimum amount of material was removed from the side wall of the ingots due to the excellent condition of "as-cast" ingots. Extrusion ingot data are given in Table 4.

The method used to encapsulate the ingots in molybdenum is shown in Figures 12 and 13. The ID of the molybdenum cylinders were machined to fit the OD of each ingot. Nose and end plugs were machined to fit snugly into each end of the molybdenum cylinders. The plugs were held in place with threaded molybdenum pins approximately 0.48 cm (3/16 inch) in diameter. The nose plug had a 2.54 cm (1 inch) radius at the OD, and the ingot was given a 0.63 cm (1/4 inch) radius. The nose plugs were a minimum of 2.54 cm (1 inch) thick.

The ingots were extruded at the ARMCO Advanced Materials Processing Laboratory in Baltimore, Maryland (formerly Fansteel Extrusion Facility). They were extruded at a reduction ratio of 3.4:1 based on the ID of the press liner which was 15.2 cm (6 inches). The clad ingot diameter was 14.6 cm (5.75 inches); the 0.63 cm (1/4 inch) difference in diameters provided for thermal expansion and ingot lubrication. Initial plans called for a 15 minute hold at the extrusion temperature, 1650°C (3000°F), prior to extrusion. Excessive oxidation of the molybdenum can in the "inert" atmosphere of the argon purged bell jar surrounding the heater caused a short circuit in the induction coil, and necessitated extrusion of the first ingot, NASVF-1000A with only a 6 to 7 minute soak at temperature. The heating procedure was modified for the remaining ingots. The ingots were heated to 1260 - 1370°C (2300 - 2500°F) and held for 15 minutes. Oxidation of the molybdenum was not a problem in this temperature range. The ingots were then heated to 1650°C (3000°F) for extrusion. Transfer time from shutdown of the heater to completion of the extrusion process was on the order of 10 to 15 seconds. The ingots were extruded through a ceramic coated die with a 8.25 cm (3.25 inch) diameter opening. The high speed recorders, which monitor extrusion pressure

Table 4. Extrusion Ingot Data

(SI Units)

Ingot Ident. NASVF	As-Cast			As-Conditioned			Mo-Clad		
	Mass (kg)	Approx. Length (cm)	Diameter (cm)	Mass (kg)	Length (cm)	Diameter (cm)	Mass (kg)	Length (cm)	Diameter (cm)
1000 A	50.0	25.4	12.52	48.0	23.6	12.50	69.3	30.5	14.6
1000 B	46.5	21.6	12.52	43.0	20.0	12.50	64.7	27.9	14.6
2000 A	47.8	22.9	12.45	43.9	22.1	12.30	64.2	27.9	14.6
2000 B	45.0	22.9	12.45	42.4	21.0	12.30	63.4	27.9	14.6

Ingot Ident. NASVF	As-Cast			As-Conditioned			Mo-Clad		
	Weight (lbs)	Approx. Length (in)	Diameter (in)	Weight (lbs)	Length (in)	Diameter (in)	Weight (lbs)	Length (in)	Diameter (in)
1000 A	110	10	4.93	105.5	9.3	4.925	152	12	5.75
1000 B	102	8-1/2	4.93	94.3	7.9	4.925	142	11	5.75
2000 A	105	9	4.90	96.4	8.7	4.850	141	11	5.75
2000 B	99	9	4.90	93.1	8.3	4.850	139	11	5.75

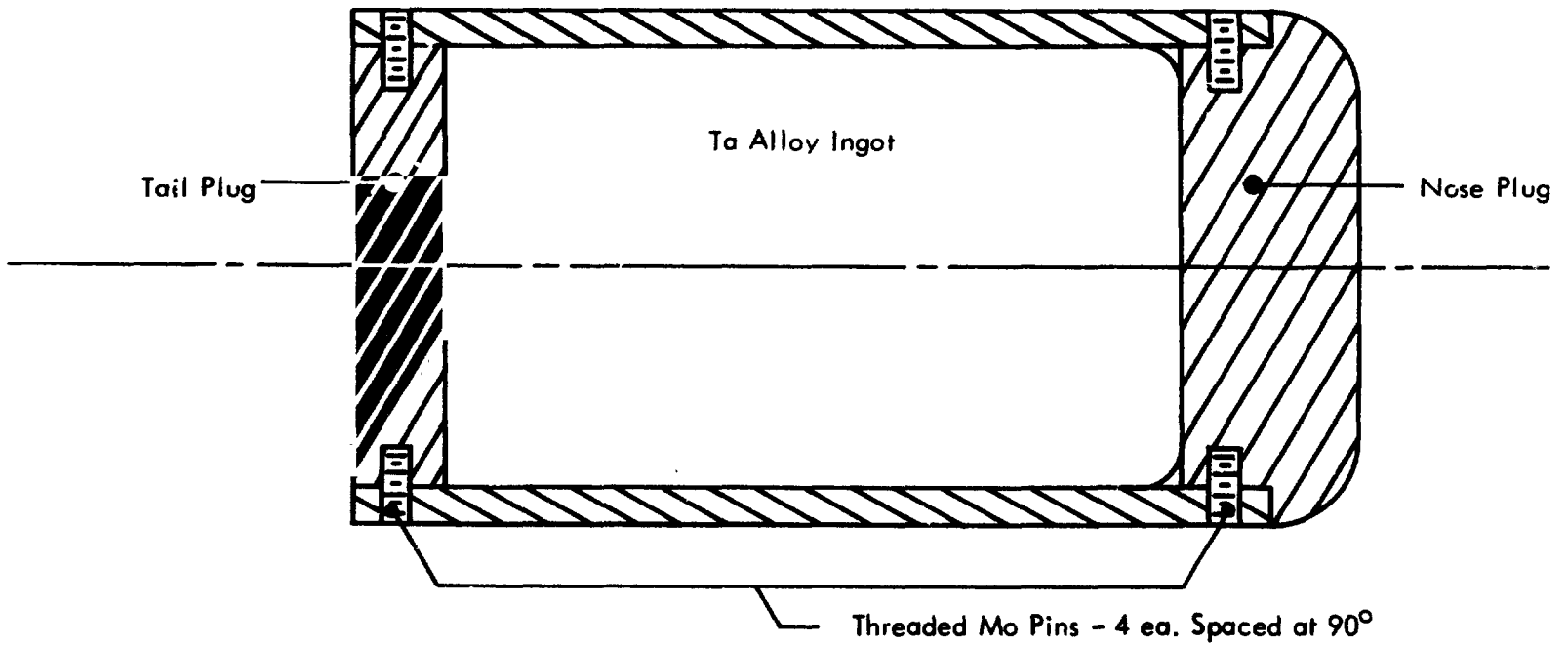

Figure 12. Molybdenum Containment Configuration for Ta Alloy Extrusion Ingots

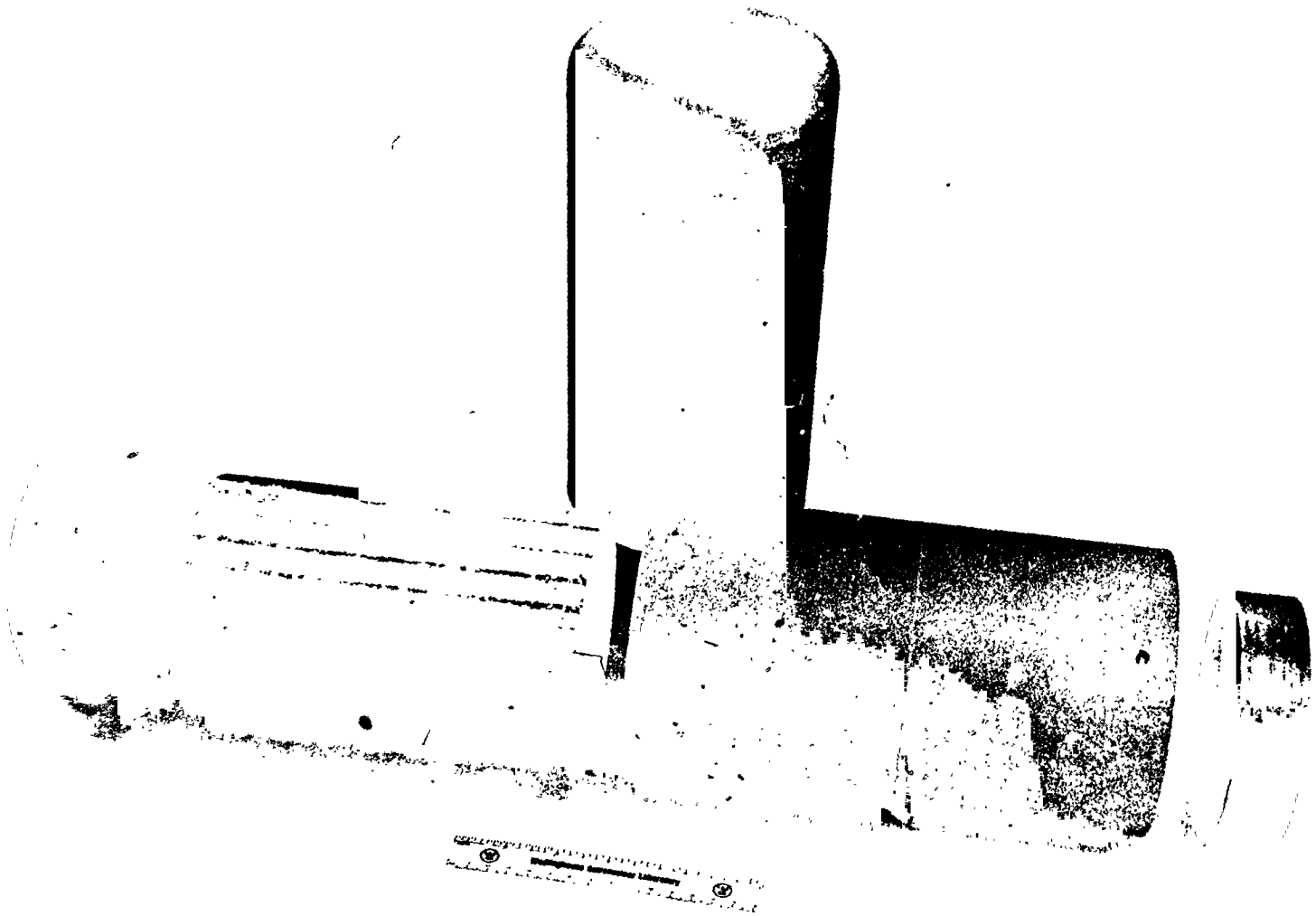

Figure 13. ASTAR 1211C Ingots Encapsulated in Molybdenum for Extrusion

and ram speed, were not operable and prevented determination of extrusion constants for these materials. Because of the speed of the extrusion process and the inertia of the gage pointer, accurate visual observation of the pressure gage readout was not possible.

The extrusions were permitted to air cool to a temperature which permitted handling with asbestos gloves. About 1 hour was sufficient to reach these conditions. The four extrusions are shown in Figure 14. The nose plugs, which separated during extrusion, are shown in the lower portion of the picture. All four extrusions were pushed through the same die. The appearance of the extrusions and the uniform diameter of the extrusions from nose to tail indicate that the coated die held up quite well. The diameter of each extrusion at the nose and tail was 8.22 cm (3.230 inches) and did not vary more than $\pm$ 25.4 μm ($\pm$ 0.001 inch) from extrusion to extrusion. All four extrusions were bowed slightly near the nose; the remaining 2/3 of the extrusion appeared to be quite straight.

The molybdenum clad was removed from the extrusions with a pickling solution of 60 percent concentrated HCl and 40 percent concentrated HNO_3. The massive molybdenum tail plug was removed from each extrusion prior to pickling. The extrusions of heats NASVF-1000A and B are shown in Figure 15. A 0.63 cm (1/4 inch) slide, which contained the oxidized portion of the nose exposed during cooldown, was removed from each extrusion. Except for the nose, the diameter of the extrusions was a uniform 7.33 cm (2-7/8 inches) for heats NASVF-1000A and B. The diameters of heats NASVF-2000A and B were not as uniform and ranged from 7.0 cm (2-3/4 inches) near the tail to 6.67 cm (2-5/8 inches) near the nose.

3.6 EXTRUSION RECRYSTALLIZATION BEHAVIOR

In order to determine the heat treatment required to recrystallize the extruded bar stock prior to further mechanical processing, a heat treatment study was conducted. A slice 1.27 cm (1/2 inch) thick was cut from the tail of each extrusion. Representative samples taken from

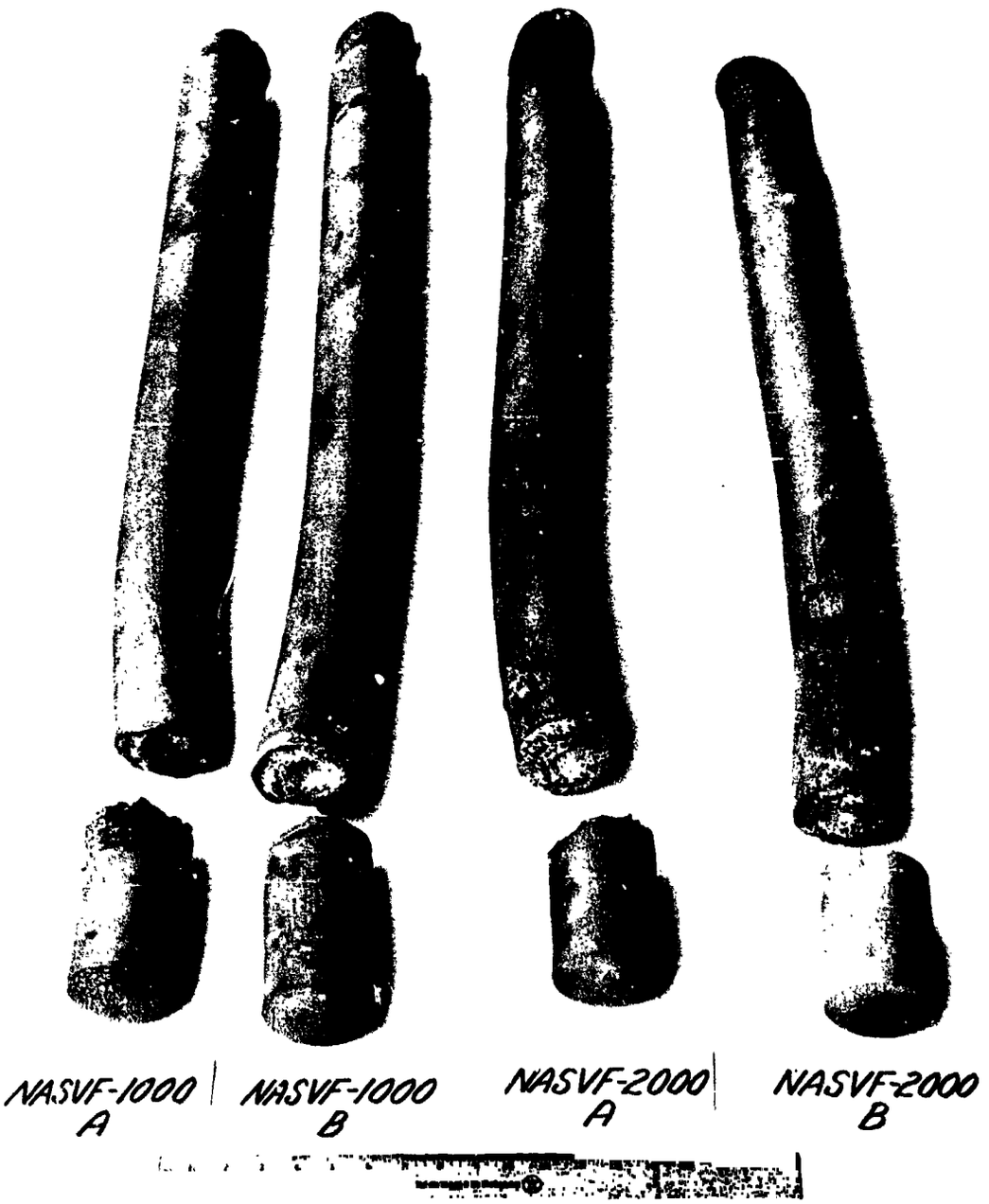

Figure 14. Extrusions of ASTAR-1211C and ASTAR-1511C

Figure 15. Declad Extrusions of ASTAR-1211C

the cross section of the extrusion were given 1 hour heat treatments at the following temperatures: 1316°C (2400°F), 1427°C (2600°F), 1482°C (2700°F), 1538°C (2800°F), 1593°C (2900°F), 1649°C (3000°F), 1816°C (3300°F), and 1960°C (3600°F). Photomicrographs of extruded and heat treated ASTAR-1211C, heat NASVF-1000A, are shown in Figure 16.* Photomicrographs of ASTAR-1511C, heat NASVF-2000B, are shown in Figure 17.* The microstructure of the material heat treated at 1316°C (2400°F), 1427°C (2600°F), 1482°C (2700°F), and 1593°C (2900°F) for both alloys, which are not shown, exhibited essentially the same structure as the "as-extruded" condition shown in Figures 16A and 17A. This behavior was typical for both heats of each alloy composition. The "as-extruded" structure for both heats of ASTAR-1211C and ASTAR-1511C was partially recrystallized. The 1649°C (3000°F) extrusion temperature was apparently high enough, and the slow cooling rate due to large mass of material involved were sufficient to permit initiation of the recrystallization process. This structure persisted up to the 1649°C (3000°F) annealing temperature. The material heat treated for 1 hour at 1649°C (3000°F) was essentially completely recrystallized; however, a duplex grain structure was produced. Numerous small grains can be seen with a fewer number of large grains interspersed among them (Figures 16B and 17B. After 1 hour at 1816°C (3300°F), a more uniform grain size is produced yielding a structure which is typical for this type alloy. (Figures 16C and 17C.) One hour at 1960°C (3600°F) produces little change compared to 1816°C (3300°F) heat treated material (Figures 16-D and 17-D).

Plots of the room temperature hardness data taken from heat treated specimens of ASTAR-1211C and ASTAR-1511C are shown in Figure 18. A consistent difference of 30 to 40 DPH points between the two compositions apparently reflects the effect of the additional 3 w/o tungsten in the ASTAR-1511C. The hardness behavior of both alloy compositions with respect to annealing temperatures was quite similar. The "as-extruded" material, although partially recrystallized, retained some residual stresses from the extrusion process. One hour exposure at 1316°C (2400°F) resulted in a lowering of the room temperature hardness indicative

*Plane of micrographs normal to extrusion direction.

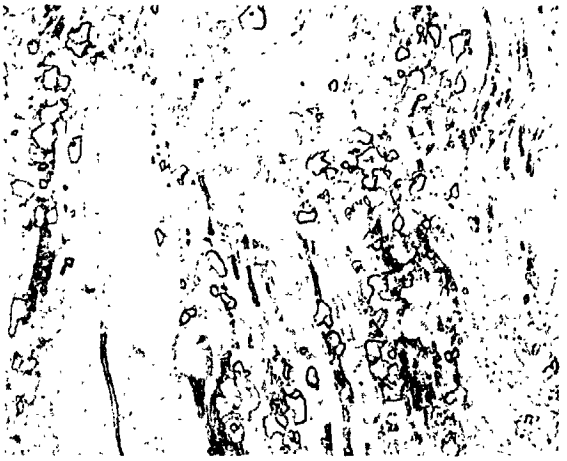

100X DPH 308

A. As Extruded

100X DPH 319

B. Extruded + 1 hr/1649°C (3000°F)

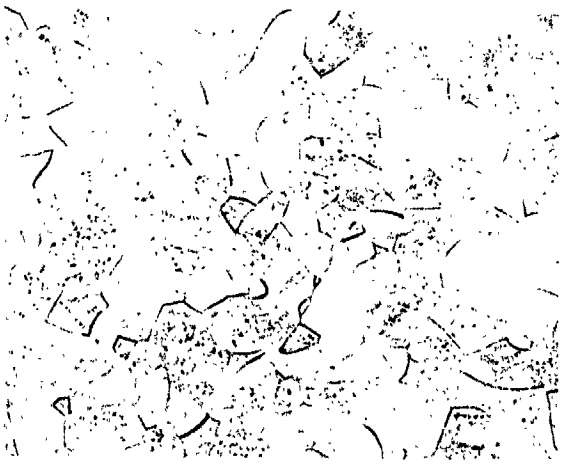

100X DPH 319

C. Extruded + 1 hr/1815°C (3300°F)

100X DPH 327

D. Extruded + 1 hr/1982°C (3600°F)

Figure 16. Microstructures of Extruded and Heat Treated ASTAR-1211C, Heat NASVF-1000 A (Transverse Sections)

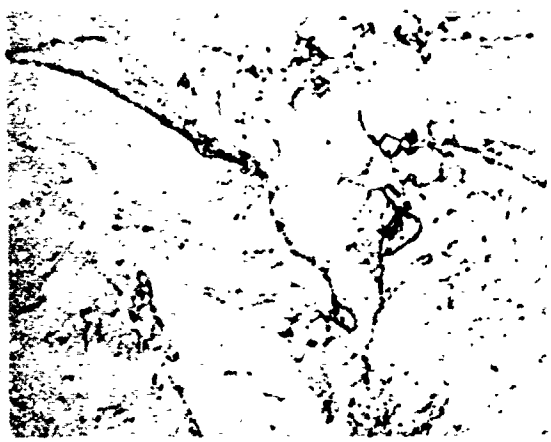

500X DPH 357

A. As Extruded

500X DPH 358

B. Extruded + 1 Hr./1649°C (3000°F)

500X DPH 361

C. Extruded + 1 Hr./1815°C (3300°F)

500X DPH 369

D. Extruded + 1 Hr./1982°C (3600°F)

Figure 17. Microstructures of Extruded and Heat Treated ASTAR-1511C, NASVF-2000-B (Transverse Sections)

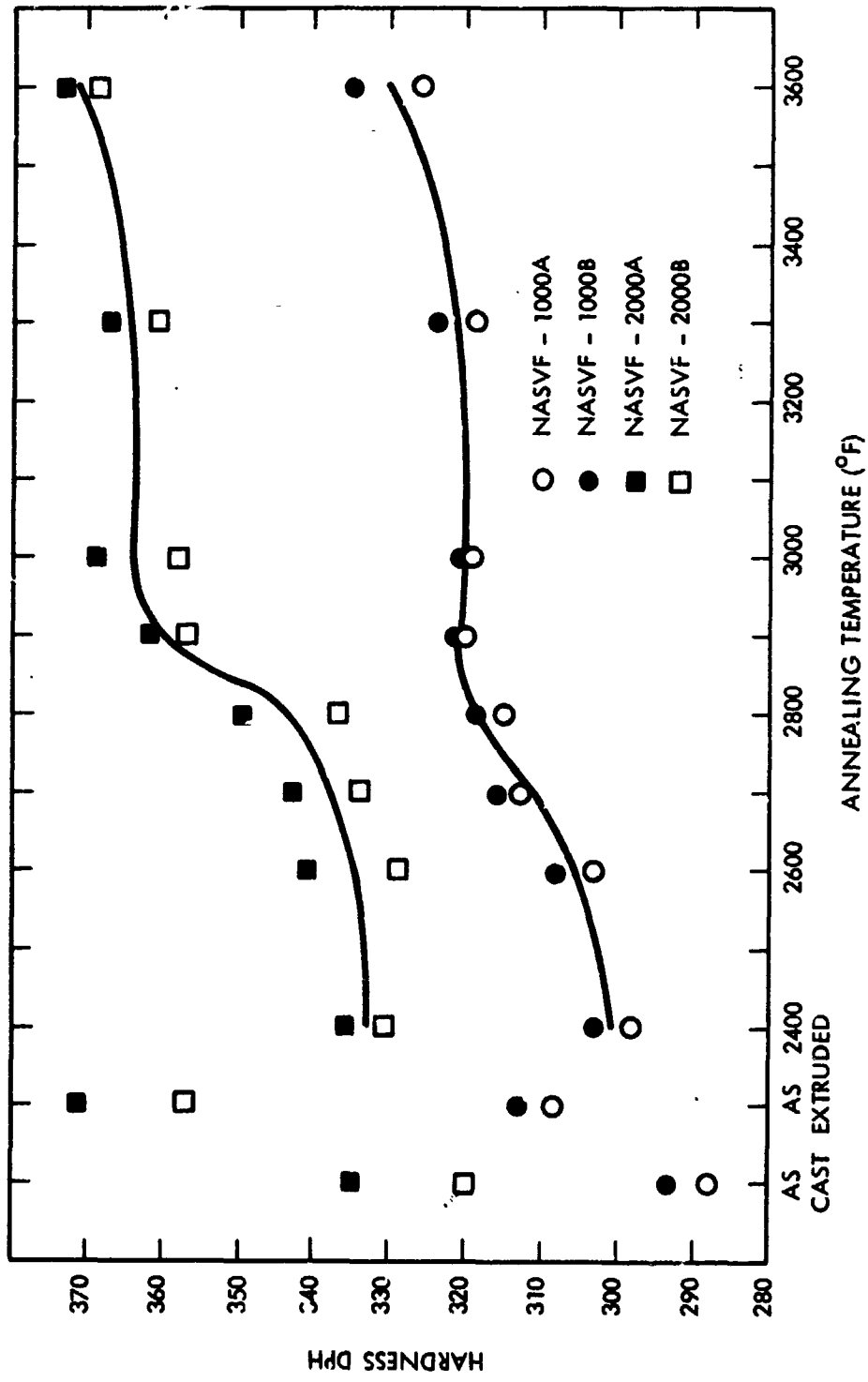

Figure 18. Hardness Data for Extruded and Heat Treated ASTAR-1211C and ASTAR-1511C

of the recovery process typical of tantalum alloys. Heat treatment at higher temperatures resulted in a gradual increase in hardness with higher annealing temperatures. The increase in hardness is most probably due to resolutioning of the carbide phase, Ta_2C, which was precipitated at lower temperatures during cooling from the extrusion temperature.

As a result of the heat treatment study of the recrystallization behavior of the primary extrusions of both alloy compositions, a 1 hour anneal at 1816°C (3300°F) was selected as the heat treatment for all extruded material. Although 1 hour exposure at 1649°C (3000°F) appeared to be adequate for complete recrystallization, the higher annealing temperature, 1816°C (3300°F), produced a more uniform microstructure with no apparent increase in room temperature hardness.

3.7 PROCESSING OF ASTAR-1211C AND ASTAR-1511C EXTRUSIONS

The extrusions of ASTAR-1211C, heats NASVF-1000A and B, and ASTAR-1511C, heats NASVF-2000A and B, were declad. The molybdenum clad was removed by pickling in a solution of 60 percent HCl and 40 percent HNO_3. The extrusions were sectioned to produce seven billets approximately 12 cm (4-3/4 inches) long and three billets 4.4 cm (1-3/4 inches) long of each composition. A diagram illustrating how the extrusions were sectioned is shown in Figure 19. The diagram does not show the curvature in the extrusions which caused some loss of material when the billet ends were squared off the axis of the billet. The billet ODs were machined to produce a maximum diameter free of surface defects.

It was noted during the "facing off" of billets A-5 and A-6 that there was a voided region common to both billets at the center of each billet. A small diameter wire probe revealed the depth of the void in billet A-6 to be 1.9 cm (3/4 inch) deep. The void in billet A-5 was found to be 1.3 cm (1/2 inch) deep. The location of the void in extrusion NASVF-1000A is shown in Figure 19. Billet A-5 was cut in half parallel to the billet axis. The defect was

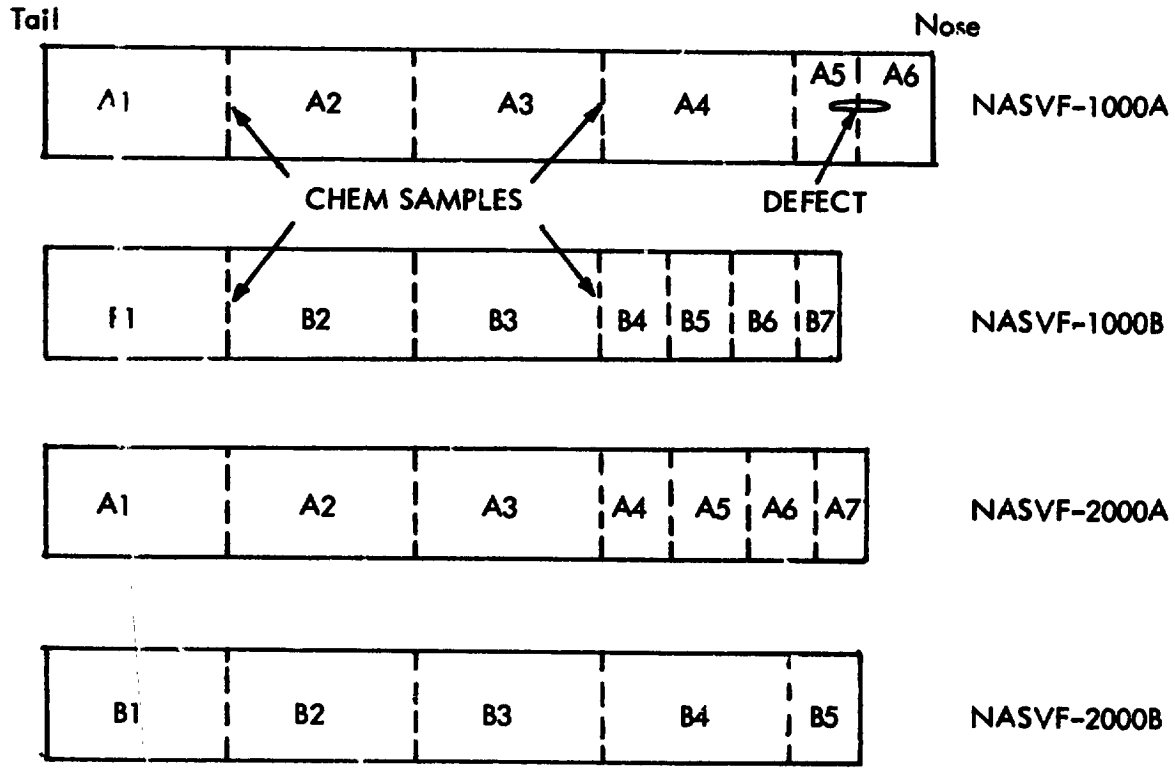

Figure 19. Sectioning of ASTAR-1211C and ASTAR-1511C Extrusions

confined to a region around the axis of billets A-5, A-6, with minor indications appearing in billet A-4 toward the nose of the extrusion. Minor indications were noted in billet B-6 of extrusion NASVF-1000B.

An extensive analysis of the central bursting defect produced in extrusion and wire drawing was made by B. Avitzur[4]. In his discussion of the factors which contribute to the formation of the noted defect, Avitzur indicated that the defect is primarily a product of the extrusion process and not necessarily characteristic of the material. Materials which are considered to be very amenable to the extrusion process can be made to exhibit the noted defect under the proper circumstances. The amount of reduction and the inlet angle of the die appear to be two of the critical factors which influence the generation of the central burst defect. The criterion for central burst as derived by Avitzur is shown in Figure 20. When extrusion is performed with a combination of semicone die inlet angle (a), reduction (r), or friction factor (m) above the solid line, no central burst is expected. When extrusion is done with a combination of factors below the line, materials may or may not burst depending on other less well defined conditions.

A review of the parameters which were used for the extrusion of the four ingots of this program revealed that the vendor used a shear die (90 degree semicone inlet angle) instead of a die with a 45 to 60 degree semicone inlet angle which is commonly used for refractory metal alloys. The combination of inlet die angle and reduction ratio, 3.4:1, clearly puts the extrusion conditions in the danger zone according to Avitzur's criterion. Even under the adverse conditions noted, the major defect appears to be confined to the nose regions of extrusion NASVF-1000A with minor indications noted in the other extrusions, also near the nose. The presence of the defects in the extrusions did not hinder the evaluation of the material. The billets cut from the extrusions were allocated to the tasks in such a manner as to eliminate possible interference of the extrusion defects in the evaluation of the material properties.

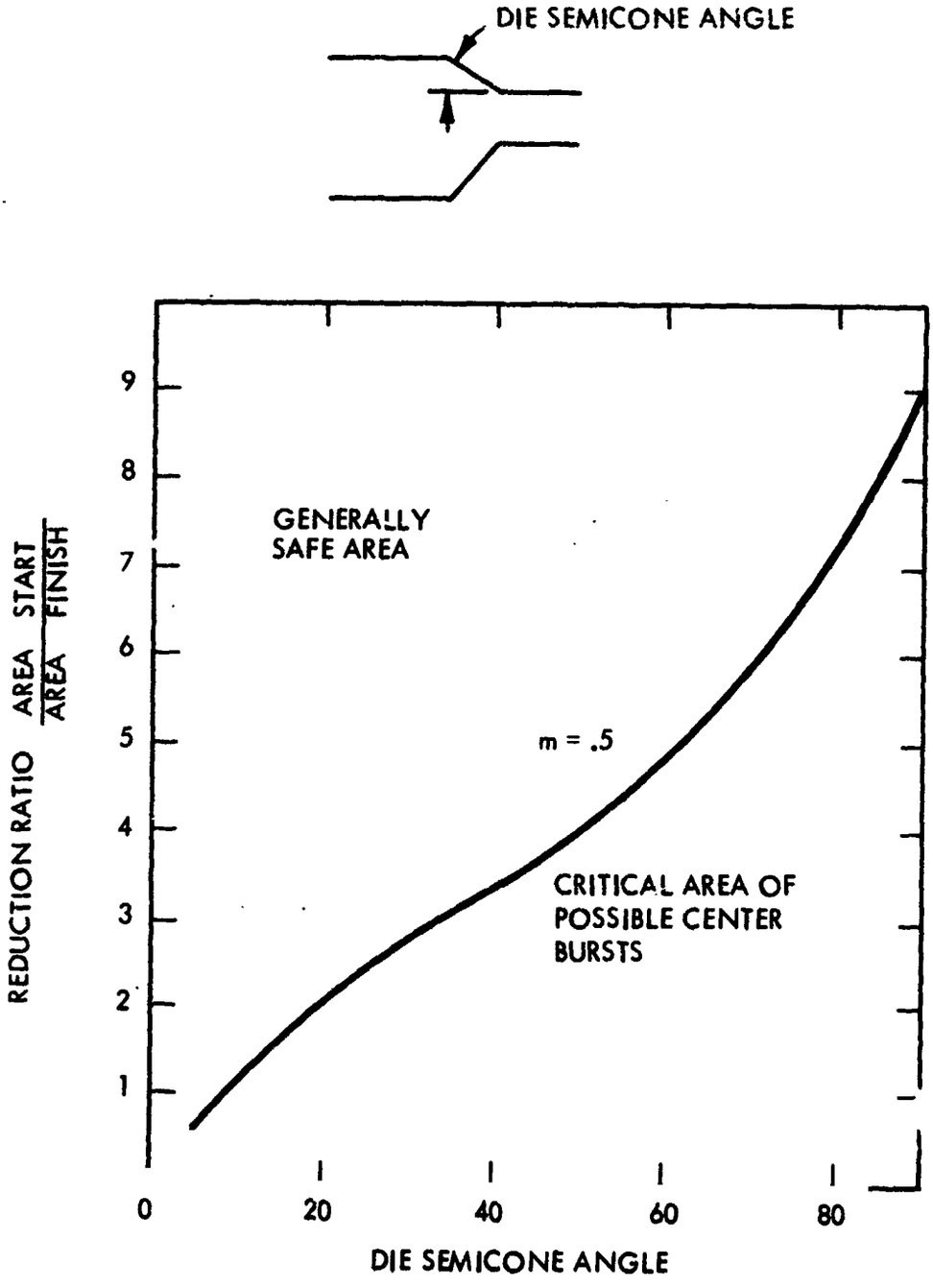

Figure 20. Avitzur"s Criterion for Avoiding Central Burst Defect[4]

3.8 CHECK CHEMICAL ANALYSIS

Results of the chemical analyses of samples taken from the top and bottom of the "as-cast" five inch diameter ingots, reported previously, indicated some variation from target values particularly with respect to hafnium at the ingot bottoms. During machining of the primary extrusion, samples were taken for check analyses from locations indicated in Figure 19. The results of the check analyses for ASTAR-1211C extrusions are given in Table 5. These data indicate that the metallic alloying additions approach the nominal alloy composition quite closely in the interior of the cast ingot. The previous explanation for the apparent disparity in alloy concentrations, particularly hafnium, in samples taken from the ends of the as-cast ingot appears to be valid.

3.9 ALLOCATION OF MATERIAL

A total of seven billets approximately 12.7 cm (5 inches) long and three billets 4.5 cm (1-3/4 inches) long of each alloy composition were required for the 4 remaining evaluation tasks. The allocation of material is shown in Table 6.

Table 5. Check Chemical Analysis of ASTAR-1211C Extrusions

Sample Location	Rhenium (wt%)	Hafnium (wt%)	Tungsten (wt%)
A-1	1.05	0.69	12.2
A-3	1.07	0.69	12.1
B-1	1.05	0.69	12.1
B-3	1.08	0.68	12.2

Table 6. Allocation of Primary Extrusion Material for Evaluation

Billet Identification	Length (cm)	Length (in)	Diameter (cm)	Diameter (in)	Mass (kg)	Weight (lbs)	Task
ASTAR-1211C							
NASVF-1000A-1	12.0	4.75	6.8	2.69	7.5	16.4	Swaged Rod
-1000A-2	12.0	4.75	6.8	2.70	7.6	16.8	Swaged Rod
-1000A-3	12.2	4.81	6.8	2.70	7.7	16.9	Tubing
-1000A-4	12.2	4.81	6.6	2.61	7.1	15.7	Tubing
-1000B-1	11.9	4.69	6.8	2.70	7.5	16.5	Swaged Rod
-1000B-2	12.2	4.81	6.4	2.63	7.2	15.9	Sheet
-1000B-3	12.0	4.75	6.6	2.62	7.1	15.7	Sheet
-1000B-4	4.5	1.75	6.6	2.60	3.7	6.0	Forged Disk
-1000B-5	4.3	1.69	6.7	2.65	3.8	5.8	Forged Disk
-1000B-6	4.3	1.69	7.0	2.76	3.6	6.1	Forged Disk
ASTAR-1511C							
NASVF-2000A-1	12.0	4.75	6.4	2.53	6.7	14.8	Sheet
-2000A-2	12.0	4.75	6.4	2.52	6.7	14.8	Sheet
-2000A-3	12.0	4.75	6.4	2.51	6.6	14.5	Tubing
-2000A-4	4.5	1.75	6.3	2.50	4.1	5.4	Forged Disk
-2000A-6	4.5	1.75	6.7	2.65	3.7	6.0	Forged Disk
-2000B-1	12.0	4.75	6.4	2.51	6.6	14.5	Swaged Rod
-2000B-2	12.0	4.75	6.4	2.51	6.6	14.5	Swaged Rod
-2000B-3	12.2	4.81	6.4	2.51	6.7	14.8	Tubing
-2000B-4	11.9	4.69	6.4	2.51	5.9	13.0	Swaged Rod
-2000B-5	4.5	1.75	6.8	2.70	3.5	6.3	Forged Disk

4.0 PROCESSING AND EVALUATION OF SWAGED BAR STOCK

This task had two primary objectives:

- The development of a thermo-mechanical process for producing swaged bar stock with optimum mechanical properties.
- The generation of tensile, creep, and ductile-to-brittle transition temperature data for material produced by the above process.

The program outline for achieving the first objective is illustrated in Figure 21. A quantity of each alloy was processed to small diameter rod using two swaging temperatures and five final annealing temperatures. The effect of swaging temperature and final annealing temperature on mechanical behavior was evaluated by creep and tensile testing. The processing schedule, which produced the optimum creep resistance and elevated temperature tensile strength without adversely affecting low temperature ductility, was selected as the standard working procedure for each alloy composition.

The outline for achieving the second objective is shown in Figure 22. Upon selection of the optimum process in the initial investigation, sufficient additional material was produced to permit a more extensive characterization of material produced by the optimum process. The development of mechanical properties included the following:

- Tensile properties from room temperature to 1650°C (3000°F) at 343°C (600°F) intervals.
- Determination of Poisson ratio from room temperature to 538°C (1000°F).
- Determination of DBTT by impact and by tensile loading. Tensile loaded specimens were tested in both the notched and unnotched condition.
- Confirmation of initial creep test results. Initial creep test results were obtained using multiple stress and temperature changes on a given test specimen. The confirmation tests in this part of the program were conducted using single-load-single-temperature test conditions.

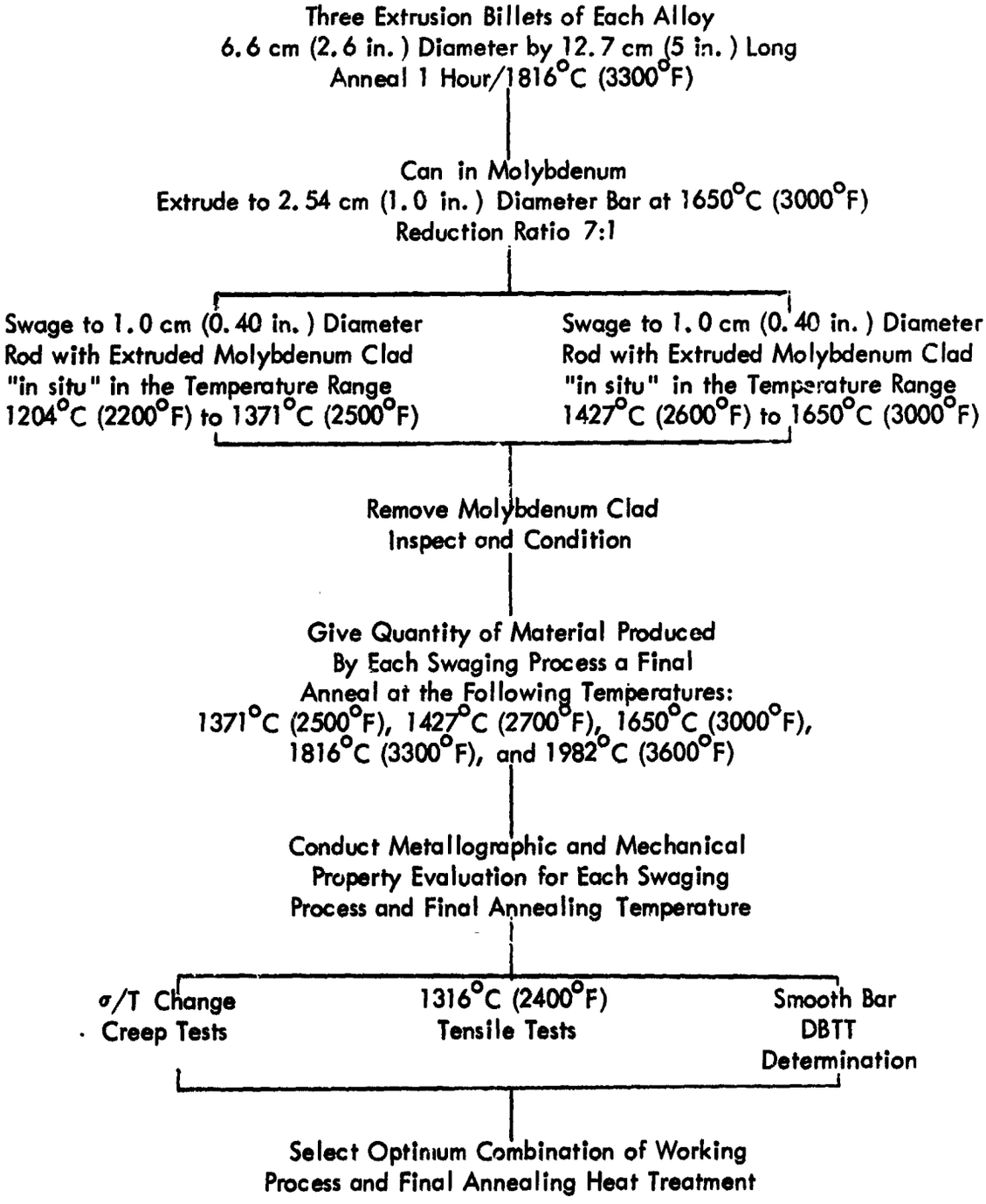

Figure 21. Schedule for Processing and Evaluating Swaged Bar Material

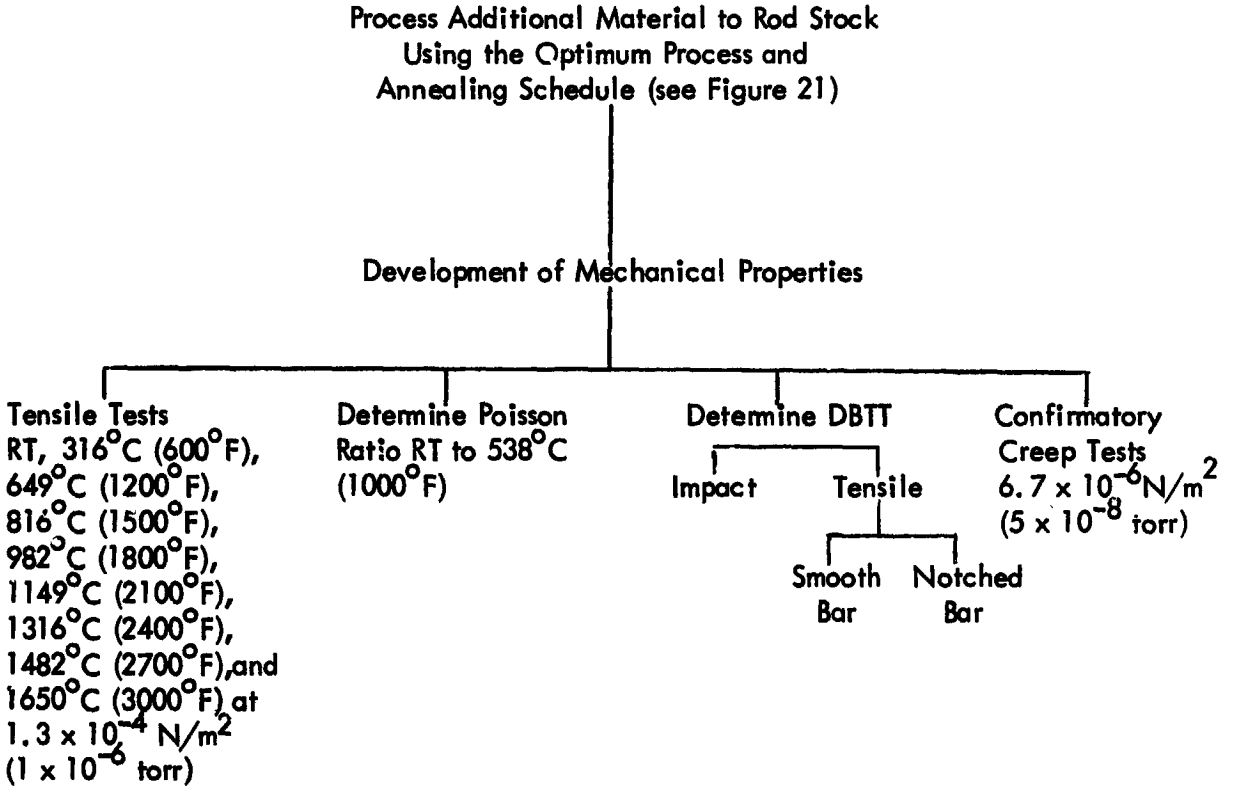

Figure 22. Development of Mechanical Properties for Swaged Bar Produced by Optimum Process and Heat Treatment Schedule

4.1 PROCESSING OF SWAGED ROD

4.1.1 Extrusion

Three billets of each alloy composition were selected for this task. For ASTAR-1211C, billets NASVF-1000A-1, -2, and B-1. For ASTAR-1511C, billets NASVF-2000B-1, -2, and -4. The billets, which had been annealed for 1 hour at 1815°C (3300°F), were canned in pressed and sintered molybdenum for re-extrusion at the Experimental Metals Processing Laboratory at Wright-Patterson AFB. The canning procedure is illustrated in Figure 23. The molybdenum cans were machined to an OD of 7.5 cm (2.95 inches) with an ID matched to the individual billets. Can walls were generally 4.7 mm (~3/16 inch) thick. A 1.9 cm (3/4 inch) thick nose plug was used with a 1.05 rad (60 degree) by 1.25 cm (1/2 inch) level. The clad billets were coated with Corning 7740 glass slurry prior to heating for extrusion. The glass coating was done by heating the billets to 77°C (170°F) to 88°C (190°F) in an oven then removing from the oven and applying while hot a colloidal suspension of glass powder. The heat in the billet caused the water in the suspension to evaporate, leaving a glass residue coating of 0.50 mm (0.02 inch) to 0.75 mm (.03 inch) thick on the billet. The bottom of the billets were left uncoated. The billets were heated for extrusion in a 30 KW (4200 Hz) induction fumace which was flushed continuously with argon. The billets were soaked at the extrusion temperature, 1650°C (3000°F), for 10 minutes. The temperature was monitored by means of a tungsten-rhenium thermocouple in contact with the bottom of the billet. When ready for extrusion, the billets were transferred manually with tongs to the press container in 10 seconds or less. A graphite follower block was used to insure complete extrusion of the billet. The billets were extruded through a zirconia coated die at a reduction ratio 8.9:1. Extrusion data are given in Table 7. Typical extrusions are shown in Figure 24. Billets NASVF-1000A-1 and A-2 were extruded through the same die. The first extrusion, A-1, had a uniform diameter of 2.62 cm (1.030 inches) from nose to tail. The second extrusion caused a washout of the zirconia coating on the die. The resulting extrusion was striated and slightly larger in diameter, 2.78 cm (1.095 inches) from nose to tail. As a result of the enlargement

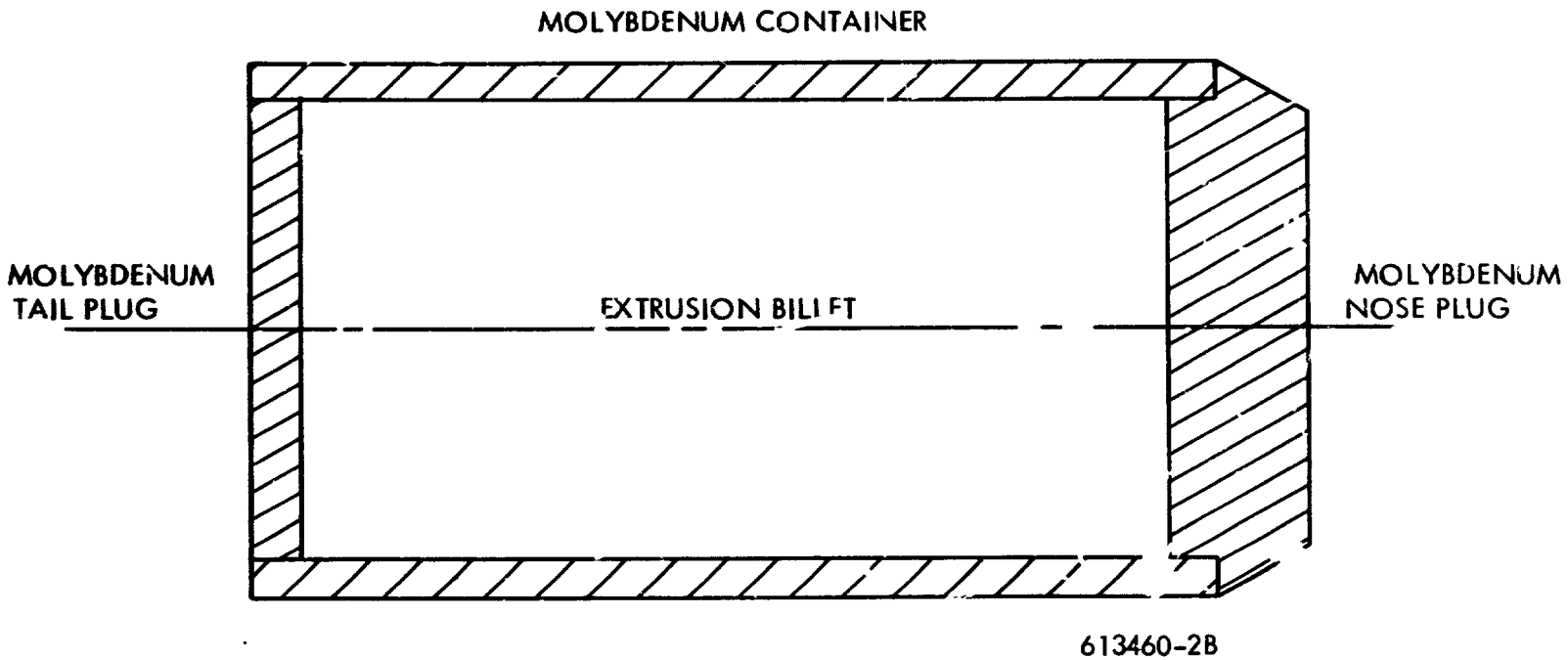

Figure 23. Cross Section of Canned Billet for Extrusion at Wright-Patterson Air Force Base

Table 7. Extrusion Data for ASTAR-1211C and ASTAR-1511C Swaged Bar Study

Billet Identification	Reduction Ratio *	Extrusion Constants			
		Breakthrough		Running	
		(MN/m^2)	(ksi)	(MN/m^2)	(ksi)
NASVF-1000 (ASTAR-1211C)					
A-1	8.9:1	521	75 6	501	72.7
A-2	7.95:1	-	-	-	-
B-1	8.9:1	520	75.4	510	74.0
NASVF-2000 (ASTAR-1511C)					
B-1	8.9:1	462	67.0	431	62.5
B-2	8.9:1	427	62.0	401	58.2
B-4	7.4:1	410	59.5	358	52.0

All billets extruded at 1650°C (3000°F) and yielded ~76 cm (~30 inches) of sound material.

* Reduction Ratio = $\left(\frac{\text{Diameter of Container}}{\text{Diameter of Extrusion}}\right)^2$

Figure 24. Extrusions of ASTAR-1211C, Billets NASVF-1000-A-1 and A-2

of the die, the true reduction ratio was closer to 8:1. Each of the remaining billets were extruded through a new die. Except for extrusion NASVF-2000B-4, the diameter of the resulting extrusions were all within a range of 2.6 cm (1.025 inches) and 2.62 cm (1.030 inches). The zirconia coating on the die face apparently spalled off during extrusion of the B-4 billet, resulting in a lower reduction ratio, 7.4:1 and a larger diameter. For some inexplicable reason, the breakthrough and running pressure during the extrusion process was significantly lower for the ASTAR-1511C compared to the ASTAR-1211C.

The extrusions were trimmed to remove the extrusion defect at the tail end then cut into four equal parts which ranged between 15.24 cm (6 inches) and 20.32 cm (8 inches) in length depending on the yield of sound material. A uniform continuous layer of molybdenum clad 1.0 mm (0.04 inch) to 1.27 mm (0.05 inch) thick from nose to tail was noted for each extrusion.

4.1.2 Swaging

As part of the evaluation to determine the effect of thermo-mechanical processing on the mechanical properties of the two alloys, two swaging temperatures were investigated. At this stage of the reduction process the objective was to compare "hot" vs "cold" working. From the primary extrusion data of the prior section, a temperature of 1371°C (2500°F) was selected for the cold working process. Selection of a hot working temperature was less certain. Two temperatures were evaluated in a preliminary processing step. Initially a swaging temperature of 1538°C (2800°F) was used for hot working.

The extruded bars with the co-extruded molybdenum clad intact were cut into four equal lengths and numbered 1 through 4 from tail to nose. Thus, ASTAR-1211C extrusion NASVF-1000A-1 become extrusion bars NASVF-1000A-11, -12, -13, and -14. The swaging procedure for the initial and subsequent processing consisted of preheating the extruded bars in an argon purged furnace to 871°C (1600°F) then transferring to a hydrogen purged furnace operating at the swaging temperature. The bars were reheated for 15 minutes between each pass. After the final swaging pass, the bars were returned to the swaging furnace and held for one hour prior to cooling to room temperature.

Reductions of 1.52 mm (.060 inch) on the diameter or 12 percent were used at the larger diameters. At mid-way in the swaging operation, the amount of reduction was changed to 0.76 mm (0.030 inch) or a reduction of 14 percent at the final diameter of 1.0 cm (0.40 inch). The total reduction from starting to finished size was on the order of 84 percent.

The temperature of the bar dropped during the swaging process. The amount of heat loss increased as the diameter of the bar decreased. In the case of the hot working process, the reheat between swaging passes was considered sufficient to facilitate recrystallization resulting in a quasi-hot working process.

The microstructures of the finished products are shown in Figures 25A and 25B. The material swaged at 1371°C (2500°F) exhibited a wrought structure. The precipitate is a carbide, most likely Ta_2C which has been identified in the tantalum-tungsten-hafnium carbon system in alloys of similar composition. The bar swaged at 1538°C (2800°F), Figure 25B, exhibited a similar microstructure with almost identical hardness, 351 DPH. The reheat temperature, 1538°C (2800°F), was approximately high enough to promote recovery without inducing recrystallization, at least within the short time period between swaging passes and during the 1 hour anneal at the swaging temperature after the final swaging pass. The objective of a "hot-worked" structure was not achieved under the given conditions.

A second extruded bar, NASVF-1000A-12, was swaged to roo 649°C (3000°F). The processing was the same as previously described. The microstructure of the processed bar is shown in Figure 25C. The combination of thermal and mechanical energy was sufficient to promote complete recrystallization. The as-swaged hardness values include an increment due to hydrogen pickup during the swaging process.

500X DPH 350

A. ASTAR-1211C Rod
Swaged at 1371°C (2500°F)

NASVF-1000-A21

500X DPH 351

B. ASTAR-1211C Rod
Swaged at 1538°C (2800°F)

NASVF-1000-11

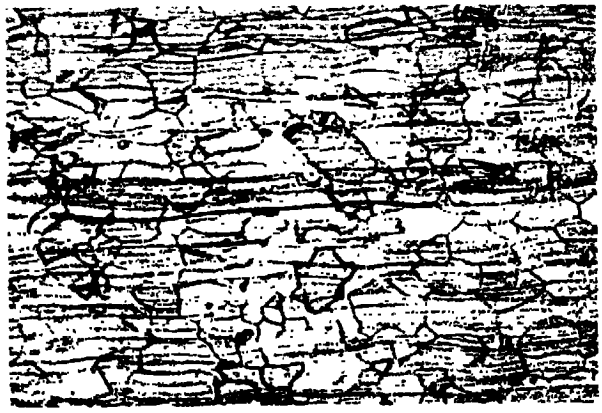

100X DPH 370

C. ASTAR-1211C Rod
Swaged at 1649°C (3000°F)

NASVF-1000-12

Figure 25. Microstructures of Swaged Rod, ASTAR-1211C

As a result of the initial investigation, the swaging process for converting both ASTAR-1211C and ASTAR-1511C extruded bar to 1.0 cm (0.4 inch) diameter rod was standardized. Approximately 406 cm (160 inches) of each alloy was processed to 1.0 cm (0.40 inch) rod. One-half wc waged at 1371°C (2500°F), and the other half was swaged at 1649°C (3000°F). The finished rod retained a molybdenum clad approximately 0.25 mm (0.010 inch) thick.

Samples of the swaged rod were analyzed for interstitial chemistry. Results are given in Table 8. The "as-swaged" material exhibited a slight increase in oxygen level over the "as-cast" ingot chemistry, Table 3. Nitrogen and carbon levels appeared unchanged. The high hydrogen level was not unexpected and was attributed to the atmosphere of the reheat furnace utilized between swaging passes. The molybdenum clad on the rod provided oxidation protection as well as lubrication for the working process. A vacuum anneal for 1 hour at a temperature as low as 1093°C (2000°F) was sufficient to reduce the hydrogen level to below 1 ppm.

The swaged rod was divided into five groups and heat treated according to the program schedule. The heat treatments were carried out under a pressure of 1.3×10^{-3} n/m^2 (1×10^{-5} torr) or less for 1 hour at 1371°C (2500°F), 1482°C (2700°F), 1649°C (3000°F), 1816°C (3300°F), and 1982°C (3600°F). The microstructures of heat treated samples are shown in Figures 26 through 29. Samples of ASTAR-1211C swaged at 1649°C (3000°F) were also heat treated at 1093°C (2000°F) and 1260°C (2300°F). The microstructures for those samples are shown in Figure 27 along with the "as-swaged" structure. The behavior of both ASTAR alloys swaged at 1371°C (2500°F) was similar. Both cold worked alloys retained a wrought structure after 1 hour at 1371°C (2500°F). Recrystallization was complete after 1 hour at 1482°C (2700°F). The grain size, however, was nonuniform in each case. A more uniform grain size was produced in the material heat treated at 1649°C (3000°F). All the microstructures were taken parallel to the rod axis; the strung-out Ta_2C precipitates indicate the working direction. As the final annealing temperature was raised to 1816°C (3300°F) and 1982°C (3600°F), the carbide

Table 8. Interstitial Chemical Analysis of ASTAR-1211C and ASTAR-1511C Swaged Rod

Identification and Condition	(ppm)			
	N_2	O_2	H_2	C
ASTAR-1211C-Rod Swaged at 1371°C (2500°F) As-swaged NASVF-1000-A-23	12	17	37	260
ASTAR-1211C-Rod Swaged at 1649°C (3000°F) As-swaged NASVF-1000-A-13	21	48	31	240
ASTAR-1511C-Rod Swaged at 1371°C (2500°F) As-swaged NASVF-2000-B-12	13	27	27	250
ASTAR-1511C-Rod Swaged at 1649°C (3000°F) As-swaged NASVF-2000-B-43	11	23	36	190
ASTAR-1211C-Rod Swaged at 1371°C (2500°F) (Swaged + 1 hr./1093°C (2000°F) in vacuum) NASVF-1000-A-23	-	5	0.2	-
ASTAR-1511C-Rod Swaged at 1649°C (3000°F) (Swaged + 1 hr./1093°C (2000°F) in vacuum) NASVF-2000-B-43	-	10	0.3	-

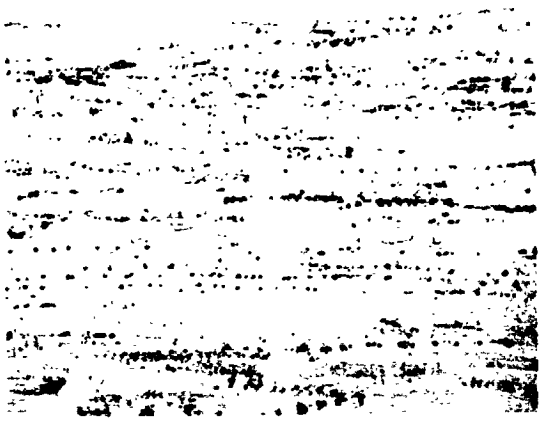

A. Swaged + 1 Hr/1371°C (2500°F)-DPH 308

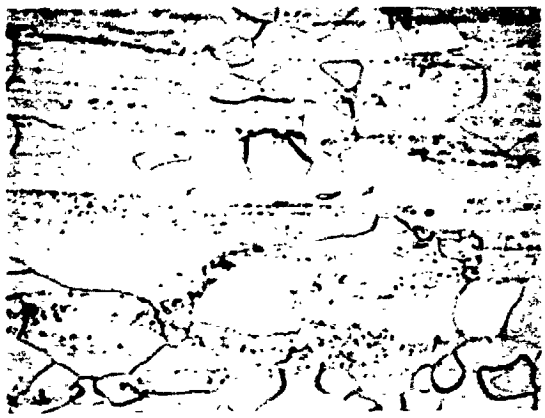

B. Swaged + 1 Hr/1482°C (2700°F)-DPH 297

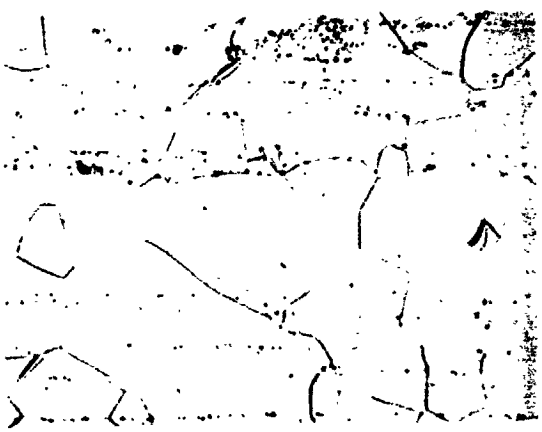

C. Swaged + 1 Hr/1649°C (3000°F)-DPH 339

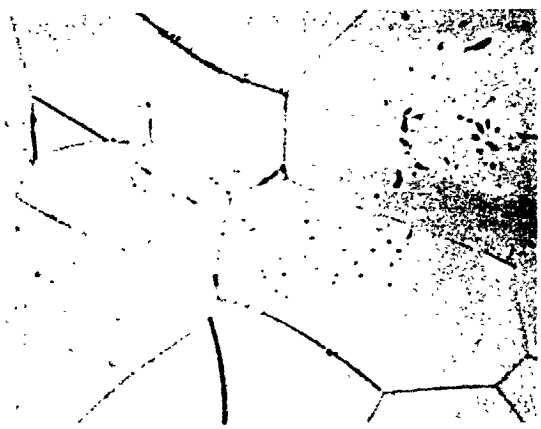

D. Swaged + 1 Hr/1815°C (3300°F) -DPH 330

E. Swaged + 1 Hr/1982°C (3600°F)-DPH 307

All Micros 500X

Figure 26. Microstructure of ASTAR-1211C Swaged at 1371°C (2500°F) and Heat Treated

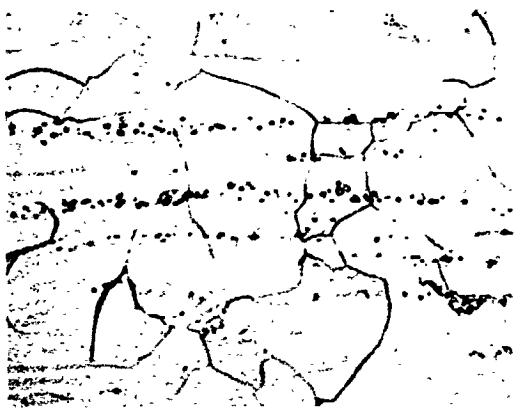

500X DPH 368

A. As Swaged

500X DPH 298

B. Swaged + 1 Hr/1093°C (2000°F)

500X DPH 276

C. Swaged + 1 Hr/1260°C (2300°F)

500X DPH 285

D. Swaged + 1 Hr/1371°C (2500°F)

Figure 27. Microstructure of ASTAR-1211C Swaged at 1649°C (3000°F) and Heat Treated

500X DPH 323

E. Swaged + 1 Hr/1482°C (2700°F)

500X DPH 308

F. Swaged + 1 Hr/1649°C (3000°F)

500X DPH 305

G. Swaged + 1 Hr/1815°C (3300°F)

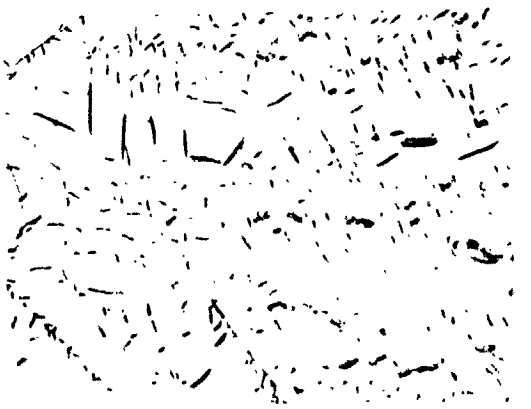

500X DPH 300

H. Swaged + 1 Hr/1982°C (3600°F)

Figure 27. Microstructure of ASTAR-1211C Swaged at 1649°C (3000°F) and Heat Treated (Continued)

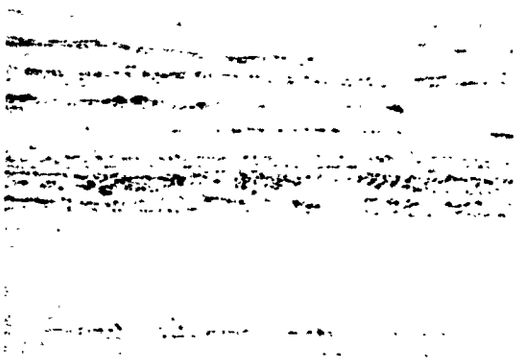

A. Swaged + 1 Hr/1371°C (2500°F)-DPH 325

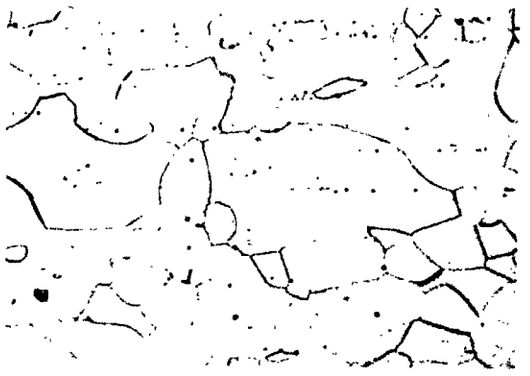

B. Swaged + 1 Hr/1482°C (2700°F)-DPH 342

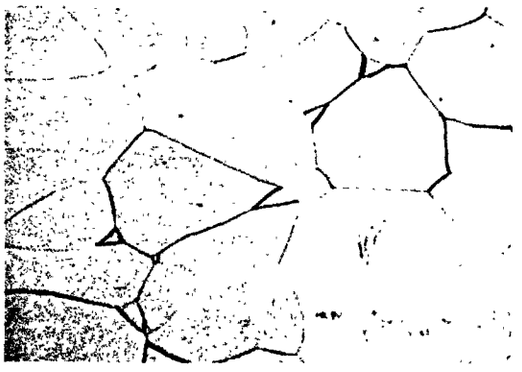

C. Swaged + 1 Hr/1649°C (3000°F)-DPH 342

D. Swaged + 1 Hr/1815°C (3300°F)-DPH 338

E. Swaged + 1 Hr/1982°C (3600°F)-DPH 333

ALL MICROS 500X

Figure 28. Microstructures of ASTAR-1511C Swaged at 1371°C (2500°F) and Heat Treated at Various Temperatures

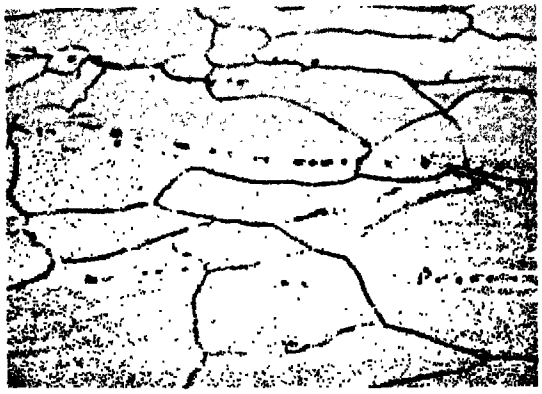

A. Swaged + 1 Hr/1371°C (2500°F)-DPH 326

B. Swaged + 1 Hr/1482°C (2700°F)-DPH 341

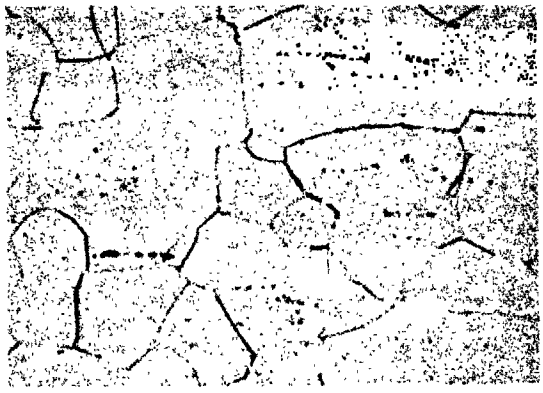

C. Swaged + 1 Hr/1649°C (3000°F)-DPH 350

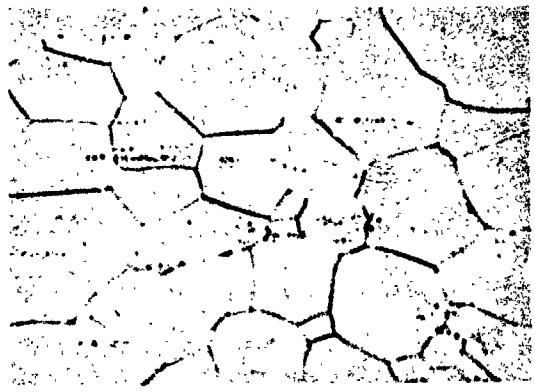

D. Swaged + 1 Hr/1815°C (3300°F)-DPH 342

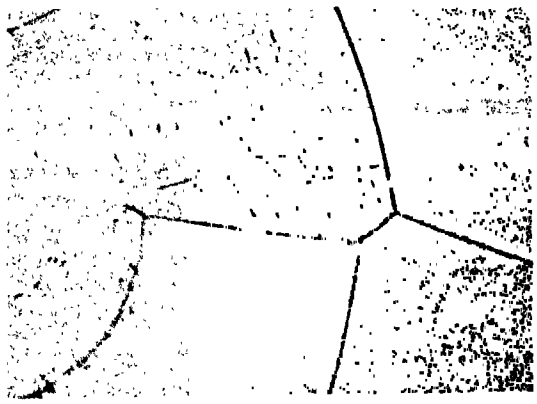

E. Swaged + 1 Hr/1982°C (3600°F)-DPH 338

ALL MICROS 500X

Figure 29. Microstructures of ASTAR-1511C Swaged at 1649°C (3000°F) and Heat Treated at Various Temperatures

precipitate was taken into solution and in some cases reprecipitated during cooldown from the annealing temperature. The grain size for hot worked material annealed at 1649°C (3000°F) and below was essentially the same.

Hardness values for the swaged ASTAR alloys are shown in Figure 30 as a function of thermo-mechanical processing and final heat treatment. The hot and cold worked ASTAR-1511C displayed hardness values which were comparable for each final heat treatment even after the 1482°C (2700°F) anneal. The hardness data for the ASTAR-1211C was more dynamic. The hot worked ASTAR-1211C exhibited a hardness minimum at 1260°C (2300°F) and a maximum at 1482°C (2700°F) while the cold worked exhibited a minimum at 1482°C (2700°F) and a maximum at 1649°C (3000°F).

The room temperature hardness of the ASTAR alloys depends to a great extent on the disposition of the carbon. The role of carbon in tantalum base alloys containing small quantities of hafnium has not been fully explored and as a result is not completely understood. The variation in hardness of ASTAR-1211C as a function of final annealing temperature and thermo-mechanical processing was more extensive than the more highly alloyed ASTAR-1511C. The reason for the difference in behavior is not known.

4.2 MECHANICAL PROPERTY EVALUATION

The effect of the thermomechanical processing on mechanical properties of the ASTAR alloys was evaluated by the following criteria: low temperature ductility, 1316°C (2400°F), tensile strength and elevated temperature creep behavior.

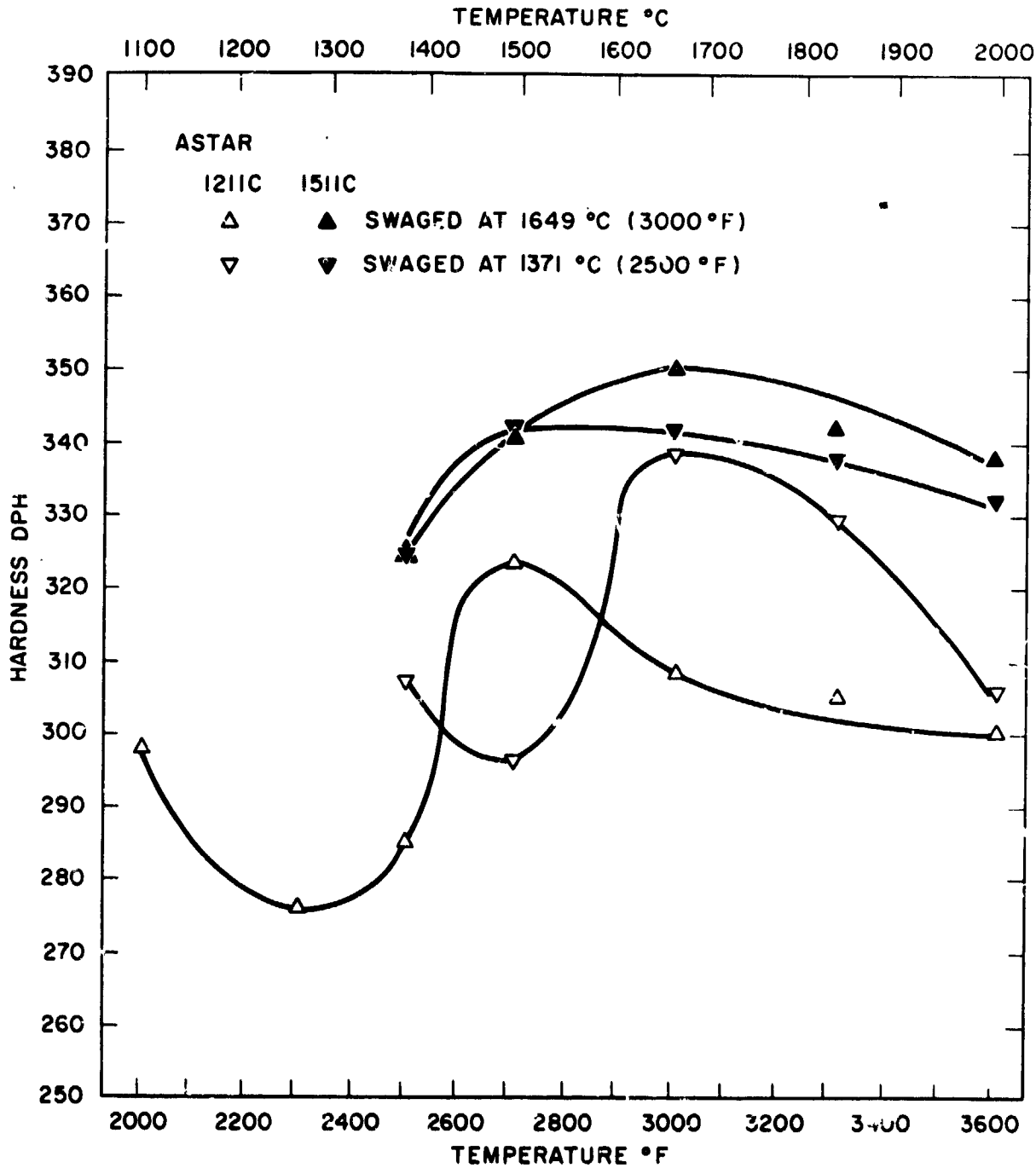

Figure 30. Room Temperature Hardness of ASTAR 1211C and ASTAR 1511C Swaged Rod as a Function of Thermal-Mechanical Processing and Various Heat Treatments

4.2.1 Low Temperature Mechanical Properties

Three tensile specimens of each composition, swaged at 1371°C (2500°F) and at 1649°C (3000°F) were heat treated at 1371°C (2500°F), 1482°C (2700°F), 1649°C (3000°F), and 1816°C (3200°F), and 1982°C (3600°F). One tensile specimen was tested at room temperature, the remaining two specimens were tested at sub-zero temperatures. Shoulder loaded round bar test specimens with a 2.9 mm (0.115 inch) uniform diameter gage length 28.6 mm (1.125 inches) were used for the mechanical property evaluation. Short time tensile tests were conducted at a constant strain rate of 0.05 per minute.

The low temperature tensile data for ASTAR-1211C and ASTAR-1511C swaged at 1371°C (2500°F) and 1649°C (3000°F), are given in Tables 9A and B, 10A and B, 11A and B, and 12A and B. The low temperature ultimate and yield strengths are shown plotted as a function of test temperature in Figures 31 and 32. The data are presented along with curves for the ultimate and yield strength of ASTAR-811C[1]. Both alloys, as would be expected, exhibited higher strength values compared to ASTAR-811C; ASTAR-1211C has 4 percent and ASTAR-1211C has 7 percent higher tungsten content than ASTAR-811C. The increased alloy content had a pronounced effect on low temperature mechanical behavior. Bar graphs in Figures 33 and 34 give comparison of the room temperature tensile properties for material swaged at the two working temperatures and as a function of final annealing temperature. No significant effect of swaging temperature was evidenced for either material. Material of both compositions swaged at 1371°C (2500°F) and annealed at 1371°C (2500°F) exhibited a high yield and ultimate strength compared to material swaged at 1649°C (3000°F). The difference in properties can be attributed to the difference in microstructure. The material swaged and heat treated at 1371°C (2500°F) displayed a wrought structure, Figures 26 and 28, while the material swaged at 1649°C (3000°F) displayed a completely recrystallized microstructure, Figures 27 and 29. Except for the 1482°C (2700°F) annealed condition, the ultimate strength of each alloy composition exhibited no significant effect of swaging temperature, although

Table 9A. Low Temperature Tensile Properties of ASTAR-1211C Rod Swaged at 1371°C (SI Units)

Annealing Temperature (°C)	Test Temperature (°C)	Yield Strength* (MN/m^2)	Ultimate Strength (MN/m^2)	Elongation		Reduction in Area (%)
				Uniform (%)	Total (%)	
1371	RT	938/931	1020	13.5	19.1	60.9
1371	-157	1233/1233	1274	9.8	14.5	52.3
1371	-196	1438/1438	1502	14.9	19.1	45.5
1482	RT	796/793	865	15.3	21.8	70.0
1482	-157	1100/1076	1144	12.5	18.2	65.4
1482	-196	1258/1258	1327	14.4	16.4	35.1
1649	RT	944/914	971	13.0	21.8	61.9
1649	-129	1169/1160	1193	9.2	14.5	52.4
1649	-157	1223/1199	1234	8.2	13.6	48.7
1816	RT	858/853	919	14.2	21.0	51.4
1816	- 73	986/984	1066	14.5	20.9	36.5
1816	-129	1089/1089	1132	6.2	6.4	6.7
1816	-157	1163	1176	0.9	1.8	1.6
1982	RT	695	853	16.3	22.7	39.1
1982	- 01	888	925	1.6	1.8	3.9
1982	-129	938	992	2.1	2.7	4.8
1982	- 46	784	936	17.0	17.0	13.9

0.05/min. strain rate used throughout test.

* Double yield figures are upper and lower yield strengths. Single yield figures are 0.2% offset yield strengths.

Table 9B. Low Temperature Tensile Properties of ASTAR-1211C Rod Swaged at 2500°F

Annealing Temperature (°F)	Test Temperature (°F)	Yield Strength* (ksi)	Ultimate Strength (ksi)	Elongation		Reduction in Area (%)
				Uniform (%)	Total (%)	
2500	RT	136.1/135.1	147.9	13.5	19.1	60.9
2500	-250	178.9/178.9	184.8	9.8	14.5	52.3
2500	-320	208.6/208.6	217.8	14.9	19.1	45.5
2700	RT	115.4/115.0	125.5	15.3	21.8	70.0
2700	-250	159.6/156.2	165.9	12.5	18.2	65.4
2700	-320	182.5/182.5	192.5	14.4	16.4	35.1
3000	RT	136.9/132.6	140.9	13.0	21.8	61.9
3000	-200	169.6/168.3	173.1	9.2	14.5	52.4
3000	-250	177.4/173.9	179.0	8.2	13.6	48.7
3300	RT	124.5/123.7	133.3	14.2	21.0	51.4
3300	-100	143.0/142.7	154.7	14.5	20.9	36.5
3300	-200	158.0/158.0	164.2	6.2	6.4	6.7
3300	-250	168.7	170.6	0.9	1.8	1.6
3600	RT	100.8	123.8	16.3	22.7	39.1
3600	-150	128.8	134.2	1.6	1.8	3.9
3600	-200	136.0	143.9	2.1	2.7	4.8
3600	-50	113 7	135.8	17.0	17.0	13.9

.05/min strain rate used throughout test.

*Double yield figures are upper and lower yield strengths.

*Single yield figures are 0.2% offset yield strengths.

Table 10A. Low Temperature Tensile Properties of ASTAR-1211C Rod Swaged at 1649°C (SI Units)

Annealing Temperature (°C)	Test Temperature (°C)	Yield Strength* (MN/m^2)	Ultimate Strength (MN/m^2)	Elongation		Reduction in Area (%)
				Uniform (%)	Total (%)	
1371	RT	771/744	872	13.1	26.4	48.8
1371	-129	995	1125	16.7	20.5	31.8
1371	-157	1050	1183	14.2	18.2	27.9
1482	RT	797/791	916	15.5	22.2	25.8
1482	-129	1135	1169	13.2	19.1	54.4
1482	-157	1095	1215	18.5	22.9	45.2
1649	RT	762	917	16.1	23.6	47.6
1649	-101	960	1106	14.8	19.4	37.0
1649	-129	1009	1149	15.1	19.0	35.0
1816	RT	714	900	14.7	22.9	36.0
1816	- 73	855	1147	11.3	16.7	18.1
1816	-101	909	1079	9.4	9.4	4.7
1982	RT	712	880	13.7	19.4	41.0
1982	- 46	848	984	7.2	7.2	5.5
1982	- 73	809	943	5.8	5.8	4.5

0.05/min. strain rate used throughout test.

* Double yield figures are upper and lower yield strengths. Single yield figures are 0.2% offset yield strengths.

Table 10B. Low Temperature Tensile Properties of ASTAR-1211C Rod Swaged at 3000°F

Annealing Temperature (°F)	Test Temperature (°F)	Yield Strength* (ksi)	Ultimate Strength (ksi)	Elongation		Reduction in Area (%)
				Uniform (%)	Total (%)	
2500	RT	111.8/107.9	126.5	13.1	26.4	48.8
2500	-200	144.3	163.2	16.7	20.5	31.8
2500	-250	152.4	171.6	14.2	18.2	27.9
2700	RT	115.7/114.8	132.8	15.5	22.2	25.8
2700	-200	164.6	169.5	13.2	19.1	54.4
2700	-250	158.8	176.2	18.5	22.9	45.2
3000	RT	110.6	133.0	16.1	23.6	47.6
3000	-150	139.3	160.4	14.8	19.4	37.0
3000	-200	146.4	166.7	15.1	19.0	35.0
3300	RT	103.6	130.6	14.7	22.9	36.0
3300	-100	124.0	151.9	15.3	16.7	18.1
3300	-150	131.9	156.5	9.4	9.4	4.7
3600	RT	103.3	127.7	13.7	19.4	41.0
3600	-50	123.0	142.8	7.2	7.2	5.5
3600	-100	117.4	136.8	5.8	5.8	4.5

0.05/min strain rate used throughout test.

*Double yield figures are upper and lower yield strengths.

*Single yield figures are 0.2% offset yield strengths.

Table 11A. Low Temperature Tensile Properties of ASTAR-1511C Rod Swaged at 1371°C (SI Units)

Annealing Temperature (°C)	Test Temperature (°C)	Yield Strength* (MN/m^2)	Ultimate Strength (MN/m^2)	Elongation		Reduction in Area (%)
				Uniform (%)	Total (%)	
1371	RT	1032/939	1086	14.7	27.0	64.2
1371	-129	1350/1313	1370	13.4	22.0	56.6
1371	-129	1353/1305	1371	14.6	23.0	58.3
1482	RT	980/928	999	16.0	25.0	67.7
1482	-129	1233/1215	1280	15.0	19.0	27.9
1482	-129	1229/1217	1273	13.6	20.0	38.1
1649	RT	962/962	984	15.0	25.0	54.8
1649	- 46	1084/1084	1032	14.7	22.0	34.2
1649	- 73	1118/1103	-	3.6	4.0	-
1816	RT	939/890	965	15.0	25.0	54.9
1816	- 73	1080/1064	1122	13.1	20.0	38.0
1816	-129	1164	1225	9.7	10.0	16.2
1982	RT	875/858	904	16.2	24.0	26.9
1982	- 46	860/956	988	10.0	11.0	7.6
1982	- 73	1002/999	1021	8.3	9.0	8.8

0.05/min. strain rate used throughout test.

* Double yield figures are upper and lower yield strengths. Single yield figures are 0.2 offset yield strengths.

Table 11B. Low Temperature Tensile Properties of ASTAR-1511C Rod Swaged at 2500°F

Annealing Temperature (°F)	Test Temperature (°F)	Yield Strength* (ksi)	Ultimate Strength (ksi)	Elongation		Reduction in Area (%)
				Uniform (%)	Total (%)	
2500	RT	149.7/136.3	157.6	14.7	27.0	64.2
2500	-200	195.8/190.5	198.7	13.4	22.0	56.6
2500	-200	196.2/189.3	198.8	14.6	23.0	58.3
2700	RT	142.2/134.7	144.9	16.0	25.0	67.7
2700	-200	178.8/176.2	185.6	15.0	19.0	27.9
2700	-200	178.2/176.6	184.7	13.6	20.0	38.1
3000	RT	139.5/139.5	142.8	15.0	25.0	54.8
3000	-50	157.2/157.2	149.7	14.7	22.0	34.2
3000	-100	162.2/160.0	----	3.6	4.0	---
3300	RT	136.2/129.1	140.0	15.0	25.0	54.9
3300	-100	156.7/154.4	162.7	13.1	20.0	38.0
3300	-200	168.8	177.7	9.7	10.0	16.2
3600	RT	126.9/124.4	131.1	16.2	24.0	26.9
3600	-50	139.2/138.6	143.3	10.0	11.0	7.6
3600	-100	145.4/145.0	148.1	8.3	9.0	8.8

0.05/min strain rate used throughout test.

*Double yield figures are upper and lower yield strengths.

*Single yield figures are 0.2% offset yield strengths.

Table 12A. Low Temperature Tensile Properties of ASTAR-1511C Rod Swaged at 1649°C (SI Units)

Annealing Temperature (°C)	Test Temperature (°C)	Yield Strength* (MN/m^2)	Ultimate Strength (MN/m^2)	Elongation		Reduction in Area (%)
				Uniform (%)	Total (%)	
1371	RT	928/911	999	12.6	20.0	52.2
1371	- 73	1109/1099	1173	14.0	23.0	49.8
1482	RT	949/942	1006	15.3	21.0	56.3
1482	-129	1251/1248	1290	12.3	19.0	23.0
1482	-129	1262/1258	1298	10.1	18.0	30.8
1649	RT	981/964	1028	12.1	19.0	47.6
1649	- 73	1118/1115	1184	12.2	16.0	20.4
1649	-129	1277	1279	9.9	14.0	25.0
1816	RT	921/921	1004	13.9	20.0	48.4
1816	- 73	1106	1159	10.0	15.0	29.1
1816	-129	1242/1239	1302	11.5	13.0	13.9
1982	RT	878/873	965	13.5	21.0	24.4
1982	- 46	964	1031	3.9	4.0	-
1982	- 73	1025	1080	2.8	3.0	4.0

0.05/min. Strain Rate used throughout test.

* Double yield figures are upper and lower yield strengths. Single yield figures are 0.2% offset yield strengths.

Table 12B. Low Temperature Tensile Properties of ASTAR-1511C Rod Swaged at 3000°F

Annealing Temperature (°F)	Test Temperature (°F)	Yield Strength* (ksi)	Ultimate Strength (ksi)	Elongation		Reduction in Area (%)
				Uniform (%)	Total (%)	
2500	RT	134.7/132.2	144.9	12.6	20.0	52.2
2500	-100	160.9/159.5	170.2	14.0	23.0	49.8
2700	RT	137.7/136.7	145.9	15.3	21.0	56.3
2700	-200	181.4/181.0	187.2	12.3	19.0	23.0
2700	-200	183.0/182.5	188.3	10.1	18.0	30.8
3000	RT	142.3/139.8	149.1	12.1	19.0	47.6
3000	-100	162.2/161.8	171.8	12.2	16.0	20.4
3000	-200	185.3	185.5	9.9	14.0	25.0
3300	RT	133.6/132.8	145.6	13.9	20.0	48.4
3300	-100	160.5	168.1	10.0	15.0	29.1
3300	-200	180.1/179.7	188.8	11.5	13.0	13.9
3600	RT	127.4/126.7	140.0	13.5	21.0	24.4
3600	-50	139.9	149.6	3.9	4.0	---
3600	-100	148.7	156.6	2.8	3.0	4.0

0.05/min strain rate used throughout test.

*Double figures are upper and lower yield strengths.

*Single figures are 0.2% offset yield strengths.

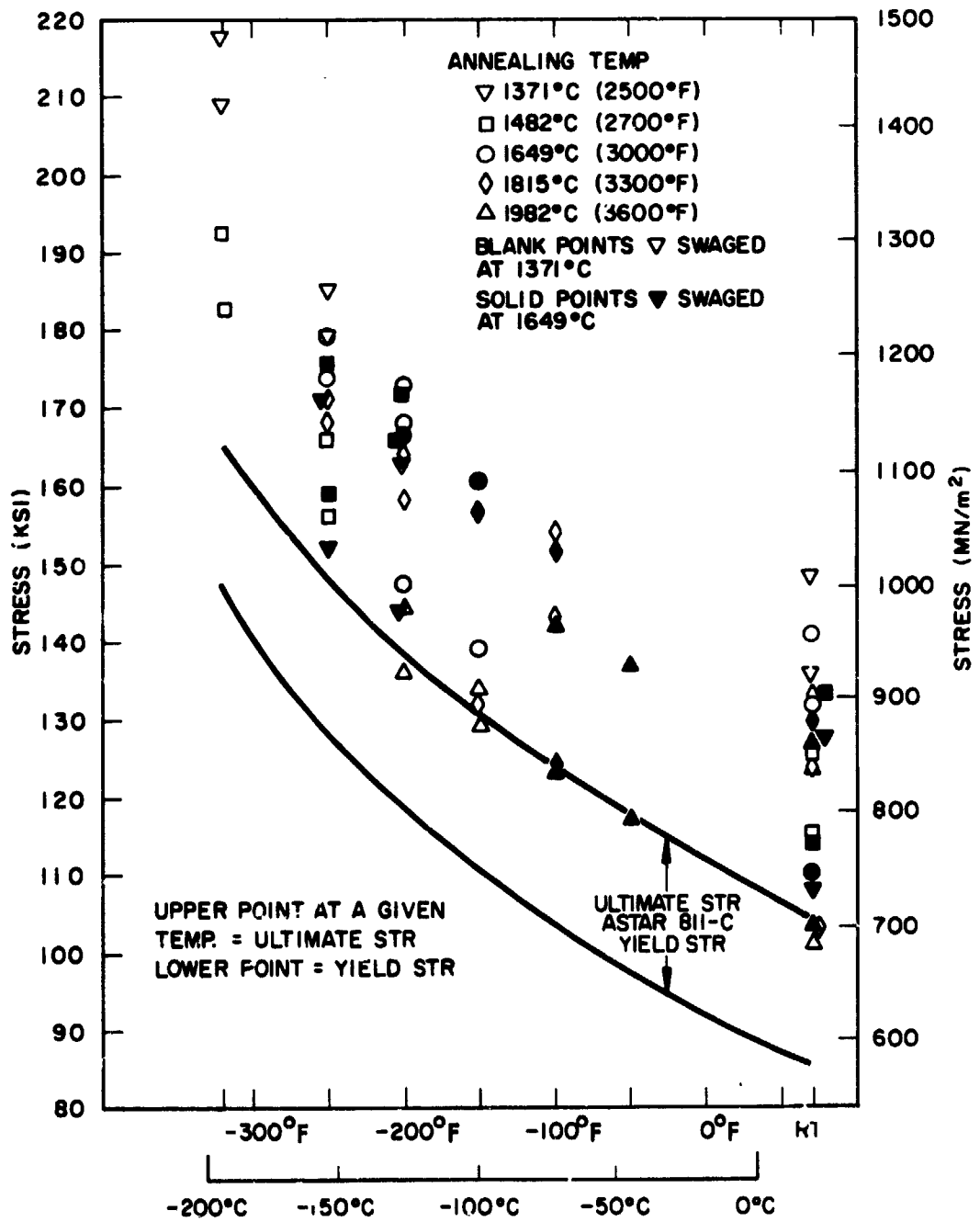

Figure 31. Low Temperature Tensile Properties of ASTAR 1211C Swaged at 1371°C (2500°F) and 1649°C (3000°F) and Annealed at Various Temperatures

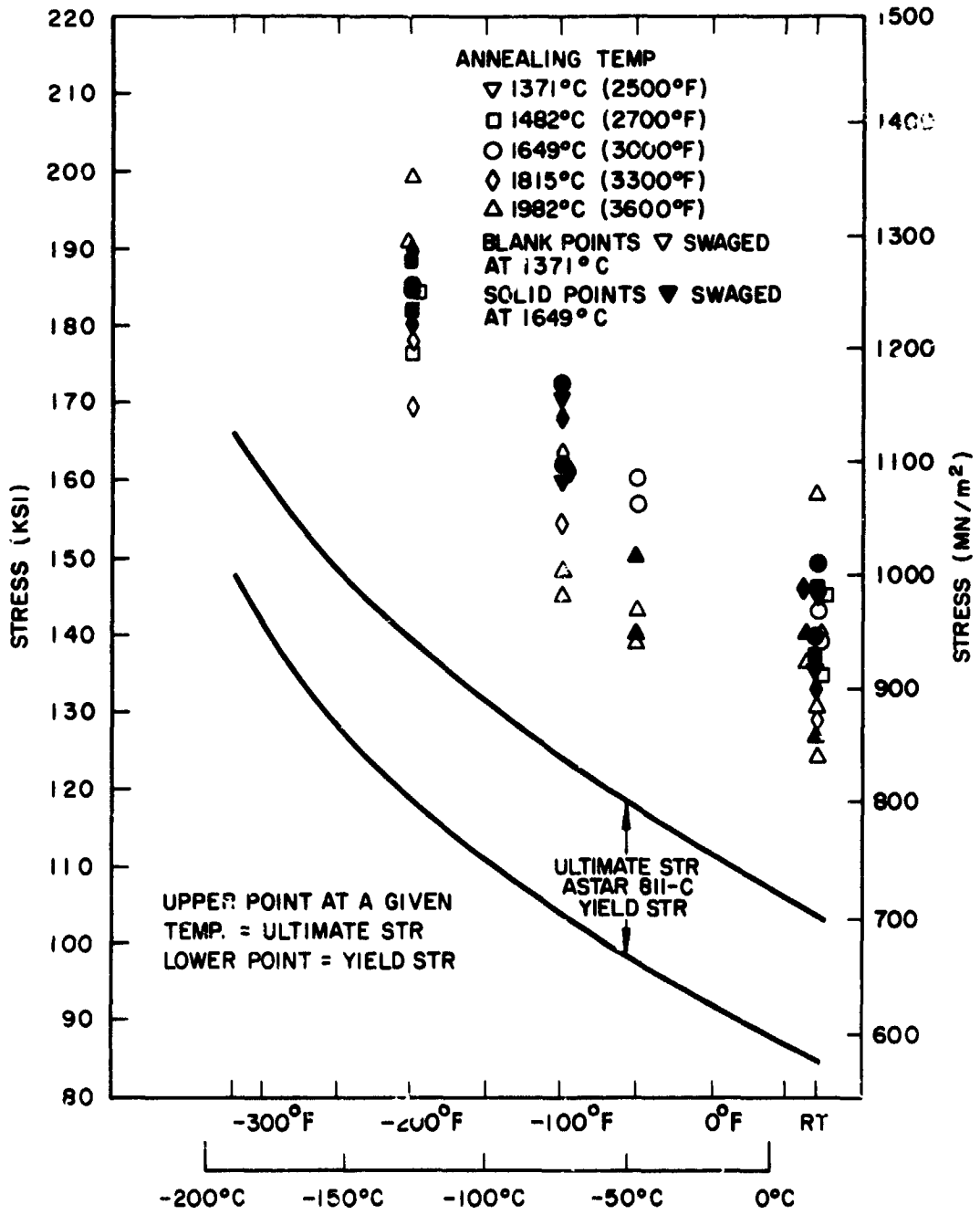

Figure 32. Low Temperature Tensile Properties of ASTAR 1511C Swaged at 1371°C (2500°F) and 1649°C (3000°F) and Annealed at Various Temperatures

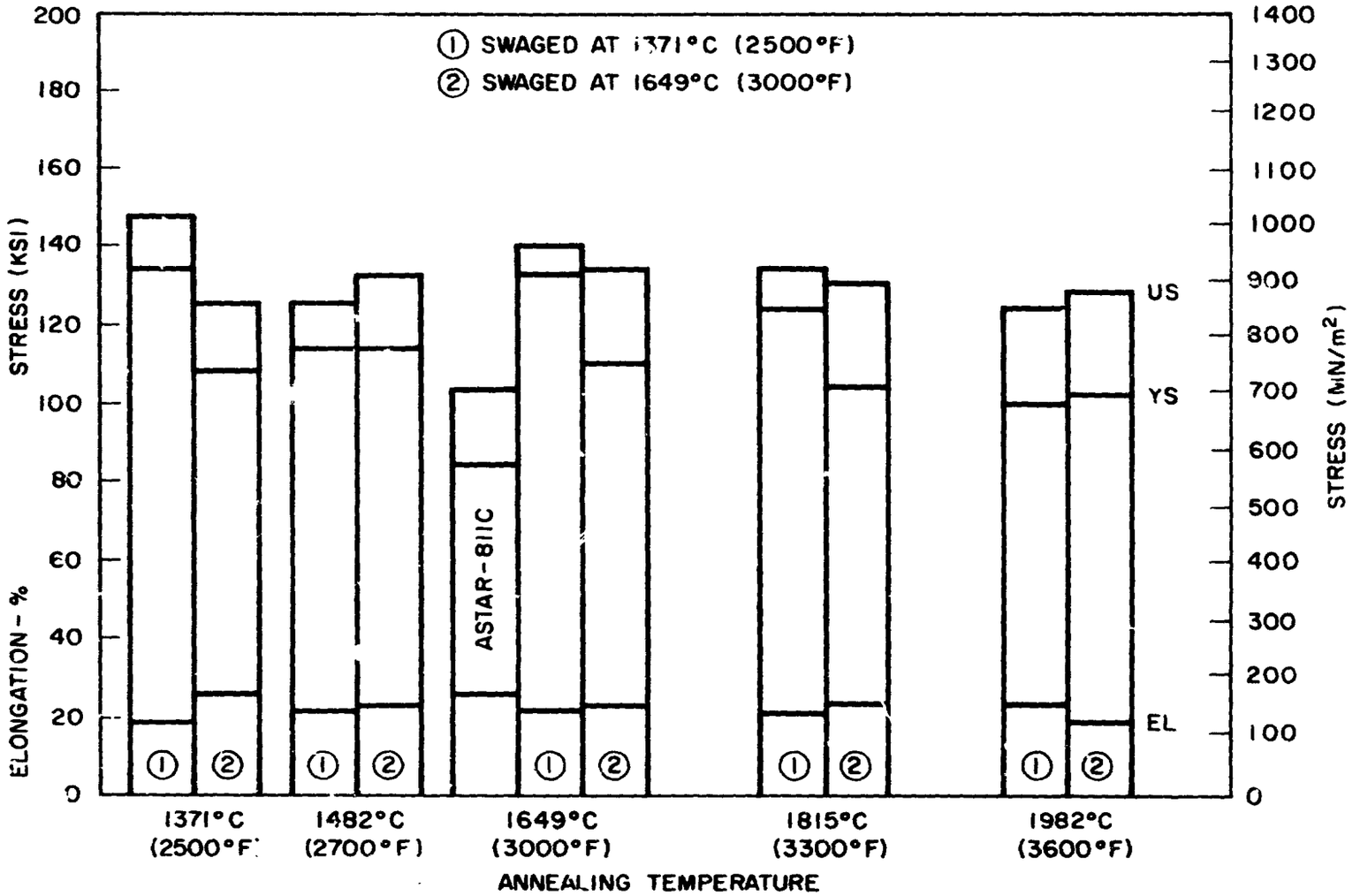

Figure 33. Room Temperature Tensile Properties of ASTAR 1211C Swaged at 1371°C (2500°F) and 1649°C (3000°F) and Annealed at Various Temperatures

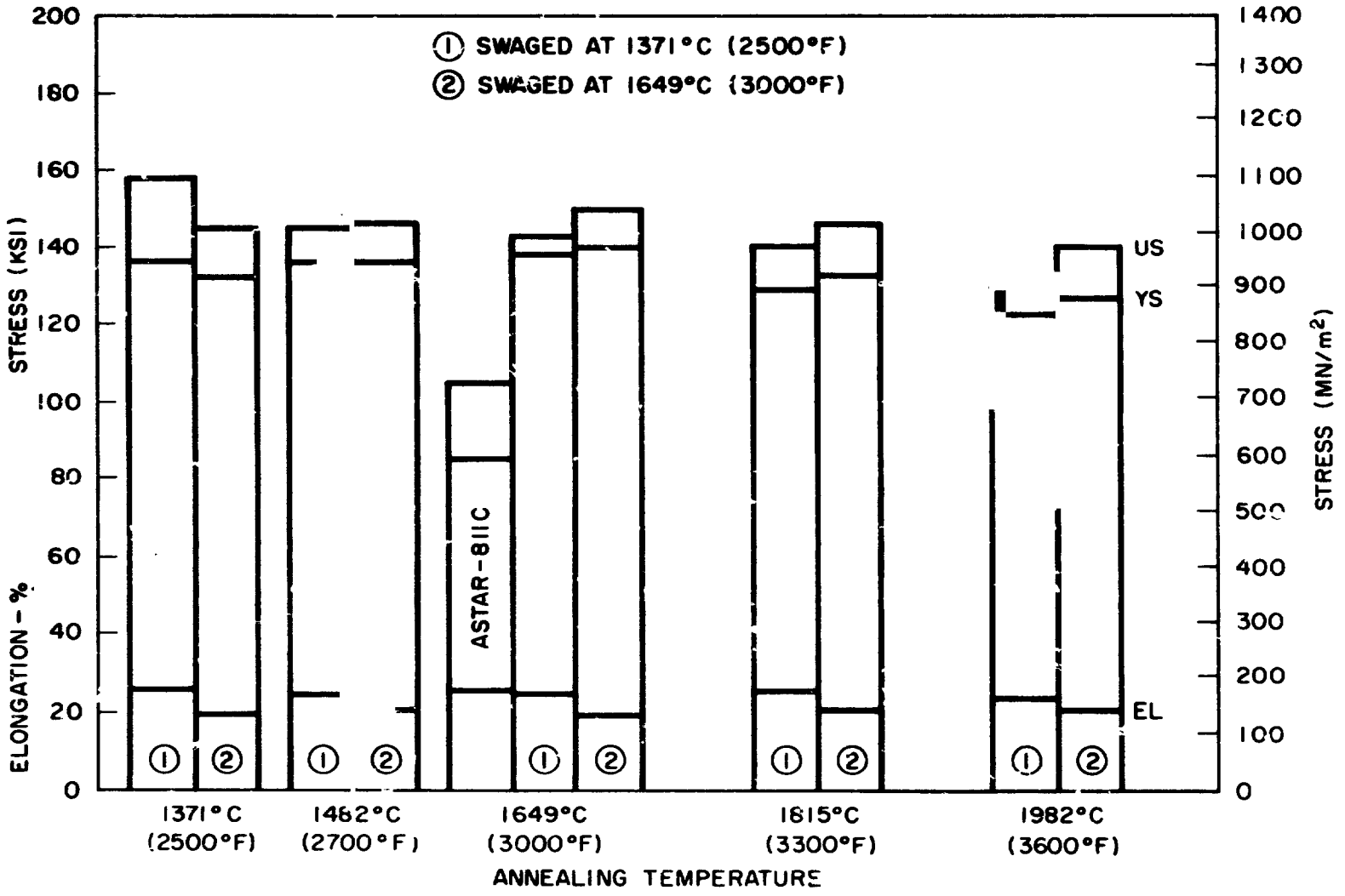

Figure 34. Room Temperature Tensile Properties of ASTAR 1511C Swaged at 1371°C (2500°F) and 1649°C (3000°F) and Annealed at Various Temperatures

the strength of each alloy tended to decrease slightly with increasing final annealing temperature. The yield strength of ASTAR-1211C displayed anomalous behavior in that material swaged at 1371°C (2500°F) and annealed at 1371°C (2500°F), 1482°C (2700°F), and 1815°C (3300°F) exhibited an upper and lower yield point phenomenon. Material swaged at 1649°C (3000°F) with two exceptions exhibited a more conventional stress-strain relationship. ASTAR-1511C in most cases displayed the upper-lower yield point behavior.

The most dramatic behavior was displayed by the tensile elongation which fell in a range between 19 and 27 percent for all thermal-mechanical and annealing treatments for both alloy compositions.

In order to appreciate the affect of prior thermal-mechanical history and final annealing temperature on low temperature ductility, the total elongation and reduction in area results are plotted as a function of test temperature in Figures 35 through 42. The data presented are the results of single point tests, and some anomalous behavior was evident. The trends that are shown are the important factors which were considered. Both the total tensile elongation and the reduction in area for both ASTAR-1211C and ASTAR-1511C showed a trend toward lower ductility as final annealing temperature was increased. In the case of ASTAR-1211C, only material annealed above 1649°C (3000°F) displayed a ductile-to-brittle transition with decreasing temperature. Material annealed at 1649°C (3000°F) and below displayed tensile elongation values well above 10 percent. This was true regardless of swaging temperature. Reduction in area data exhibited similar behavior for ASTAR-1211C. ASTAR-1511C exhibited more or less similar tensile-elongation and reduction-in-area behavior with decreasing temperature.

Grain size is known to have a significant influence on the low temperature ductility of refractory metals and alloys. In unalloyed columbium, molybdenum and tungsten a dependency

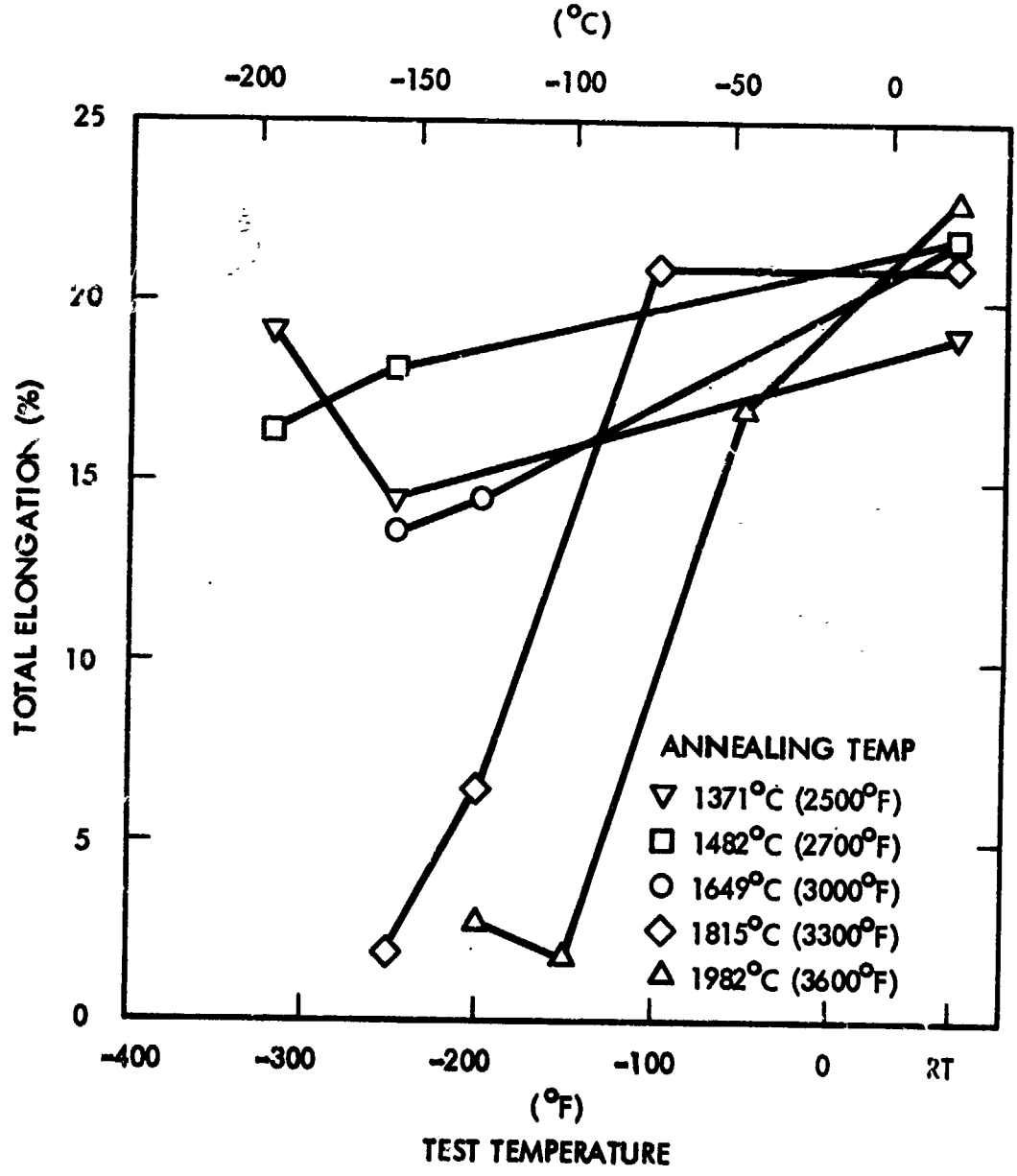

Figure 35. Low Temperature Tensile Elongation of ASTAR 1211C Swaged at 1371°C (2500°F)

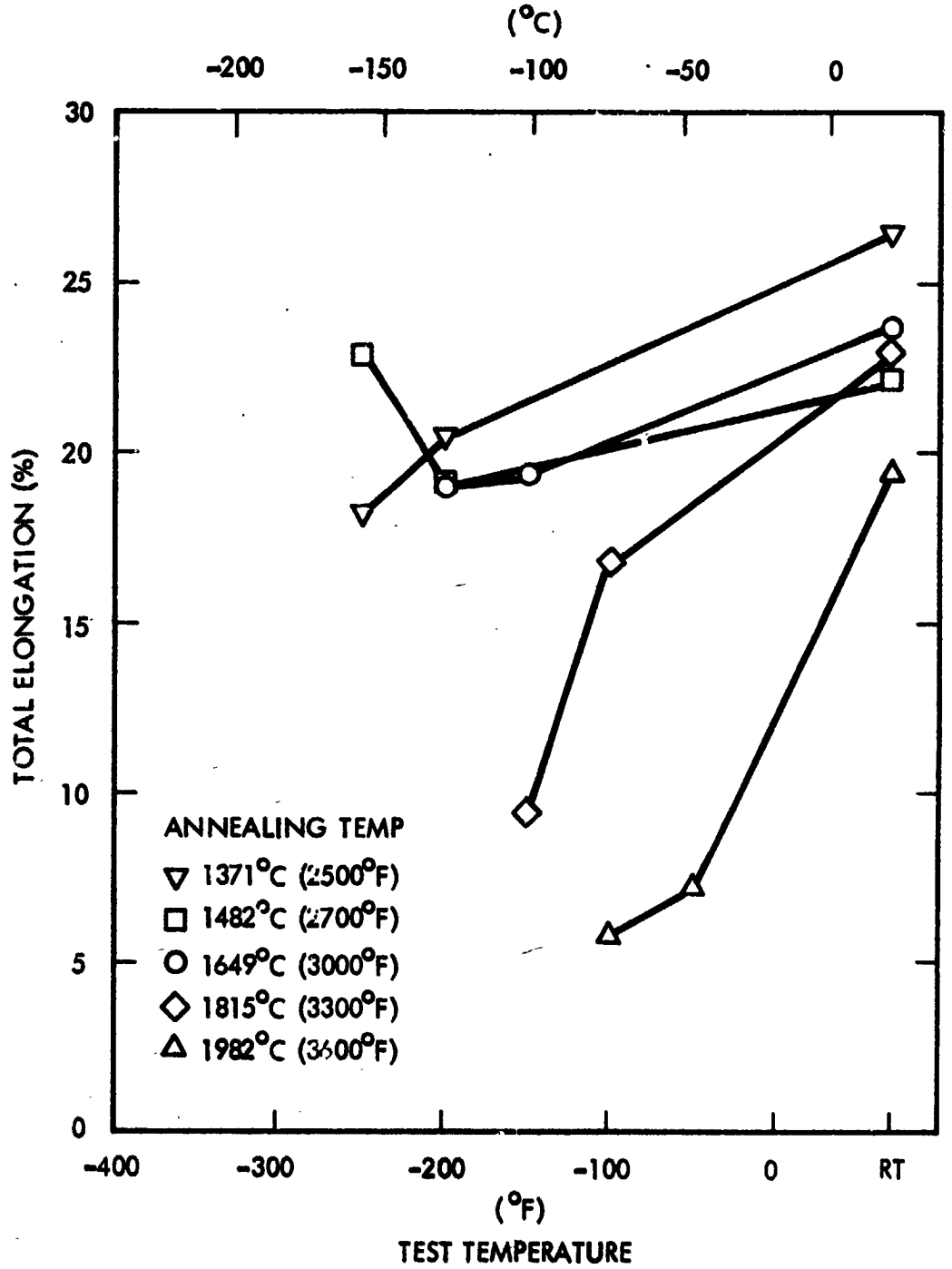

Figure 36. Low Temperature Tensile Elongation of ASTAR-1211C Swaged at 1649°C (3000°F)

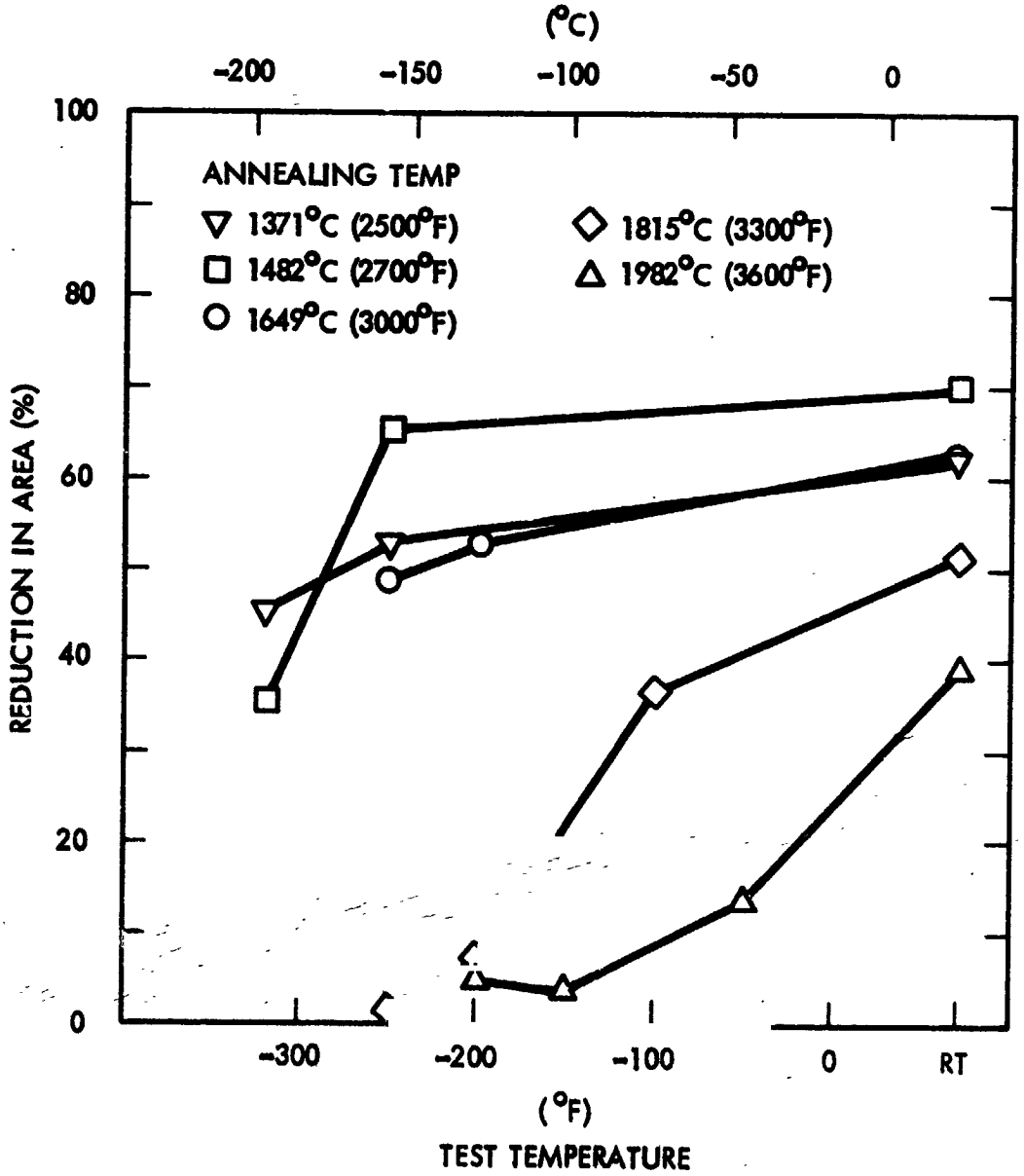

Figure 37. Reduction in Area of ASTAR-1211C Swaged at 1371°C (2500°F)

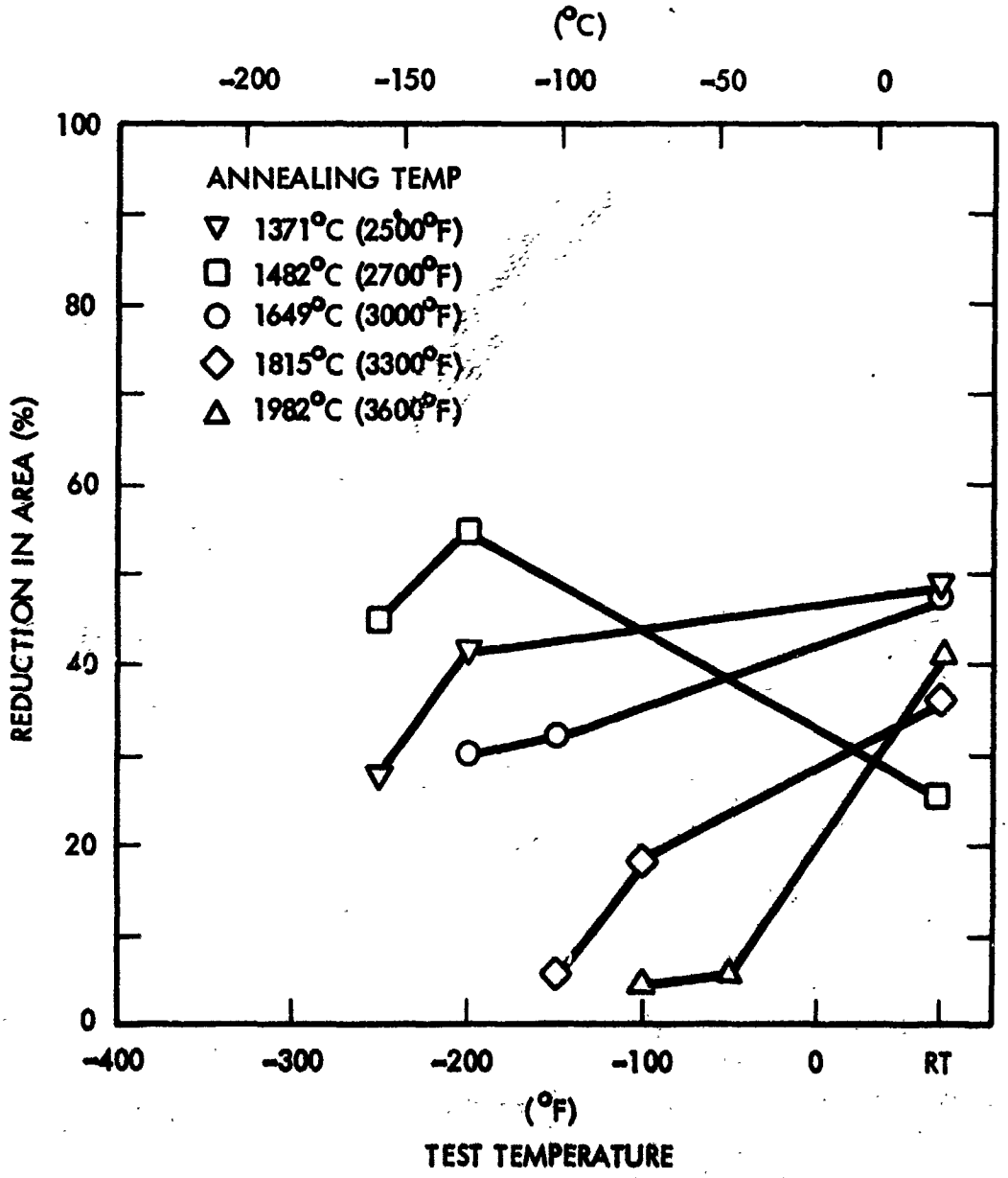

Figure 38. Reduction in Area of ASTAR-1211C Swaged at 1649°C (3000°F)

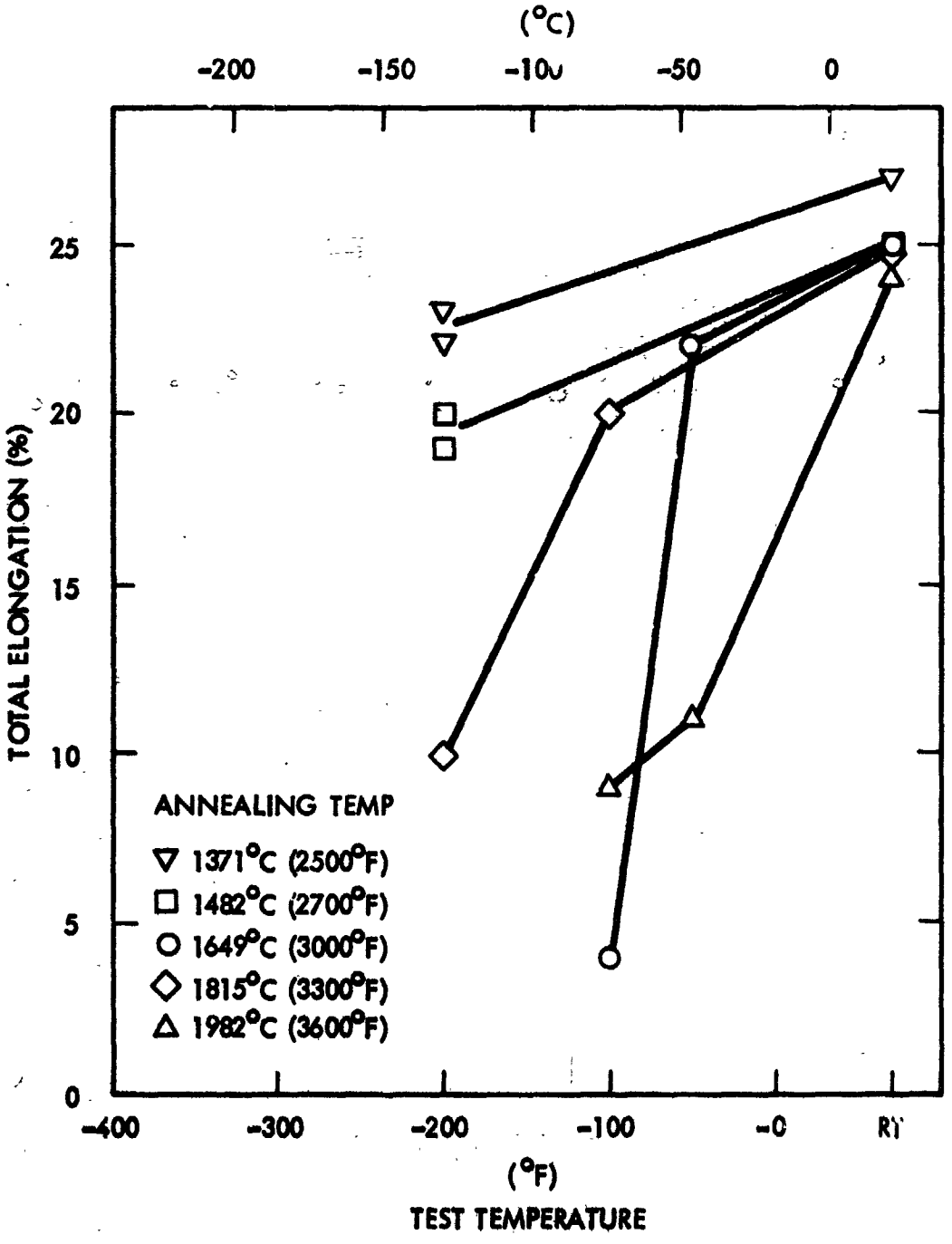

Figure 39. Low Temperature Tensile Elongation of ASTAR-1511C Swaged at 1371°C (2500°F)

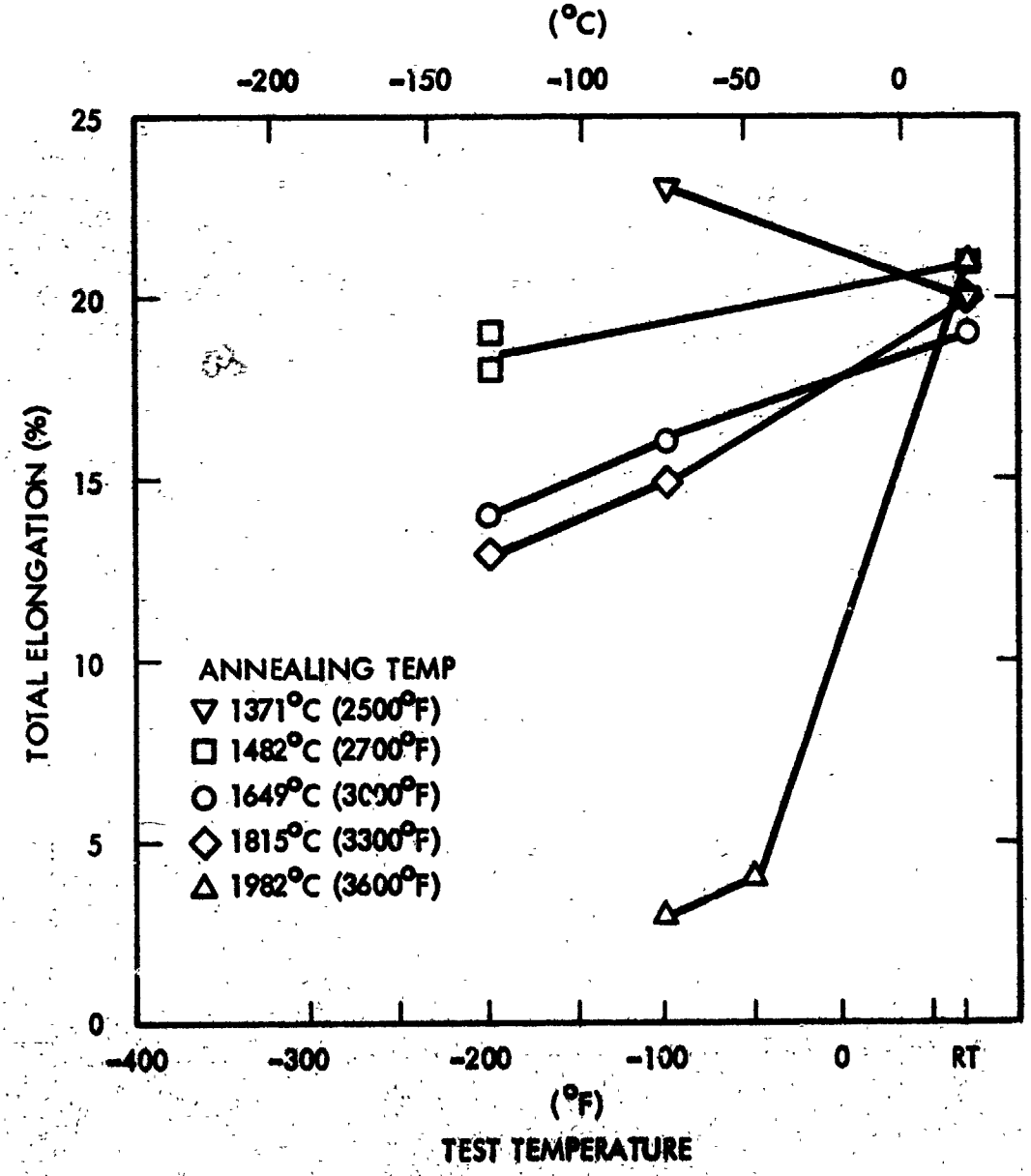

Figure 40. Low Temperature Tensile Elongation of ASTAR-1511C Swaged at 1649°C (3000°F)

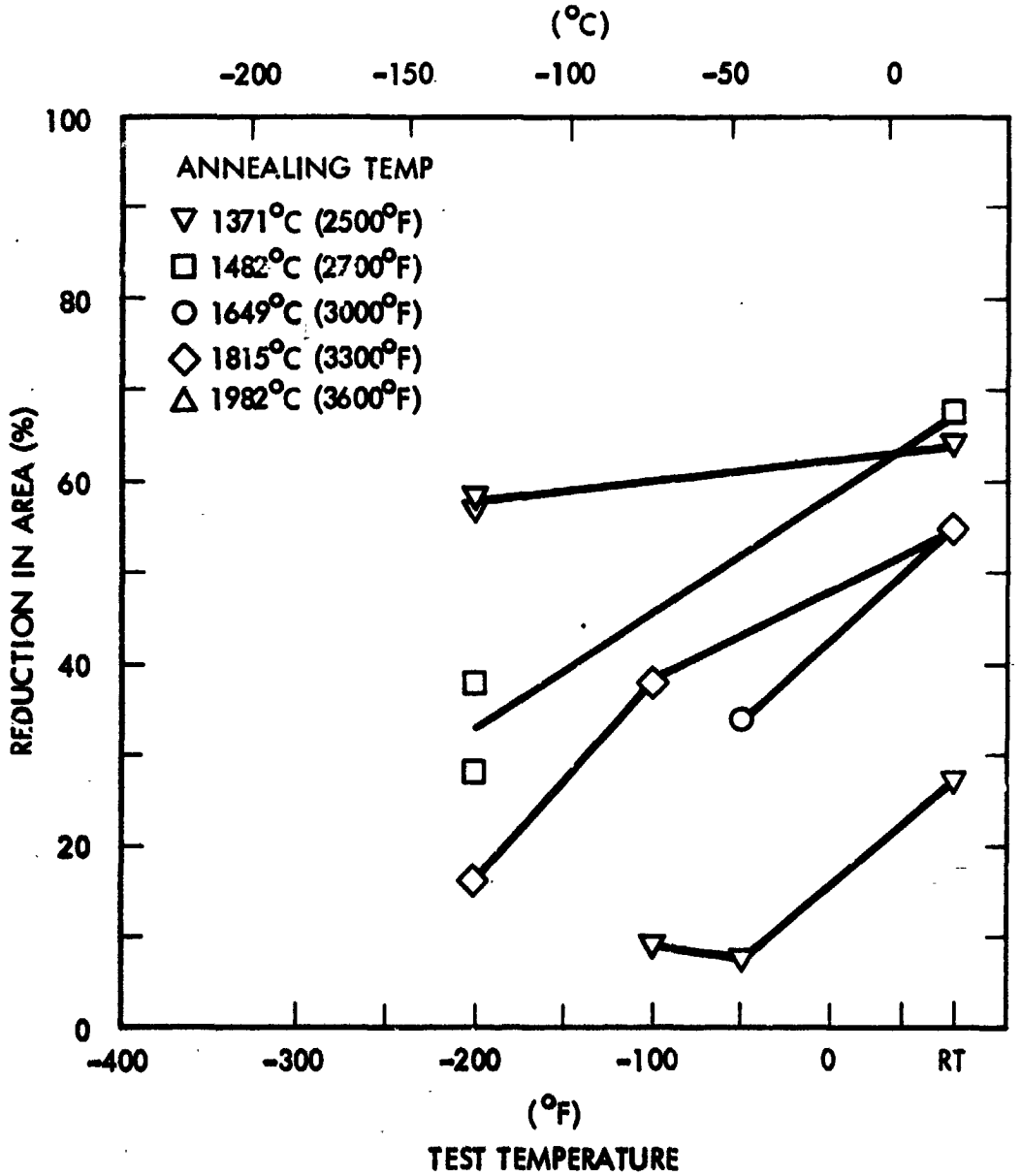

Figure 41. Reduction in Area of ASTAR-1511C Swage at 1371°C (2500°F)

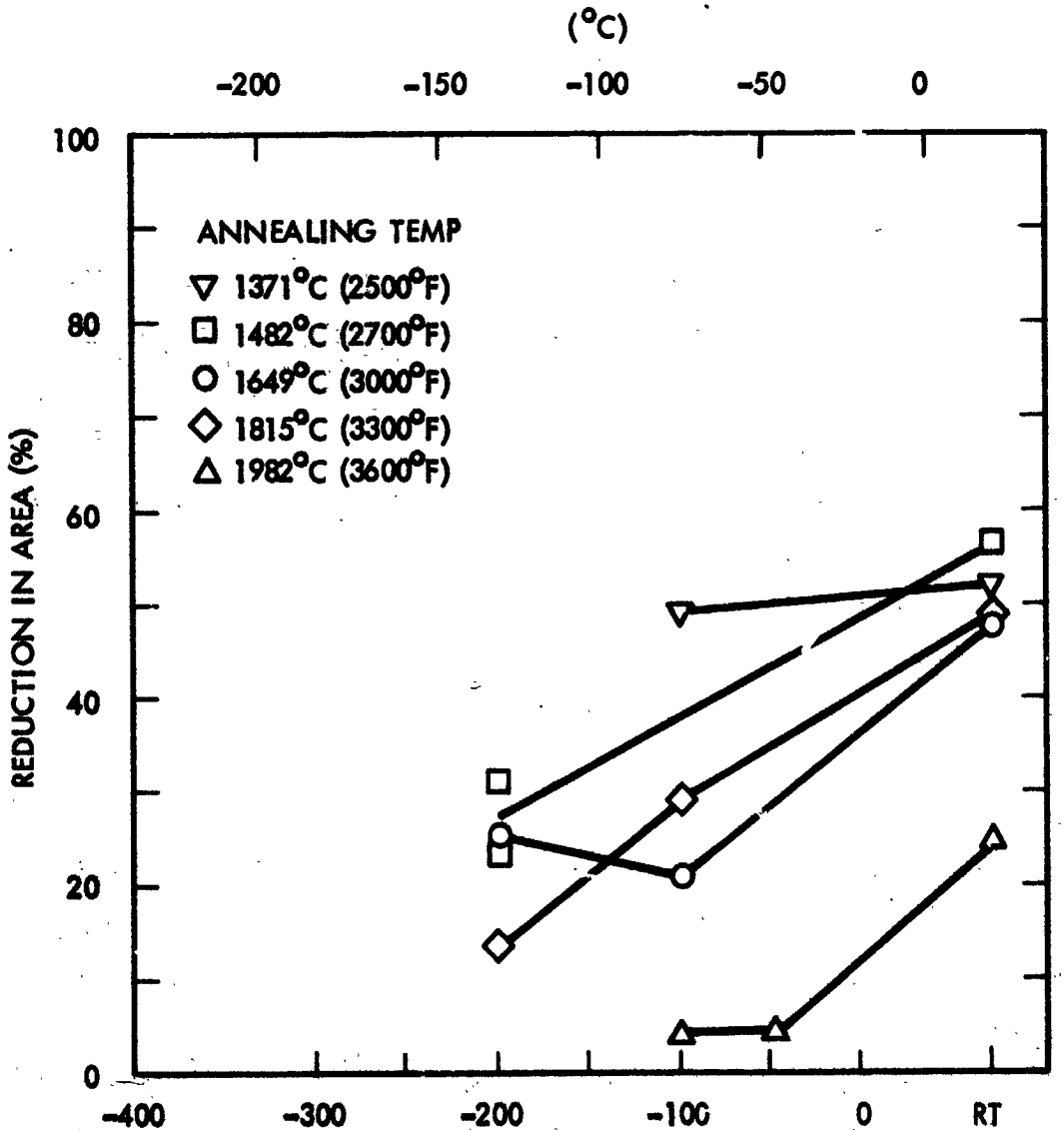

Figure 42. Reduction in Area of ASTAR-1511C Swaged at 1649°C (3000°F)

of ductile-to-brittle transition temperature has been noted[5]. As grain size decreases, the transition temperature shifts to lower values. The tantalum base ASTAR alloys appear to behave in a similar manner. As shown in Figures 26 through 29, the grain size of each alloy increases with final annealing temperature.

4.2.2 Elevated Temperature Tensile Properties

The elevated temperature tensile behavior of swaged ASTAR-1211C and ASTAR-1511C rod stock was evaluated at 1316°C (2400°F). The tensile tests were conducted in vacuum of $1.3 \times 10^{-4} N/m^2$ (1×10^{-6} torr) or lower. The tensile specimens had the same geometry as the low temperature specimens, 2.9 mm (0.115 inch) gage diameter and gage length of 28.6 mm (1.125 inch). One specimen was heat treated at each of the final annealing temperatures, 1371°C (2500°F), 1482°C (2700°F), 1649°C (3000°F), 1815°C (3300°F), and 1982°C (3600°F) prior to testing. The tests were carried out at a strain rate of 0.05/min. Test results are listed in Tables 13 and 14 and are depicted in bar graphs in Figures 43 and 44. Data for ASTAR-811C were included for comparison purposes.

The ASTAR-1211C alloy exhibited little or no affect of swaging temperature on elevated temperature tensile properties. The difference in properties noted at 1371°C (2500°F) was attributed to the difference in microstructure. The material, which was swaged and annealed at 1371°C (2500°F), had a wrought microstructure, Figure 26A; the material swaged at 1649°C (3000°F) and annealed at 1371°C (2500°F) had a recrystallized microstructure. The apparently retained residual stresses in the wrought material were responsible for the difference in strength level at 1371°C (2500°F). The ASTAR-1211C tensile results were consistent for material annealed at 1482°C (2700°F) and above. The 1815°C (3300°F) annealed material displayed the highest strength level of the recrystallized material. The variation in mechanical properties was not large enough to attribute to the effect of final annealing temperature, since the variation could fall within the normal data scatter band.

Table 13A. 1316°C Tensile Properties of ASTAR-1211C Swaged at 1371 and 1649°C (SI Units)

Swage Temperature (°C)	Annealing Temperature (°C)	Yield Strength 0.2% Offset (MN/m^2)	Ultimate Strength (MN/m^2)	Elongation		Reduction in Area (%)
				Uniform (%)	Total (%)	
1371	1371	487	520	1.8	16.4	66.1
1649	1371	293	396	11.0	26.5	61.6
1371	1482	287	367	7.7	13.6	45.0
1649	1482	298	400	9.4	31.5	69.0
1371	1649	287	400	9.4	34.6	75.0
1649	1649	286	392	12.0	30.7	68.0
1371	1816	326	446	7.4	20.0	67.1
1649	1816	316	442	11.0	27.4	66.2
1371	1982	303	417	8.8	24.5	61.9
1649	1982	301	414	11.0	26.4	62.4

0.05/min. strain rate used throughout test.

Table 13B. 2400°F Tensile Properties of ASTAR-1211C Swaged at 2500°F and 3000°F

Swage Temperature (°F)	Annealing Temperature (°F)	Yield Strength (.2% Offset) (ksi)	Ultimate Strength (ksi)	Elongation		Reduction in Area (%)
				Uniform (%)	Total (%)	
2500	2500	70.7	75.5	1.8	16.4	66.1
3000	2500	42.5	57.4	11.0	26.5	61.6
2500	2700	41.6	53.3	7.7	13.6	45.0
3000	2700	43.2	58.0	9.4	31.5	69.0
2500	3000	41.7	58.0	9.4	34.6	75.0
3000	3000	41.5	56.9	12.0	30.7	68.0
2500	3300	47.3	64.7	7.4	20.0	67.1
3000	3300	45.9	64.1	11.0	27.4	66.2
2500	3600	44.0	60.5	8.8	24.5	61.9
3000	3600	43.7	60.0	11.0	26.4	62.4

0.05/min strain rate used throughout test.

Table 14A. 1316°C Tensile Properties of ASTAR-1511C Swaged at 1371 and 1649°C (SI Units)

Swage Temperature (°C)	Annealing Temperature (°C)	Yield Strength 0.2 Offset (MN/m^2)	Ultimate Strength (MN/m^2)	Elongation		Reduction in Area (%)
				Uniform (%)	Total (%)	
1371	1371	494	527	3.3	21.0	70
1649	1371	492	527	1.4	19.0	66
1371	1482	291	400	11.9	47.0	74
1649	1482	440	500	4.8	16.0	60
1371	1649	292	406	12.2	35.0	67
1649	1649	405	481	5.6	22.0	68
1371	1816	298	411	11.9	32.0	68
1649	1816	403	481	6.9	26.0	67
1371	1982	299	430	10.8	24.0	58
1649	1982	317	452	11.6	24.0	55

0.05/min. strain rate throughout test.

Table 14B. 2400°F Tensile Properties of ASTAR-1511C Swaged at 2500 and 3000°F

Swage Temperature (°F)	Annealing Temperature (°F)	Yield Strength (0.2 Offset) (ksi)	Ultimate Strength (ksi)	Elongation		Reduction in Area (%)
				Uniform (%)	Total (%)	
2500	2500	71.6	76.5	3.3	21.0	70
3000	2500	71.4	76.5	1.4	19.0	66
2500	2700	42.2	58.0	11.9	47.0	74
3000	2700	63.8	72.5	4.8	16.0	60
2500	3000	42.4	58.9	12.2	35.0	67
3000	3000	58.7	69.8	5.6	22.0	68
2500	3300	43.3	59.6	11.9	32.0	68
3000	3300	58.5	69.7	6.9	26.0	67
2500	3600	43.4	62.4	10.8	24.0	58
3000	3600	46.0	65.6	11.6	24.0	55

Strain Rate 0.05/Min.

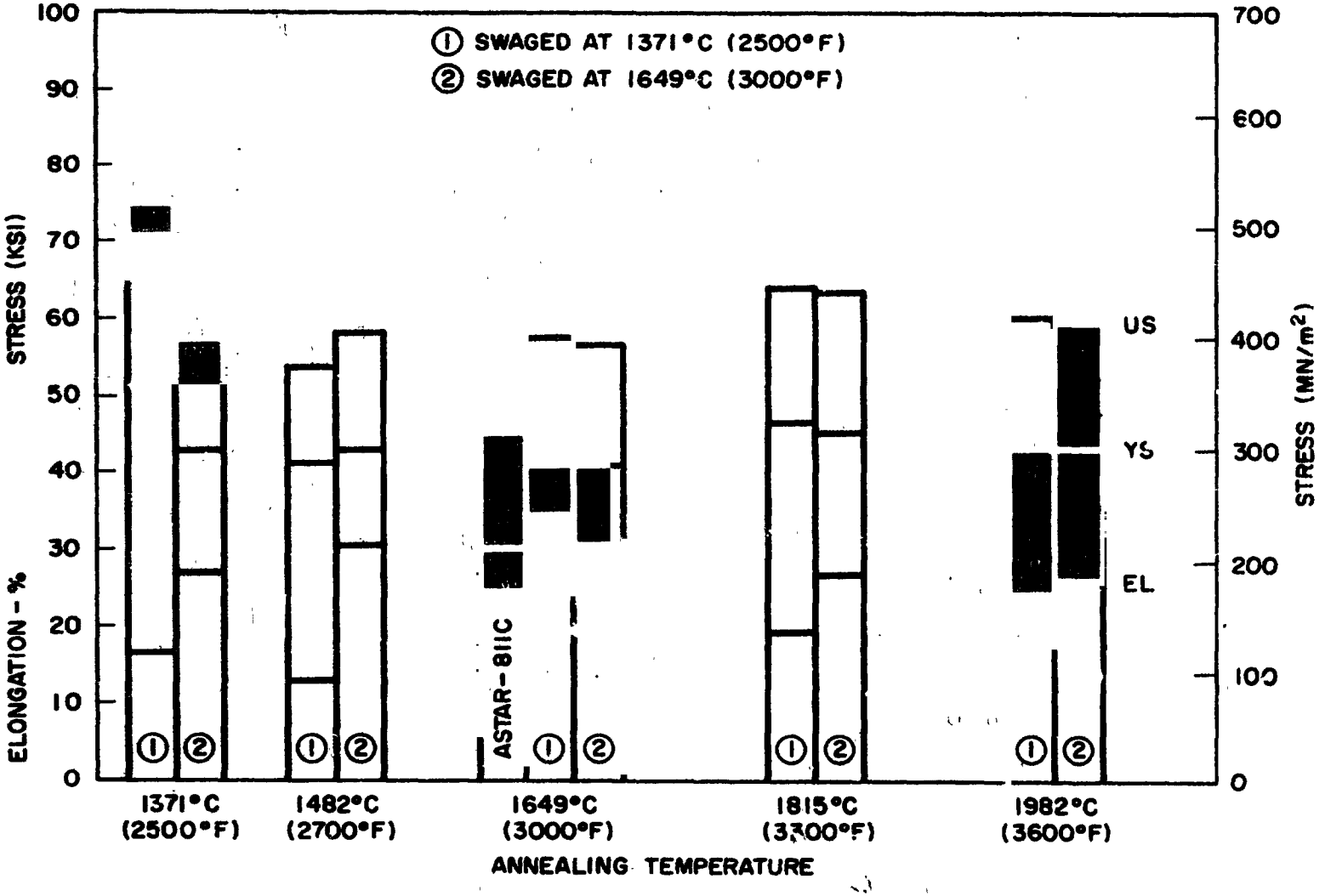

Figure 43. 1316°C (2400°F) Tensile Properties of ASTAR-1211C Swaged at 1371°C (2500°F) and 1649°C (3000°F) and Annealed at Various Temperatures

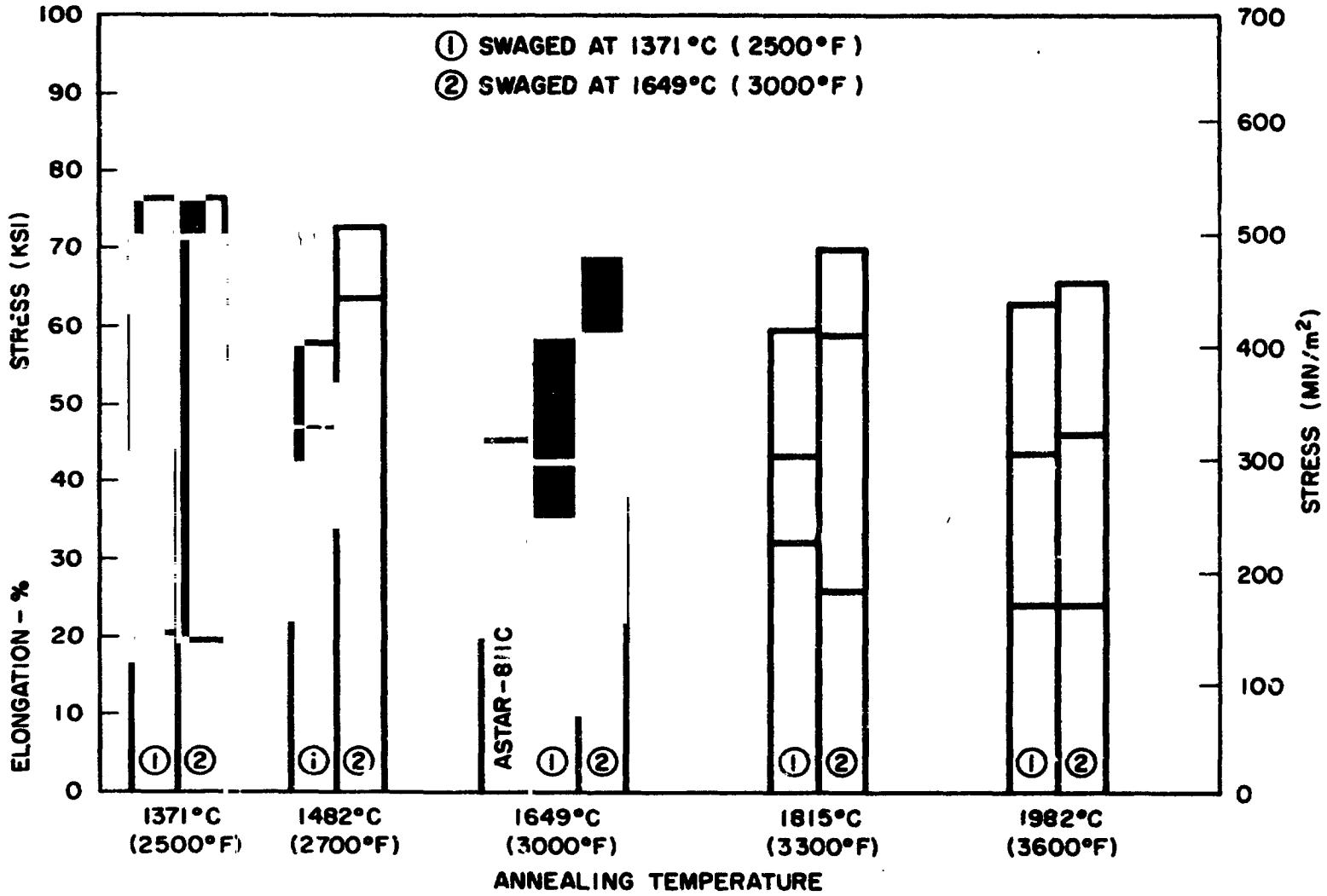

Figure 44. 1316°C (2400°F) Tensile Properties of ASTAR-1511C Swaged at 1371°C (2500°F) and 1649°C (3000°F) and Annealed at Various Temperatures

In contrast to the results for ASTAR-1211C, the elevated temperature tensile results for ASTAR-1511C indicated a possible influence of swaging temperature. Material given a final anneal at 1482°C (2700°F), 1649°C (3000°F), and 1815°C (3300°F) displayed a significant difference in mechanical properties for the two swaging temperatures. Results for material annealed at 1371°C (2500°F) and 1982°C (3600°F) were approximately the same for the two swaging temperatures. The 1982°C (3600°F) final annealing temperature, as in the case of the ASTAR-1211C, produced a large grain size in both swaged materials (Figures 28E and 29E). The effect of prior thermomechanical history was apparently minimized by the 1982°C (3600°F) final anneal. The similarity of results for the 1371°C (2500°F) annealed ASTAR-1511C was less certain. The material swaged and annealed at 1371°C (2500°F) had a wrought structure, Figure 28A, while the 1649°C (3000°F) swaged material exhibited a recrystallized grain structure, Figure 29A. The similarity of mechanical behavior was most likely fortuitous and would require additional tests to verify the results.

Both ASTAR-1211C and ASTAR-1511C exhibited significantly higher strength levels at 1316°C (2400°F) compared to ASTAR-811C with a similar processing history. ASTAR-1511C, in general, had higher strength properties compared to ASTAR-1211C in all process conditions. In both alloys the most stable condition with respect to microstructure and mechanical properties occurs in material annealed at 1649°C (3000°F) and above, regardless of prior thermomechanical history.

4.2.3 Creep Properties

Creep testing was conducted in accordance with procedures developed under prior programs, NAS 3-2542 and NAS 3-10939[1,2]. A shoulder loaded creep specimen with a 2.5 mm (0.1 inch) diameter by 0.54 mm (1.0 inch) long gage section was used. Tests were carried out in a dead-weight load machine equipped with a 400 liter-per-second ion pumping system capable of maintaining an internal pressure of 1.3×10^{-6} N/m^2 (1×10^{-8} torr) or better at test

temperature. Strain was measured by means of an optical extensometer. Test temperature was monitored and controlled by means of a Pt/Pt-Rh thermocouple attached to the gage section.

A multi-load, multi-temperature testing procedure was used to determine creep behavior. One creep specimen for each final annealing and swaging condition was used. Each specimen was initially loaded to a stress level of 276 MN/m^2 (40 ksi) at 1093°C (2000°F). After establishment of a stable secondary creep rate, the load and temperature were changed. Generally, the stress level was reduced, and the temperature was increased. After establishment of a stable secondary creep rate, the load and temperature were again changed. This procedure was repeated until the test temperature reached 1316°C (2400°F) to 1343°C (2450°F) or the stress level dropped to 69 MN/m^2 (10 ksi) or 86 MN/m^2 (12.5 ksi). Although prior strain may have had an effect on subsequent creep behavior, comparison of creep data produced by the above described procedure with single-load, single-temperature test results produced and discussed under another section of this report, confirmed the validity of the creep test procedure used here.

Results of the multi-load, multi-temperature creep tests of ASTAR-1211C and ASTAR-1511C are listed in Tables 15 through 18. Larson-Miller plots of 1 percent creep strain, as determined from secondary creep rate, for each alloy are given in Figures 45 and 46. The time to 1 percent creep strain was determined by extrapolation of secondary creep rate in most cases. Where creep strain exceeded 1 percent during a particular increment of the creep test, the actual time was used to calculate the Larson-Miller parameter. In Figure 45, the data for material swaged at 1649°C (3000°F) and 1482°C (2700°F) are the average of duplicate tests.

Table 15. Creep Data for ASTAR-1211C Rod Swaged at 1371°C (2500°F) and Annealed at Various Temperatures

Specimen Identification and Final Annealed Condition	Test Temperature		Stress Level		Secondary Creep Time (hrs.)	Secondary Creep Strain (%)	Secondary Creep Rate (%/hr.)	Time to 1% Strain (hrs.)	P $T_{Ro}(15+\log t)\times10^{-3}$
	(°C)	(°F)	(MN/m^2)	(ksi)					
1-A-22-25 Annealed 1 hr/1371°C (2500°F)	1093	2000	276	40	232.9	0.76	0.0033	308	43.0
	1204	2200	207	30	101.9	2.57	0.0252	39	44.1
	1149	2100	207	30	41.6	0.31	0.0075	134	43.8
	1149	2100	173	25	150.0	0.81	0.0054	185	44.2
	1149	2100	138	20	186.6	0.42	0.0023	443	45.2
	1204	2200	122	17.6	169.6	1.25	0.0068	148	45.7
	1204	2200	86	12.5	171.0	0.28	0.0016	610	47.3
	1232	2250	86	12.5	18.5	0.09	0.0049	206	46.9
	1260	2300	86	12.5	120.3	0.30	0.0025	400	48.6
1-A-22-27 Annealed 1 hr/1482°C (2700°F)	1093	2000	276	40	90.0	1.14	0.0126	79	41.6
	1093	2000	242	35	192.0	0.37	0.0019	526	43.6
	1204	2200	173	25	167.0	1.30	0.0078	128	45.5
	1204	2200	138	20	163.0	0.49	0.0031	332	46.6
	1260	2300	104	15	72.0	0.72	0.0038	264	48.2
	1260	2300	86	12.5	125.0	0.21	0.0017	595	48.8
1-A-22-30 Annealed 1 hr/1649°C (3000°F)	1093	2000	276	40	188.6	0.94	0.0056	179	42.4
	1204	2200	207	30	144.4	1.67	0.0116	87	45.0
	1204	2200	138	20	168.5	0.20	0.0012	840	47.7
	1316	2400	86	12.5	149.7	0.61	0.0041	246	49.7
	1316	2400	69	10	240.0	0.57	0.0024	420	50.4
1-A-22-33 Annealed 1 hr/1815°C (3300°F)	1093	2000	276	40	285.3	1.16	0.0041	224	42.8
	1204	2200	207	30	74.0	.08	0.0011	910	47.8
	1232	2250	207	30	142.0	.69	0.0046	217	47.0
	1316	2400	138	20	120.0	.54	0.0045	222	49.6
	1316	2400	104	15	42.4	.04	0.00094	1060	51.6
1-A-22-36 Annealed 1 hr/1982°C (3600°F)	1093	2000	276	40	114.0	0.49	0.0049	233	42.7
	1204	2200	276	40	24.3	6.09	0.25	4	41.5
	1204	2200	207	30	124.1	0.52	0.0042	239	46.2
	1316	2400	104	15	187.0	0.43	0.0023	434	50.4
	1343	2450	104	15	104.9	0.48	0.0046	217	50.4
	1343	2450	86	12.5	148.9	0.39	0.0026	385	51.2

Table 16. Creep Data for ASTAR-1211C Rod Swaged at 1649°C (3000°F) and Annealed at Various Temperatures

Specimen Identification and Final Annealed Condition	Test Temperature		Stress Level		Secondary Creep Time (hrs.)	Secondary Creep Strain (%)	Secondary Creep Rate (%/hr.)	Time to 1% Strain (hrs.)	P $T_{R^o}(15+\log t)\times 10^{-3}$
	(°C)	(°F)	(MN/m^2)	(ksi)					
1-A-12-25 Annealed 1 hr/1371°C (2500°F)	1093	2000	276	40	191	0.35	0.0018	545	42.8
	1204	2200	207	30	235	0.41	0.0018	574	47.2
	1316	2400	138	20	119	0.65	0.0055	183	49.4
	1316	2400	104	15	213	0.49	0.0023	435	50.5
1-A-12-27 Annealed 1 hr/1482°C (2700°F)	1093	2000	276	40	383	0.11	0.00039	2570	45.3
	1204	2200	207	30	310	0.21	0.00068	1472	48.3
	1316	2400	138	20	195	0.14	0.00072	1390	51.9
	1343	2450	104	15	42	0.03	0.00071	1400	52.8
	1371	2500	104	15	330	0.57	0.00173	578	52.6
1-A-12-30 Annealed 1 hr/1649°C (3000°F)	1093	2000	276	40	162	0.25	0.0015	648	43.8
	1204	2200	207	30	192	0.75	0.0039	255	46.3
	1316	2400	138	20	52	0.40	0.0077	130	48.9
	1316	2400	104	15	170	0.31	0.0018	550	50.8
1-A-12-33 Annealed 1 hr/1815°C (3300°F)	1093	2000	276	40	162	0.25	0.0015	648	43.8
	1204	2200	207	30	265	0.35	0.0013	760	47.5
	1316	2400	138	20	148	0.50	0.0034	296	50.0
	1316	2400	104	15	265	0.09	0.00034	2945	52.8
1-A-12-36 Annealed 1 hr/1982°C (3600°F)	1093	2000	276	40	257	0.35	0.0013	735	43.9
	1204	2200	207	30	220	0.30	0.0013	735	47.5
	1316	2400	138	20	193	0.66	0.0034	292	49.9

Table 17. Creep Data for ASTAR-1511C Rod Swaged at 1371°C (2500°F) and Annealed at Various Temperatures

Specimen Identification and Final Annealed Condition	Test Temperature (°C)	Test Temperature (°F)	Stress Level (MN/m^2)	Stress Level (ksi)	Secondary Creep Time (hrs.)	Secondary Creep Strain (%)	Secondary Creep Rate (%/hr.)	Time to 1% Strain (hrs.)	P $T_R o(15+\log t)\times 10^{-3}$
2-8-41-25 Annealed 1 hr/1371°C (2500°F)	1093	2000	276	40	211	0.25	0.0012	844	44.1
	1149	2100	207	30	111	0.24	0.0022	463	45.3
	1260	2300	138	20	76	0.44	0.0058	173	47.6
	1260	2300	104	15	265	1.27	0.0048	209	47.8
2-8-41-27 Annealed 1 hr/1482°C (2700°F)	1093	2000	276	40	44	0.26	0.0059	170	42.4
	1093	2000	207	30	121	0.00	--	--	--
	1149	2100	207	30	161	0.37	0.0023	436	45.0
	1260	2300	138	20	166	0.31	0.0019	536	47.7
	1260	2300	104	15	282	0.78	0.0028	362	48.5
2-8-41-30 Annealed 1 hr/1649°C (3000°F)	1093	2000	276	40	216	0.20	0.00093	1080	44.4
	1204	2200	207	30	311	0.69	0.0022	452	47.0
	1316	2400	138	20	167	0.94	0.0056	178	49.3
	1316	2400	104	15	247	0.40	0.0016	677	50.9
2-8-41-33 Annealed 1 hr/1815°C (3300°F)	1093	2000	276	40	211	0.26	0.0016	620	43.8
	1204	2200	207	30	313	0.44	0.0014	712	47.5
	1316	2400	138	20	166	0.84	0.0051	196	49.5
	1316	2400	104	15	266	0.77	0.0029	346	50.2
2-8-41-36 Annealed 1 hr/1982°C (3600°F)	1093	2000	276	40	150	0.00	--	--	--
	1149	2100	276	40	41	0.67	0.0163	61	43.0
	1149	2100	207	30	161	0.12	0.00075	1330	46.4
	1204	2200	173	25	280	0.13	0.00046	2150	48.7
	1316	2400	138	20	163	0.30	0.0018	542	50.7
	1343	2450	138	20	89	0.35	0.0039	254	50.6
	1371	2500	104	15	258	0.54	0.0021	476	52.3

Table 18. Creep Data for ASTAR-1511C Rod Swaged at 1649°C (3000°F) and Annealed at Various Temperatures

Specimen Identification and Final Annealed Condition	Test Temperature (°C)	Test Temperature (°F)	Stress Level (MN/m^2)	Stress Level (ksi)	Secondary Creep Time (hrs.)	Secondary Creep Strain (%)	Secondary Creep Rate (%/hr.)	Time to 1% Strain (hrs.)	$T_{RO}(15+\log t)\times 10^{-3}$
2-8-11-25 Annealed 1 hr/1371°C (2500°F)	1093	2000	276	40	264	0.08	0.0003	3300	45.6
	1204	2200	207	30	161	0.20	0.0012	805	47.6
	1316	2400	138	20	151	0.84	0.0056	180	49.4
	1316	2400	104	15	166	0.44	0.0027	378	50.3
2-8-11-27 Annealed 1 hr/1482°C (2700°F)	1093	2000	276	40	331	0.14	0.0004	2360	45.3
	1204	2200	207	30	144	0.37	0.0026	389	46.8
	1316	2400	138	20	70	0.64	0.0092	109	48.7
	1316	2400	104	15	125	0.39	0.0031	321	50.1
	1316	2400	86	12.5	194	0.57	0.0029	340	50.1
2-8-11-30 Annealed 1 hr/1649°C (3000°F)	1093	2000	276	40	376	0.09	0.0002	4170	45.8
	1204	2200	207	30	216	0.20	0.0009	1080	48.0
	1316	2400	138	20	123	0.68	0.0055	181	49.4
	1316	2400	104	15	459	1.22	0.0027	376	50.3
2-8-11-33 Annealed 1 hr/1815°C (3300°F)	1093	2000	276	40	282	0.12	0.0004	2350	45.2
	1204	2200	207	30	311	0.39	0.0012	800	47.6
	1316	2400	138	20	148	0.68	0.0046	218	49.6
	1316	2400	104	15	247	0.52	0.0021	475	50.6
2-8-11-36 Annealed 1 hr/1982°C (3600°F)	1093	2000	276	40	231	0.07	0.0003	3300	45.6
	1149	2100	276	40	143	0.33	0.0023	433	45.2
	1204	2200	207	30	212	0.07	0.0003	3030	49.2
	1316	2400	138	20	163	0.16	0.0010	1020	51.6
	1343	2450	138	20	89	0.19	0.0021	470	51.4
	1371	2500	104	15	-	-	-	-	-

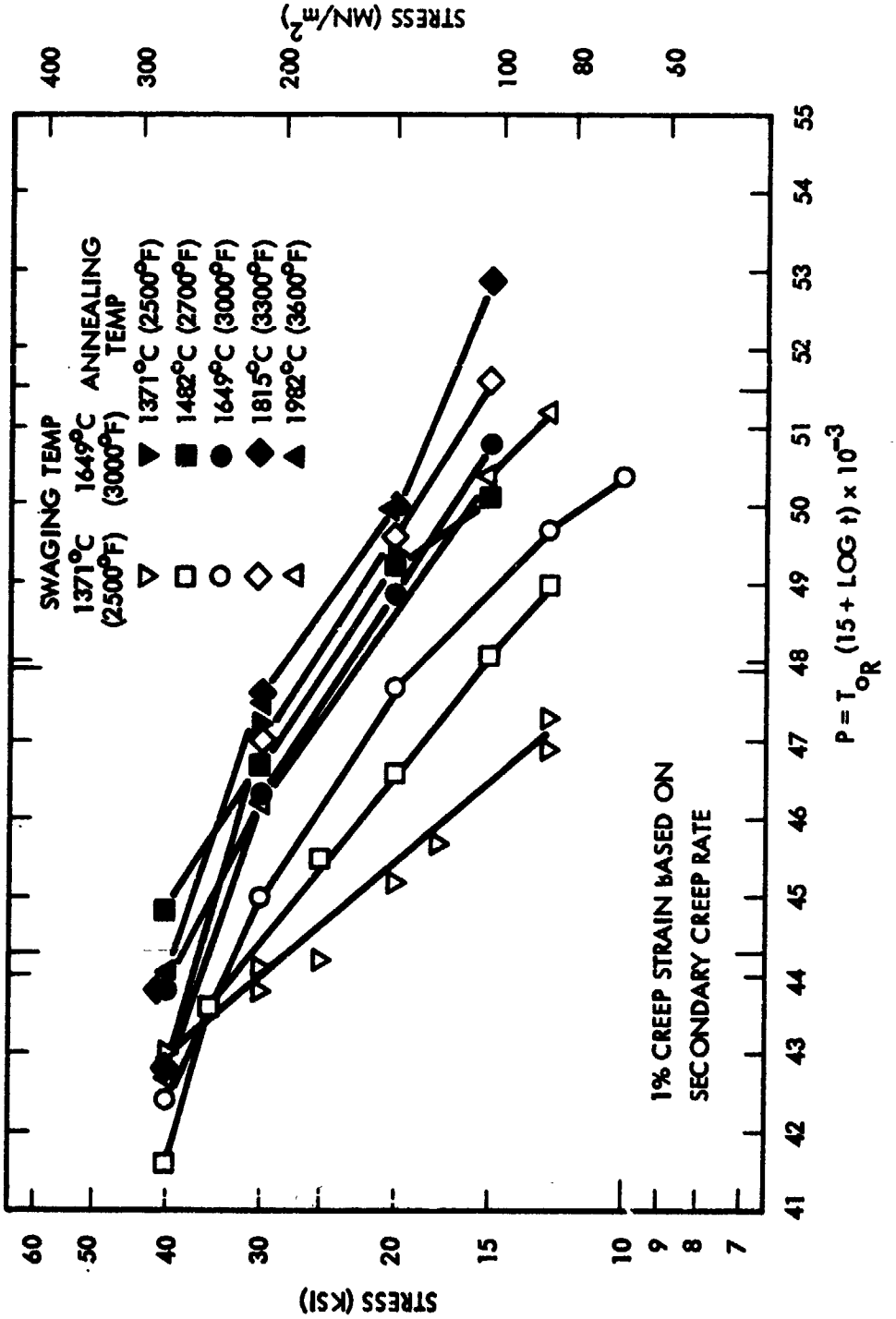

Figure 45. Creep Data for ASTAR-1211C Swaged Bar Stock

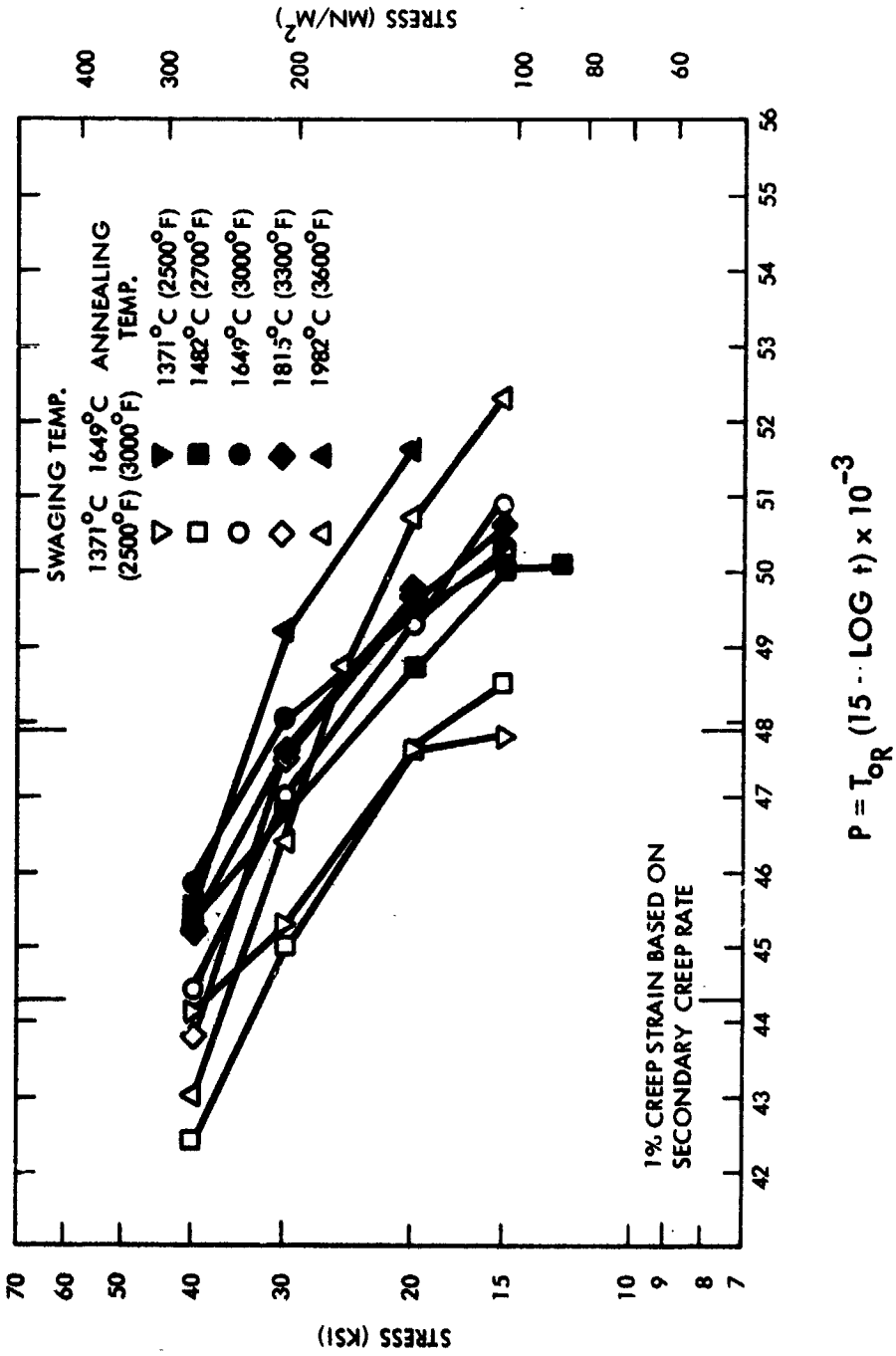

Figure 46. Creep Data for ASTAR-1511C Swaged Bar Stock

The effects of swaging temperature and final annealing temperature are more clearly illustrated in Figures 47 and 48. The stress to produce 1 percent creep strain in 1000 hours at three selected temperatures; 1093°C (2000°F), 1204°C (2200°F), and 1316°C (2400°F) are plotted as a function of swaging temperature and final annealing temperature. In almost all cases for ASTAR-1211C and ASTAR-1511C, the material swaged at 1649°C (3000°F) was the most creep resistant, regardless of final annealing temperature. The difference in creep resistance due to swaging temperature was greatest for annealing temperatures below 1649°C (3000°F).

The effects of final annealing temperature are also clearly illustrated. The trend to higher stress levels, particularly at higher creep temperatures, is evident. For ASTAR-1211C, the highest stress levels, indicating the best creep resistance, were material annealed at 1815°C (3300°F) for either swaging temperature. The trend was slightly different for ASTAR-1511C, the highest stress levels, shifted from the 1649°C (3000°F) annealed material at creep temperature of 1093°C (2000°F) to material annealed at 1982°C (3600°F) and creep tested at 1316°C (2400°F).

The low creep resistance of material swaged at 1371°C (2500°F) and final annealed at temperatures below 1649°C (3000°F) was attributed to the metallurgical condition of the microstructure and changes in the structure which occurred during creep testing. Metallographic examination of post-test creep specimens of ASTAR-1211C was conducted. Photomicrographs are shown in Figure 49,and pertinent relative data are listed in Table 19.

The material swaged and annealed at 1371°C (2500°F) had a wrought structure prior to creep testing (see Figure 26). The microstructure of the creep tested specimen, Figure 49A, shows that recrystallization occurred during creep testing. The material swaged at 1371°C (2500°F) and annealed at 1482°C (2700°F), Figure 49B, also showed a completely recrystallized microstructure. This material was partially recrystallized prior to creep testing. Prior experience

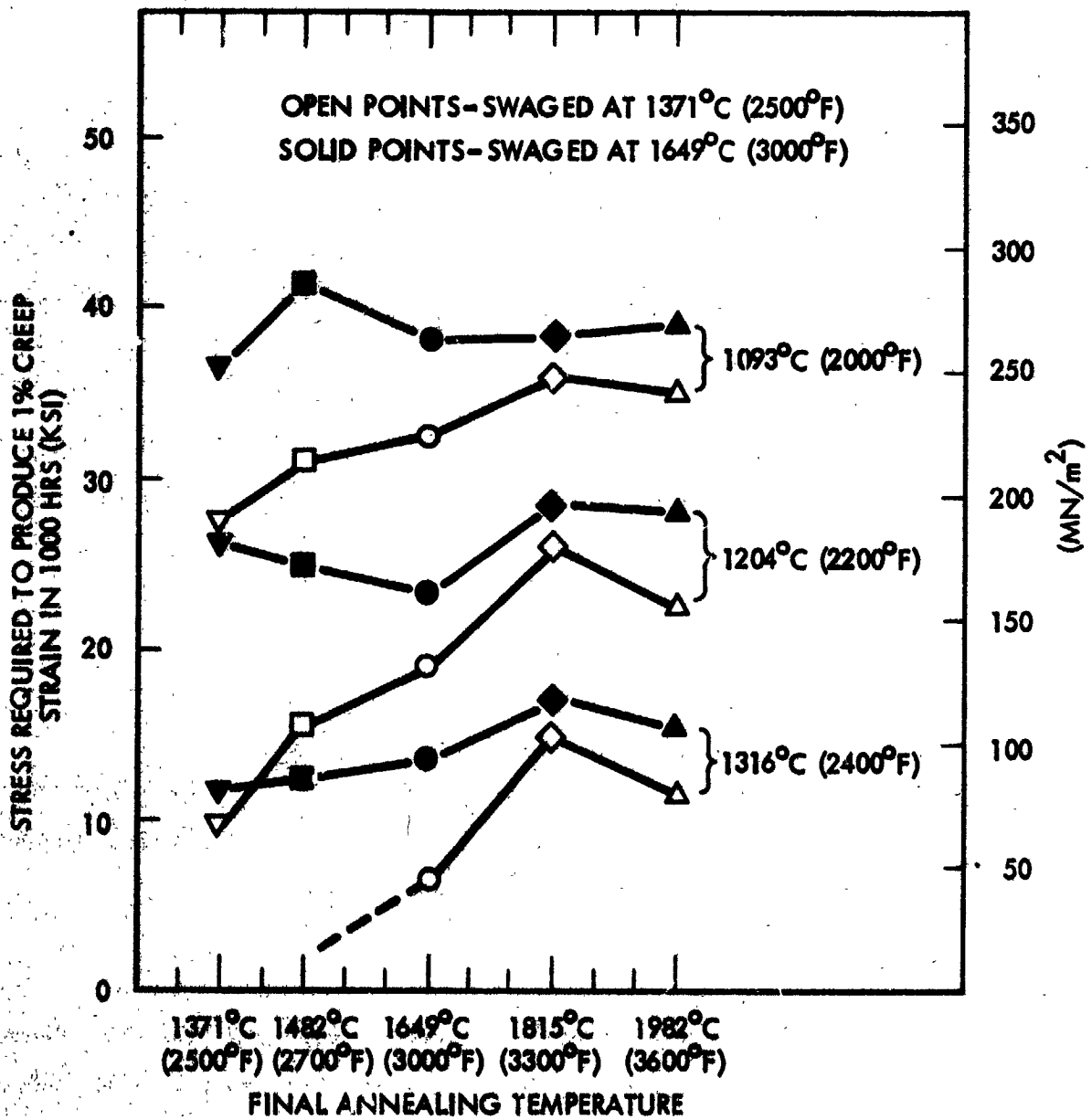

Figure 47. Stress to Produce 1 Percent Creep Strain in ASTAR-1211C as a Function of Processing and Final Annealing Temperature

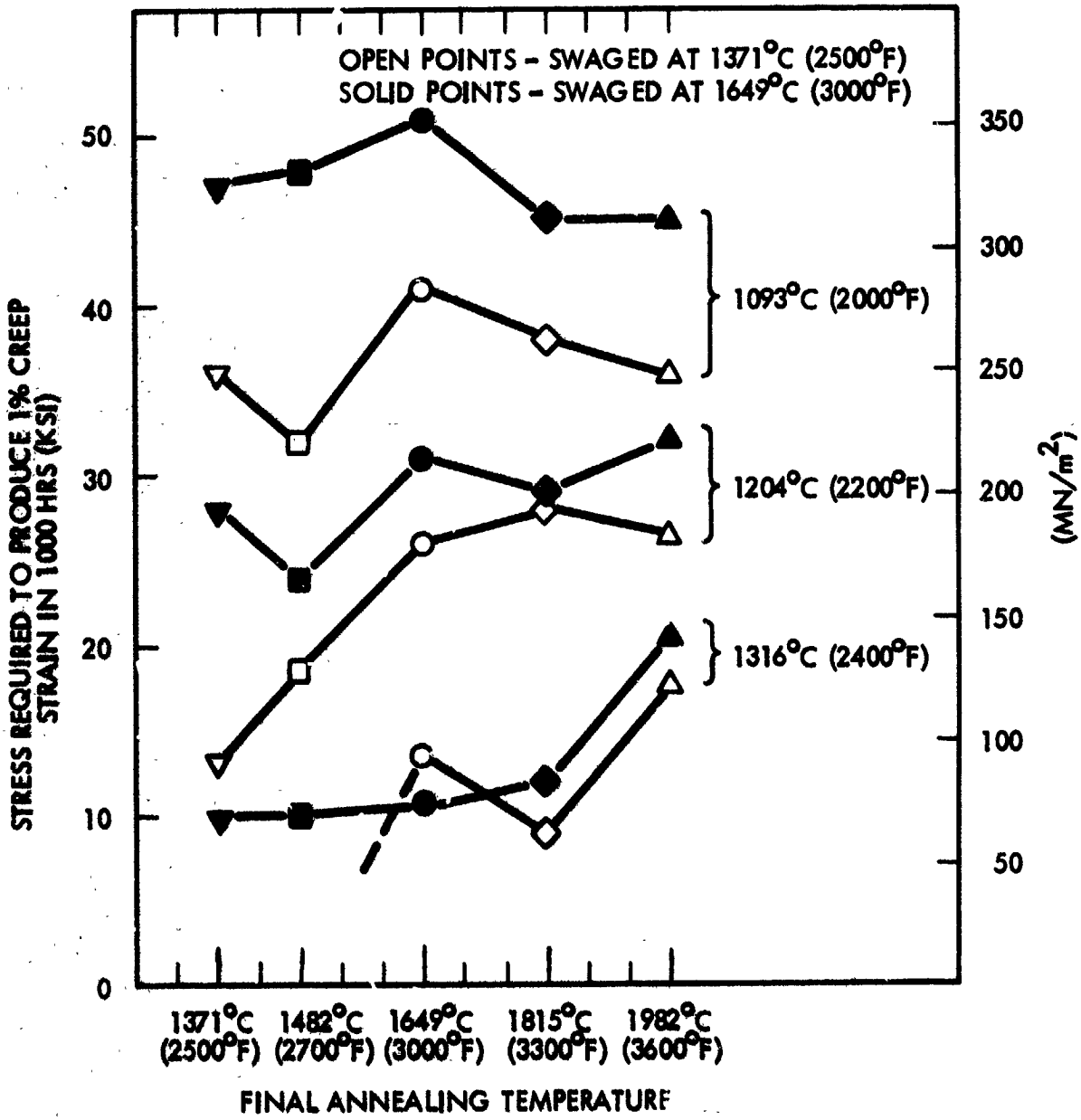

Figure 48. Stress to Produce 1 Percent Creep Strain in ASTAR-1511C as a Function of Processing and Final Annealing Temperature

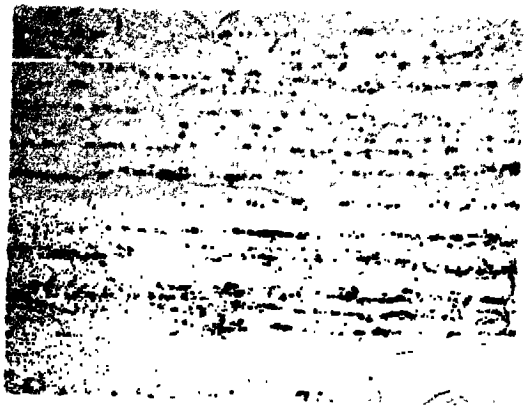

A

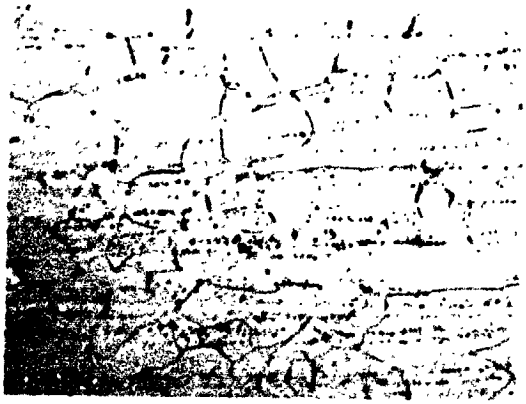

B

C

D

E

Figure 49. Post Test Microstructure of ASTAR-1211C Creep Specimens

F

G

H

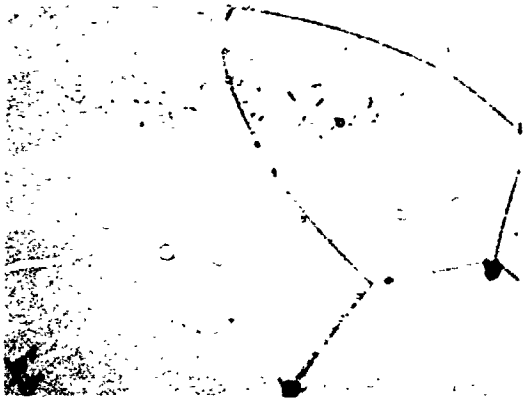

I

Figure 49. Post Test Microstructure of ASTAR-1211C Creep Specimens (Continued)

Table 19. Data for Post-Test Creep Specimens of ASTAR-1211C

Micro-graph Ident.	Swage Temperature		First Anneal Temperature		Initial Grain Size (mm)	Total Creep Test Time (hrs)	Total Creep Strain (%)	Pre-Test Hardness (DPH)	Post-Test Hardness (DPH)
	(°C)	(°F)	(°C)	(°F)					
A	1371	2500	1371	2500	W	1274	7.40	308	286
B	1371	2500	1482	2700	0.015	818	4.36	297	277
C	1371	2500	1649	3000	0.024	891	5.12	339	307
D	1371	2500	1815	3300	0.036	853	3.12	330	279
E	1371	2500	1932	3600	0.120	796	8.93	307	296
F	1649	3000	1482	2700	0.025	1249	1.96	323	273
G	1649	3000	1649	3000	0.026	600	2.51	308	274
H	1649	3000	1815	3300	0.038	865	1.79	305	276
I	1649	3000	1982	3600	0.125	720	2.01	300	285

W = Wrought Structure

with tantalum alloys has shown that recrystallization during creep testing has an adverse affect on creep rate[6].

The carbon solubility in the ASTAR-1211C alloy matrix was also graphically demonstrated in the series of micrographs. The tantalum carbide phase, Ta_2C, which precipitated during the 1371°C (2500°F) swaging process, was gradually taken back into solution as the final annealing temperature was increased. The carbon in solution then reprecipitated at the grain boundaries as large massive blocks during creep testing at the lower temperatures.

The material swaged at 1649°C (3000°F) exhibited a completely recrystallized microstructure for all final annealing conditions. The grain sizes of the 1649°C (3000°F) swaged material were similar, except for the 1982°C (3600°F) annealed material. Material annealed at 1649°C (3000°F) and above had similar microstructures regardless of swaging temperature. Grain size was increased for the 1982°C (3600°F) annealed material.

4.2.4 Supplemental Testing of ASTAR-1211C

At the conclusion of the initial mechanical property evaluation of this task, four supplemental final annealing conditions were selected for further evaluation. The additional final annealing conditions selected were as follows:

- ASTAR-1211C - Swaged at 1371°C (2500°F) + 1 hr/1760°C (3200°F)
- ASTAR-1211C - Swaged at 1371°C (2500°F) + 1 hr/1649°C (3000°F) + 1 hr/1260°C (2300°F)
- ASTAR-1211C - Swaged at 1371°C (2500°F) + 1 hr/1815°C (3300°F) + 1 hr/1260°C (2300°F)
- ASTAR-1211C - Swaged at 1649°C (3000°F) + 1 hr/1649°C (3000°F) + 1 hr/1316°C (2400°F).

The first annealing condition was selected to investigate the temperature range between 1649°C (3000°F) and 1815°C (3300°F). Material annealed 1815°C (3300°F) exhibited the best creep resistance of the five initial annealing temperatures investigated; while material annealed at 1649°C (3000°F) and below displayed the better low temperature ductility behavior. The intermediate temperature of 1760°C (3200°F) was selected to provide additional information concerning the effects of final annealing temperature on the low temperature ductility behavior and elevated temperature creep properties of swaged ASTAR-1211C rod stock.

The remaining three annealing conditions were selected to investigate the effect of duplex heat treatment on high and low temperature mechanical properties of ASTAR-1211C. It was noted during the processing of ASTAR-1211C swaged rod that material swaged at 1649°C (3000°F) and subsequently heat treated at lower temperatures exhibited a room temperature hardness minima for annealing temperatures between 1093°C (2000°F) and 1316°C (2400°F). This effect is illustrated in Figure 30. The hardness minima was verified by a subsequent hardness study. Samples of ASTAR-1211C swaged at 1371°C (2500°F) were annealed for one hour at 1815°C (3300°F). Samples were then annealed at 1093°C (2000°F), 1204°C (2200°F), 1260°C (2300°F), and 1371°C (2500°F). Room temperature hardness data for the duplex heat treated samples are given in Table 20.

Table 20. RT Hardness of Duplex Heat Treated ASTAR-1211C Swaged Rod

Secondary Annealing Temperature	Primary Annealing Temperature	
	1649°C (3000°F) DPH	1815°C (3300°F) DPH
1093°C (2000°F)	298	298
1204°C (2200°F)	-	288
1260°C (2800°F)	276	283
1371°C (2500°F)	285	285

The RT hardness values for the ASTAR-1211C annealed at 1815°C (3300°F) and subsequently heat treated at the lower temperature verify the hardness reduction noted previously. Material subjected to the three differing duplex heat treatments, as listed above, were evaluated to determine if the hardness decrease also reflected a change in creep properties and low temperature ductility.

4.2.4.1 Low Temperature Mechanical Properties

Mechanical properties of the four supplemental annealing conditions are listed in Table 21. Room temperature tensile data are plotted in Figure 50 along with data for the five previously tested final annealing conditions. The yield and ultimate strength for the 1760°C (3200°F) annealed material were unexpectedly low while ductility, as expressed by total elongation, was consistent with other results. The yield and ultimate strengths of the duplex annealed material were lower as expected and as indicated by the lower hardness values. There was no significant change in the values for ductility of the duplex annealed material.

Sub-room temperature total elongation and reduction in area data for the supplemental test conditions are plotted in Figures 51 through 54 along with data for the five previously tested final annealing conditions. The elongation and reduction in area data for the 1760°C (3200°F) annealed material fell in line with the 1649°C (3000°F) and 1815°C (3300°F) as expected. The results for the duplex annealed materials were not as predictable. The material annealed at 1649°C (3000°F)/1260°C (2300°F) exhibited elongation values compared to the single 1649°C (3000°F) annealed material, while the opposite was true of the 1815°C (3300°F)/ 1260°C (2300°F) heat treated material.

The microstructure of three of the supplemental test materials are shown in Figure 55. The photomicrographs were taken of sectioned heads of room temperature tensile specimens. The 1760°C (3200°F) annealed material exhibited a microstructure similar to the material annealed

Table 21A. Supplemental Tensile Data for ASTAR-1211C Rod Swaged and Annealed at Various Temperatures (SI Units)

Specimen Identification and Final Heat Treatment	Test Temp. (°C)	Yield Strength (MN/m^2)	Ultimate Strength (MN/m^2)	Elongation		Reduction in Area (%)
				Uniform (%)	Total (%)	
1-A-23-32	RT	715	869	17.9	21.3	54.2
Swaged at 1371°C	- 73	865	1007	16.3	18.5	41.3
Annealed 1 hr/1760°C	-129	957	1078	11.8	11.8	16.0
	1316	290	381	7.6	23.6	68.2
1-A-23-30/23	RT	686	802	21.6	26.0	62.2
Swaged at 1371°C	- 73	812	927	18.8	22.4	51.0
Annealed 1 hr/1649°C	-129	890	994	13.4	16.1	51.2
+ 1 hr/1260°C	1316	255	348	11.9	45.4	79.0
1-A-23-33/23	RT	646	776	19.9	22.9	49.1
Swaged at 1371°C	- 73	807	871	6.2	6.2	4.9
Annealed 1 hr/1815°C	-129	760	837	6.1	6.1	5.2
+ 1 hr/1260°C	1316	229	321	10.8	31.0	56.2
1-A-14-30/24	RT	690	731	19.4	24.0	52.6
Swaged at 1649°C	-129	841	942	11.1	18.7	30.4
Annealed 1 hr/1649°C	-196	966	1069	1.9	1.9	1.5
+ 1 hr/1316°C	1316	226	359	9.2	29.7	65.7

Strain Rate 0.05/min.

Table 21B. Supplemental Tensile Data for ASTAR-1211C Rod Swaged and Annealed at Various Temperatures

Specimen Identification and Final Heat Treatment	Test Temp. (°F)	Yield Strength (ksi)	Ultimate Strength (ksi)	Elongation		Reduction in Area (%)
				Uniform (%)	Total (%)	
1-A-23-32	RT	103.6	126.0	17.9	21.3	54.2
Swaged at 2500°F	-100	125.4	146.0	16.3	18.5	41.3
Annealed 1 hr/3200°F	-200	138.7	156.2	11.8	11.8	16.0
	2400	42.1	55.2	7.6	23.6	68.2
1-A-23-30/23	RT	99.5	116.2	21.6	26.0	62.2
Swaged at 2500°F	-100	117.7	134.3	18.8	22.4	51.0
Annealed 1 hr/3000°F	-200	129.0	144.0	13.4	16.1	51.2
+ 1 hr/2300°F	2400	36.9	50.4	11.9	45.4	79.0
1-A-23-33/23	RT	93.6	112.5	19.9	22.9	49.1
Swaged at 2500°F	-100	116.9	126.3	6.2	6.2	4.9
Annealed 1 hr/3300°F	-200	110.2	121.3	6.1	6.1	5.2
+ 1 hr/2300°F	2400	33.2	46.6	10.8	31.0	56.2
1-A-14-30/24	RT	101.5	123.8	19.4	24.0	52.6
Swaged at 3000°F	-200	142.3	159.7	11.1	18.7	30.4
Annealed 1 hr/3000°F	-320	163.6	181.0	1.9	1.9	1.5
+ 1 hr/2400°F	2400	37.7	52.1	9.2	29.7	65.7

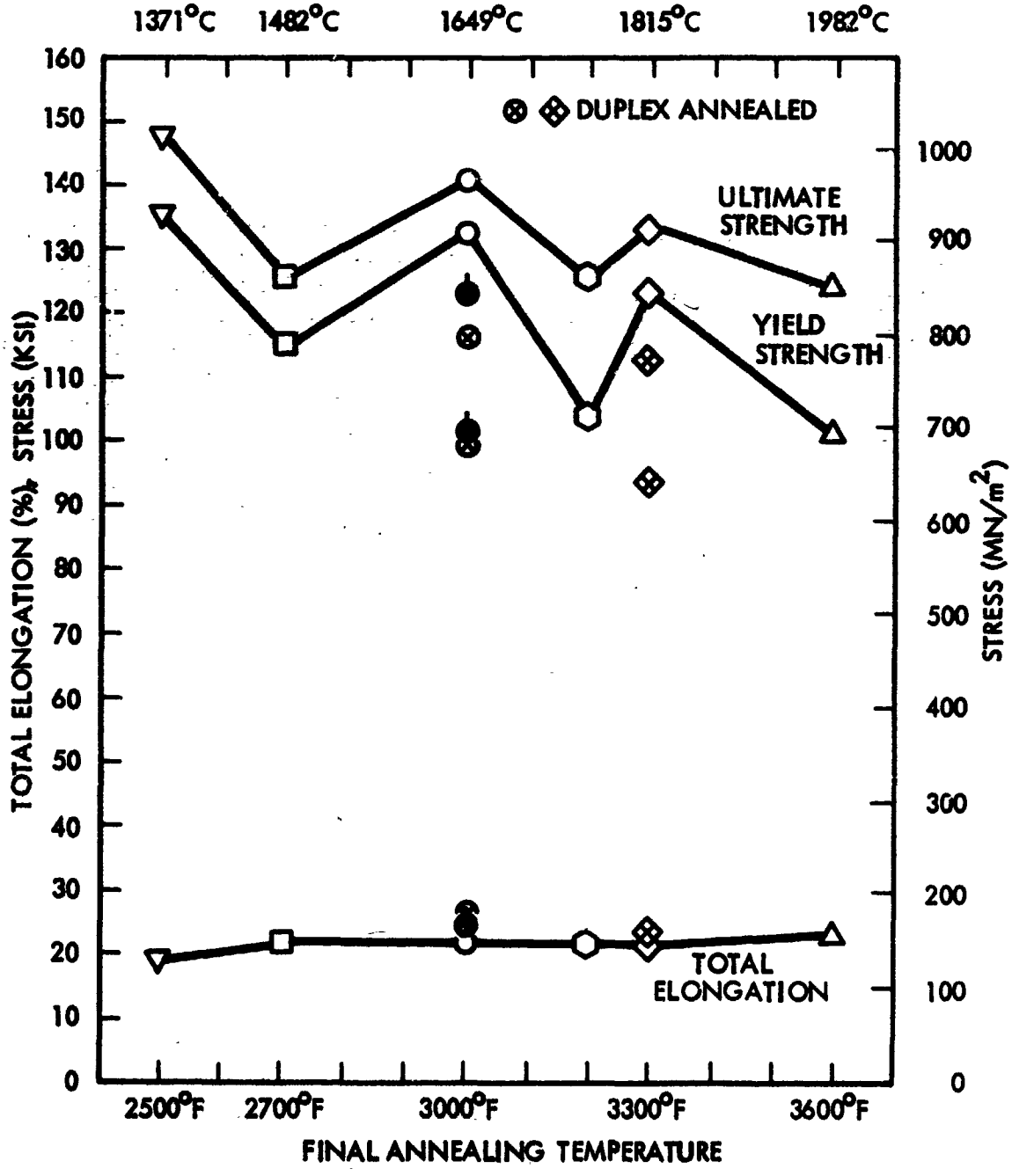

Figure 50. Room Temperature Tensile Properties of ASTAR-1211C Swaged at 1371°C (2500°F) and Annealed at Various Temperatures

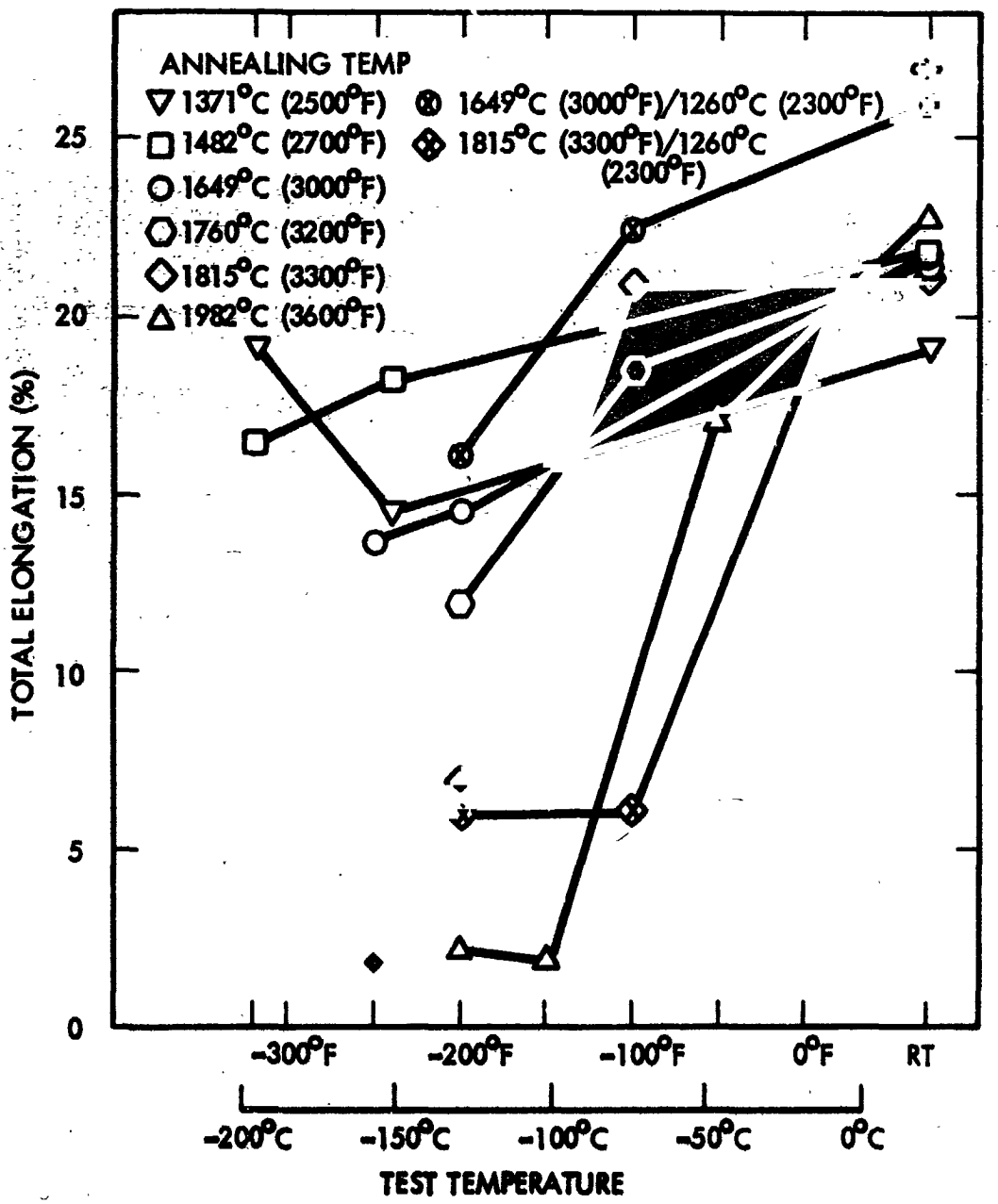

Figure 51. Low Temperature Tensile Elongation of ASTAR-1211C Swaged at 1371°C (2500°F)

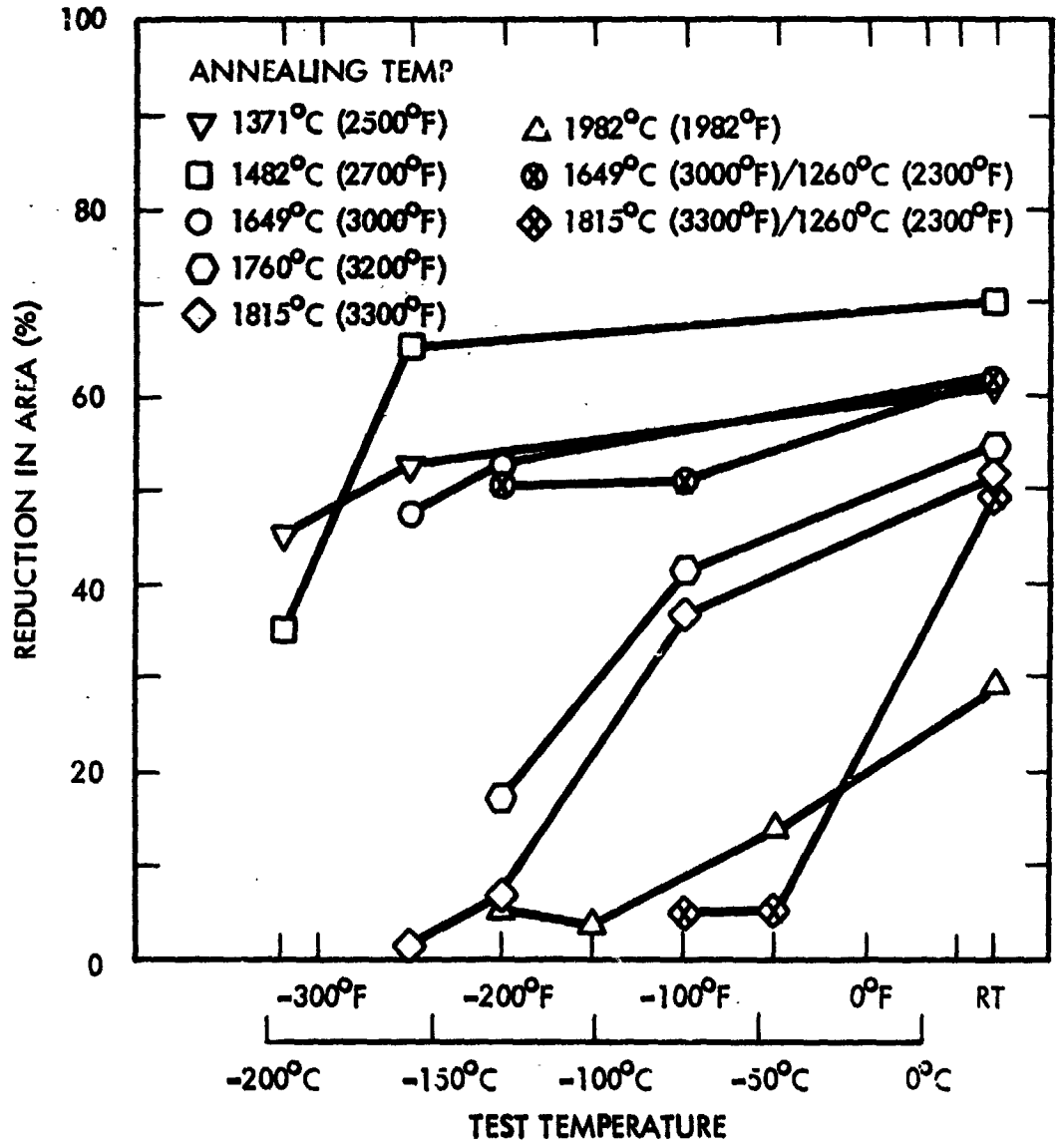

Figure 52. Low Temperature Reduction in Area of ASTAR-1211C Swaged at 1371°C (2500°F)

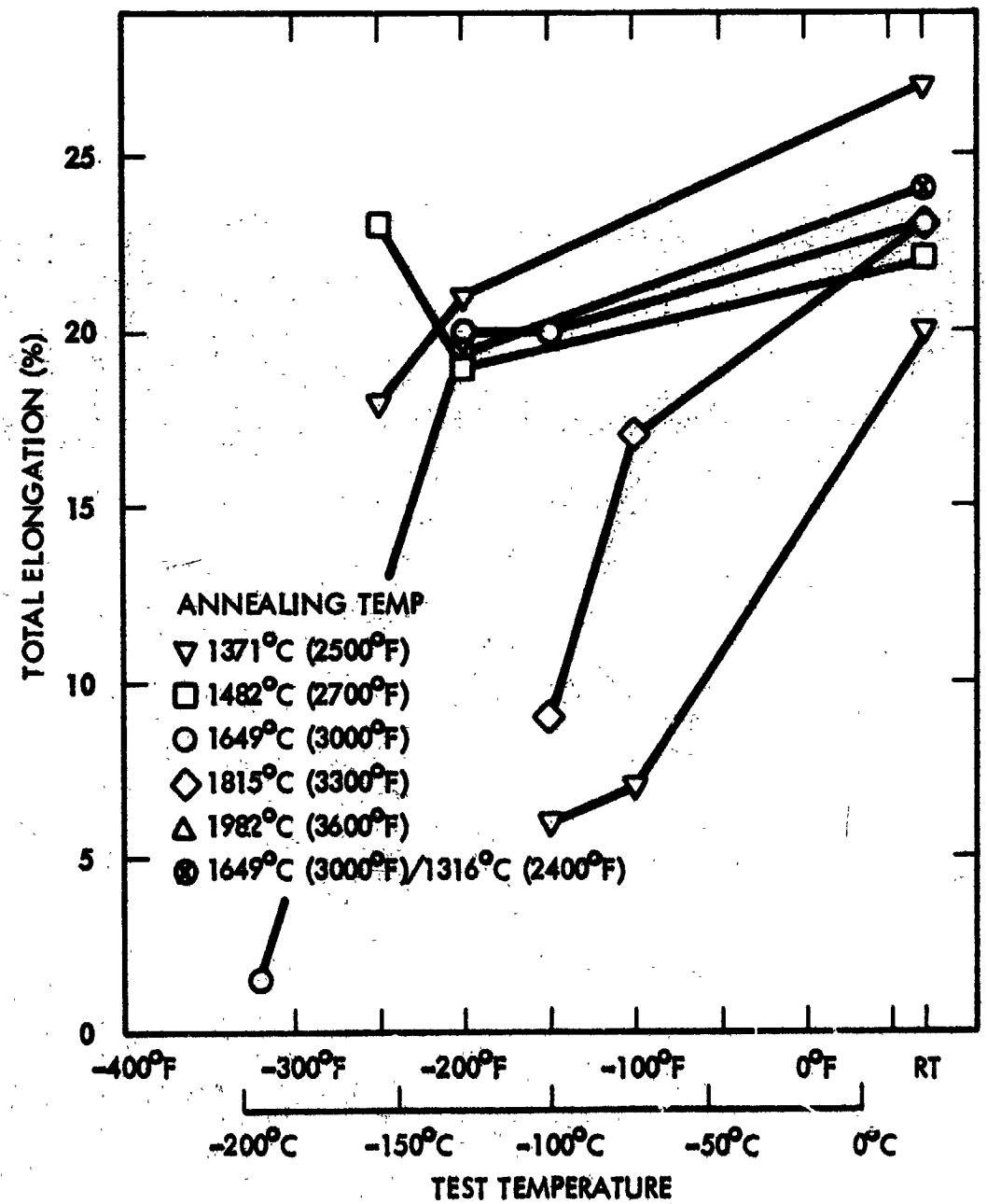

Figure 53. Low Temperature Tensile Elongation of ASTAR-1211C Swaged at 1649°C (3000°F)

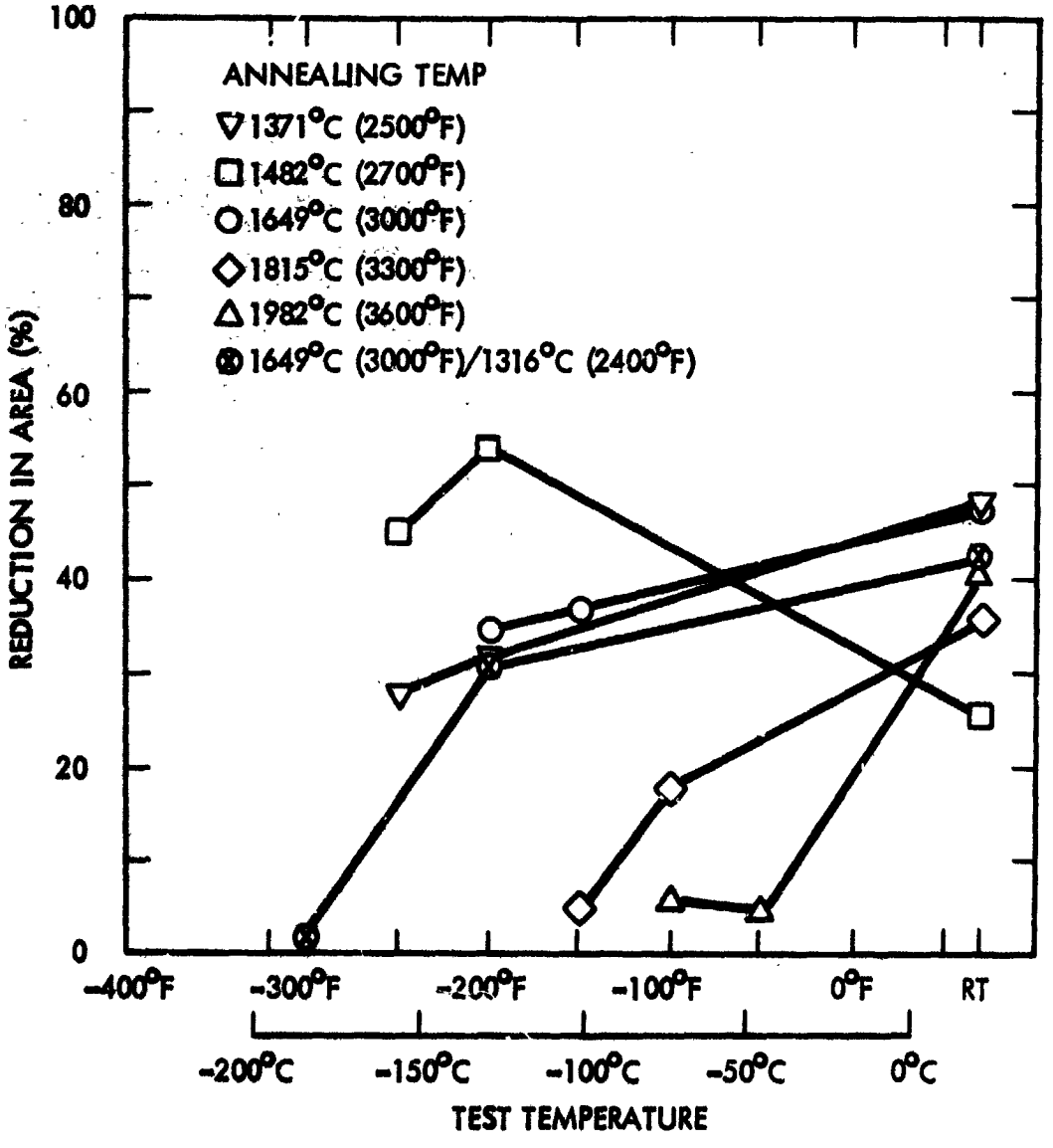

Figure 54. Reduction in Area of ASTAR-1211C Swaged at 1649°C (3000°F)

ASTAR-1211C
Swaged at 1371°C (2500°F)
Annealed 1 hr/1769°C (3200°F)

500X DPH 308

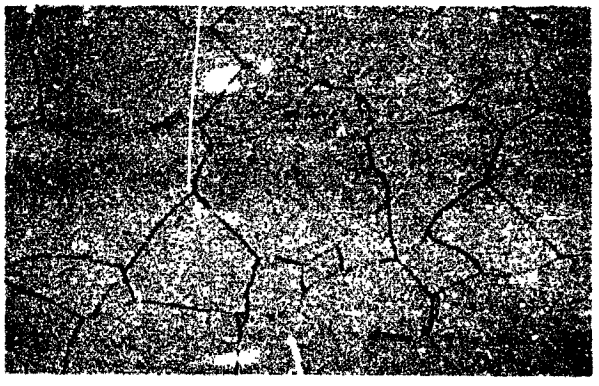

ASTAR-1211C
Swaged at 1371°C (2500°F)
Annealed 1 hr/1649°C (3000°F)
1 hr at 1260°C (2300°F)

500X DPH 271

ASTAR-1211C
Swaged at 1371°C (2500°F)
Annealed 1 hr/1815°C (3300°F)
1 hr at 1260°C (2300°F)

500X DPH 280

Figure 55. Microstructures of ASTAR-1211C Swaged at 1371°C (2500°F) and Annealed at Various Temperatures

at 1815°C (3300°F) shown in Figure 26D. Both the grain boundary and grain matrix were decorated with a fine precipitate which occurred during cooling. The duplex annealed material exhibited a fairly clean matrix with large discontinuous precipitate confined to the grain boundary. The second lower temperature anneal, 1260°C (2300°F) was below the carbon solvus where precipitation of the Ta_2C phase occurs preferentially at the grain boundary. The removal of carbon from solid solution was responsible for the lowering of the room temperature hardness.

4.2.4.2 Elevated Temperature Properties

The 1316°C (2400°F) tensile data of the supplemental test program are plotted in Figure 56 along with data for the five initial final anneal conditions. The 1760°C (3200°F) annealed material data fall within a reasonable scatter band with respect to the strength of the five initial annealing conditions. Fracture elongation values for the duplex annealed materials were also higher than the single temperature annealed material. Considering that the 1260°C (2300°F) secondary annealing temperature was below the actual test temperature, a significant difference in mechanical properties would not be expected unless a time dependent structural change was occurring within the alloys during the secondary anneal. Metallographically, it was noted that massive carbides at the grain boundaries were promoted by such heat treatment. These results indicate that the disposition of carbon in these alloys has a significant effect on short time mechanical properties.

4.2.4.3 Creep Properties

The duplex annealed materials were creep tested using the multi-temperature, multi-load technique previously described. Creep data are listed in Table 22. A Larson-Miller plot of one percent life based on secondary creep rate is presented in Figure 57. A reference curve for single annealed material, 1649°C (3000°F), was included for reference. The secondary anneal, which was above the initial creep test temperature, 1260°C (2300°F) and

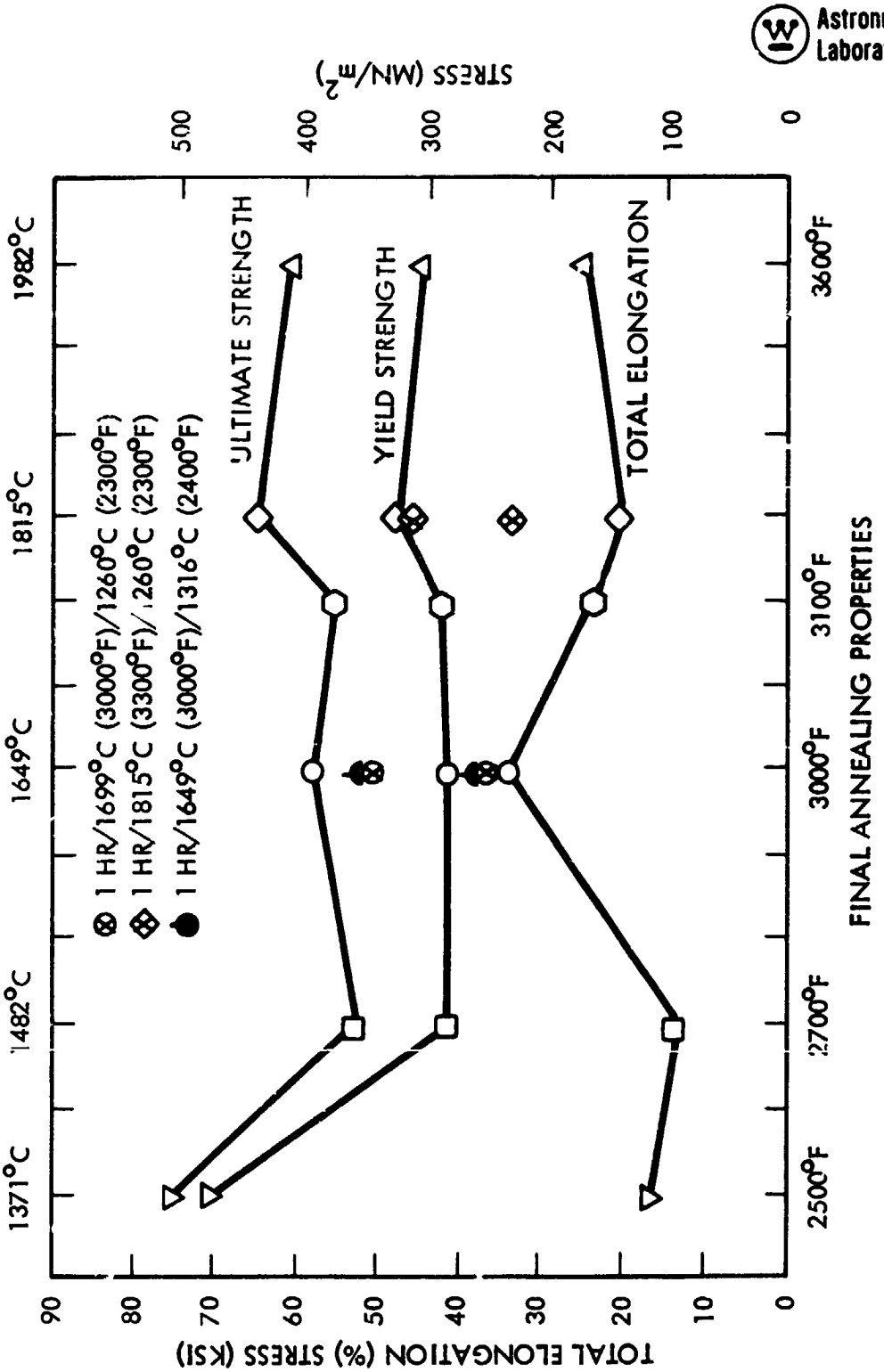

Figure 56. 1316°C (2400°F) Tensile Properties of ASTAR-1211C Swaged 1371°C (2500°F) and Annealed at Various Temperatures

Table 22. Supplemental Creep Data for ASTAR-1211C Rod Swaged and Annealed at Various Temperatures

Specimen Identification and Final Annealed Condition	Test Temperature		Stress Level		Secondary Creep Time (hrs.)	Secondary Creep Strain (%)	Secondary Creep Rate (%/hr.)	Time to 1% Strain (hrs.)	P $T_{Ro}(15+\log t)\times 10^{-3}$
	(°C)	(°F)	(MN/m^2)	(ksi)					
1-A-13-27	1093	2000	276	40	168	0.15	0.00089	1120	44.3
Swaged at 1649°C(3000°F)	1204	2200	207	30	138	1.52	0.01100	91	45.1
Annealed 1 hr/1482°C	1204	2200	138	20	145	0.40	0.00276	362	46.6
(2700°F)	1260	2300	104	15	161	0.90	0.00560	178	47.6
1-A-23-32	1093	2000	276	40	256	0.34	0.00133	753	43.9
Swaged at 1371°C(2500°F)	1204	2200	207	30	155	0.25	0.00161	620	47.3
Annealed 1 hr/1750°C	1316	2400	138	20	136	0.45	0.00330	320	49.8
(3200°F)	1316	2400	104	15	185	0.21	0.00114	880	51.4
1-A-23-30/23	1093	2000	276	40	89	0.70	0.00787	127	42.1
Swaged at 1371°C(2500°F)	1093	2000	207	30	198	0.00	--	--	--
Annealed 1 hr/1649°C	1149	2100	207	30	208	0.29	0.00139	718	45.7
(3000°F)+1 hr/1260°C(2300°F)	1260	2300	138	20	113	0.50	0.00442	226	47.9
	1260	2300	104	15	65	0.11	0.00169	598	49.0
1-A-23-33/23	1038	1900	276	40	137	0.05	0.00036	2740	43.6
Swaged at 1371°C(2500°F)	1093	2000	276	40	163	0.39	0.00240	418	43.3
Annealed 1 hr/1815°C	1204	2200	207	30	208	0.43	0.00207	483	47.0
(3300°F)+1 hr/1260°C(2300°F)	1316	2400	138	20	136	0.53	0.00390	257	49.8
	1316	2400	104	15	304	0.33	0.00108	922	51.4
1-A-14-30/24	1038	1900	276	40	283	0.18	0.00064	1570	43.0
Swaged at 1649°C(3000°F)	1149	2100	207	30	211	0.11	0.00052	1920	46.7
Annealed 1 hr/1649°C	1260	2300	138	20	136	0.28	0.00208	485	48.8
(3000°F)+1 hr/1316°C(2400°F)	1260	2300	104	15	328	0.21	0.00064	1560	50.2

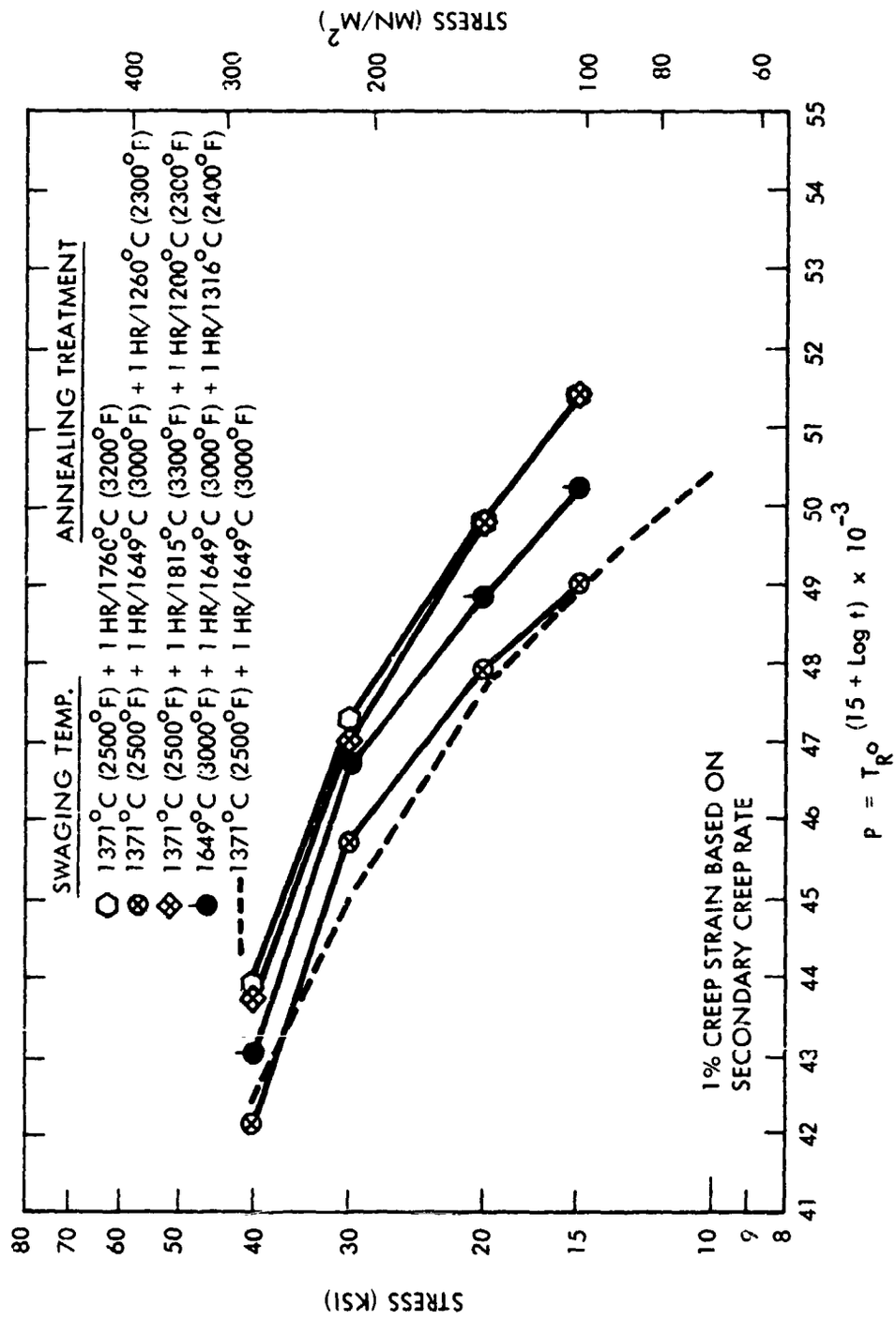

Figure 57. Supplemental Creep Data for ASTAR-1211C Rod Swaged and Annealed at Various Temperatures

1316°C (2400°F) vs 1093°C (2000°F), appears not to have had any effect on the creep behavior. The primary or highest annealing temperature appears to control creep properties. Grain size appears to have a more pronounced influence on creep behavior than disposition of carbon in matrix.

4.2.5 Selection of Optimum Processing Schedule

The mechanical property data for both alloys were reviewed with the objective of selecting an optimum working and annealing schedule. The optimized thermomechanical process was selected on the basis of the best compromise between low temperature ductility and high temperature creep strength. Practical aspects, such as available vacuum annealing facilities for large sections, were also considered.

The following general observations were highly influential in the selection of the optimum process.

- Material swaged at 1371°C (2500°F) required a minimum annealing temperature of 1649°C (3000°F) in order to produce a stable, uniform, recrystallized grain size. Material swaged at 1649°C (3000°F) exhibited a stable recrystallized grain size prior to final annealing treatment. Because of the difference in microstructure produced by the swaging process, structure sensitive properties were affected at the lower final annealing temperatures, and difference in mechanical behavior diminished as final annealing temperature increased producing similar microstructures in both materials.
- Creep resistance tended to be better for material swaged at the higher temperature.
- Low temperature ductility as measured by ductile-to-brittle transition temperature is favored by small grain size produced by final annealing temperatures below 1649°C (3000°F).

- Creep resistance is favored by large grain size produced by final annealing temperatures of 1649°C (3000°F) and above.
- The economics of materials processing favors cold working of tantalum alloys over hot working.

On the basis of the above mentioned observations, the processing schedule selected for both ASTAR-1211C and ASTAR-1511C, consisted of swaging at 1371°C (2500°F) followed by a final anneal of 1 hour at 1649° C (3000°F).

4.3 DEVELOPMENT OF MECHANICAL PROPERTY DATA

The final portion of this task was devoted to developing mechanical and physical property data for both alloys, ASTAR-1211C and ASTAR-1511C, processed by the standard processing schedule developed in the prior section of this task. The data developed under this task portion are outlined in Figure 22. Elevated temperature tensile data from 316°C (600°F) to 1649°C (3000°F) in 167°C (300°F) increments were determined. An ultrasonic technique was used to determine modulus data to 871°C (1600°F) from which Poisson's Ratio was determined. The ductile-to-brittle transition temperatures, DBTT, for both alloys were determined by impact testing and by smooth and notched tension tests. Finally, single-load, single temperature creep tests were performed to confirm the creep properties of the alloys processed by the standard processing schedule.

To provide the material for this task, extruded bar stock of both alloys, which had been reserved, was processed to 10 mm (3/8 inch) diameter swaged bar stock. The material was swaged from a nominal 25.4 mm (1 inch) diameter extruded bar stock clad in a thin layer of molybdenum. The bars were swaged in approximately 10 percent reductions at 1371°C (2500°F) to the final size. Appropriate test specimens were machined from the swaged rod prior to the final heat treatment of 1 hour at 1649°C (3000°F).

4.3.1 Elevated Temperature Tensile Properties

Tensile property data for ASTAR-1211C and ASTAR-1511C at elevated temperatures are given in Table 23. Tensile properties as a function of temperature are shown in Figure 58. The strain-aging peak in ultimate strength in the temperature range 549°C (1200°F) to 1149°C (2100°F) was evident. This behavior is typical for tantalum base alloys which contain an intentional addition of carbon.

4.3.2 Elastic Properties

Elastic properties of ASTAR-1211C and ASTAR-1511C were determined in the temperature range of room temperature to 877°C (1609°F) in 111°C (200°F) increments. Shear and Young's modulii were determined by Panametrics, a subsidiary of Esterline Corporation of Waltham, Mass. The determinations were made using an ultrasonic thin-line technique developed by Panametrics[7]. Recrystallized samples 3.2 mm (0.125 inch) in diameter by 7.62 cm (3 inches) long were used. Elevated temperature tests were conducted in vacua. Results are given in Table 24. Poisson's ratio was calculated from the modulii data according to the relationship:

$$\mu = \frac{E}{2G} - 1$$

where

μ = Poisson's Ratio
E = Young's Modulus
G = Shear Modulus

The elastic properties are plotted as a function of temperature in Figure 59.

Table 23A. Elevated Temperature Tensile Properties of ASTAR-1211C and ASTAR-1511C Produced by the Standard Process (SI Units)

Test Temperature (°C)	Yield Strength (MN/m^2)	Ultimate Strength (MN/m^2)	Elongation		Reduction in Area (%)
			Uniform (%)	Total (%)	
ASTAR-1211C					
316	-	-	-	-	-
649	477	724	13.0	17.6	61.5
816	361	724	13.0	16.6	58.1
982	334	638	15.2	19.4	64.3
1149	337	564	10.9	19.0	67.8
1316	268	359	8.0	38.9	73.4
1482	250	286	4.5	30.1	39.6
1649	199	204	2.3	54.7	72.3
ASTAR-1511C					
316	676	733	9.0	15.2	66.3
649	582	788	9.9	13.9	52.5
816	457	800	15.5	17.5	58.2
982	368	745	18.9	21.3	58.8
1149	359	699	18.8	23.3	62.1
1316	288	403	9.4	28.6	61.5
1482	274	331	5.3	36.8	58.0
1649	242	244	0.7	46.2	49.2

Standard Process - Swaged at 1371°C (2500°F)/final anneal 1 hour/ 1649°C (3000°F)

Table 23B. Elevated Temperature Tensile Properties of ASTAR-1211C and ASTAR-1511C Produced by the Standard Process

Test Temperature (°F)	Yield Strength (ksi)	Ultimate Strength (ksi)	Elongation		Reduction in Area (%)
			Uniform (%)	Total (%)	
ASTAR-1211C					
600	-	-	-	-	-
1200	69.2	105.9	13.5	17.6	61.5
1500	52.3	104.9	13.0	16.6	58.1
1800	48.4	92.4	15.2	19.4	64.3
2100	48.8	81.7	10.9	19.0	67.8
2400	38.8	52.1	8.0	38.9	73.4
2700	36.2	41.4	4.5	30.1	39.6
3000	28.9	29.5	2.3	54.7	72.3
ASTAR-1511C					
600	98.0	106.2	9.0	15.2	66.3
1200	84.3	114.2	9.9	13.9	52.5
1500	66.3	115.9	15.5	17.5	58.2
1800	53.3	108.0	18.9	21.3	58.8
2100	52.1	101.3	18.8	23.3	62.1
2400	41.8	58.4	9.4	28.6	61.5
2700	39.7	48.0	5.3	36.8	58.0
3000	35.0	35.4	0.7	46.2	49.2

Standard Process - Swaged at 1371°C (2500°F)/final anneal 1 hour/ 1649°C (3000°F)

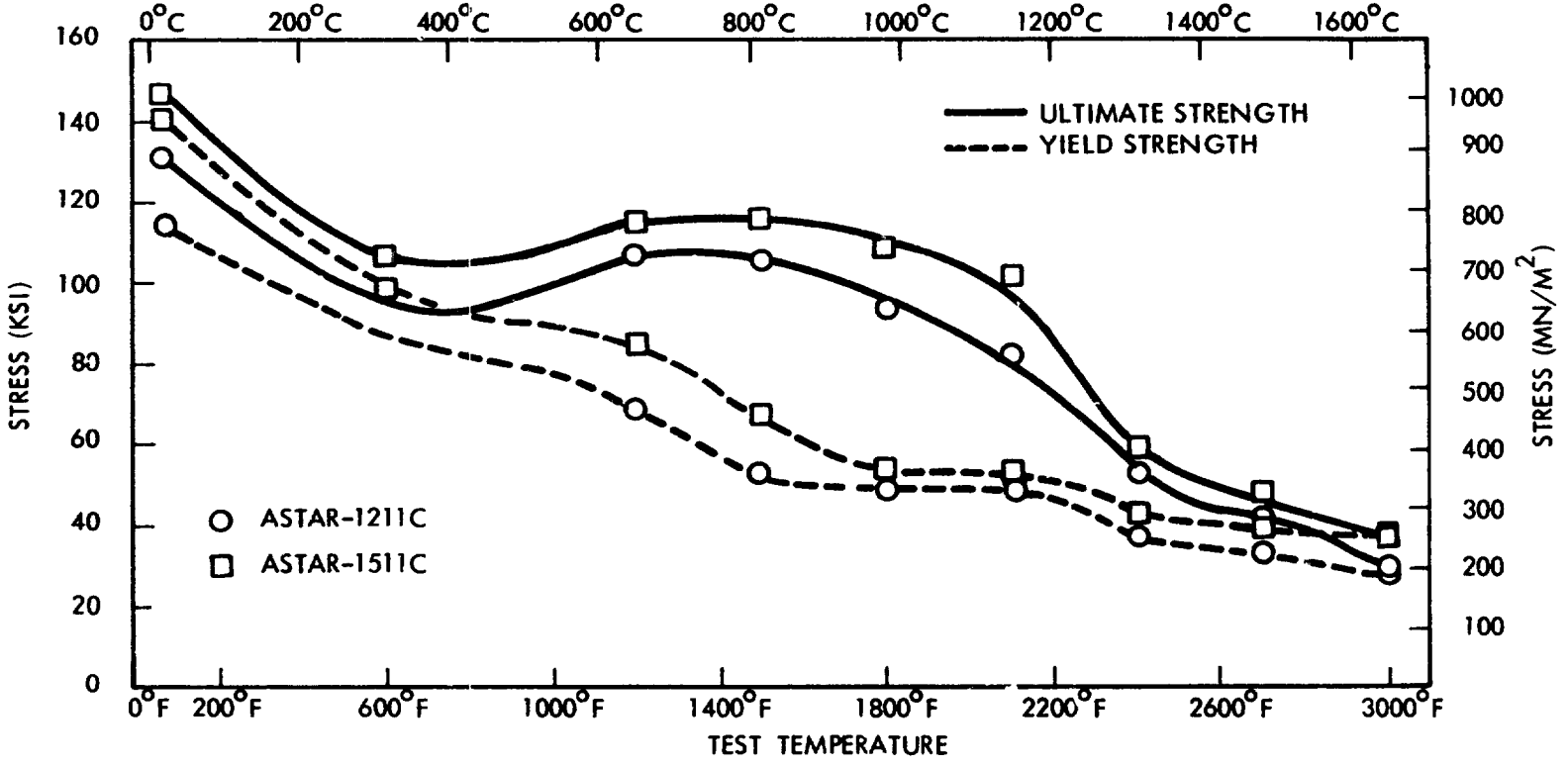

Figure 58. Elevated Temperature Tensile Properties of ASTAR-1211C and ASTAR-1511C Produced by the Standard Process

Table 24. Elastic Properties of ASTAR-1211C and ASTAR-1511C

Temperature		Young's Modulus		Shear Modulus		Poisson's Ratio
(°C)	(°F)	(GN/m^2)	(psi x 10^6)	(GN/m^2)	(psi x 10^6)	
ASTAR-1211C						
RT	RT	196.1	28.42	74.7	10.82	0.313
93	200	195.3	28.30	74.0	10.72	0.319
208	407	193.1	27.98	73.3	10.63	0.316
315	598	191.8	27.80	72.7	10.54	0.318
438	821	190.1	27.55	72.0	10.44	0.319
543	1010	188.8	27.37	71.6	10.37	0.319
651	1204	187.2	27.13	70.9	10.28	0.319
763	1405	185.1	26.83	70.5	10.22	0.312
877	1609	184.0	26.66	70.1	10.16	0.312
ASTAR-1511C						
RT	RT	199.1	28.85	76.8	11.13	0.296
82	179	198.2	28.72	76.1	11.03	0.302
191	376	196.4	28.47	75.7	10.97	0.297
299	570	195.1	28.28	75.3	10.91	0.296
421	791	193.4	28.03	74.7	10.83	0.294
527	980	192.0	27.83	74.1	10.74	0.295
635	1175	190.9	27.67	73.6	10.66	0.298
745	1374	189.7	27.49	72.9	10.57	0.300
858	1576	188.4	27.30	72.5	10.51	0.298

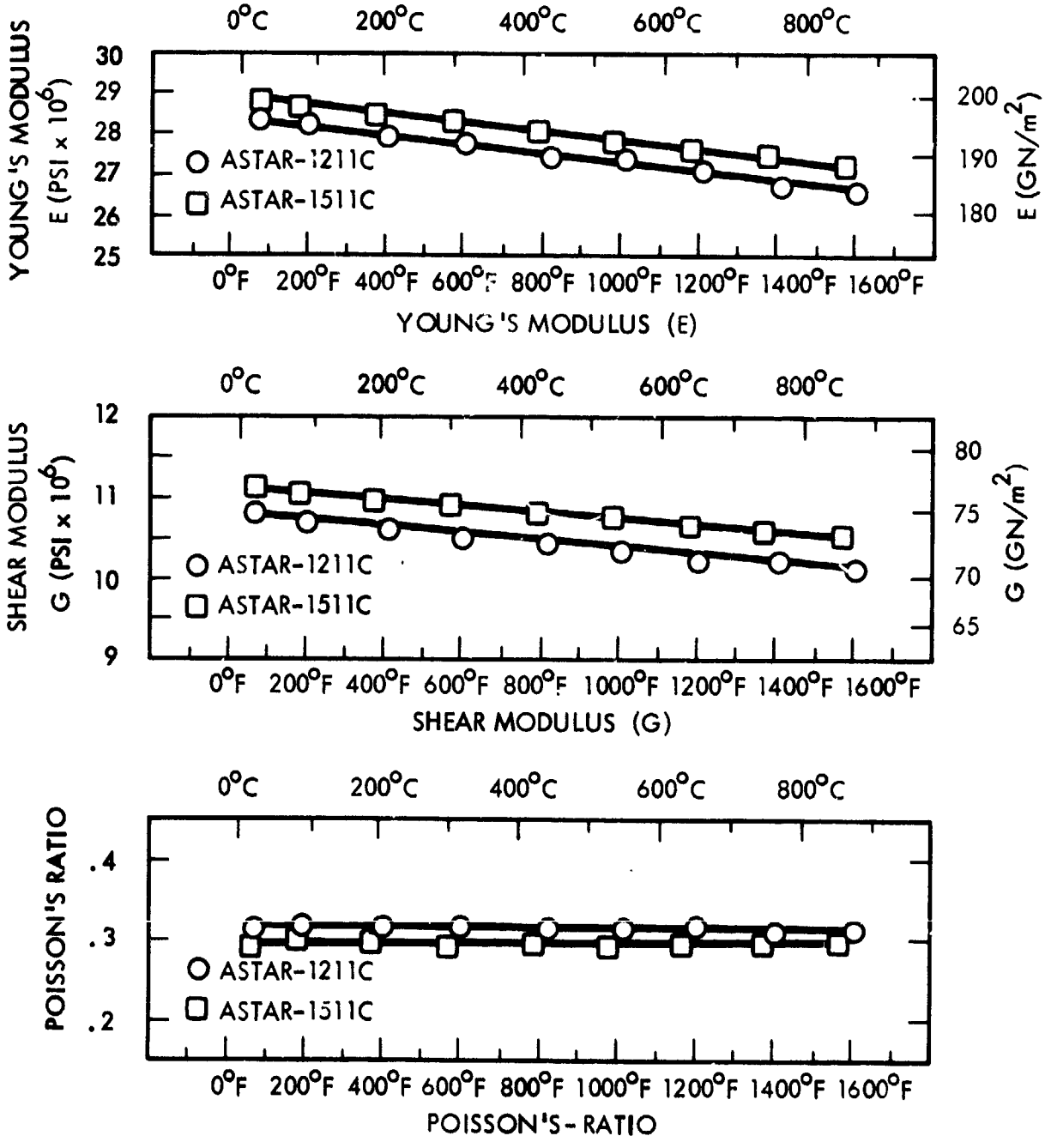

Figure 59. Elastic Properties of ASTAR-1211C and ASTAR-1511C

4.3.3 Ductile-to-Brittle Transition Temperature Behavior

The ductile-to-brittle behavior of ASTAR-1211C and ASTAR-1511C processed by the standard process were determined by impact testing and by smooth and notched tension tests.

4.3.3.1 Impact Properties

Impact tests of ASTAR-1211C and ASTAR-1511C were conducted over a temperature range from room temperature to 538°C (1000° F). The notched specimens were cylindrical in shape with a major diameter of 5.7 mm (0.225 inch) and a minor diameter of 3.8 mm (0.150 inch). The specimens were 28.6 mm (1.125 inches) long. They were machined with an included angle of 0.78 rad (45°) with a root radius of 12.7 μm (0.005 inch). The stress concentration factor, K_t, was 3.8. The specimens were tested in a Baldwin Impact tester of Bell Telephone Laboratory design for miniature specimens. The machine had a capacity of 21.7 J (192 inch-pounds). The specimens were heated in place with a hot-air torch until an attached shielded thermocouple indicated the desired test temperature. The temperature was stabilized by holding at temperature for several minutes, then the test was conducted. Test results are recorded in Table 25. The data are plotted in Figure 60.

The plot of absorbed energy for both alloys does not exhibit classical impact behavior. Only a gradual increase in absorbed energy is shown; no abrupt transition to ductile behavior was noted.

Examination of the fractured surfaces by optical microscopy revealed little or no evidence of ductile fracture behavior, even at 538°C (1000°F). SEM micrographs of the fracture surfaces are shown in Figure 61. Figures 61A, B, and C show fracture surfaces of ASTAR-1211C. In Figure 61D, the fracture surface of ASTAR-1511C tested at 538°C (1000°F) is shown. In all cases, classical surface features indicating brittle cleavage type failure is evident. The transition to ductile impact behavior may reside at higher temperatures for both alloys.

Table 25. Impact Test Results for Standard Processed ASTAR-1211C and ASTAR-1511C

Test Temperature		Absorbed Energy			
		ASTAR-1211C		ASTAR-1511C	
(°C)	(°F)	(Joules)	(in-lbs.)	(Joules)	(in-lbs.)
RT	RT	2.0	17.8	1.1	9.6
260	500	4.4	38.4	-	-
316	600	-	-	3.2	28.8
427	800	6.6	58.6	-	-
538	1000	10.0	89.3	4.4	38.4

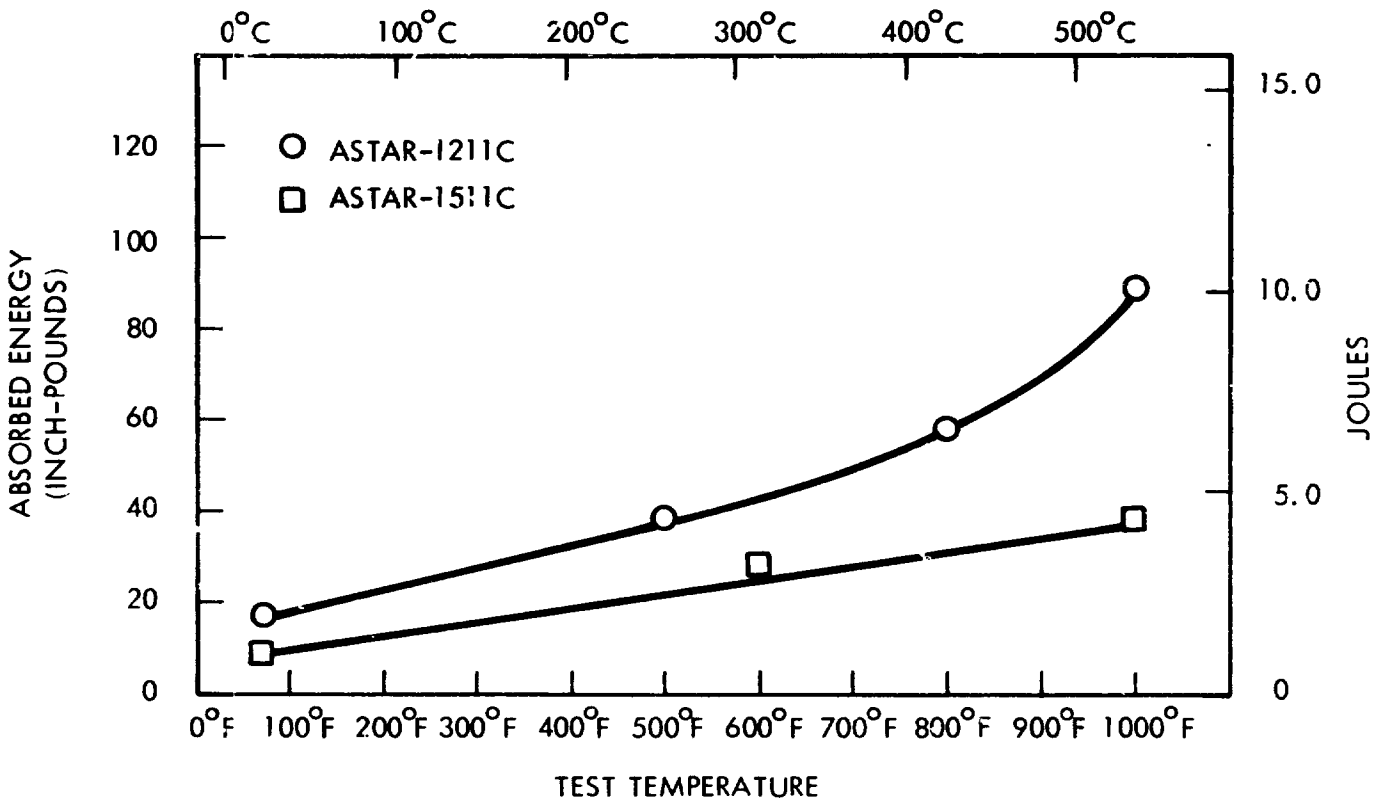

Figure 60. Impact Data for Standard Processed ASTAR-1211C and ASTAR-1511C

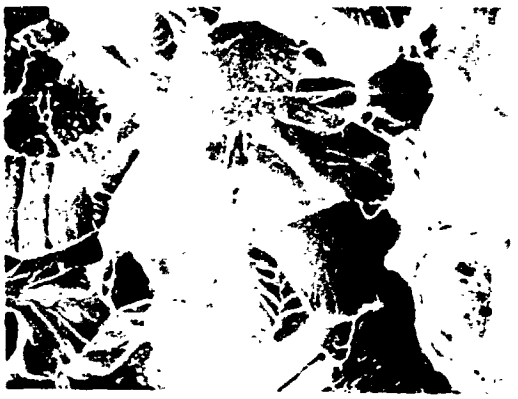

575X

A. ASTAR-1211C - Room Temperature

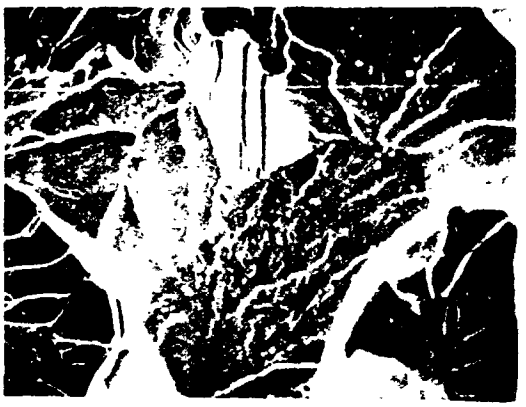

1200X

B. ASTAR-1211C - 427°C (800°F)

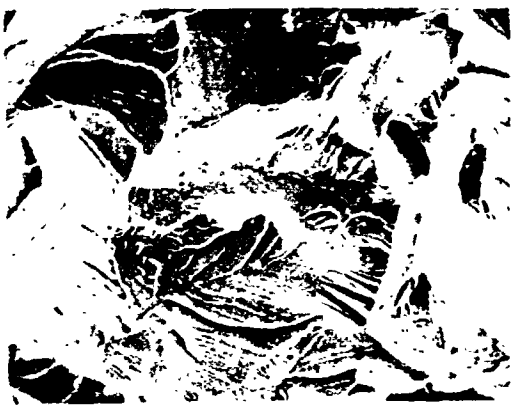

575X

C. ASTAR-1211C - 538°C (1000°F)

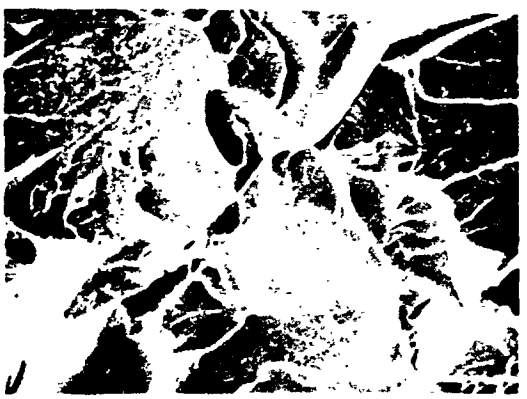

1200X

D. ASTAR-1511C - 538°C (1000°F)

Figure 61. SEM Micrographs of Fractured ASTAR-1211C and ASTAR-1511C Impact Specimens

4.3.3.2 Low Temperature Tensile Properties

Low temperature ductile behavior of ASTAR-1211C and ASTAR-1511C was determined in tension for smooth and notched specimens. The notched specimen had a major diameter of 4.6 mm (0.180 inch) and a minor diameter of 3.2 mm (0.125 inch). The notch angle was 1.02 rad (60°) with a root radius of 17.8 μm (0.007 inch) giving a stress concentration factor, K_t, of 3.1.

Tensile tests of both smooth and notched specimens were conducted at the same temperatures over the range room temperature to -196°C (-320°F). The test results are tabulated in Table 26. In Figure 62, total elongation and reduction in area for unnotched tests are plotted as a function of test temperature. ASTAR-1211C exhibited a lower transition-temperature to brittle behavior compared to ASTAR-1511C. Th· higher alloy content in ASTAR-1511C was responsible for the higher DBTT in ASTAR-1511C. This behavior was not unexpected. The notched-unnotched strength ratios are given in Table 27.

The notched-unnotched ratio for both alloys was well over 1.0 at room temperature and in each case decreased as test temperature decreased. In neither case, did the ratio fall below 1.0 indicating a reasonable resistance to notch sensitivity for both alloys under the imposed test conditions.

4.3.4 Creep Properties

Confirmatory creep testing was conducted to determine the creep properties of ASTAR-1211C and ASTAR-1511C produced by the standard proces·. The purpose of the test program was to expand the data base with respect to creep behavior. Creep tests were conducted using a single-load, single temperature test procedure. The pertinent creep data are given in Table 28. The actual creep curves are shown in Figure 63 for ASTAR-1211C and in Figure 64 for ASTAR-1511C. A Larson-Miller plot of 1 percent creep as determined from the curves is shown in Figure 65.

Table 26. Low Temperature Tensile Properties of ASTAR-1211C and ASTAR-1511C Produced by the Standard Process

Test Temperature		Yield Strength		Ultimate Strength		Elongation		Reduction in Area (%)
(°C)	(°F)	(MN/m^2)	(ksi)	(MN/m^2)	(ksi)	Uniform (%)	Total (%)	
ASTAR-1211C								
RT	RT	789	114.3	900	130.5	13.2	29	58
RT*	RT*	-	-	1441	208.8	-	-	-
-73	-100	908	131.6	1027	148.9	11.8	25	51.3
-73*	-100*	-	-	1590	230.5	-	-	-
-129	-200	962	139.5	1134	164.4	15.8	25	49.0
-129*	-200*	-	-	1589	230.3	-	-	-
-157	-250	1094	158.5	1211	175.5	15.9	26	38.4
-157*	-250*	-	-	1432	207.5	-	-	-
-196	-320	1227	177.9	1327	192.3	7.3	9.0	8.7
-196*	-320*	-	-	1569	227.4	-	-	-
ASTAR-1511C								
RT	RT	969	140.5	1001	146.0	14.0	25	59.5
RT*	RT*	-	-	1551	224.8	-	-	-
-73	-100	1074	155.7	1136	164.7	13.9	22	53.3
-73*	-100*	-	-	1441	208.8	-	-	-
-129	-200	1163	168.6	1237	179.3	15.3	14	18.2
-129*	-200*	-	-	1487	215.5	-	-	-
-196	-320	1412	204.7	1437	208.3	2.4	3.0	3.6
-196*	-320*	-	-	1528	221.4	-	-	-

* Notched

Strain Rate 0.05/min; $K_t = 3.1$

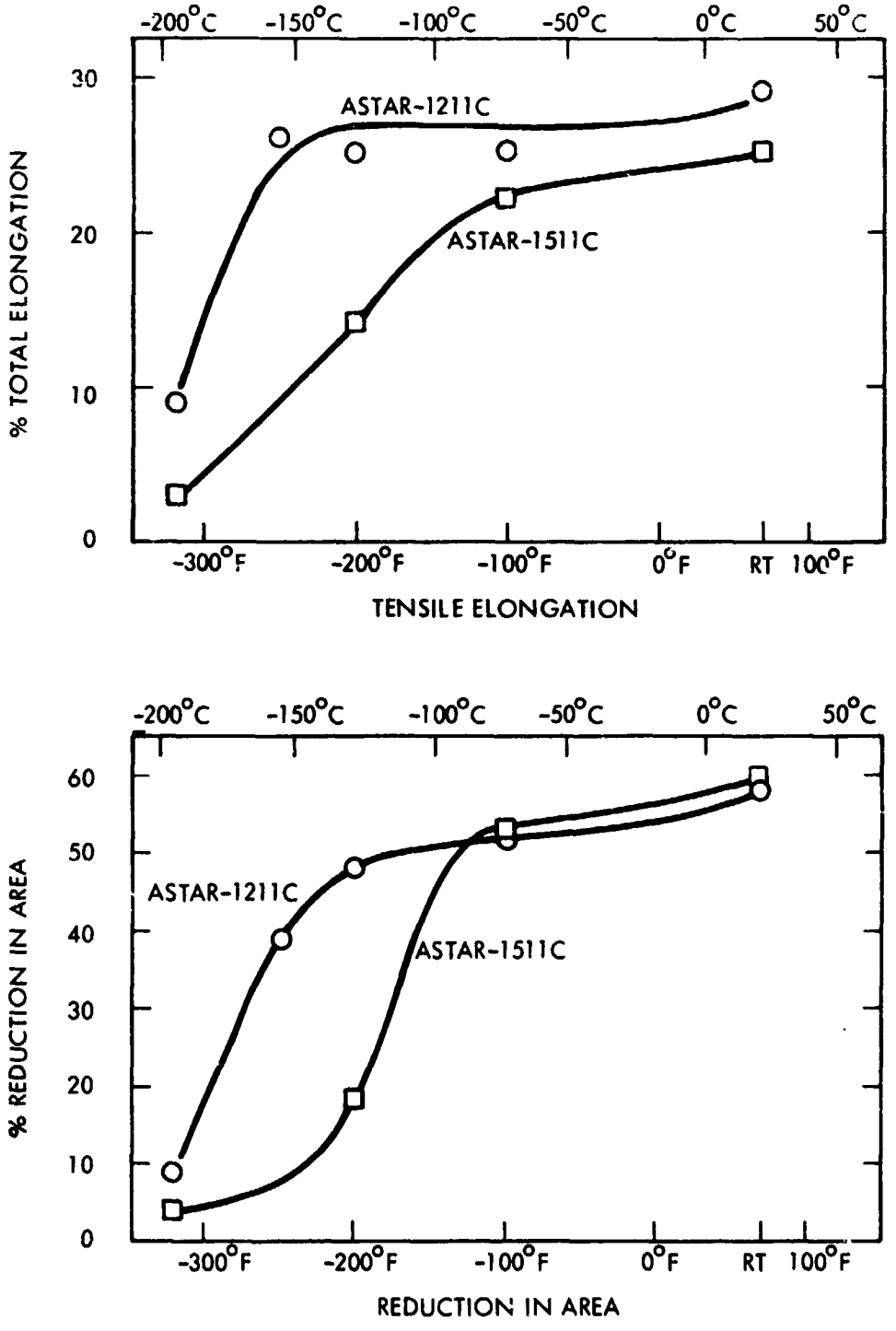

Figure 62. Smooth Bar DBTT for ASTAR-1211C and ASTAR-1511C Produced by the Standard Process

Table 27. Low Temperature Notched-Unnotched Strength Ratio of ASTAR-1211C and ASTAR-1511C

Test Temperature		Notched-Unnotched Strength Ratio	
(°C)	(°F)	ASTAR-1211C	ASTAR-1511C
RT	RT	1.60	1.54
- 73	-100	1.55	1.27
-129	-200	1.40	1.20
-157	-250	1.19	-
-196	-320	1.18	1.06

Table 28. Confirmatory Creep Data for Swaged ASTAR-1211C and ASTAR-1511C Rod

Specimen Identification	Test Temperature (°C)	Test Temperature (°F)	Stress Level (MN/m^2)	Stress Level (ksi)	Secondary Creep Time (hrs.)	Secondary Creep Strain (%)	Secondary Creep Rate (%/hr.)	Time to 1% Strain (hrs.)	P $T_{R^o}(15+\log t)\times 10^{-3}$
ASTAR-1211C									
1-B-11-30-A	1038	1900	276	40	792	.51	0.00064	1960	43.2
1-B-11-30-B	1149	2100	207	30	565	1.00	0.00177	565	45.4
1-B-11-30-C	1260	2300	138	20	585	1.00	0.00171	585	49.0
1-B-11-30-D	1316	2400	104	15	560	1.00	0.00172	560	50.8
ASTAR-1511C									
2-B-14-30-A	1093	2000	276	40	793	1.41	0.00178	575	43.7
2-B-14-30-B	1204	2200	207	30	764	3.39	0.00443	355	46.7
2-B-14-30-C	1316	2400	138	20	530	3.34	0.00630	275	49.9
2-B-14-30-D	1343	2450	104	15	500	4.34	0.00880	195	50.4

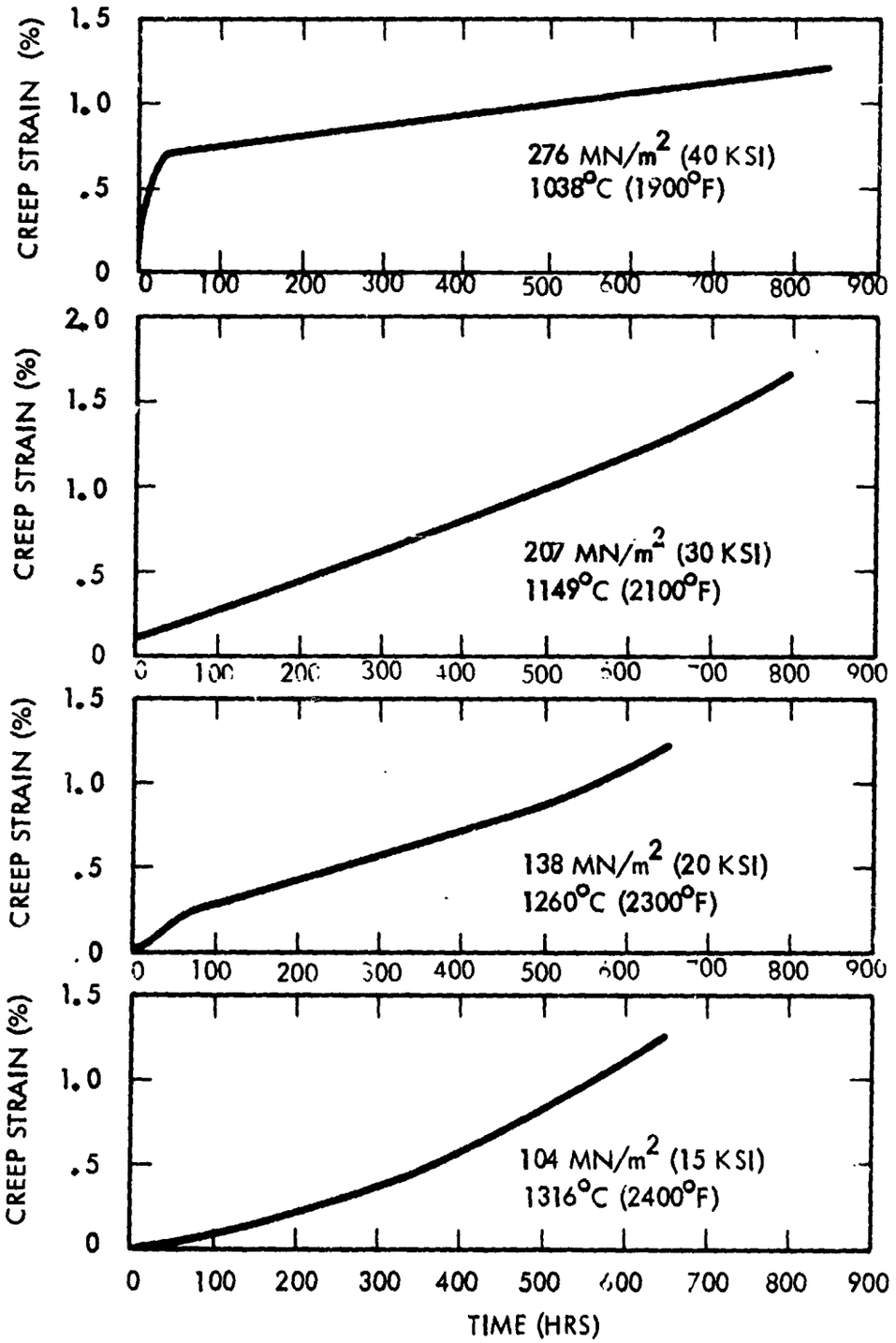

Figure 63. Creep Curves for ASTAR-1211C

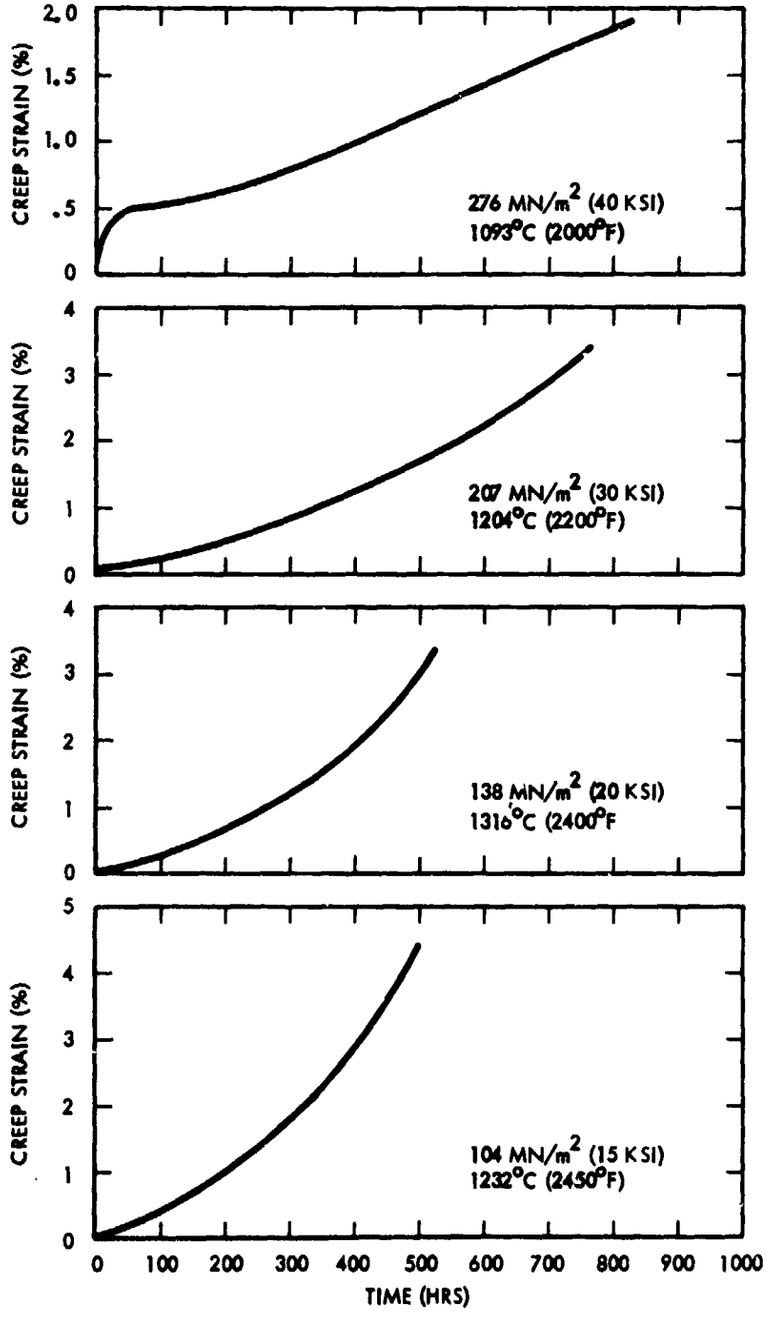

Figure 64. Creep Curves for ASTAR-1511C

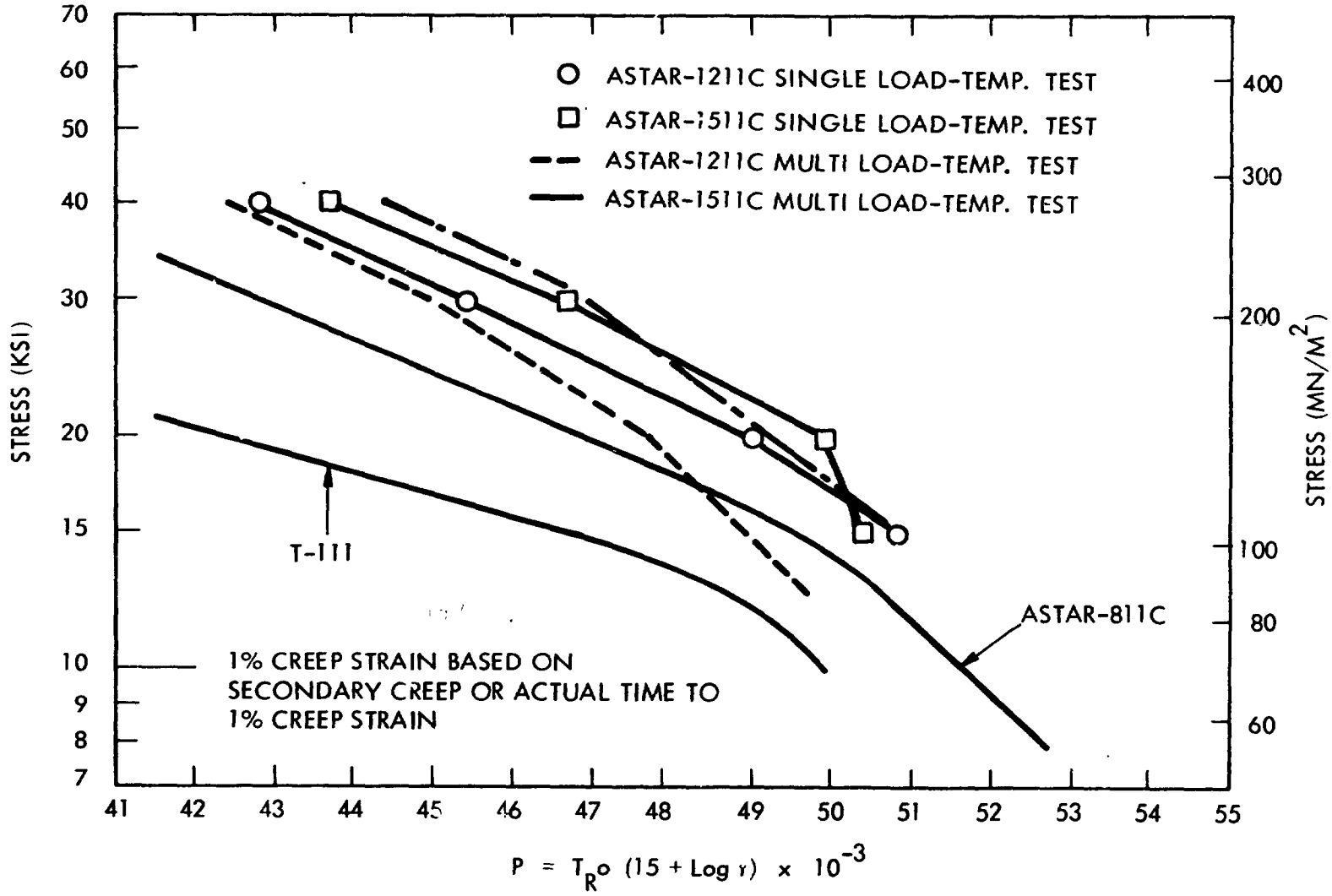

Figure 65. Comparison of Single Load-Temp and Multi Load-Temp Creep Data for Standard Processed ASTAR-1211C and ASTAR-1511C

The creep curve shapes are typical for tantalum base alloys and have been observed in prior programs[2,8]. In the high stress, low temperature test for each alloy, a primary or first stage was noted. In the case of ASTAR-1211C, a classical second stage occurred with a constant creep rate. In all other tests, the creep rate increased constantly with time. The Larson-Miller parameters were calculated from secondary creep rates, when available, or actual time to 1 percent creep, when a constant secondary creep rate was not in evidence.

Included on the Larson-Miller plot are data from the multi-load, multi-temperature tests conducted as part of the screening program in the prior section of this task. Also included under data for T-111 and ASTAR-811C, developed on prior programs[1,2].

The results of the single-load-temperature creep tests when compared to the results of the multi-load-temperature creep tests were as predicted. In the multi-load-temperature creep tests, prior strain apparently affected subsequent creep properties as temperature and load changes were made. Prior experience indicated that the multi-load-temperature test results would become conservative as the test proceeded[8]. The single-load-temperature data are more representative of the creep behavior of both alloys. Data for T-111 and ASTAR-811C were also included for comparison. The effect of the higher alloying addition of tungsten is quite evident at the lower temperatures and higher stress levels. The difference in creep properties diminished as test temperature increased. The difference was still quite significant at the 130 MN/m^2 (20 ksi) stress level. The 104 MN/m^2 (15 ksi) results for ASTAR-1511C appear to be anomolus. There was no rationale to explain the reversal of creep behavior at that stress level.

5.0 PROCESSING AND EVALUATION OF SHEET

The objective of this task was to produce and evaluate ASTAR-1211C and ASTAR-1511C sheet. The probability of rolling ASTAR-1511C to sheet was considered quite low due to the high solute content of the alloy. Initially, the processing schedule outlined in Figure 66 was used to produce ASTAR-1211C sheet. The same schedule with minor modifications was used to produce a limited quantity of ASTAR-1511C sheet.

The sheet evaluation program consisted primarily of characterization of weld deformation behavior in tension and bending. The evaluation schedule is outlined in Figure 67.

5.1 PROCESSING OF ASTAR-1211C AND ASTAR-1511C SHEET

5.1.1 Extrusion and Forging of ASTAR-1211C and ASTAR-1511C

In order to expedite the production of ASTAR-1211C sheet and gain information on the extrusion, forging, and rolling process, a pilot billet was processed to sheet initially to establish the working procedures. The pilot billet was produced from the second melt electrode stubs remaining from the casting of heat NASVF-1000A and B. The electrode stubs were cut longitudinally and fabricated into an electrode suitable for melting into a 7.1 cm (2.8 inch) diameter mold using AC power. The resulting ingot,designated NASVF-1000C, was machined to a 6.6 cm (2.6 inch) diameter by 12.7 cm (5 inch) long billet for extrusion. The pilot billet and subsequent ASTAR-1211C and ASTAR-1511C billets designated for utilization in this task were encapsulated in pressed and sintered molybdenum cans as shown in Figure 23 and described in Section 4.1.1. The canned billets were extruded to a sheet bar configuration at the Experimental Metals Processing Laboratory at Wright-Patterson AFB. Data for the extrusion of ASTAR-1211C and ASTAR-1511C billets to sheet bar are presented in Table 29. A typical sheet bar extrusion is shown in Figure 68. The extrusion temperature was 1649°C (3000°F), and the reduction ratios were nominal 4:1. The resulting extrusions were

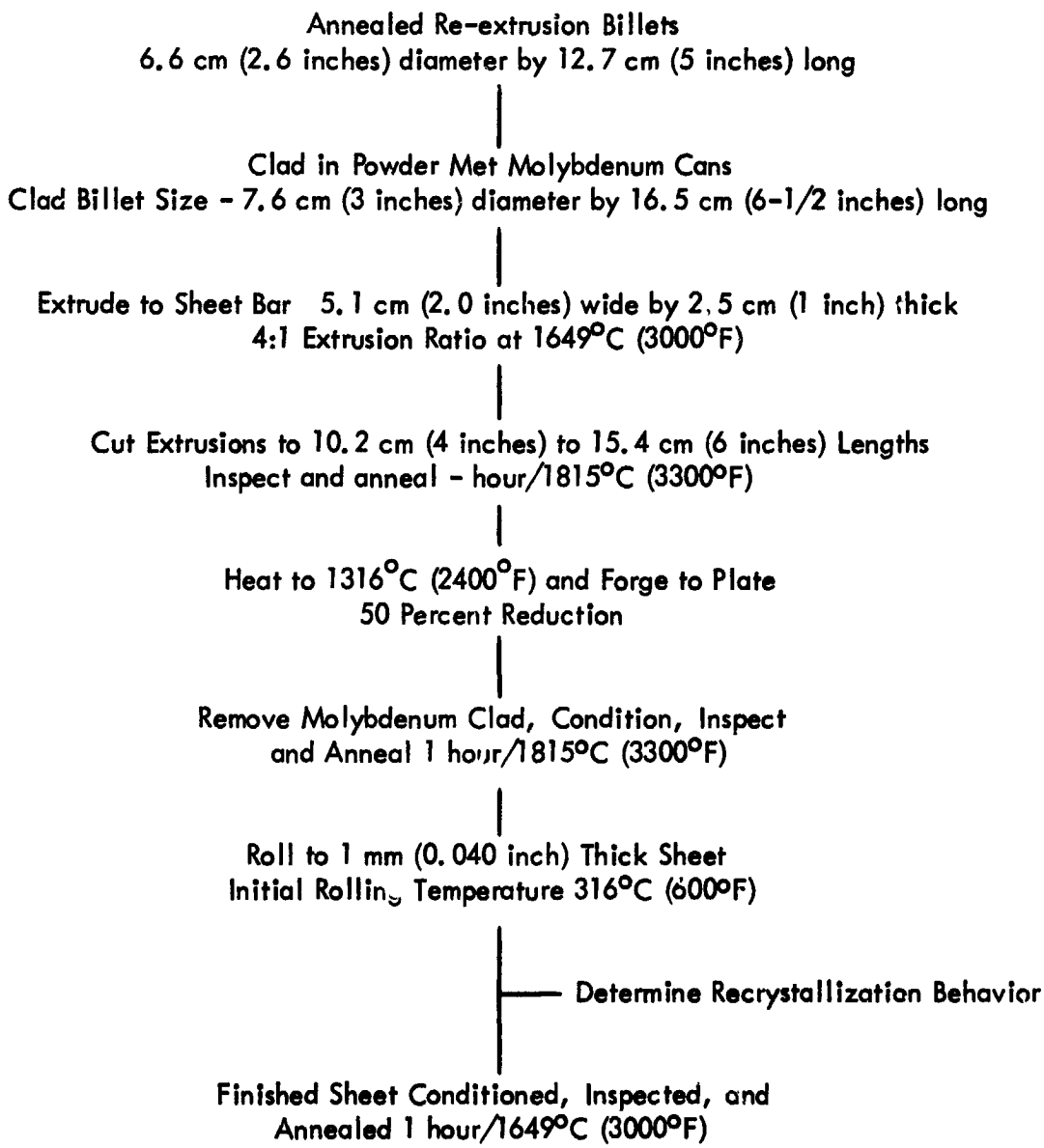

Figure 66. Processing Schedule for ASTAR-1211C Sheet

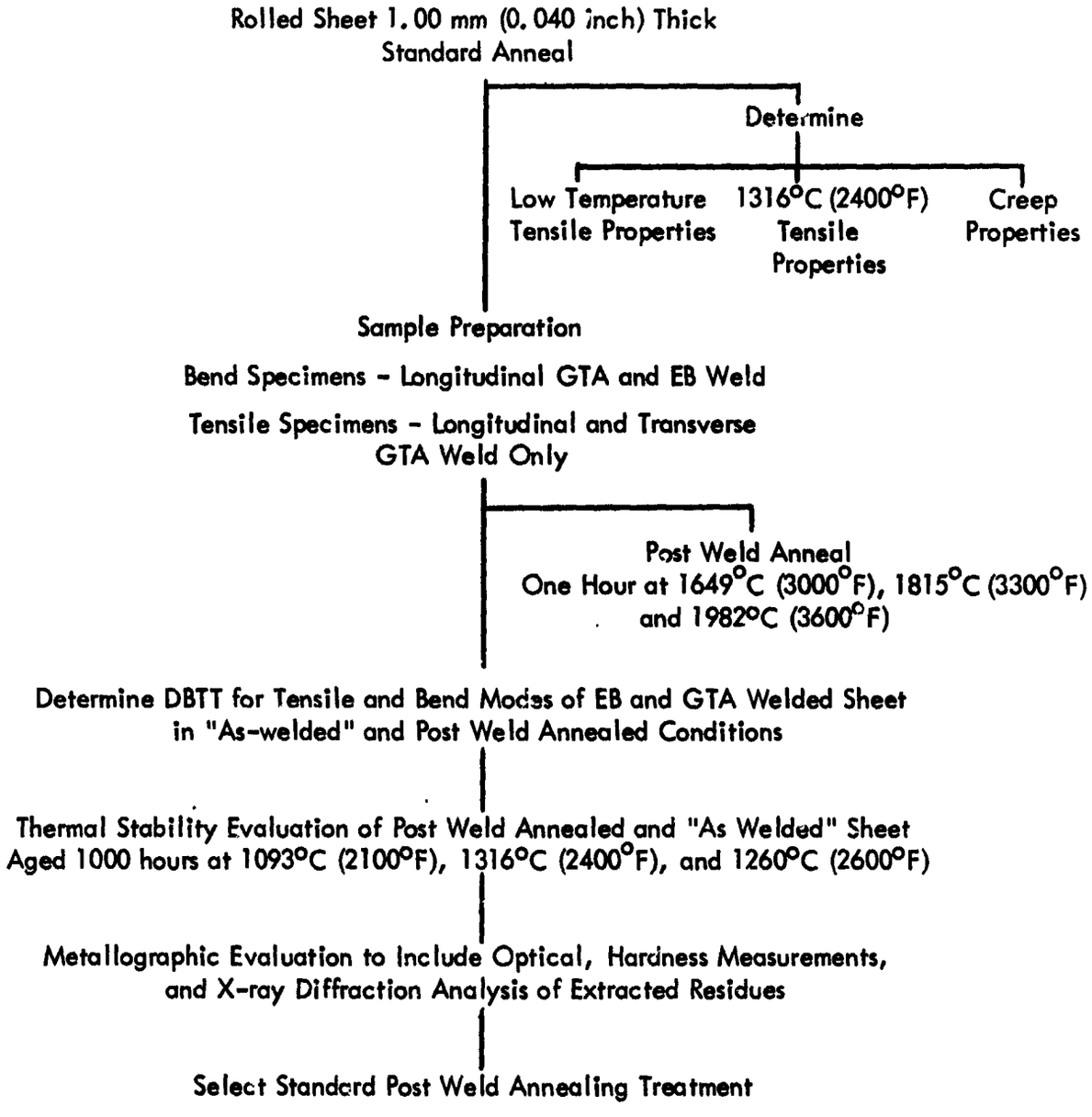

Figure 67. Evaluation Schedule for ASTAR-1211C Sheet

Table 29. Extrusion Data for ASTAR-1211C and ASTAR-1511C Sheet Study

Billet Identification	Reduction Ratio	Extrusion Constants			
		Breakthrough		Running	
		(MN/m^2)	(ksi)	(MN/m^2)	(ksi)
NASVF-1000 (ASTAR-1211C)					
C	4.3:1	537	77.8	497	72.0
B2	4.1:1	646	93.7	618	89.5
B3	4.4:1	462	67.0	388	56.3
NASVF-2000 (ASTAR-1511C)					
A-1	4.2:1	480	69.6	428	62.0
A-2	4.4:1	458	66.4	397	57.5

All billets extruded at 1649°C (3000°F) and yielded 38 cm (15 inches) of sound material.

$$\text{Reduction Ratio} = \frac{\text{area of container}}{\text{cross sectional area of extrusion}}$$

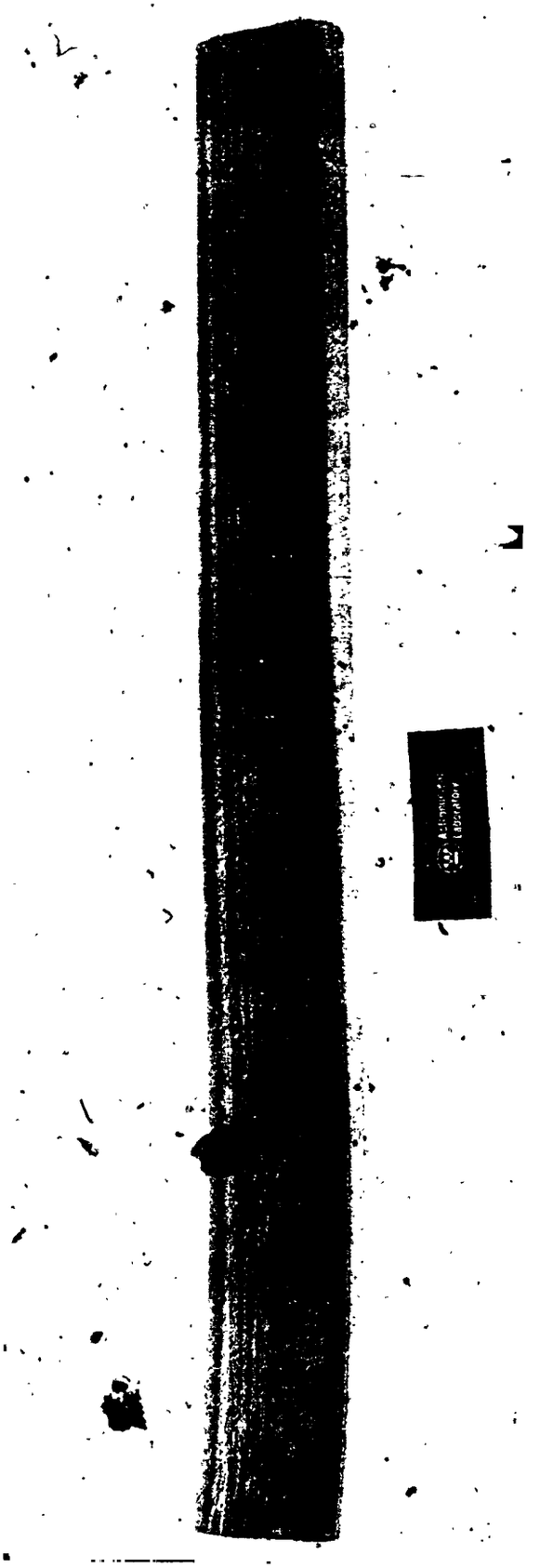

Figure 68. Sheet Bar Extrusion of ASTAR-1211C, Heat NASVF-1000-C

approximately 5.0 cm (2 inches) wide by 2.5 cm (1 inch) thick with 6.5 mm (0.25 inch) radii at the comers. The extrusion lengths varied from 51 cm (20 inches) to 60 cm (23.5 inches). The nose and tail were cropped from each extrusion as shown in Figure 68. The remaining sound material was cut into three equal lengths generally 12.5 cm (5 inches) to 15.0 cm (6 inches) long. The front one-third of the extrusion was designated with a "N", center section with a "C", and the tail section with a "T".

The extrusion bar stock was cleaned by sand blasting to remove oxidized scale from the surface then vacuum annealed for 1 hour at 1815°C (3300°F) to completely recrystallize the micrc structure. The co-extruded molybdenum clad was left intact to provide protection from the atmosphere during the forging operation.

For forging, the extruded bar stock sections were heated, one at a time, in an induction coil situated in an argon purged container. The pieces were heated to 1316°C (2400°F) and soaked for 10 minutes at temperature. The pieces were then transferred to the Dynapak, a high-energy-rate forging machine, and forged to plate in 1 hour. Reductions were on the order of 45 percent. The molybdenum clad was chemically removed from the forged plates. A set of forged plates of ASTAR-1511C is shown in Figure 69. In general, only minor edge cracking at the ends where molybdenum clad was lacking was noted. The forged plates were trimmed to rectangular shape, approximately 5.0 cm (2 inches) wide by 15 cm (16 inches) long. The m surfaces were machined to produce smooth even parallel surfaces for rolling. Approximately 0.6 mm (0.025 inch) was removed from each surface. The plates were then vacuum annealed 1 hour at 1815°C (3300°F).

5.1.2 Rolling of ASTAR-1211C Sheet

A pilot run was conducted, initially to determine the rolling characteristics of ASTAR-1211C. One plate, designated NASVF-1000CN, was rolled at 482°C (900°F) at 10 percent reduction per rolling pass. The plate was successfully reduced to 1.27 mm (0.050 inch) without an

Figure 69. Forged Plates of ASTAR-1511C

intermediate anneal. At a thickness of 1.9 mm (0.075 inch) double passes at the same mill setting were required to achieve the desired reduction. At 1.27 mm (0.050 inch), the separating force of the mill was not sufficient to reduce the sheet any further. The rolling mill used was a Stanat two-high laboratory rolling mill with 19.32 cm (8 inch) diameter rolls. The total reduction from plate to 1.27 mm (0.050 inch) thick sheet was 87 percent. The sheet was given a stress-relief anneal of 1 hour at 1093°C (2000°F) in vacuum. The sheet was then easily finish rolled to a final thickness of 1.0 mm (0.040 inch). The final total reduction from plate to 1.0 mm (0.040 inch) sheet was 89 percent. In view of the high resistance to deformation encountered at the high reduction, the rolling schedule was modified.

Two plates, NASVF-1000CM and CT, were rolled 60 percent at the rate of 10 percent reduction per rolling pass through the mill then annealed 1 hour at 1815°C (3300°F) and finished rolled 60 percent to the final 1.0 mm (0.040 inch) thickness. Some material was lost due to severe edge cracking which occurred during rolling after the intermediate anneal. One plate split longitudinally through the plate thickness from nose to tail. A total of 2 kg (4.5 lbs.) of 1.0 mm (0.040 inch) thick sheet was produced with a yield of 28 percent from the starting billet and a yield of 57 percent from starting plate. ASTAR-1211C billets NASVF-1000B2 and B3 were processed to sheet using the same modified rolling schedule. The yield of finished sheet similar to the NASVF-1000C resulted.

5.1.3 Rolling of ASTAR-1511C Sheet

It was anticipated that the rolling of ASTAR-1511C would be more difficult than ASTAR-1211C due to the higher room temperature hardness and yield strength. In the evaluation of swaged ASTAR-1211C, it was noted that a duplex heat treatment reduced room temperature hardness and flow stress. In order to explore the possible advantage of the duplex heat treatment, a plate of annealed ASTAR-1511C, NASVF-2000A1, was cut in half, and one piece was

given an additional 1 hour anneal at 1260°C (2300°F). The hardness of the plate annealed 1 hour at 1815°C (3300°F) was 333 DPH. The duplex annealed plate had a hardness of 297 DPH, a reduction of 10 percent in hardness. Both pieces were rolled at 316°C (600°F) at 10 percent reduction per rolling pass. At a thickness of 3.9 mm (0.153 inch),a reduction of 48 percent, the single annealed piece split from nose to tail. On the next pass, the duplex annealed piece at a thickness of 3.4 mm (0.135 inch), a reduction of 54 percent, split in a similar catastrophic manner. The failed plates are shown in Figure 70. It was noted during the rolling process, that the duplex annealed material yielded reductions which were approximately equal to the mill settings. This behavior was attributed to the lower initial hardness of the duplex annealed material and may also have been indicative of a lower work hardening rate. A piece of material, 31.8 mm (1.25 inches) wide by 17.5 cm (7 inches) long was salvaged from the single annealed plate which split.

This strip was annealed 1 hour at 1649°C (3000°F) followed by 1 hour at 1260°C (2300°F). The initial annealing temperature was decreased from 1815°C (3300°F) to 1649°C (3000°F) to reduce the recrystallized grain size in an attempt to minimize the catastrophic type failure observed previously. The strip was rolled at 316°C (600°F) at 10 percent reductions per pas to a thickness of 1.7 mm (0.067 inch), a reduction of 48 percent. The strip was cleaned, pickled, and annealed 1 hour at 1649°C (3000°F) followed by 1 hour at 1260°C (2300°F). The strip was finished rolled to 1.0 mm (0.040 inch) without difficulty. The remaining plates of ASTAR-1511C were then processed to 1.0 mm (0.040 inch) thick sheet using a rolling schedule consisting of 40 to 45 percent reductions at 10 percent per pass followed by the duplex anneal, 1 hour at 1649°C (3000°F) followed by 1 hour at 1261°C (2300°F). Three intermediate anneals were required to reach the final gage thickness. A total of 1.0 kg (2.25 lbs.) of 1.0 mm (0.040 inch) thick ASTAR-1511C sheet was produced, a yield of 15 percent from the billets or 34 percent from the conditioned plate. The yield data includes the material lost during the initial pilot rolling program, thus a higher yield would be expected for material processed by the revised rolling schedule.

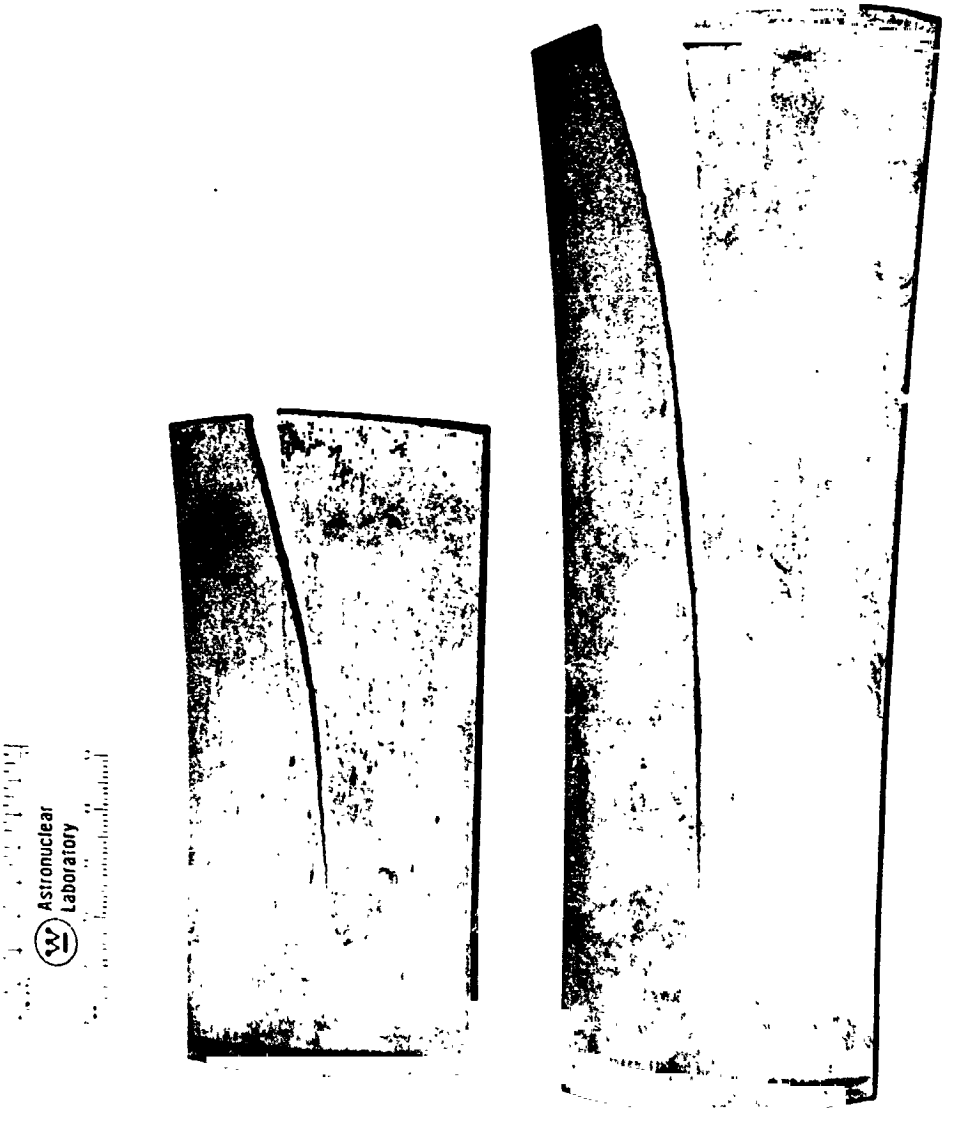

Figure 70. Failed Plates of ASTAR-1511C

5.1.4 Metallography of ASTAR-1211C and ASTAR-1511C Sheet

Samples of finished rolled sheet of ASTAR-1211C and ASTAR-1511C were annealed for 1 hour at 982°C (1800°F), 1093°C (2000°F), 1260°C (2300°F), 1371°C (2500°F), 1482°C (2700°F), 1649°C (3000°F), 1815°C (3300°F), and 1982°C (3600°F). Hardness data for the annealed sheet are shown in Figure 71. The "as-rolled" hardness of ASTAR-1211C was higher than that of ASTAR-1511C. The ASTAR-1211C sheet was reduced 87 percent, stress relieved 1 hour at 1093°C (2000°F), and then reduced an additional 5 percent. The microstructure of the ASTAR-1211C sheet exhibited a highly wrought structure in the "as-rolled" condition and after 1260°C (2300°F) anneal (Figures 72A and 72C). After 1 hour at 1371°C (2500°F) the microstructure, Figure 72D, was over 50 percent recrystallized. After the 1482°C (2700°F) heat treatment, the sheet was essentially 100 percent recrystallized. The hardness minima at 1371°C (2500°F) and the hardness peak at 1649°C (3000°F) are not unusual behavior for tantalum alloys of this type.

The ASTAR-1511C, which underwent a different processing schedule, reflects the difference in microstructure and hardness behavior. The ASTAR-1511C was reduced 40 percent after the last intermediate duplex anneal. There was no change in the microstructure after 1 hour at 982°C (1800°F), Figure 73A. The "as-rolled" microstructure is not shown since it was identical to Figure 73A. The duplex annealed ASTAR-1511C exhibited the large Ta_2C precipitate at the grain boundaries during the low temperature, 1261°C (2300°F) portion of the duplex anneal. The elongated grains produced by the 40 percent rolling reduction are evident. The lower amount of cold work was responsible for the lower hardness values for the ASTAR-1511C sheet even after the 1093°C (2000°F), 1260°C (2300°F), and 1371°C (2500°F) anneals. There was no significant change in the microstructure as a result of these anneals.

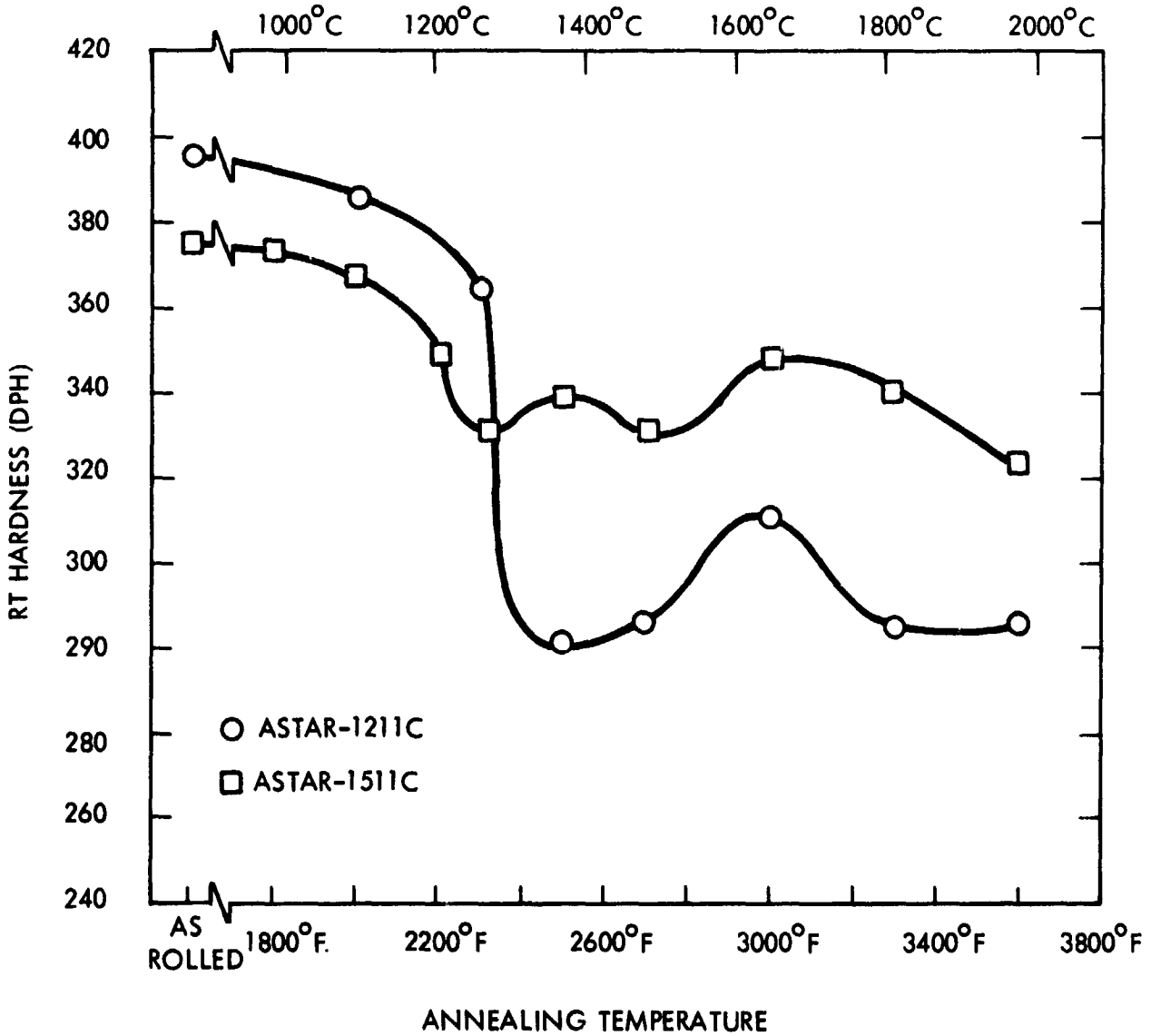

Figure 71. Hardness of ASTAR-1211C and ASTAR-1511C Sheet as Function of Isochronal Annealing Temperature

500X DPH 395

A. As Rolled

500X DPH 385

B. Rolled + 1 Hr/1093°C (2000°F)

500X DPH 365

C. Rolled + 1 Hr/1260°C (2300°F)

500X DPH 291

D. Rolled + 1 Hr/1371°C (2500°F)

Figure 72. Microstructure of Heat Treated ASTAR-1211C Sheet (NASVF-1000-C)

500X DPH 296

E. Rolled + 1 Hr/1482°C (2700°F)

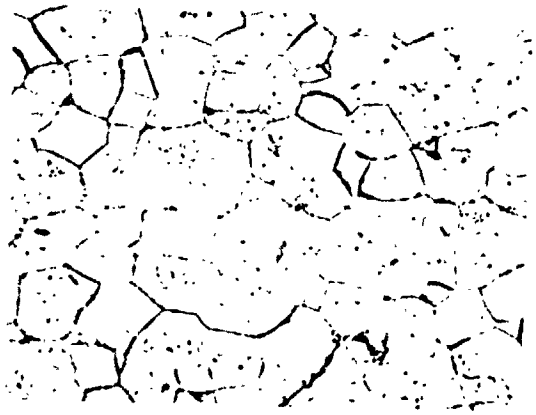

500X DPH 311

F. Rolled + 1 Hr/1649°C (3000°F)

500X DPH 295

G. Rolled + 1 Hr/1815°C (3300°F)

500X DPH 296

H. Rolled + 1 Hr/1982°C (3600°F)

Figure 72. Microstructure of Heat Treated ASTAR-1211C Sheet (NASVF-1000-C) (Continued)

500X DPH 372

A. Rolled + 1 hr/982°C (1800°F)

500X DPH 367

B. Rolled + 1 hr/1093°C (2000°F)

500X DPH 331

C. Rolled + 1 hr/1260°C (2300°F)

500X DPH 339

D. Rolled + 1 hr/1371°C (2500°F)

Figure 73. Microstructure of Heat Treated ASTAR-1511C Sheet (NASVF-2000-A1)

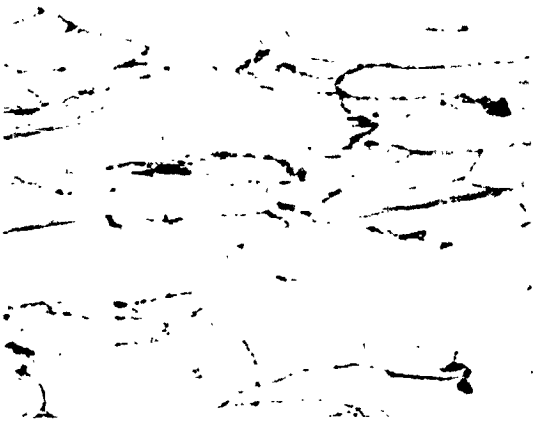

500X DPH 331

E. Rolled " 1 hr/1482°C (2700°F)

500X DPH 3 8

F. Rolled + 1 hr/1649°C (3000°F)

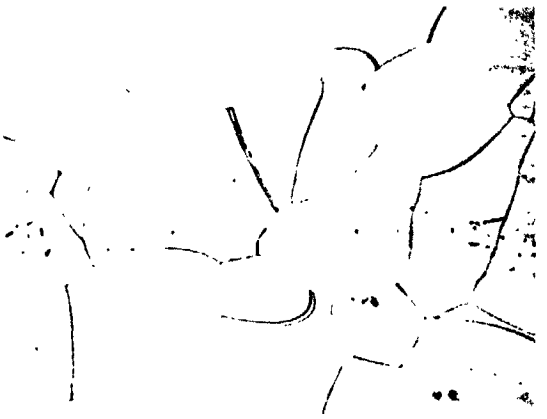

500X DPH 340

G. Rolled + 1 hr/1815°C (3300°F)

500X DPH 323

H. Rolled + 1 hr/1982°C (3600°F)

Figure 73. Microstructure of Heat Treated ASTAR-1511C Sheet NASVF-2000-Al (continued)

The onset of recrystallization can be seen in the material annealed at 1482°C (2700°F). After 1 hour at 1649°C (3000°F), the ASTAR-1511C sheet had a completely recrystallized grain structure. The hardness values assumed proper relationship to ASTAR-1211C for annealing temperatures above 1371°C (2500°F). As the annealing temperature was increased, the grain size increased, and evidence of the Ta_2C precipitate at the grain boundary diminished, disappearing entirely after 1 hour at 1982°C (3600°F). The hardness values for both ASTAR-1211C and ASTAR-1511C also declined after the 1982°C (3600°F) heat treatment.

5.1.5 Check Chemistry of Processed Sheet

Upon completion of the rolling operation, chemistry samples were taken for analysis of interestitial content. The ingot chemistry of heat NASVF-1000C with respect to alloying additions was also determined. The results are listed in Table 30.

Table 30. Check Chemical Analysis of ASTAR-1211C and ASTAR-1511C

Sample Identification	Chemical Analysis						
	W w/o	Re w/o	Hf w/o	C ppm	O_2 ppm	N_2 ppm	H_2 ppm
NASVF-1000-C (Ingot) ASTAR-1211C	12.2	1.09	0.69	-	-	-	-
NASVF-1000-C (Sheet) ASTAR-1211C	-	-	-	260	8	13	0.2
NASVF-2000-A1 (Sheet) ASTAR-1511C	-	-	-	190	45	12	0.4

5.2 MECHANICAL PROPERTIES OF ASTAR-1211C AND ASTAR-1511C SHEET

Mechanical property data for ASTAR-1211C and ASTAR-1511C sheet were determined at low temperature and at 1316°C (2400°F). Creep properties were also determined in the temperature range 1093°C (2000°F) and 1316°C (2400°F). Data includes properties for standard annealed material, one hour final anneal at 1649°C (3000°F) and duplex annealed materials, 1 hour at 1649°C (3000°F) followed by 1 hour at 1260°C (2300°F).

5.2.1 Tensile Properties

Low temperature and 1316°C (2400°F) tensile properties for ASTAR-1211C and ASTAR-1511C were determined using sheet tensile specimens with a 6.4 mm (0.250 inch) wide by 2.5 cm (1 inch) long gage section. The gage thickness was nominally 1 mm (0.040 inch). The test results are listed in Table 31.

The room temperature tensile strength properties of the standard annealed ASTAR-1211C and ASTAR-1511C sheet were comparable to data for material swaged at 1371°C (2500°F) and annealed 1 hour at 1649°C (3000°F). The duplex annealed material exhibited strength values that were approximately 10 percent lower. This reduction in strength was also exhibited by swaged ASTAR-1211C rod which had been given a duplex anneal. Like the swaged rod data, the duplex anneal had no effect on low temperature ductility for both alloys. This fact is illustrated in Figure 74. Elongation values for standard annealed and duplex annealed ASTAR-1211C and ASTAR-1511C sheet are plotted as a function of test temperature. ASTAR-1211C retains a fair level of ductility down to -129°C (-200°F) for both conditions. The reduction in elongation values for ASTAR-1511C in both annealed conditions is apparent. The test results for ASTAR-1211C and ASTAR-1511C sheet corroborates the test results obtained for swaged rod. The tensile DBTT for ASTAR-1211C sheet is -148°C (-200°F) for both heat treatments. The ASTAR-1511C DBTT is higher, as would be expected, -18°C (0°F). In the case of ASTAR-1511C there is little difference in tensile elongation below room temperature, while the duplex heat treatments appear to have a beneficial affect on room temperature ductility. The sub-zero ductile behavior of duplex annealed ASTAR-1211C was affected to some extent by heat treatment. The -129°C (-200°F) value appears to be anomolous, the 30 percent value was greater than the room temperature result, contrary to expected behavior.

Table 31A. Tensile Data for ASTAR-1211C and ASTAR-1511C Sheet (SI units)

Specimen Identification and Final Heat Treatment	Test Temp. (°C)	Yield Strength (MN/m^2)	Ultimate Strength (MN/m^2)	Elongation	
				Uniform (%)	Total (%)
1-B-2-30 (ASTAR-1211C) Annealed 1 hr/1649°C	RT	747	862	14.8	28
	- 73	879	978	13.8	15
	-129	000	1088	13.2	15
	-196	1227	1254	2.4	4
	1316	259	353	7.8	27
1-B-2-30/24 (ASTAR-1211C) Annealed 1 hr/1649°C + 1 hr/1316°C	RT	690	789	17.6	28
	- 73	822	918	18.4	20
	-129	911	1023	24.6	30
	-196	1160	1172	2.3	4
	1316	250	340	8.7	38
2-A-2-30 (ASTAR-1511C Annealed 1 hr/1649°C	RT	791	967	12.6	22
	- 73	1008	1032	12.0	21
	-129	1035	1071	14.5	15
	-196	1093	1107	6.3	8
	1316	305	417	6.0	26
2-A-2-30 + (ASTAR-1511C) Annealed 1 hr/1649°C + 1 hr/1316°C	RT	781	883	16.2	29
	- 73	842	944	15.9	21
	-129	880	976	11.9	13
	-196	922	1009	9.7	10
	1316	286	390	8.4	28

Strain Rate 0.05/min.

Table 31B. Tensile Data for ASTAR-1211C and ASTAR-1511C Sheet

Specimen Identification and Final Heat Treatment	Test Temp. (°F)	Yield Strength (ksi)	Ultimate Strength (ksi)	Elongation	
				Uniform (%)	Total (%)
1-B-2-30 (ASTAR-1211C) Annealed 1 hr/3000°F	RT	108.3	125.0	14.8	28
	-100	127.4	141.8	13.8	15
	-200	144.9	157.7	13.2	15
	-320	177.8	181.7	2.4	4
	2400	37.5	51.2	7.8	27
1-B-2-30/24 (ASTAR-1211C) Annealed 1 hr/3000°F) + 1 hr/2400°F)	RT	100.1	114.4	17.6	28
	-100	119.1	133.1	18.4	20
	-200	132.0	148.3	24.6	30
	-320	168.2	169.8	2.3	4
	2400	36.2	49.3	8.7	38
2-A-2-30 (ASTAR-1511C) Annealed 1 hr/3000°F	RT	138.9	140.1	12.6	22
	0	146.1	149.5	12.0	21
	- 50	150.0	155.2	14.5	15
	-100	158.4	160.5	6.3	8
	2400	44.2	59.7	6.0	26
2-A-2-30/24 (ASTAR-1511C) Annealed 1 hr/3000°F + 1 hr/2400°F	RT	113.2	128.0	16.2	29
	0	122.0	136.8	15.9	21
	- 50	127.5	141.4	11.9	13
	-100	133.6	146.2	9.7	10
	2400	41.4	56.5	8.4	28

Strain Rate 0.05/min.

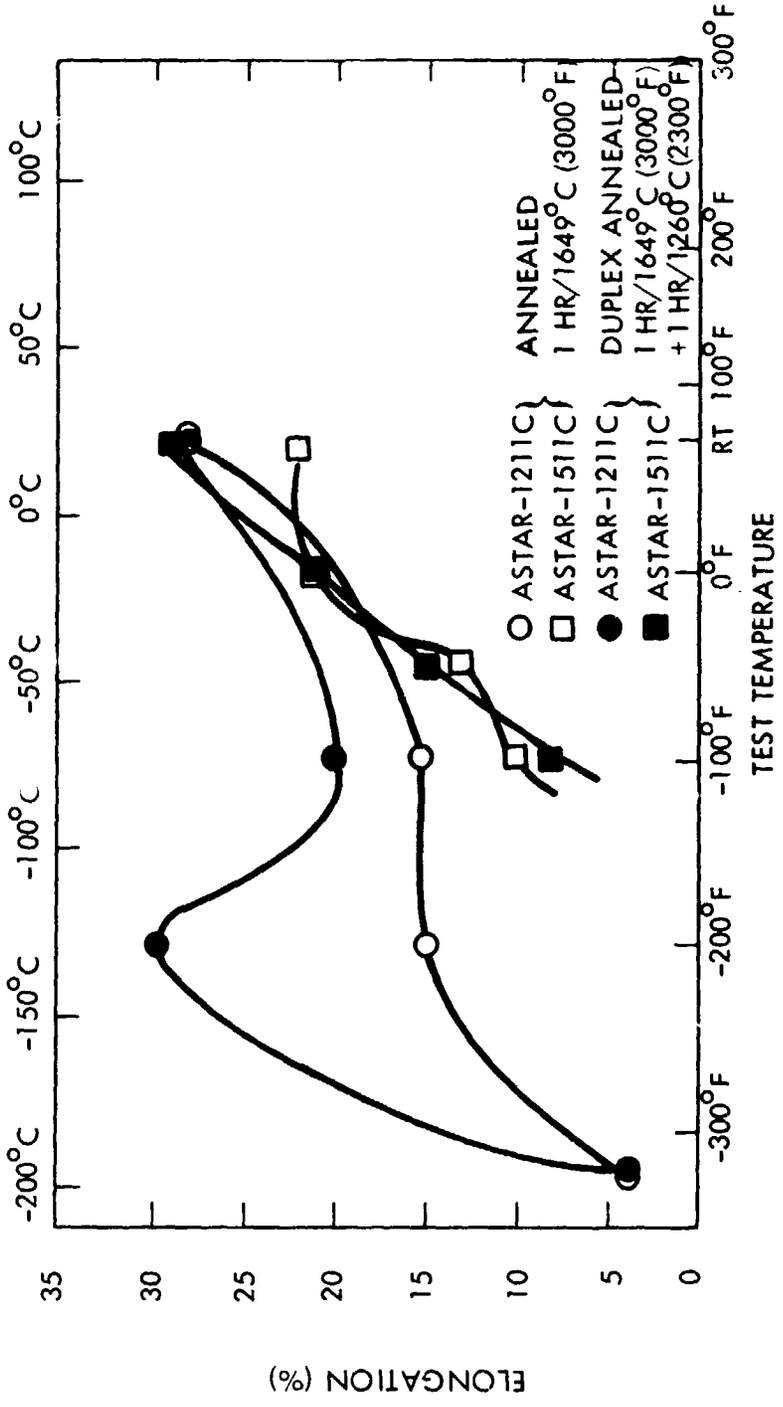

Figure 74. Tensile Ductility of ASTAR-1211C and ASTAR-1511C Sheet

The elevated temperature tensile properties of ASTAR-1211C and ASTAR-1511C sheet were lower than values obtained for swaged rod with similar heat treatments. The decreases in yield and ultimate strengths were on the order of 10 percent which was considered significant. The thermomechanical histories of the sheet and swaged were not the same. The sheet was rolled in the temperature range 316°C (600°F) to 482°C (900°F), while the swaged material was processed at 1371°C (2500°F). The difference in elevated temperature tensile properties may well be due to the difference in working temperature.

5.2.2 Creep Properties of Sheet

Creep testing of ASTAR-1211C and ASTAR-1511C sheet was also conducted for the standard annealed and duplex annealed conditions. The creep tests were multi-load, multi-temperature type using pin loaded specimens with a 6.4 mm (0.250 inch) wide by 2.54 cm (1 inch) long gage section. The gage thickness was 0.9 mm (0.036 inch). The creep data are listed in Table 32, and a Larson-Miller plot for 1 percent creep strain is shown in Figure 75. The creep resistance of the sheet material for both alloys in both heat treated conditions was equivalent to or slightly better than the creep resistance of swaged rod in a comparably annealed condition. The duplex annealed material of both alloys exhibited creep properties which were not significantly different from the standard annealed material. The duplex heat treatment, which produced large grain boundary precipitates of Ta_2C, appears to have had little or no affect on creep behavior of material tested at temperature below the secondary duplex annealing temperature, 1260°C (2300°F). The presence of the large Ta_2C grain boundary precipitate appears to neither enhance nor degrade creep properties.

Table 32. Creep Data for ASTAR-1211C and ASTAR-1511C Sheet

Specimen Identification and Final Annealed Condition	Test Temperature		Stress Level		Secondary Creep Time (hrs.)	Secondary Creep Strain (%)	Secondary Creep Rate (%/hr.)	Time to 1% Strain (hrs.)	P $T_R(15+\log t)\times 10^{-3}$
	(°C)	(°F)	(MN/m^2)	(ksi)					
1-B-2-30	1093	2000	276	40	77	0.50	0.00650	154	42.2
ASTAR-1211C Sheet	1149	2100	207	30	161	0.10	0.00062	1610	46.6
Annealed	1260	2300	138	20	234	0.39	0.00167	600	49.0
1 hr/1649°C (3000°F)	1316	2400	104	15	136	0.30	0.00221	454	50.5
1-B-2-30/24	1093	2000	276	40	168	0.65	0.00387	258	42.9
ASTAR-1211C Sheet	1204	2200	207	30	143	0.71	0.00496	202	46.0
Annealed 1 hr/1649°C	1316	2400	138	20	67	0.74	0.01105	91	48.5
(3000°F) + 1 hr/1316°C	1316	2400	104	15	98	0.45	0.00459	218	49.6
(2400°F)									
2-A-2-30	1093	2000	276	40	169	0.09	0.00053	1880	44.9
ASTAR-1511C Sheet	1204	2200	209	30	184	0.20	0.00109	920	47.8
Annealed	1316	2400	138	20	160	0.40	0.00250	400	50.4
1 hr/1649°C (3000°F)	1316	2400	104	15	160	0.10	0.00063	1600	52.1
2-A-2-30/24	1093	2000	276	40	160	0.15	0.00094	1070	44.3
ASTAR-1511C Sheet	1204	2200	207	30	187	0.19	0.00102	980	49.9
Annealed 1 hr/1649°C	1316	2400	138	20	136	0.33	0.00243	412	50.4
(3000°F) + 1 hr/1316°C	1316	2400	104	15	144	0.15	0.00104	958	51.5
(2400°F)									

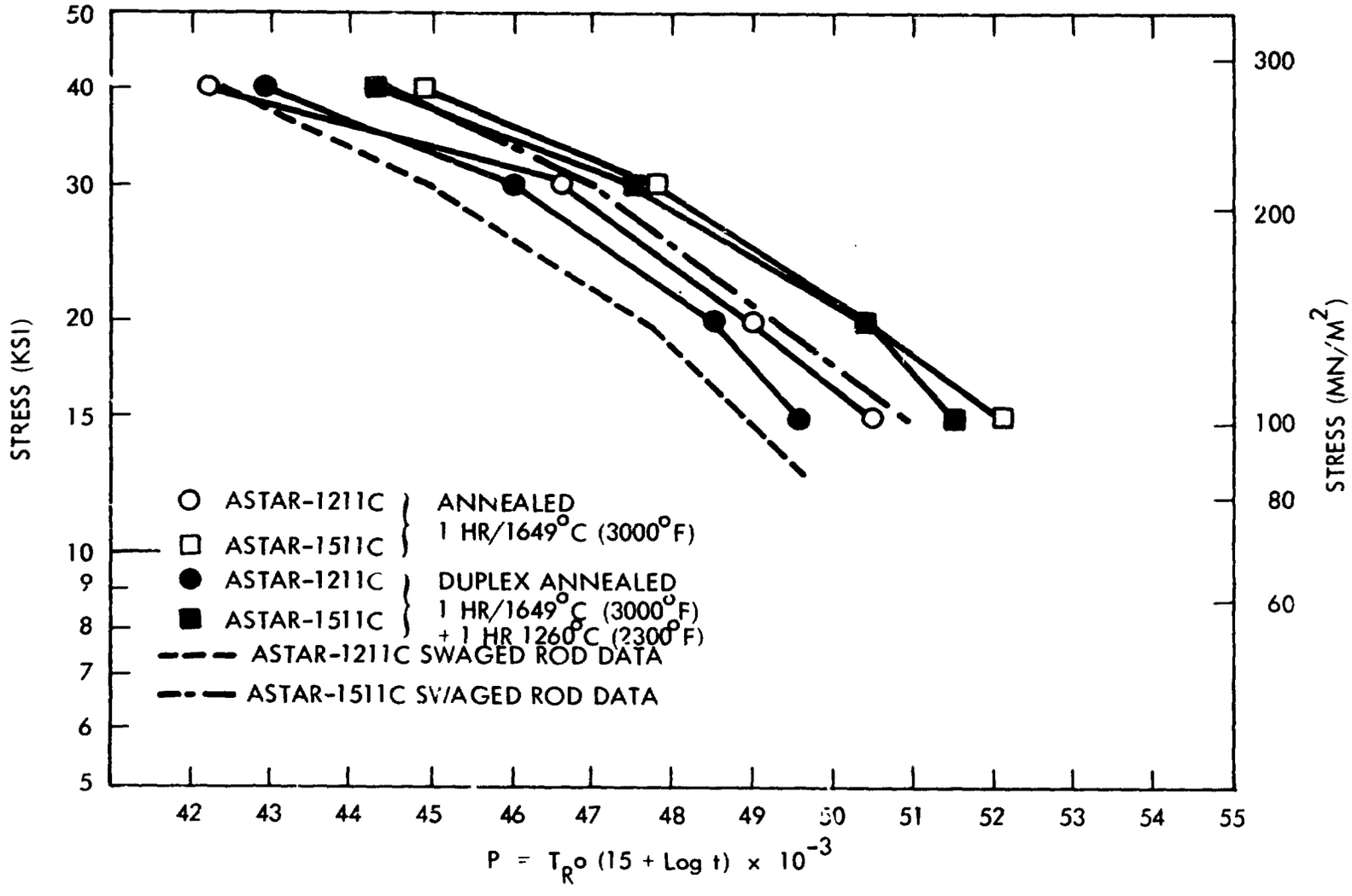

Figure 75. Creep Data for ASTAR-1211C and ASTAR-1511C Sheet

5.3 EVALUATION OF WELDED ASTAR-1211C AND ASTAR-1511C SHEET

The evaluation of ASTAR-1211C and ASTAR-1511C sheet under this task consisted primarily of the investigation of the effect of EB and GTA welds on the ductile-to-brittle transition behavior of sheet material. Standard EB and GTA procedures developed for ASTAR-811C under NASA Contract NAS 3-11827 were used to produce test specimens for this program[9]. The DBTT for GTA and EB welded sheet of both alloys were determined in the bend mode as a function of post-weld annealing temperatures and for sheet in the "as-welded" condition. The weld bend DBTT was determined using longitudinal welded specimens, i.e., the weld parallel to the rolling direction and long dimension of the test specimen. Under this condition, weld metal, HAZ, and base metal were subjected to the same stress level at the outer bend surface. The bend specimens used were 12 t wide by 24 t long -- approximately 1.3 cm (0.5 inch) by 2.54 cm (1 inch) long, respectively. The test span was 15 t. The punch had a radius of 1 t and was driven at a speed of 2.54 cm (1 inch) per minute. The testing procedures and criteria for assessing failure of bend specimens were the same as those developed under Contract NAS 3-2540[10].

The tensile DBTT for GTA welded ASTAR-1211C sheet was determined using both longitudinal and transverse weld specimens as shown in Figure 76. Longitudinal weld tensile specimens had the axis of the weld coicident with the axis of the tensile gage section. In this configuration, the gage section contained the weld metal plus the heat affected zone on each side of the weld. Transverse weld specimens had the weld axis normal to the stress axis of the tensile specimen. Under this condition, the weld metal, HAZ, and base metal sustained the same tensile load, and failure occurred in the material with the lowest ductility or lowest strength. Tension tests were conducted of GTA welded ASTAR-1211C sheet in the "as-welded" and "post-weld" annealed conditions.

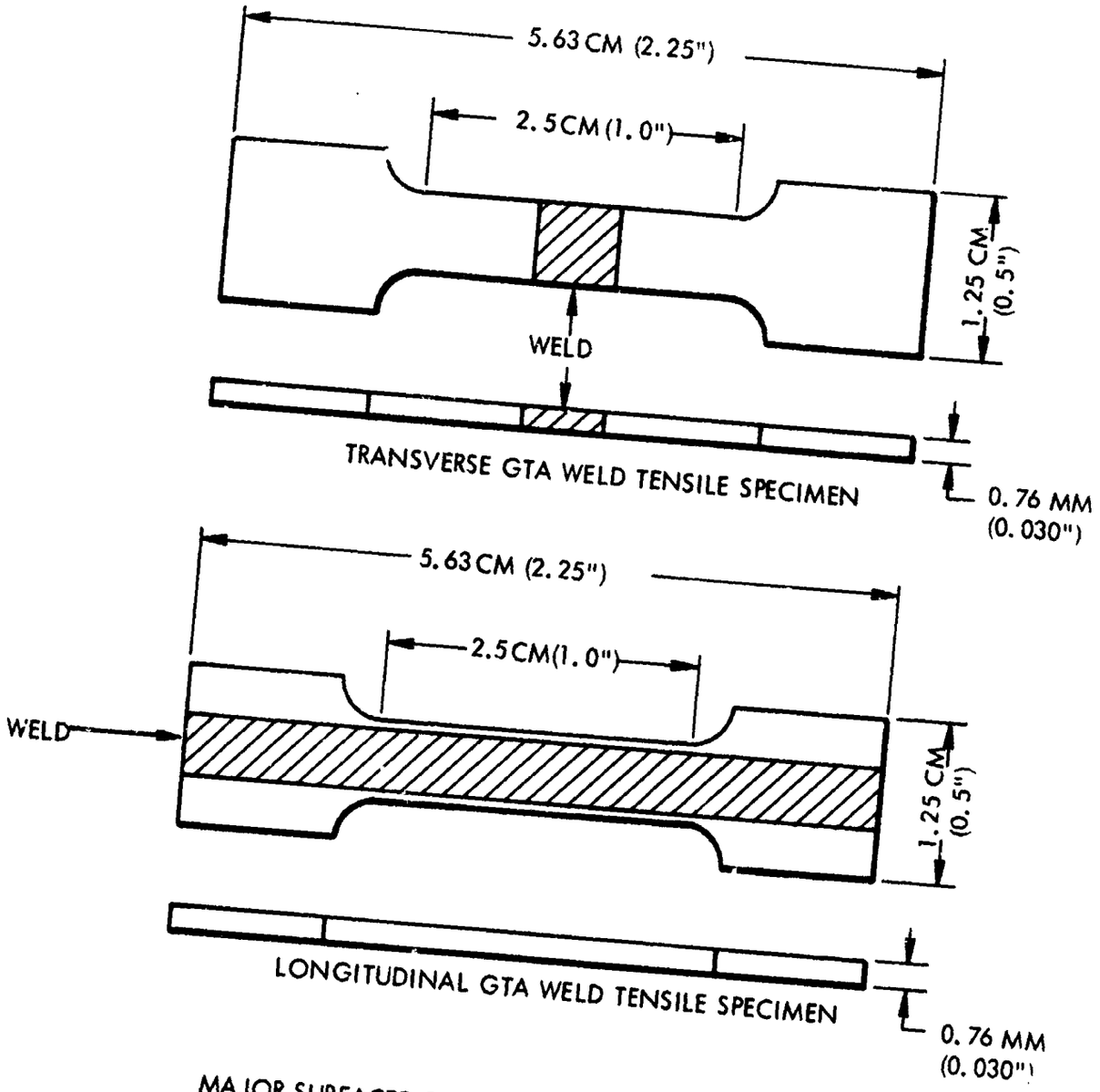

Figure 76. Longitudinal and Transverse GTA Weld Tensile Specimen Geometry

The post-weld heat treatments selected were 1 hour at 1649°C (3000°F), 1815°C (3300°F), and 1982°C (3600°F). The lower temperatures straddle the carbon solvus, and the 1982°C (3600°F) is well above, thus the disposition of carbon within the alloy matrix would be affected to the greatest extent in this temperature range.

The remainder of this task was concemed with the thermal stability of welded ASTAR-1211C and ASTAR-1511C sheet. ASTAR-1211C tensile specimens containing both longitudinal and transverse GTA welds and ASTAR-1511C specimens containing only longitudinal GTA welds were given post-weld anneals of 1 hour at 1649°C (3000°F), 1815°C (3300°F), and 1982°C (3600°F). The "post-weld" annealed specimens along with "as-welded" specimens were thermally aged for 1000 hours at 1149°C (2100°F), 1316°C (2400°F), and 1427°C (2600°F). In the temperature range covered by the aging temperature, the tendency for carbide precipitation, Ta_2C, is greatest in the ASTAR-type alloys.

5.3.1 Evaluation of Welded ASTAR-1211C Sheet

Sheet specimens were prepared for welding by hec y pickling of the as-rolled sheet followed by vacuum annealing for 1 hour at 1649°C (3000°F). Individual weld specimens were prepared by shearing to lengths and widths convenient for welding. No evidence of edge cracking or delamination was observed due to the shearing operation. All material used for these evaluations was 1.0 mm (0.040 inch) thick sheet produced from NASVF-1000CM and CT.

No problems were encountered in either EB or GTA welding of this alloy. Welding parameters are listed in Table 33.

Table 33. Weld Parameters for ASTAR-1211C and ASTAR-1511C Sheet

GTA Welds	Parameters	EB Welds
38 cm/min (15 IPM)	Speed	635 cm/min (25 IPM)
140 A	Current	9.5 mA
18 V	Voltage	120 KV
8.8 mm (0.375 inch)	Clamping Space	6.3 mm (0.25 inch)

Weld Quality appeared comparable to that previously observed for similar welds in ASTAR-811C. Visual and dye penetrant inspection revealed no defects.

Bend and tensile specimen blanks were prepared by cold shearing the as-welded sheet to the appropriate sizes. The post-weld anneals required to satisfy the test requirements were accomplished by 1 hour annealing at 1649°C (3000°F), 1815°C (3300°F), and 1987°C (3600°F) at pressures below 1.33×10^{-6} N/m^2 (1×10^{-8} torr).

5.3.1.1 Bend Tests

Bend tests were conducted only on longitudinal specimens; i.e., with the bending surface of the punch lying normal to both the rolling and welding direction of the test specimens. Tests were conducted and evaluated using those procedures previously established under Contract NAS 3-2540[10]. All tests were conducted using a 1 t bend radius. This corresponds to a nominal outer fiber strain of 33%. To provide a proper base of comparison the 1 t bend DBTT was also determined for the ASTAR-1211C base metal after 1 hour anneal at 1649°C (3000°F).

The results of the bend tests on ASTAR-1211C are shown in Figures 77, 78, and 79 and are presented in tabular form in Table 34. The bend DBTT of the EB welds is seen to compare well with that of the base metal, the total range being from 24°C (75°F) to 52°C (125°F) for all of the conditions evaluated. The GTA welds had, by comparison, slightly higher bend transition temperatures. This was due to the greater heat input of the GTA welds and reflects the general loss of low temperature ductility associated with increased grain size in tantalum-base alloys. Post-weld anneals were seen to have some beneficial effect, lowering the bend DBTT to within approximately 10°C (50°F) to 38°C (100°F) of that of the base metal. Fractures during bend testing appeared to be largely the result of cleavage-type cracking and in that respect the data represents a true ductile-to-brittle transition behavior. This was in contrast to the "ductile tear" type fractures generally observed in bend tests of GTA and EB welds in T-111 and ASTAR-811C[10].

5.3.1.2 Hardness

Hardness traverses were conducted on specimens representing each of the welded and post-weld annealed conditions. Measurements were made on base metal, heat-affected zone (HAZ), and weld metal regions of each using a 10 Kg load on a Vickers hardness tester. The results of these measurements are plotted in Figures 80-83. Results for both EB and GTA welds were similar in that one hour post-weld anneals were effective in reducing the very high hardness of the as-welded fusion and heat-affected zones. Values observed on the base metal seem to agree well with the 317 DPH determined for as-rolled and recrystallized base metal.

5.3.1.3 Tensile Transition Temperature Tests

Tensile tests were conducted over a range of temperatures in an effort to identify the tensile DBTT of GTA welds in ASTAR-1211C. Tests were conducted on material in the as-welded condition as well as after the various one hour post-weld anneals employed. Tests were

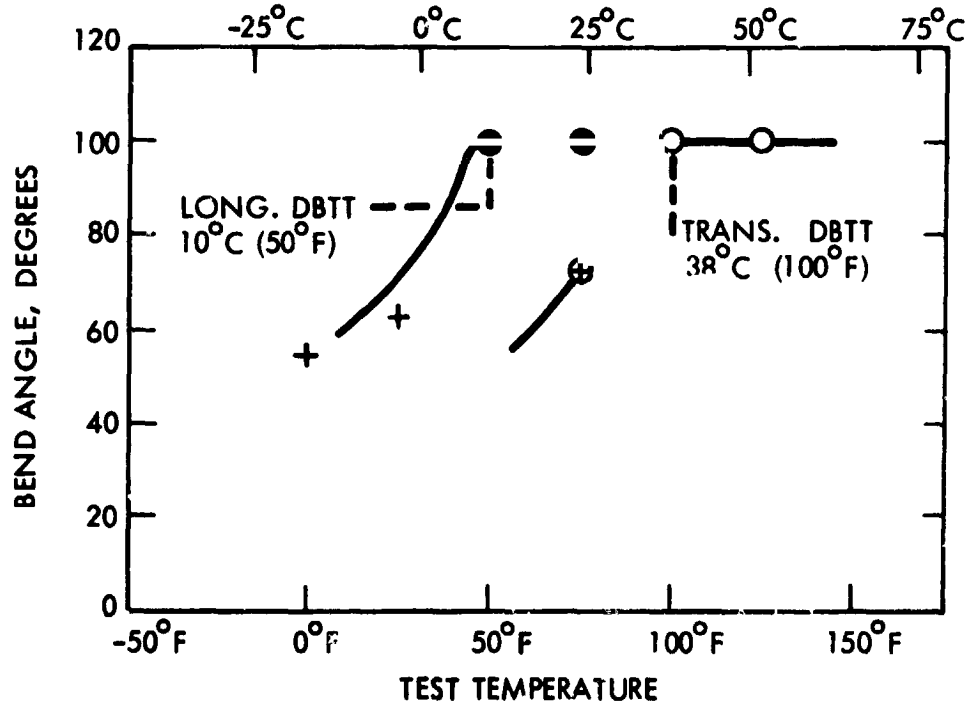

Figure 77. Results of 1 t Bend Tests on ASTAR-1211C Base Metal

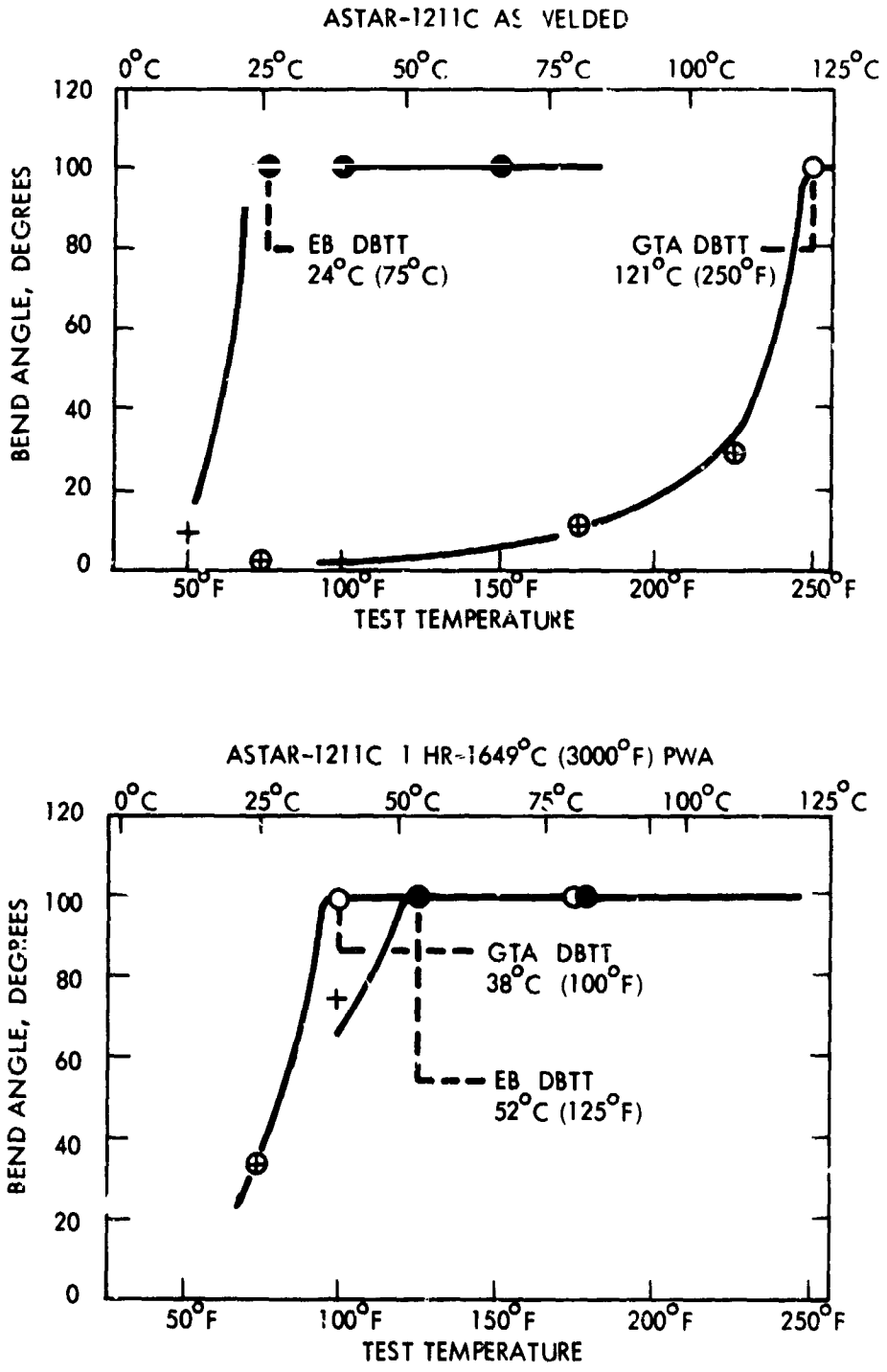

Figure 78. Results of 1 t Bend Tests on EB and GTA Welds in 1.0 mm (0.040 inch) ASTAR-1211C Sheet. Thermal History as Indicated.

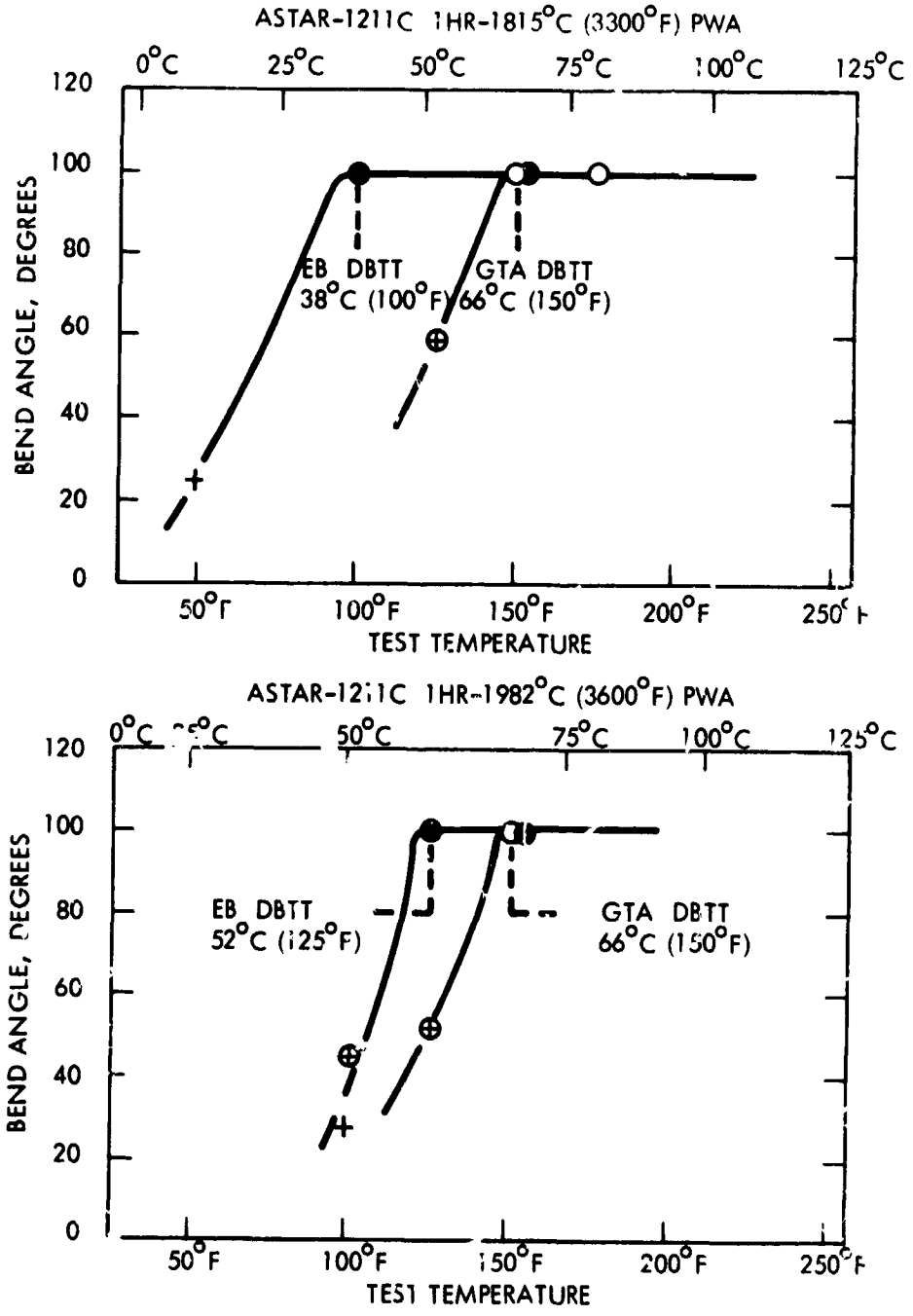

Figure 79. Results of 1 t Bend Tests on EB and GTA Welds in 1.0 mm (0.040 inch) ASTAR-1211C Sheet. Thermal History as Indicated.

Table 34. Summary of Bend Ductile-Brittle Transition Temperature Results for GTA and EB Welded ASTAR-1211C Sheet. (Thermal exposure as indicated)

Test Condition	1t Bend DBTT			
	GTA Welds		EB Welds	
	(°C)	(°F)	(°C)	(°F)
As-welded	121	250	24	75
1 hr/1649°C (3000°F) PWA	38	100	52	125
1 hr/1815°C (3300°F) PWA	66	150	38	100
1 hr/1982°C (3600°F) PWA	66	150	52	125
Base Metal	Longt. 10	50	Trans. 38	100

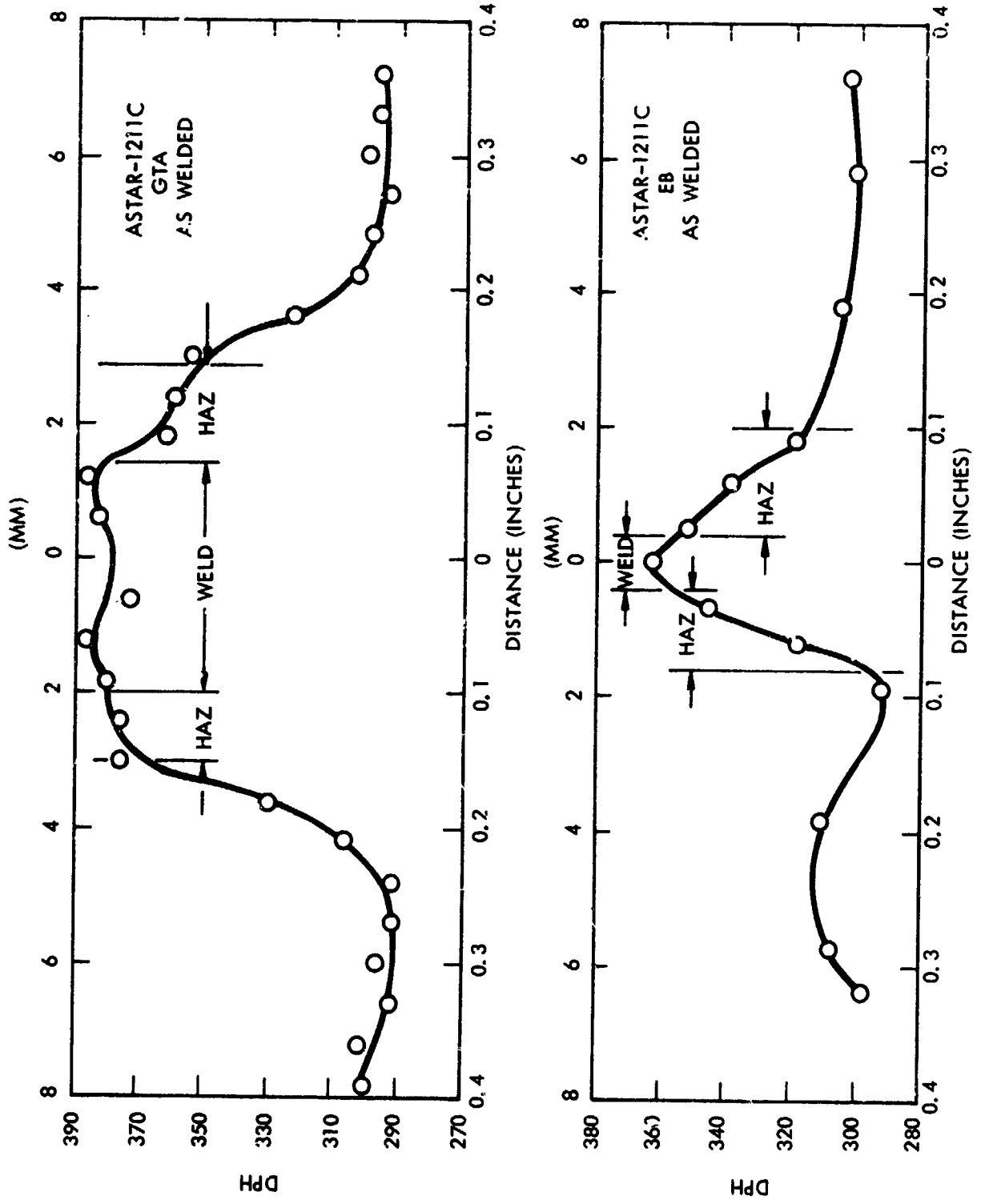

Figure 80. Hardness Traverses on EB and GTA Welds in 1.0 mm (0.040 inch) ASTAR-1211C Sheet Tested in the As-Welded Condition

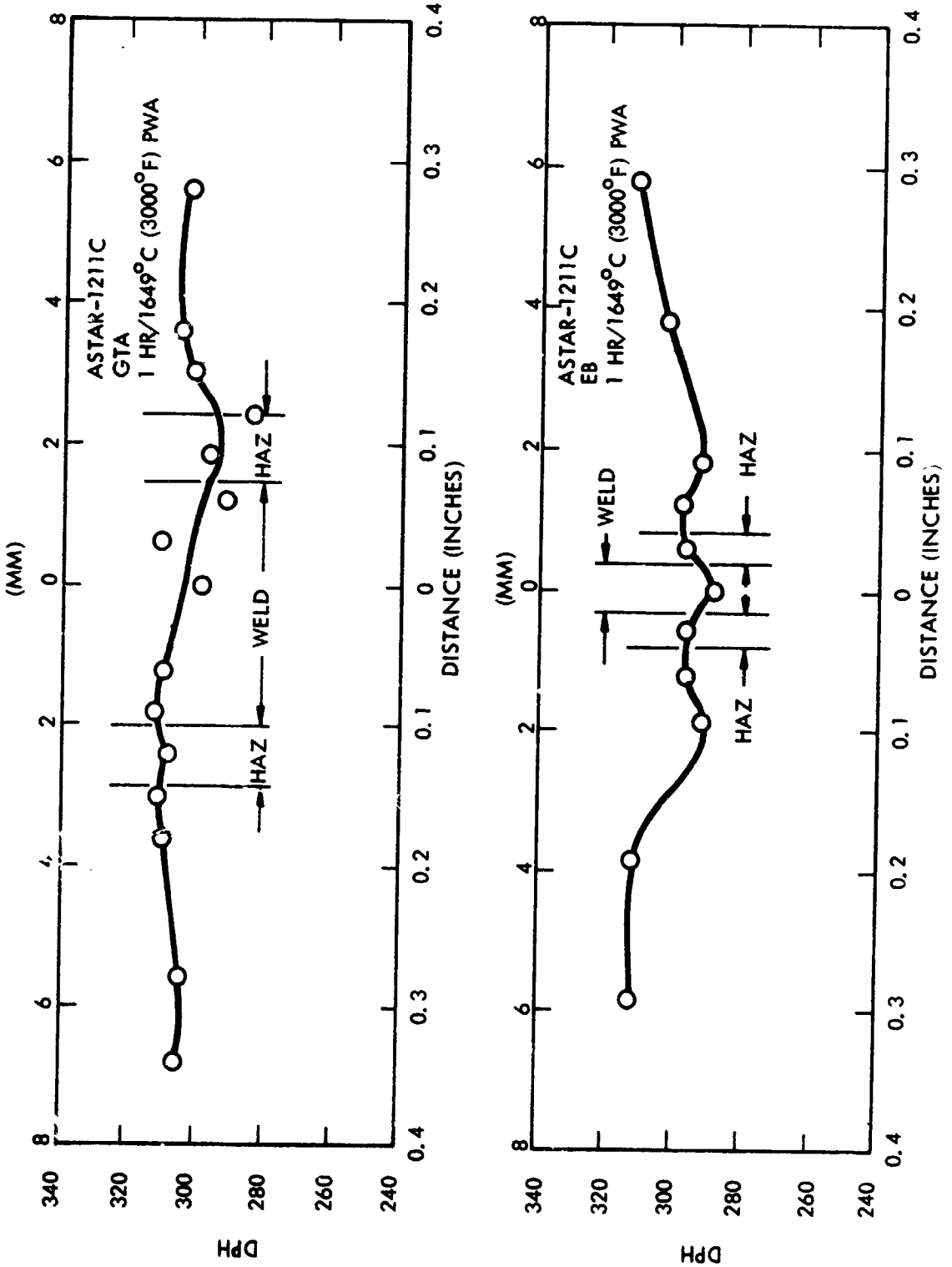

Figure 81. Hardness Traverses on EB and GTA Welds in 1.0 mm (0.040 inch) ASTAR-1211C Sheet - Tested After 1 HR/1649°C (3000°F) PWA

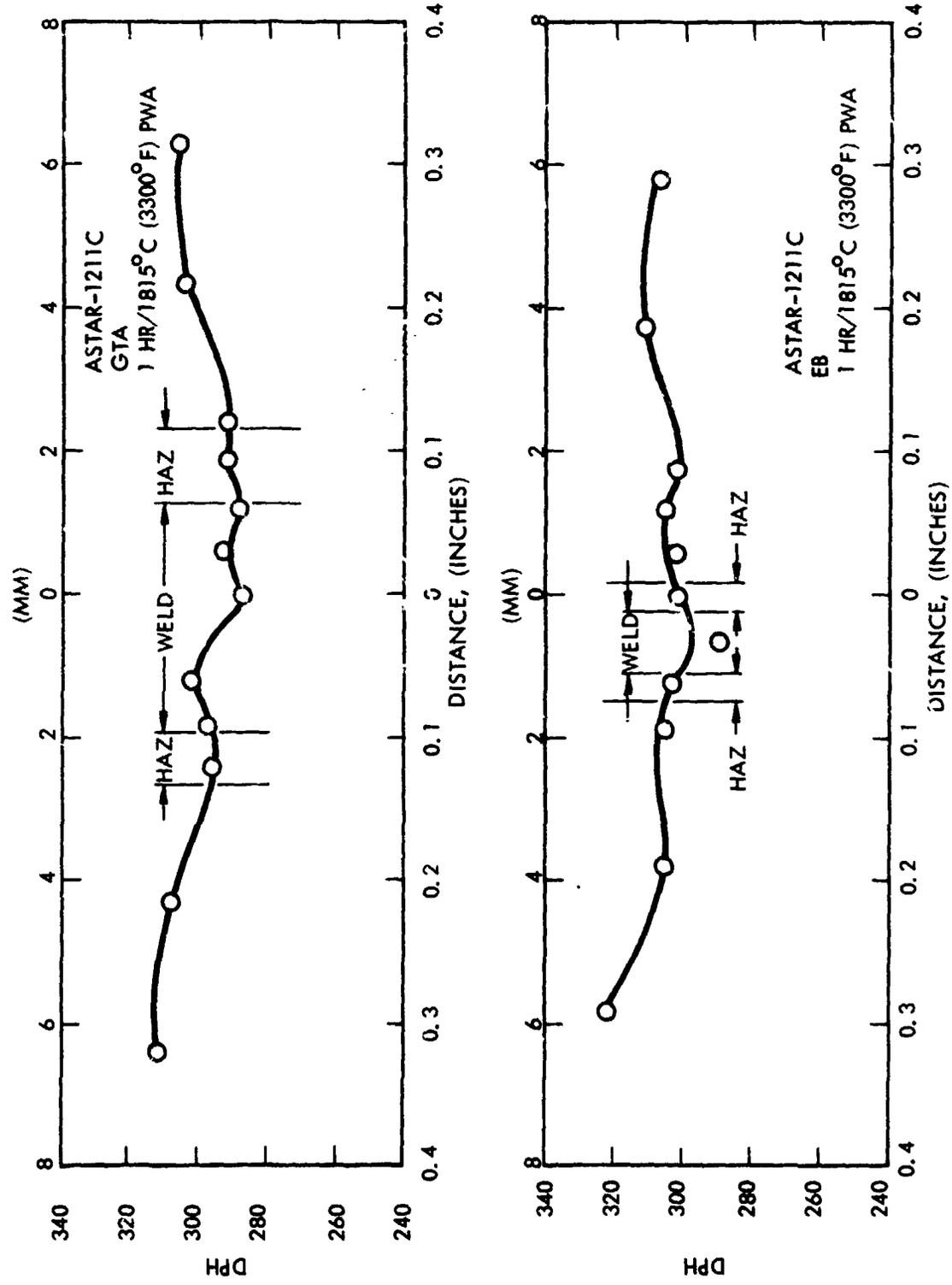

Figure 82. Hardness Traverses on EB and GTA Welds in 1.0 mm (0.040 inch) ASTAR-1211C Sheet. Tested After 1 HR/1815°C (3300°F) PWA.

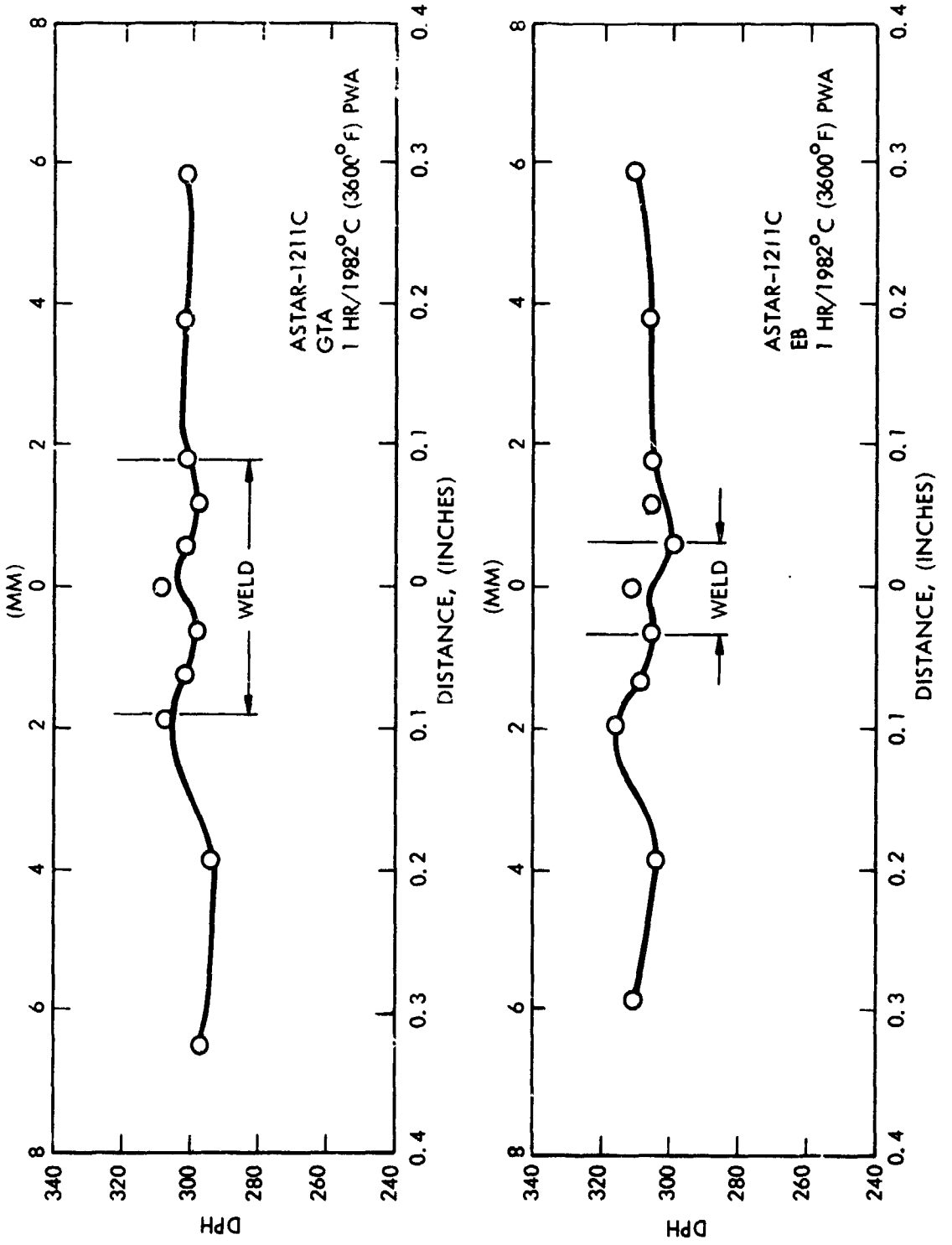

Figure 83. Hardness Traverses on EB and GTA Welds in 1.0 mm (0.040 inch) ASTAR-1211C Sheet. Tested After 1 HR/1982°C (3600°F) PWA.

performed on specimens having the weld zone oriented both longitudinal and transverse (i. e., parallel and normal) to the tensile axis of the specimen.

The test results are listed in Table 35 and are plotted in Figures 84 and 85 in terms of percent elongation at fracture vs test temperature. A constant strain rate of 0.05 $min.^{-1}$ was used throughout all tests. The only qualification required for these data is tc point out the curve indicated for the transverse tests on as-welded specimens (Figure 84) was characteristic of the base metal rather than the weld metal since fracture occurred in the base metal. This is a direct consequence of the specimen design since base metal, HAZ, and weld metal are subjected to the same tensile load,and failure will inevitably occur in the region of lowest strength and/or ductility. Note these results are in agreement with the as-welded hardness data of Figure 80.

The strength values listed in Table 35 are also plotted in Figures 86 and 87 as a function of testing temperature. In the "as-welded" condition, the ultimate and yield strengths of longitudinal tested specimens were shifted to much higher levels compared to base metal. The transverse test condition exhibited instability at temperatures below 93°C (200°F). All three past weld annealing treatments appear to have normalized the strength behavior. Both longitudinal and transverse strength properties for each PWA were similar; normal flow and fracture behavior to low temperatures was restored in each case.

5.3.1.4 Metallography

To provide further information on the effect of the various thermal exposures on the mechanical properties of the EB and GTA welds in ASTAR-1211C, specimens representing each condition evaluated were examined metallographically. Typical microstructures are shown in Figures 88 through 92.

Table 35. Longitudinal and Traverse Tensile Properties of GTA Welded and PWA ASTAR-1211C Sheet

Test Condition	Type Spec.	Test Temperature (°C)	Test Temperature (°F)	Yield Strength (MN/m²)	Yield Strength (ksi)	Ultimate Strength (MN/m²)	Ultimate Strength (ksi)	Total Elong. (%)
As-welded	L	RT	RT	-	-	668	96.8*	0
	L	93	200	883	128.0	887	128.5	4.2
	L	149	300	807	117.0	840	121.7	10.9
	L	204	400	762	110.5	790	114.5	13.3
	T	RT	RT	779	112.9	916	132.8	14.7**
	T	-46	-50	778	112.8	938	136.0	3.4**
	T	93	200	651	94.3	773	112.0	7.3
	T	149	300	656	95.0	778	112.7	15.2**
	T	204	400	-	-	706	102.3	15.0**
1 hr/1649°C (3000°F) PWA	L	RT	RT	700	101.4	834	120.9	8.6
	L	-73	-100	842	122.0	883	128.0	2.3
	L	93	200	655	94.9	756	109.6	14.8
	L	149	300	571	82.8	713	103.4	14.1
	T	RT	RT	737	106.8	804	116.5	2.3
	T	-46	-50	858	124.3	927	134.3	2.0
	T	93	200	624	90.4	753	109.1	9.9
	T	149	300	580	84.0	709	102.7	10.9
1 hr/1815°C (3300°F) PWA	L	RT	RT	642	93.0	759	110.0	4.7
	L	-46	-50	796	115.3	856	124.1	1.7
	L	66	150	618	89.6	760	110.1	8.9
	L	149	300	547	79.3	701	101.6	16.0
	T	RT	RT	682	98.8	794	115.0	5.2
	T	-46	-50	776	112.5	863	125.0	2.8
	T	66	150	645	93.5	773	112.1	7.0
	T	149	300	562	81.5	718	104.0	9.1
1 hr/1982°C (3600°F) PWA	L	RT	RT	676	98.0	794	115.0	4.2
	L	-46	-50	-	-	664	96.3*	0
	L	66	150	649	94.0	768	111.3	4.7
	L	149	300	571	82.7	700	101.5	12.7
	T	RT	RT	690	100.0	704	102.0	1.3
	T	-46	-50	858	124.3	884	128.1	0.9
	T	66	150	702	101.8	767	111.1	11.3
	T	149	300	618	89.6	700	101.4	12.9

Strain Rate 0.05/min.
L = Longitudinal
T = Transverse

* Fracture Stress - broke on loading curve
** Failed in base metal

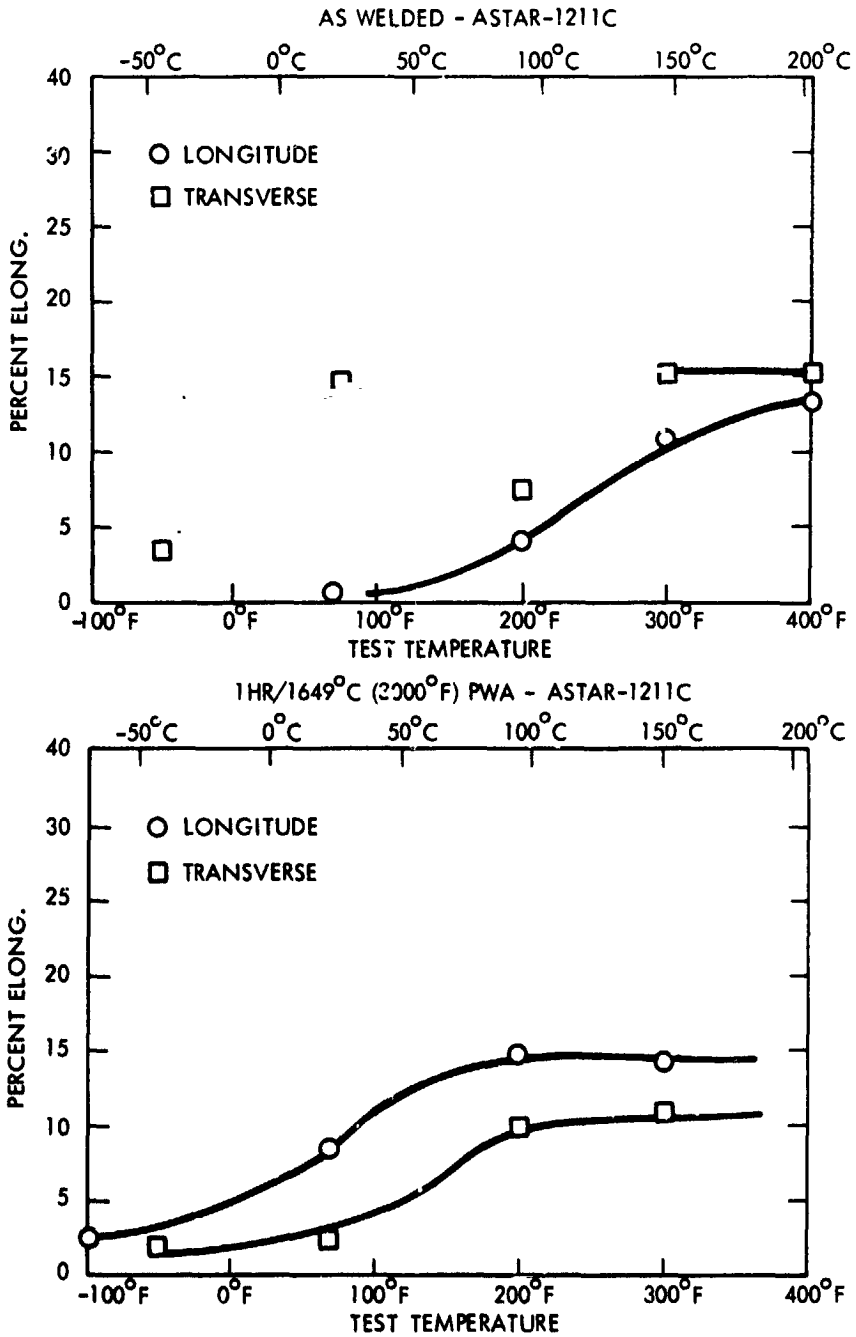

Figure 84. Results of Tensile Transition Temperature Tests on GTA Welds in 1.0 mm (0.040 inch) ASTAR-1211C Sheet. Thermal History as Indicated.

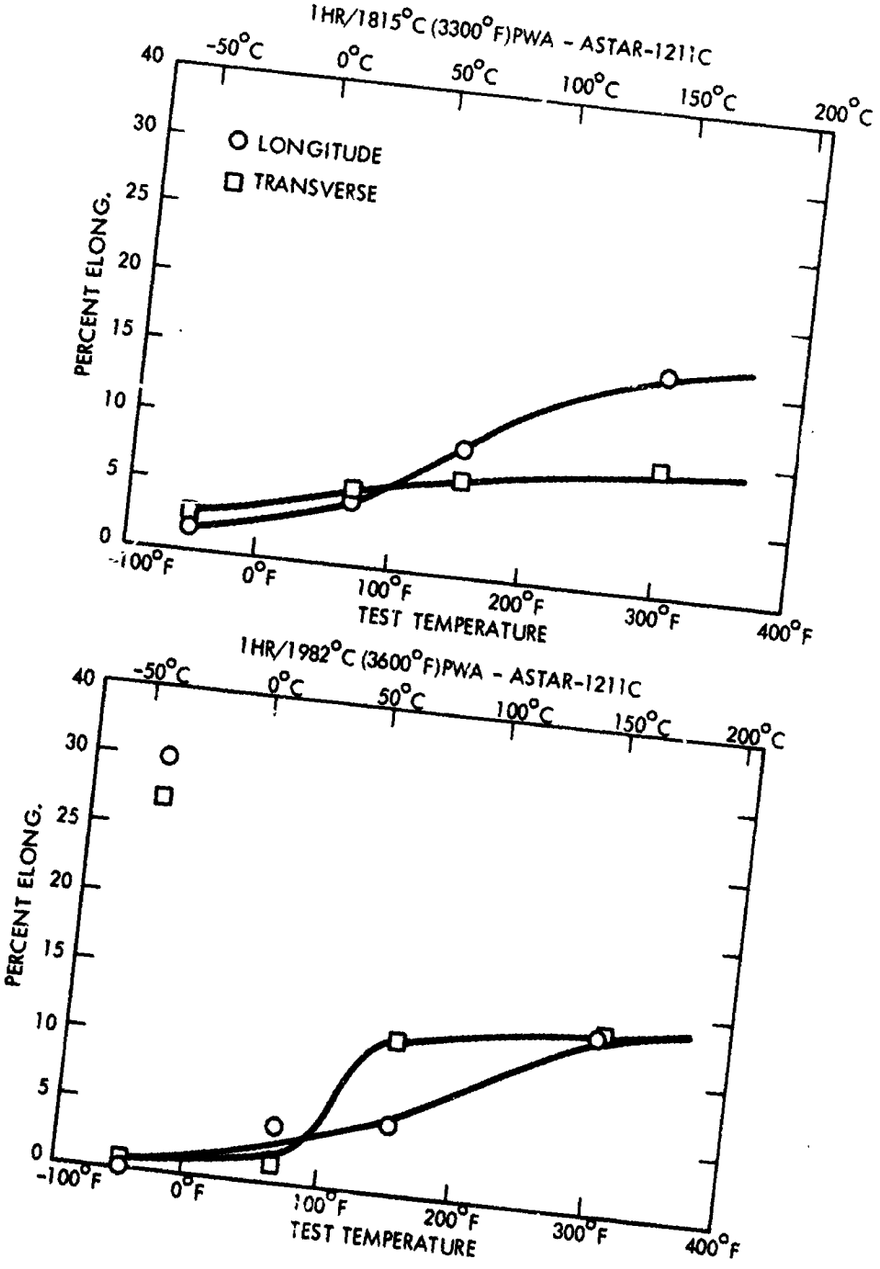

Figure 85. Results of Tensile Transition Temperature Tests on GTA Welds in 1.0 mm (0.040 inch) ASTAR-1211C Sheet. Thermal History as Indicated.

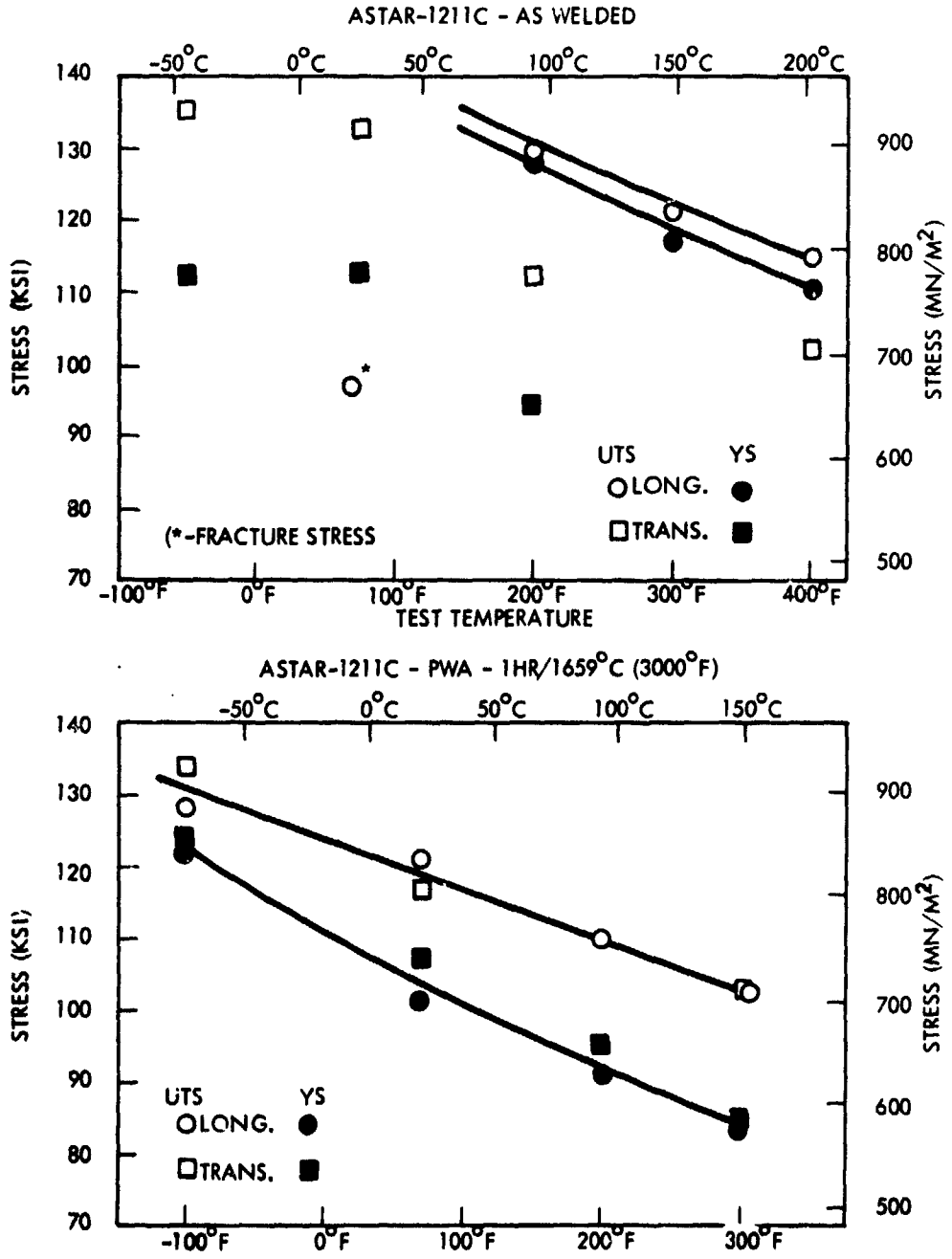

Figure 86. Tensile Strength Properties of GTA Welded and PWA ASTAR-1211C Sheet

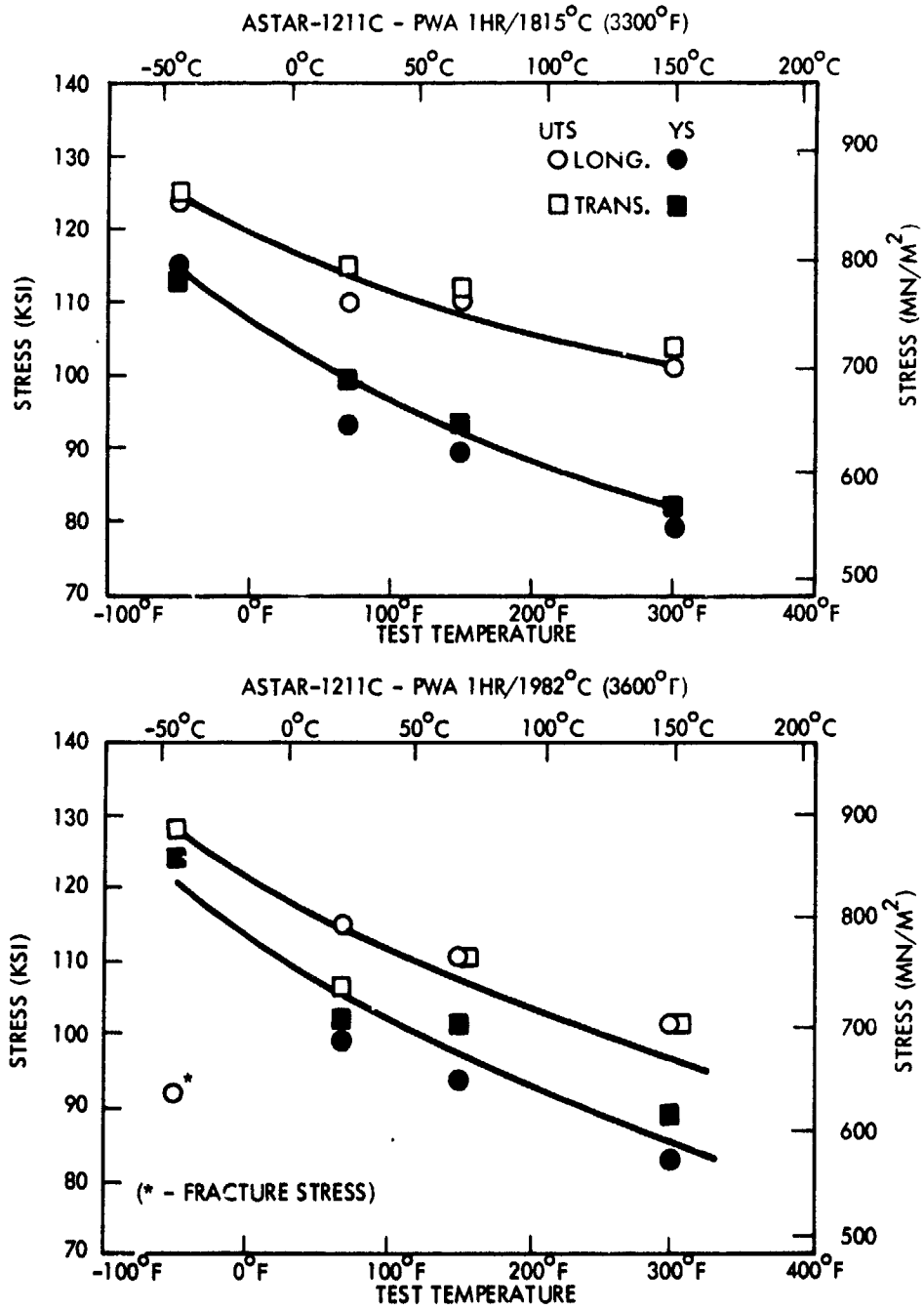

Figure 87. Tensile Strength Properties of GTA Welded and PWA ASTAR-1211C Sheet

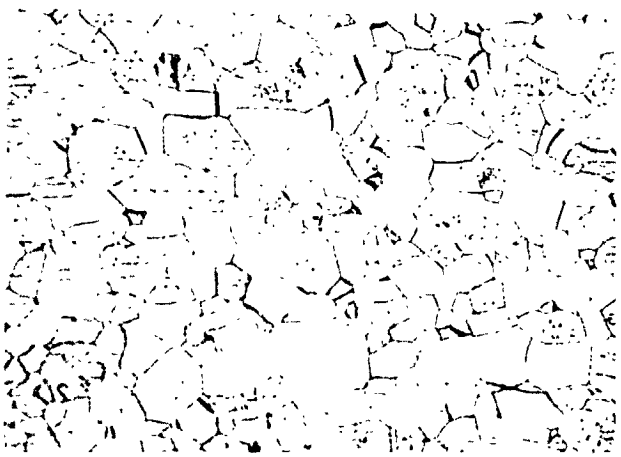

Base Metal 200X

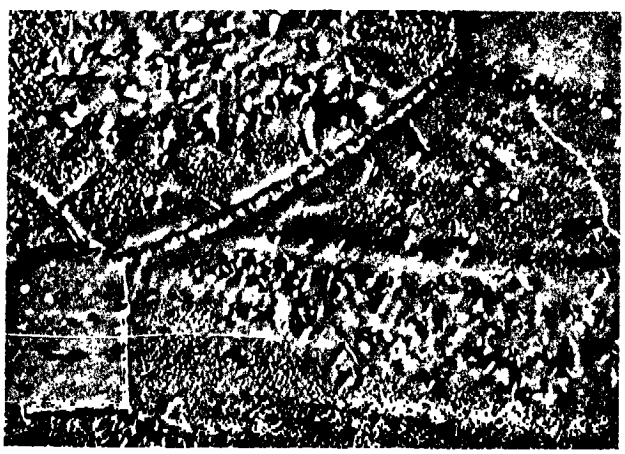

Base Metal 1500X

Figure 88. Microstructure of ASTAR-1211C Base Metal. Material Shown after 1 Hour-1649°C (3000°F) Anneal Following Rolling.

Weld

W/HAZ

GTA Weld 1500X

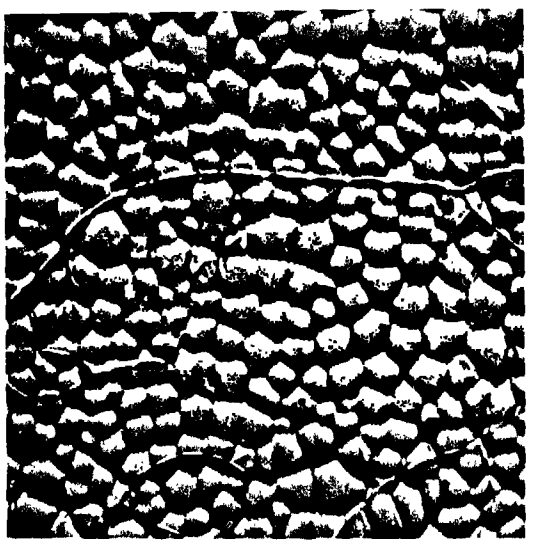

Weld

W/HAZ

EB Weld 1500X

Figure 89. As-Welded Microstructure of GTA and EB Welds in 1.0 mm (0.040 inch) ASTAR-1211C Sheet.

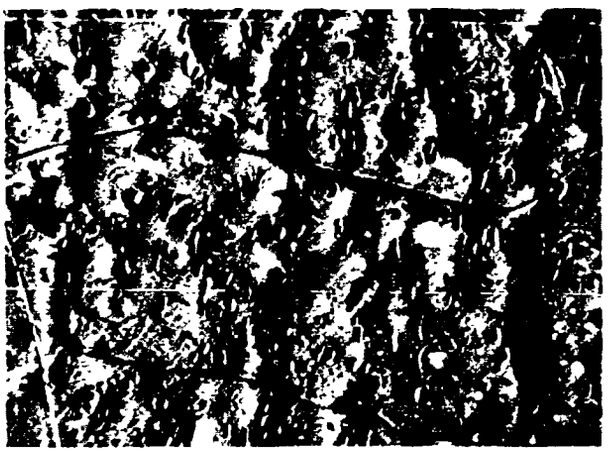

GTA Weld 1500X

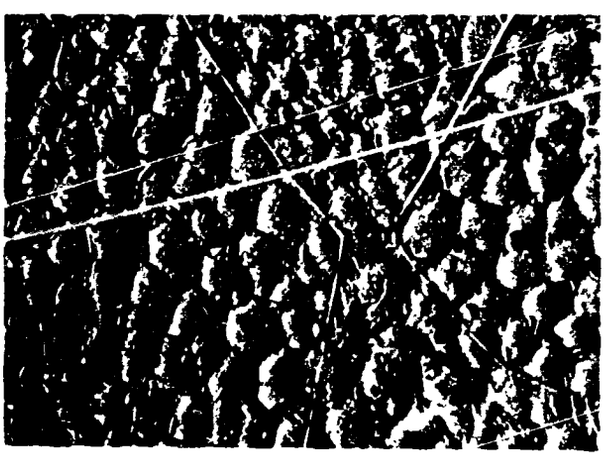

EB Weld 1500X

Figure 90. Microstructure of GTA and EB Welds in 1.0 mm (0.040 inch) ASTAR-1211C Sheet Following 1 Hour-1649°C (3000°F) PWA.

GTA Weld 1500X

EB Weld 1500X

Figure 91. Microstructure of GTA and EB Welds in 1.0 mm (0.040 inch) ASTAR-1211C Sheet Following 1 Hour-1815°C (3300°F) PWA.

GTA Weld 1500X

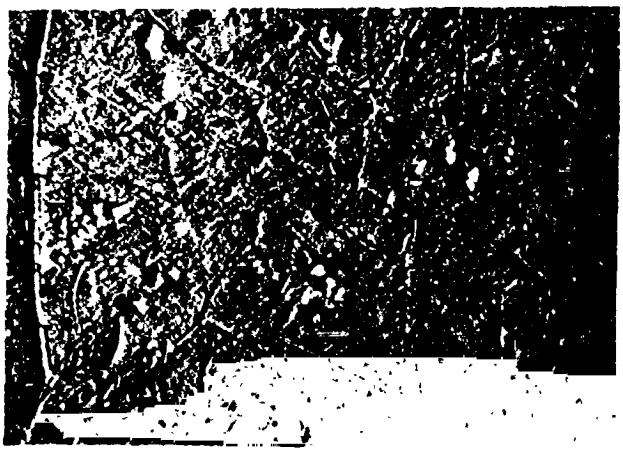

EB Weld 1500X

Figure 92. Microstructure of GTA and EB Welds in 1.0 mm (0.040 inch) ASTAR-1211C Sheet Following 1 Hour-1982°C (3600°F) PWA.

The as-welded microstructures, Figure 89, are seen to be exceptionally "clean". Post-weld annealing for 1 hour at 1649°C (3000°F), Figure 90, results in the appearance of precipitates in both the GTA and EB weld zones. In the EB welds there is a clear association between the precipitates and the interdendritic boundaries while in the GTA weld such an association is not obvious. The effect of post-weld annealing at 1815°C (3300°F), Figure 91, appeared to be mainly one of continuing the general development seen at 1649°C (3000°F) and somewhat alleviating the evidence of weld zone inhomogeneity residual from the weld solidification. One hour post-weld annealing at 1982° (3600°F), Figure 92, completely eradicates all evidence of the prior weld zone structure except for the delineation of the prior dendrite boundaries by precipitates. These now represent low angle sub-grain boundaries, probably of simple dislocation character, and are hence ready sites for the nucleation and growth of the precipitating phase. In addition to the precipitates located at the grain and sub-grain boundaries, a blockier appearing phase can be seen in both the GTA and EB weld zones.

5.3.2. Evaluation of ASTAR-1511C Sheet

The ductile-brittle transition temperatures of GTA and EB welds in 1.0 mm (0.040 inch) ASTAR-1511C sheet was determined using 1t bend tests.

Sheet specimens were prepared for welding by heavy pickling of the as-rolled sheet followed by vacuum annealing for 1 hour at 1649°C (3000°F). Preliminary attempts to prepare the individual weld specimens by shearing resulted in edge cracking. Hence, all weld specimen and subsequent bend test specimen preparation was achieved by cutting with a water cooled cut-off wheel. All material used for these evaluations was 1.0 mm (0.040 inch) thick sheet produced from NASVF-2000-AIN. GTA and EB welds were prepared using the same weld parameters already reported in this report for ASTAR-1211C. Visual and dye penetrant

inspection revealed no evidence of defects of any kind. Post-weld anneals were performed for 1 hour at 1649°C (3000°F), 1815°C (3300°F), and 1982°C (3600°F) at pressures below 1.3×10^{-6} N/M^2 (1×10^{-8} torr).

5.3.2.1 Bend Tests

Specimen orientation and testing procedures were identical to those used for ASTAR-1211C welds reported previously. Again, all tests were conducted using a 1t bend radius, corresponding to a nominal outer fiber strain of 33%. The 1t bend DBTT was also determined for the ASTAR-1511C base metal after a 1 hour 1649°C (3000°F) anneal.

The results of the bend tests on ASTAR-1511C are shown in Figures 93, 94, and 95 and are presented in tabular form in Table 36. The bend DBTT of the EB welds is seen to be slightly higher than that of the base metal and is relatively unaffected by the post-weld anneals, remaining consistently around 98°C (200°F). As was noted for ASTAR-1211C previously, the bend DBTT of the GTA welds is higher than those of the EB welds. However, the loss of ductility in the GTA welds is much more severe for ASTAR-1511C and even for the best post-weld anneal at 1815°C (3300°F) remains at 149°C (300°F). Fractures appeared to be invariably the result of cleavage.

5.3.2.2 Hardness

Hardness traverses were conducted on specimens of each of the conditions evaluated by bend testing. Hardness measurements were made on base metal, heat-affected zone (HAZ), and weld metal regions of each using a 10 Kg load on a Vickers hardness tester. The results of these measurements are plotted in Figures 96 through 99. Results were similar to those observed for ASTAR-1211C in that the very high hardness of the as-welded fusion and heat-affected zones was decreased by post-weld annealing. The 1 hour - 1649°C (3000°F) post-weld

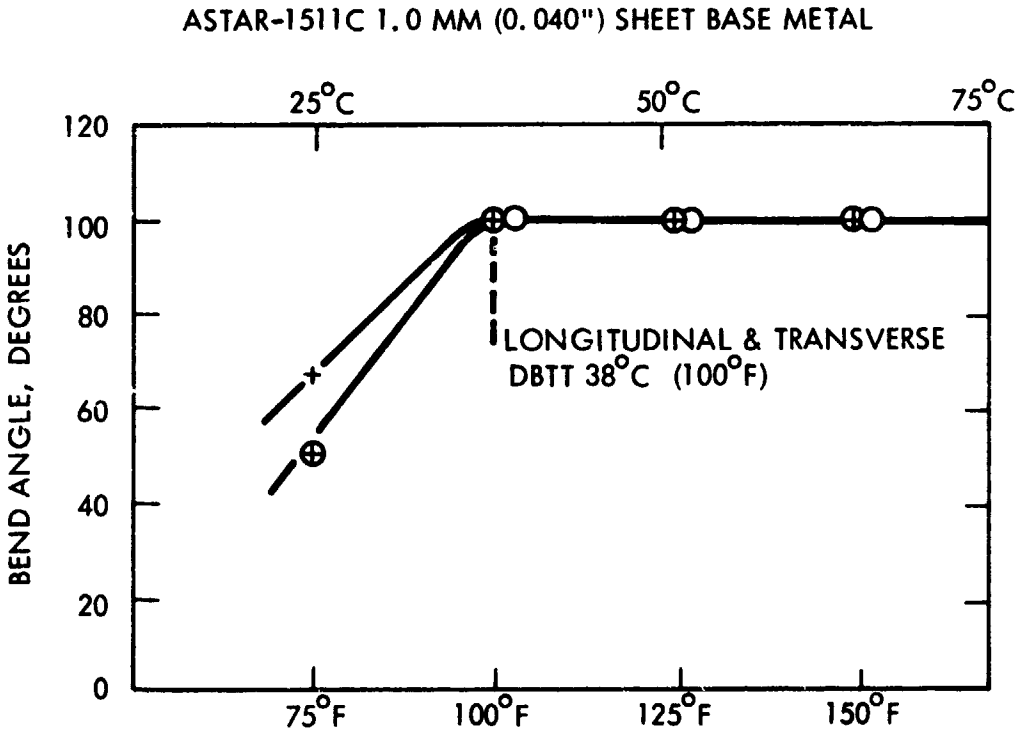

Figure 93. Results of 1 t Bend Tests on ASTAR-1511C Base Metal

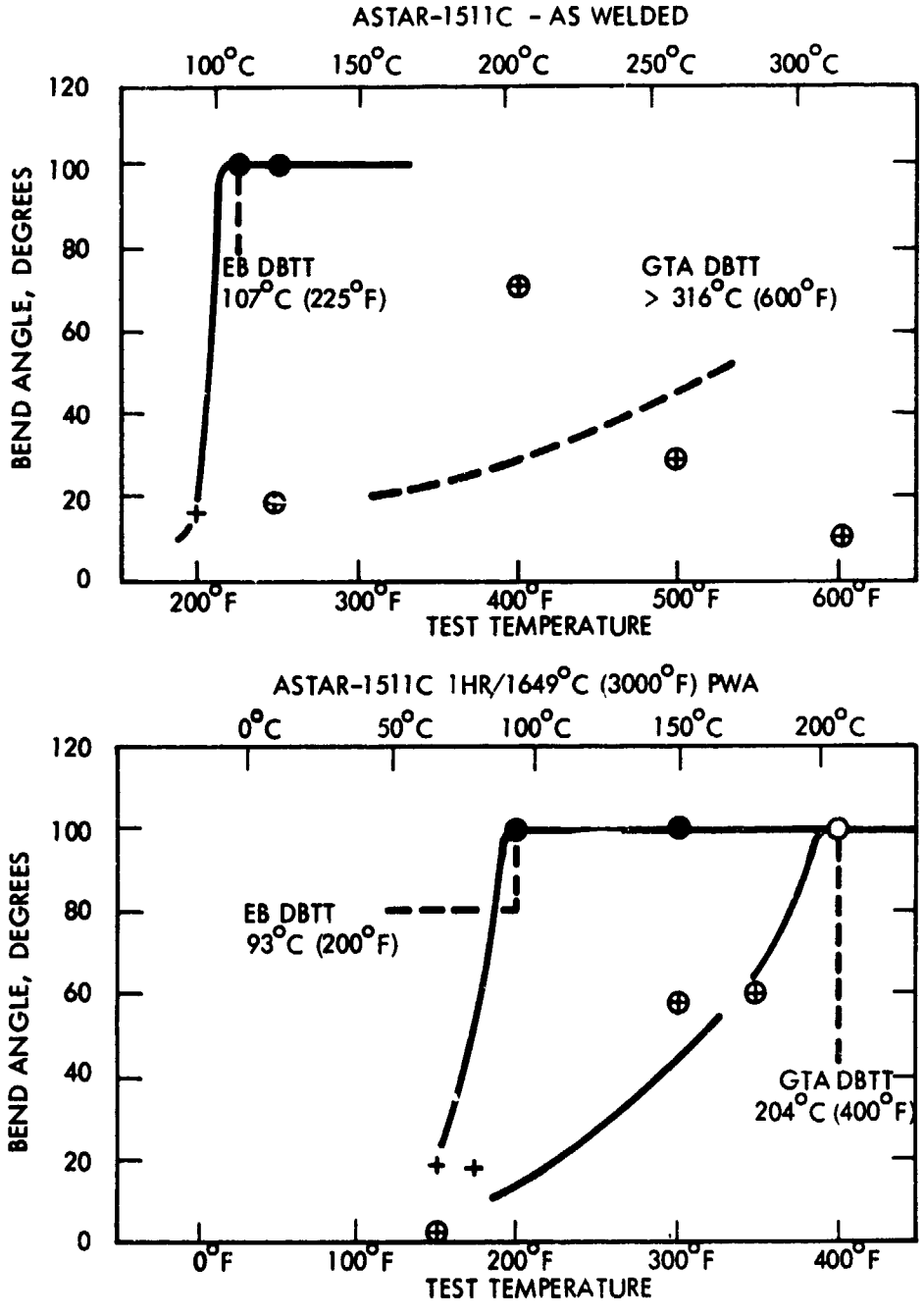

Figure 94. Results of 1 t Bend Tests on EB and GTA Welds in 1.0 mm (0.040 inch) ASTAR-1511C Sheet. Thermal History as Indicated.

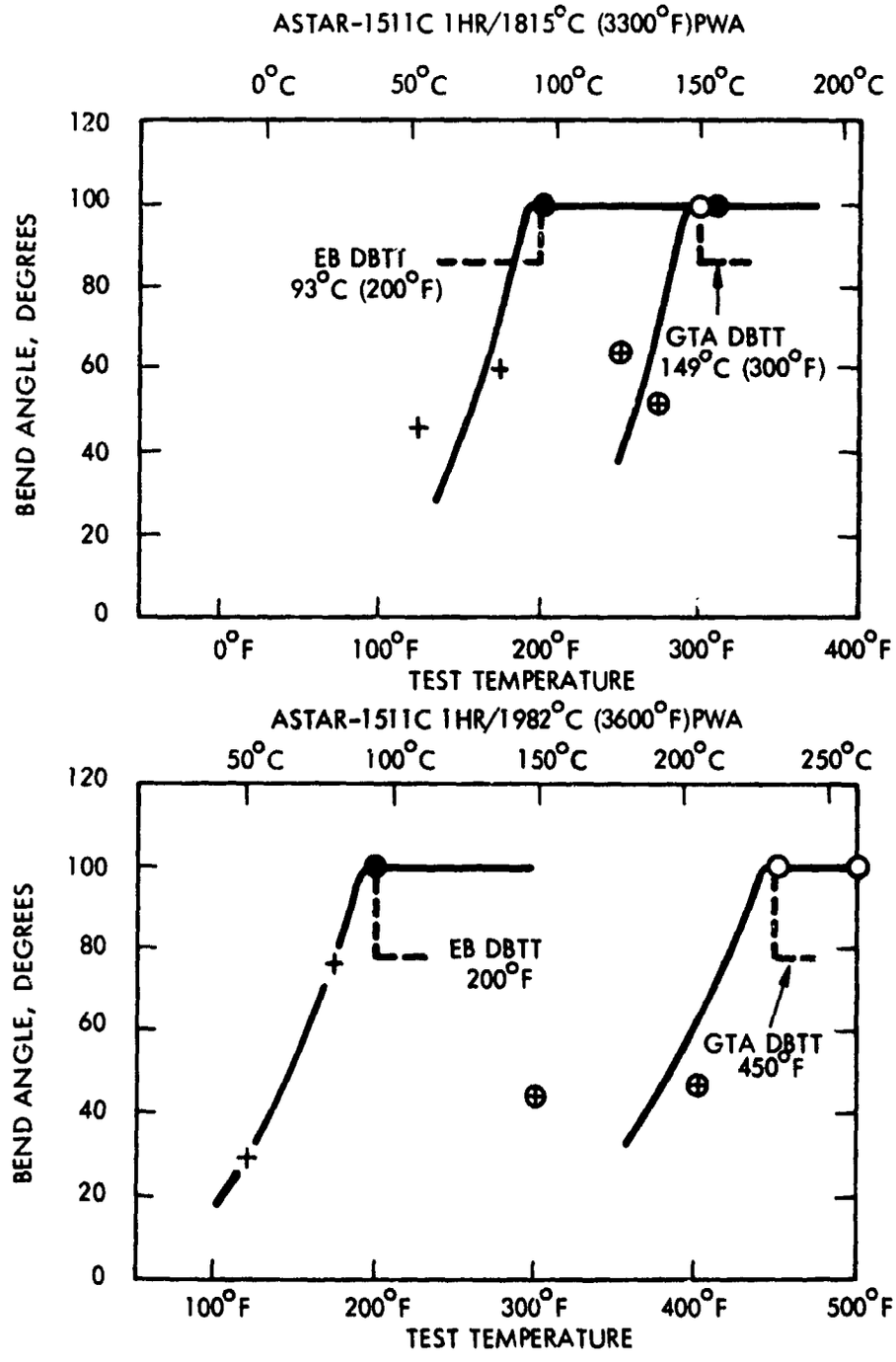

Figure 95. Results of 1t Bend Tests on EB and GTA Welds on 1.0 mm (0.040 inch) ASTAR-1511C Sheet. Thermal History as Indicated.

Table 36. Summary of Bend Ductile-Brittle Transition Temperatures Results for GTA and EB Welded ASTAR-1511C Sheet. (Thermal exposures as indicated)

Test Condition	1t Bend DBTT			
	GTA Welds		EB Welds	
	(°C)	(°F)	(°C)	(°F)
As-welded	>316	>600	107	225
1 hr/1649°C (3000°F) PWA	204	400	93	200
1 hr/1815°C (3300°F) PWA	149	300	93	200
1 hr/1982°C (3600°F) PWA	232	450	93	200
Base Metal	Longt. 38	100	Trans. 38	100

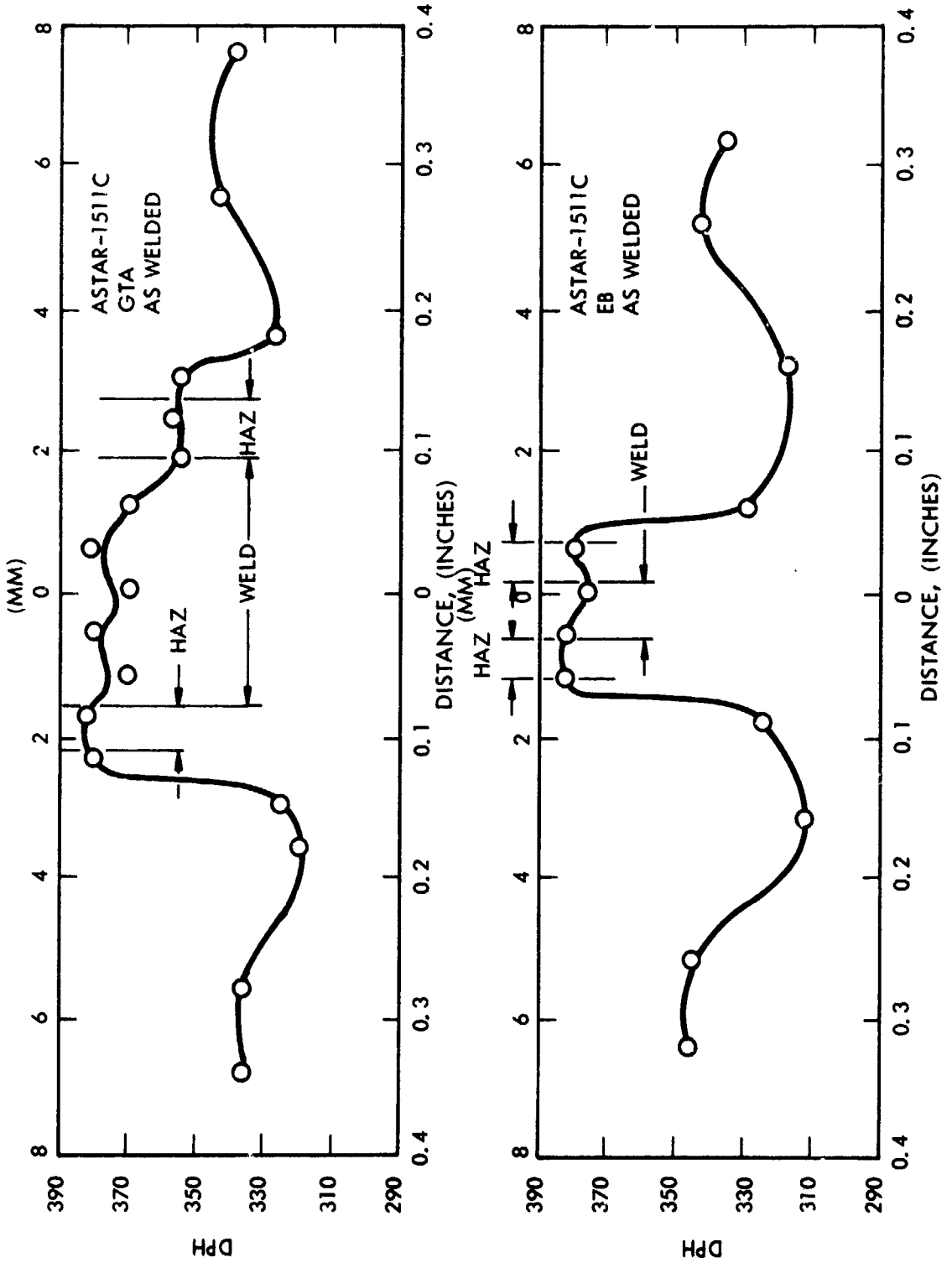

Figure 96. Hardness Traverses on EB and GTA in 1.0 mm (0.040 inch) ASTAR-1511C Sheet. Tested in the As-Welded Condition.

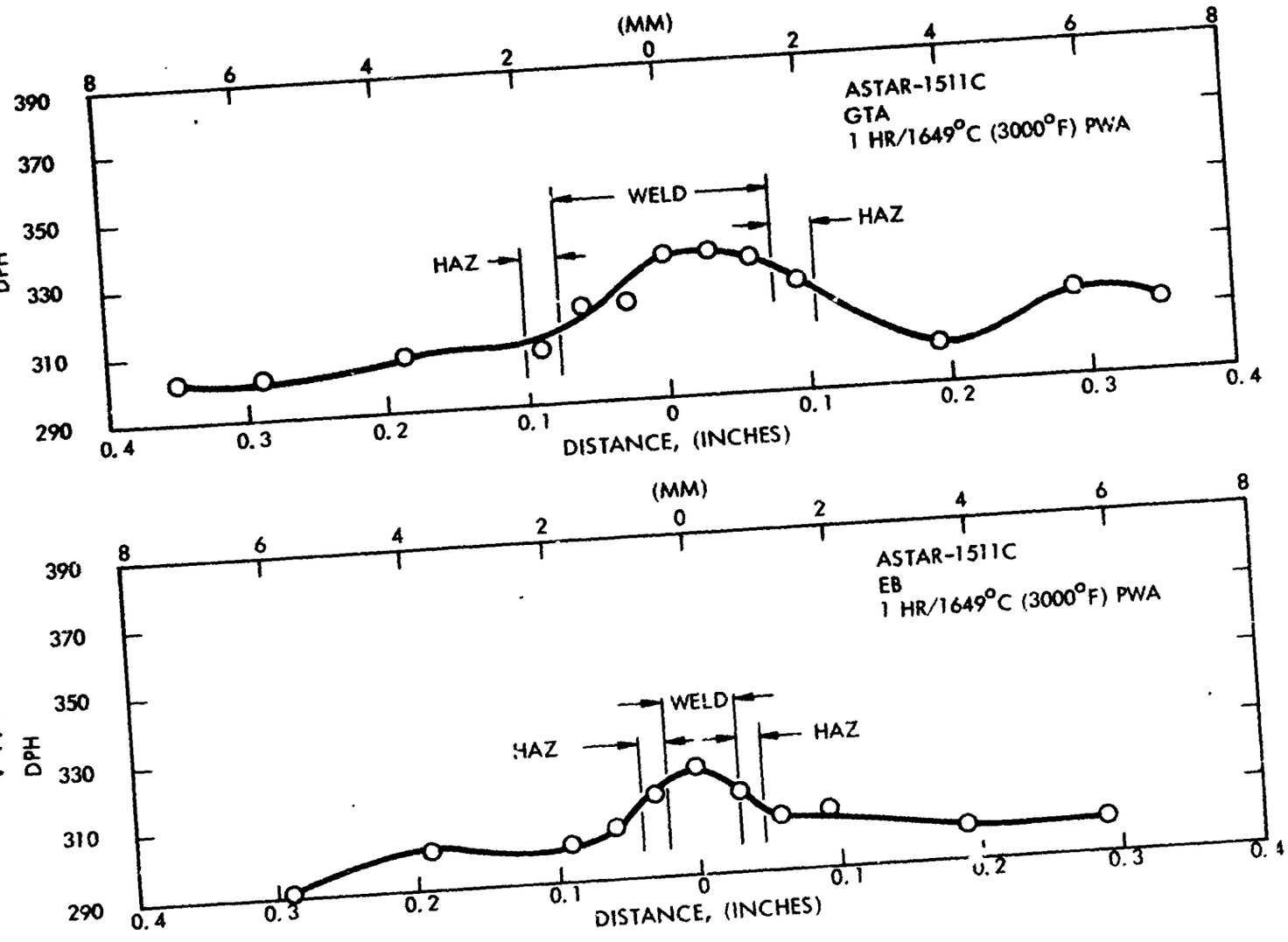

Figure 97. Hardness Traverses on EB and GTA Welds in 1.0 mm (0.040 inch) ASTAR-1511C Sheet. Tested After 1 HR/1649°C (3000°F) PWA.

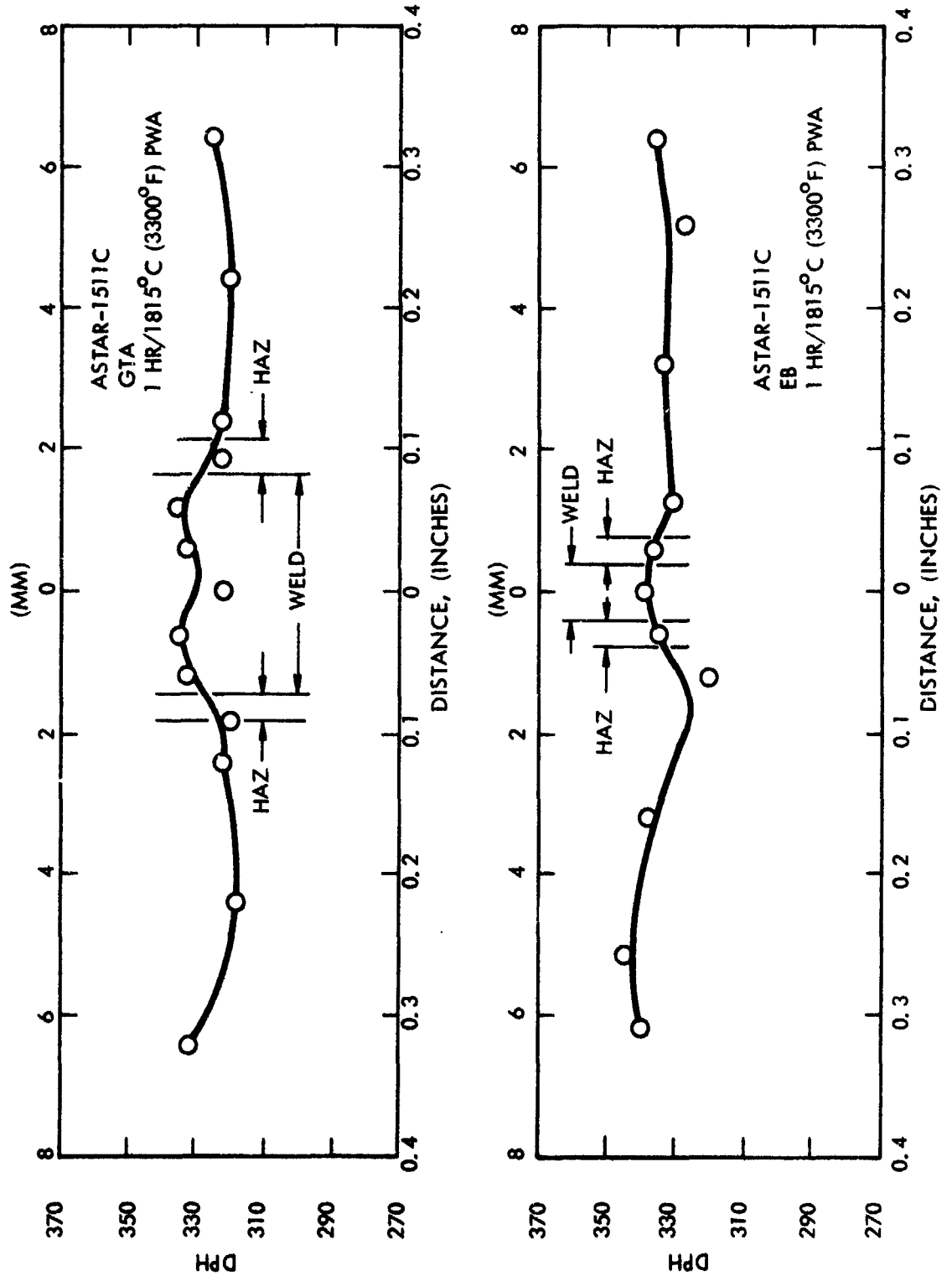

Figure 98. Hardness Traverses on EB and GTA Welds in 1.0 mm (0.040 Inch) ASTAR-1511C Sheet. Tested After 1 HR/1815°C (3300°F) PWA.

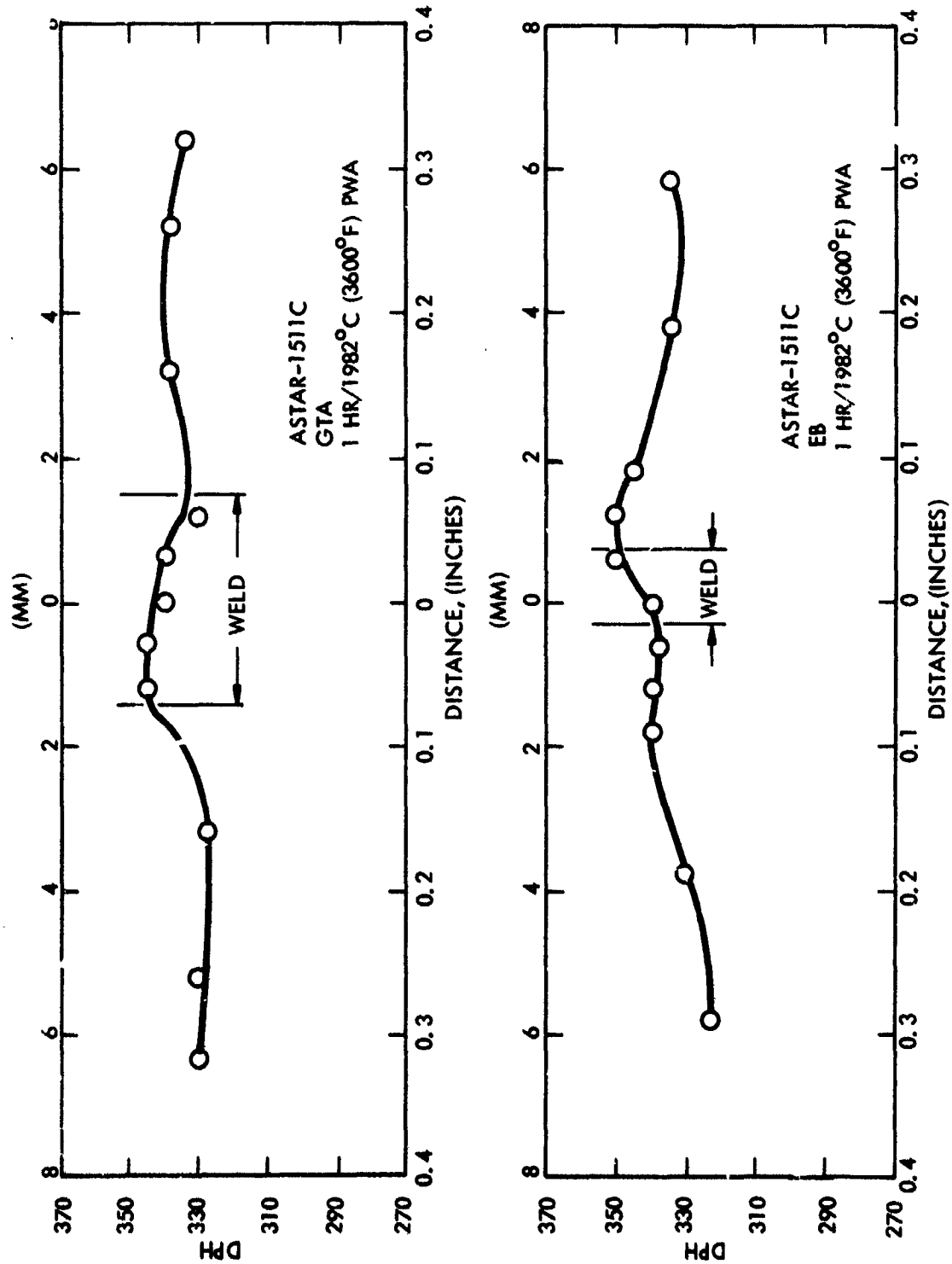

Figure 99. Hardness Traverses in EB and GTA Welds in 1.0 mm (0.040 inch) ASTAR-1511C Sheet. Tested After 1 HR/1982°C (3600°F) PWA.

anneals appear to have been unable to completely relieve the weld zone hardness. However, comparing these data with the fact the hardness of the as-rolled and recrystallized (1 hour - 1649°C (3000°F) base metal was DPH 344 suggests it is the base metal readings of Figure 97 that are low, rather than the weld and HAZ values being high. The base metal hardness values are more typical of ASTAR-1211C than ASTAR-1511C.

5.3.2.3 Metallography

Microstructures of the GTA and EB welds produced in the ASTAR-1511C sheet are shown in Figures 100 through 104. In the as-welded condition, Figure 101, both the fusion zone and heat-affected zone of GTA and EB welds appear exceptionally clean, i.e., free of evidence of precipitation.

Post-weld annealing for 1 hour at 1649°C (3000°F) resulted in the appearance of two types of precipitates, Figure 102. In both the GTA and EB fusion zones precipitates have formed in the interdendritic regions and, in addition, a cellular, discontinuous precipitate has appeared at some of the grain boundaries. This latter form of precipitate has been previously noted on ASTAR-811C welds but only after 1000 hour aging treatments at 1149°C (2100°F).

One hour post-weld annealing at 1815°C (3300°F), Figure 103, has resulted in the general development of the precipitates in the weld fusion zones to approximately the same condition realized by 1 hour annealing at 1649°C (3000°F) in the ASTAR-1211C. This can be seen by comparing Figure 103 to Figures 90 and 91. This implies that the higher tungsten content of ASTAR 1511C may be retarding the kinetics of the annealing reaction for that alloy.

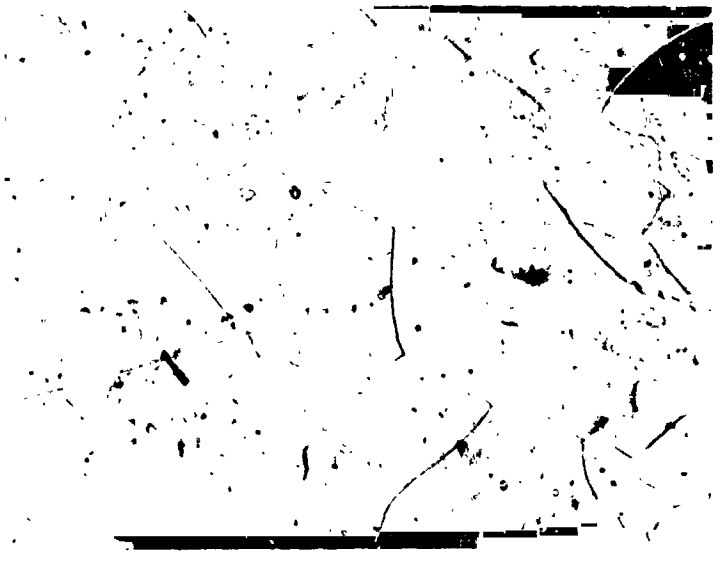

1500X

Figure 100. Microstructure of ASTAR-1511C Base Metal. Shown After 1 Hour-1649°C (3000°F) Anneal Following Rolling.

Astronuclear Laboratory

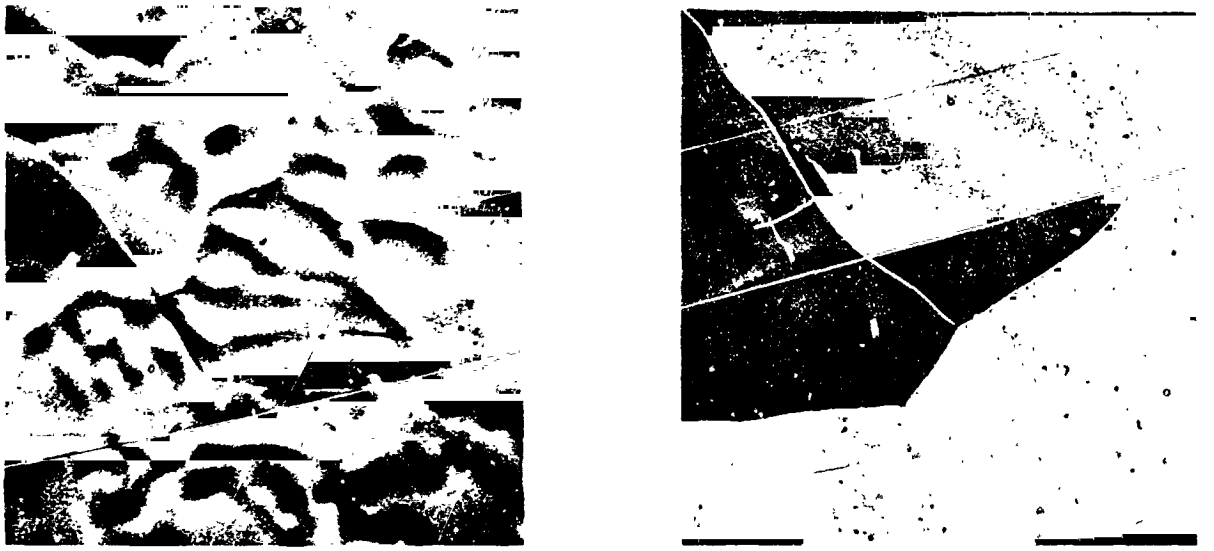

Weld W/HAZ

GTA Weld 1500X

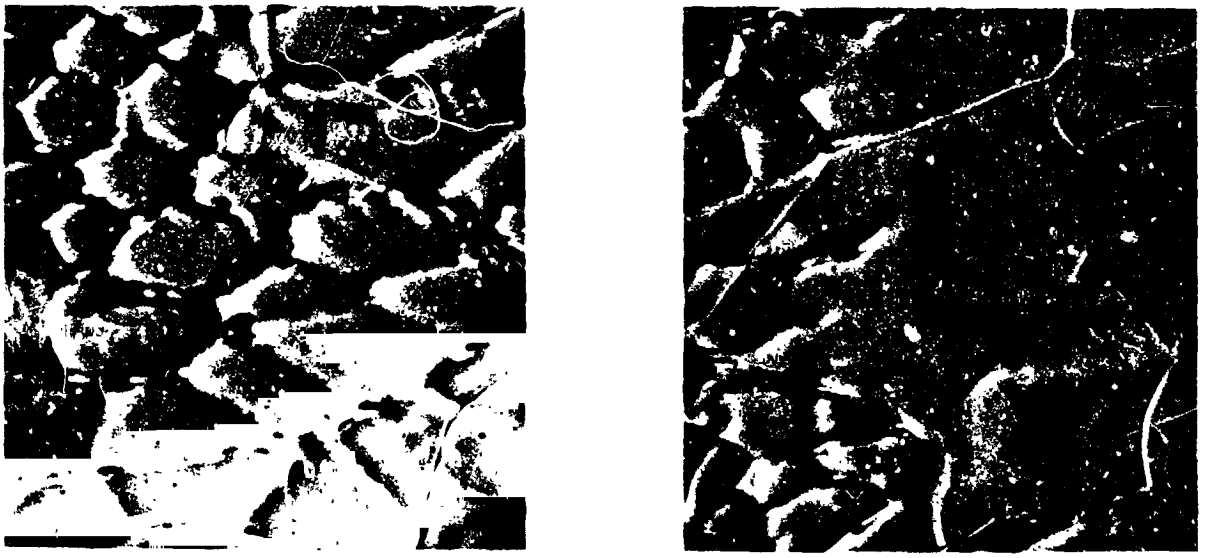

Weld W/HAZ

EB Weld 1500X

Figure 101. As-Welded Microstructure of GTA and EB Welds in 1.0 mm (0.040 inch) ASTAR-1511C Sheet.

GTA Weld 1500X

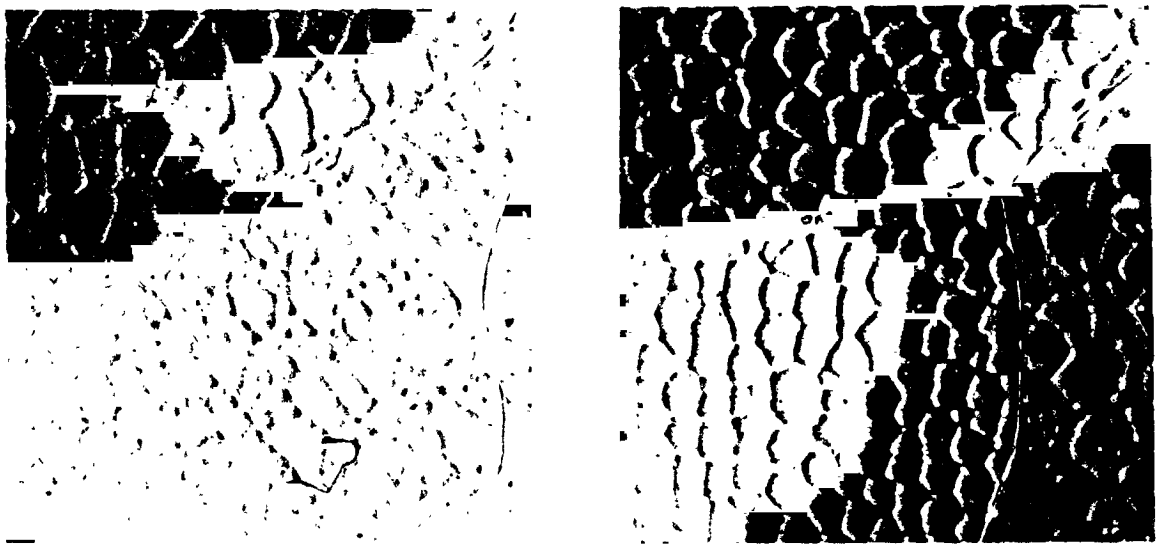

EB Weld 1500X

Figure 102. Microstructure of GTA and EB Welds in 1.0 mm (0.040 inch) ASTAR-1511C Sheet Following 1 Hour-1649°C (3000°F) PWA.

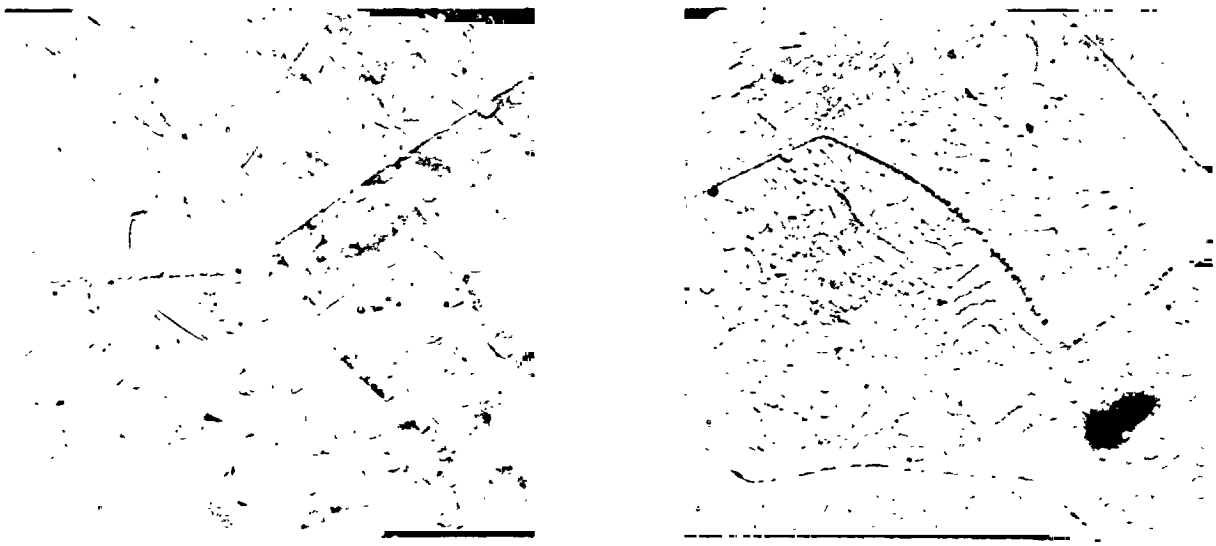

Fusion Zone

Base Metal

GTA Weld 1500X

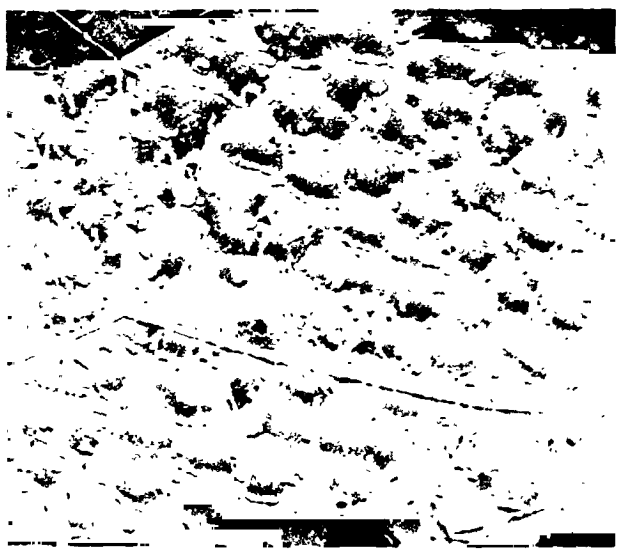

EB Weld 1500X

Figure 103. Microstructure of GTA and EB Welds in 1.0 mm (0.040 inch) ASTAR-1511C Sheet Following 1 Hour-1815°C (3300°F) PWA.

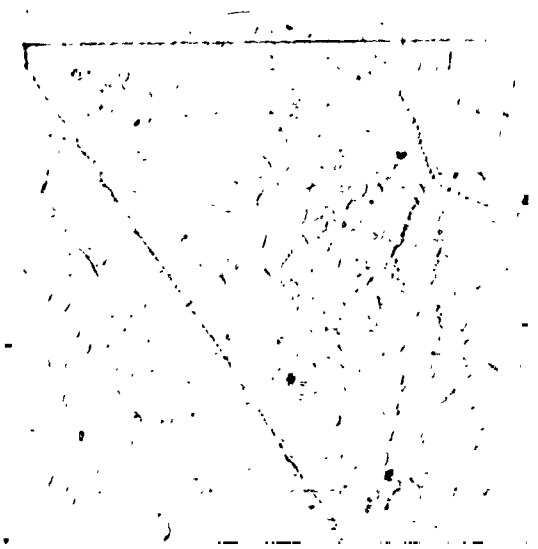

1500X

400X

GTA Weld

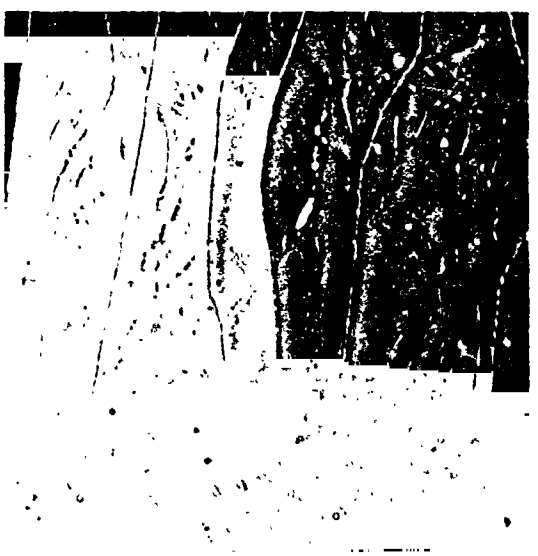

1500X

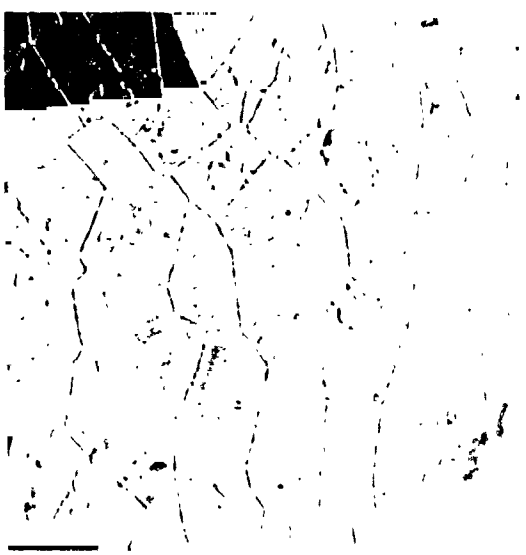

1500X

EB Weld

Figure 104. Microstructure of GTA and EB Welds in 1.0 mm (0.40 inch) ASTAR-1511C Sheet Following 1 Hour-1982°C (3600°F) PWA.

The effect of 1 hour post-weld annealing at 1982°C (3600°F) is shown in Figure 104. This anneal has had the effect of substantially increasing the grain size as well as resulting in extensive grain and sub-grain boundary precipitation. Note the very regular and complete decoration of the sub-grain boundaries in the EB weld. Where it has been possible, for example near the intersection of grain and sub-grain boundaries, polygonization has occurred, and subsequent cooling from the annealing temperature has resulted in precipitation on the polygonized boundaries. There also appears to be very fine, intragranular precipitates within the grain and sub-grain interiors. The considerable change in structure noted between the 1815°C (3300°F) and the 1649°C (3000°F) anneals implies the temperature for complete carbon solutioning lies within that range.

5.3.3 Evaluation of Thermally Aged, GTA Welded Sheet

The final portion of this task involved the tensile testing of GTA welded, post-weld annealed, and thermally aged material. Longitudinal and transverse welded specimens of ASTAR-1211C and longitudinal welded specimens of ASTAR-1511C were post-weld annealed 1 hour at 1649°C (3000°F), 1815°C (3300°F), and 1982°C (3600°F). Four tensile specimens of each post-weld anneal along with four specimens in the "as-welded" condition were thermally aged for 1000 hours at 1149°C (2100°F), 1316°C (2400°F), and 1427°C (2600°F). The aging treatments were done in a vacuum of 1.3×10^{-6} N/m^2 (1×10^{-8} torr) or better in ultra-high vacuum annealing furnaces.[10]

5.3.3.1 Determination of Tensile DBTT of GTA Welded ASTAR-1211C Sheet

Tensile tests of PWA and thermally aged specimens were conducted over a range of temperatures. Initial testing was carried out at room temperature, and subsequent test temperatures were selected on the basis of prior results. The tensile test data are listed in Table 37. The total elongation values were plotted as a function of test temperature in Figures 105, 106,

Table 37. Low Temperature Tensile Properties of GTA Welded, PWA, and Aged ASTAR-1211C Sheet

Specimen Thermal History	Spec. Type	Test Temperature (°C)	Test Temperature (°F)	Yield Strength (MN/m^2)	Yield Strength (ksi)	Ultimate Strength (MN/m^2)	Ultimate Strength (ksi)	Total Elong. (%)
As-welded + 1000 hrs/1149°C (2100°F)	T	RT	RT	658	95.4	718	104.1	4.6
	T	93	200	595	86.3	682	98.9	7.9
	T	149	300	524	75.9	623	90.3	8.7
	T	204	400	502	72.7	587	85.0	8.2
	L	RT	RT	665	96.4	707	102.5	3.0
	L	93	200	576	83.5	689	99.8	15.9
	L	149	300	535	77.6	646	93.7	18.0
PWA-1 hr/1649°C (3000°F) + 1000 hrs/ 1149°C (2100°F)	T	-129	-200	877	127.1	908	131.6	1.7
	T	-73	-100	771	111.8	822	119.1	5.0
	T	RT	RT	663	96.1	735	106.5	8.8
	T	149	300	519	75.2	618	89.5	9.9
	L	-73	-100	776	112.4	796	115.3	1.3
	L	-18	0	690	100.0	753	109.2	5.6
	L	RT	RT	635	92.1	742	107.5	17.4
	L	149	300	535	77.6	642	93.0	18.0
PWA-1 hr/1815°C + 1000 hrs/1149°C (2100°F)	T	RT	RT	651	94.3	710	102.9	4.7
	T	93	200	572	82.9	662	96.0	9.0
	T	149	300	512	74.2	623	90.3	9.7
	T	204	400	484	70.2	569	82.5	8.4
	L	-73	-100	782	113.3	801	116.1	1.3
	L	-18	0	691	100.2	739	107.1	3.9
	L	RT	RT	651	94.4	748	108.4	12.4
	L	149	300	507	73.5	630	91.3	19.8
PWA-1 hr/1982°C (3600°F) + 1000 hrs/ 1149°C (2100°F)	T	RT	RT	643	93.2	693	100.4	4.2
	T	66	150	589	85.3	679	98.4	9.6
	T	93	200	562	81.5	643	93.2	8.9
	T	149	300	515	74.7	607	87.9	9.7
	L	RT	RT	641	92.9	702	101.8	6.2
	L	66	150	595	86.3	637	92.3	3.1
	L	93	200	553	80.1	648	93.9	20.1
	L	149	300	519	75.2	608	88.1	15.3

Strain Rate 0.05/min.
T = Transverse
L = Longitudinal

Table 37. Low Temperature Tensile Properties of GTA Welded, PWA, and Aged ASTAR-1211C Sheet (Cont'd.)

Specimen Thermal History	Spec. Type	Test Temperature (°C)	Test Temperature (°F)	Yield Strength (MN/m^2)	Yield Strength (ksi)	Ultimate Strength (MN/m^2)	Ultimate Strength (ksi)	Total Elong. (%)
As-welded +1000 hrs/1316°C (2400°F)	T	-46	-50	774	112.2	824	119.4	5.2
	T	RT	RT	674	97.7	752	109.0	8.5
	T	93	200	607	88.0	718	104.0	9.4
	T	149	300	549	79.5	642	93.0	8.8
	L	RT	RT	676	98.0	708	102.6	3.7
	L	66	150	635	92.0	731	105.9	12.6
	L	93	200	609	88.3	701	101.6	15.3
	L	149	300	562	81.5	652	94.5	18.3
PWA-1 hr/1649°C (3000°F) + 1000 hrs/ 1316°C (2400°F)	T	-101	-150	846	122.7	902	130.8	7.1
	T	-46	-50	744	107.8	818	118.5	8.6
	T	RT	RT	676	98.0	769	111.4	12.6
	T	149	300	553	80.2	635	92.0	10.6
	L	-101	-150	853	123.7	901	130.6	4.4
	L	-46	-50	756	109.5	839	121.6	9.9
	L	RT	RT	675	97.8	778	112.8	23.4
	L	149	300	538	77.9	637	92.7	20.8
PWA-1 hr/1815°C (3300°F) + 1000 hrs/ 1316°C (2400°F)	T	-101	-150	840	121.7	881	127.7	3.8
	T	-46	-50	753	109.2	834	120.9	9.7
	T	RT	RT	659	95.5	741	107.4	9.3
	T	149	300	534	77.4	624	90.5	10.0
	L	-101	-150	847	122.8	894	129.5	4.3
	L	-46	-50	740	107.2	813	117.8	8.5
	L	RT	RT	680	98.5	760	110.2	15.0
	L	149	300	531	77.0	642	93.0	17.5
PWA-1 hr/1982°C (3600°F) + 1000 hrs/ 1316°C (2400°F)	T	-46	-50	747	108.2	747	108.2	.2
	T	RT	RT	666	96.5	738	107.0	7.5
	T	149	300	539	78.1	621	90.0	9.0
	T	204	400	480	69.5	572	82.9	13.0
	L	RT	RT	652	94.5	660	95.7	1.3
	L	149	300	535	77.5	599	86.8	6.5
	L	177	350	513	74.4	610	88.4	19.7
	L	232	450	459	66.5	560	81.2	19.2

Strain Rate 0.05/min.
T = Transverse
L = Longitudinal

Table 37. Low Temperature Tensile Properties of GTA Welded, PWA, and Aged ASTAR-1211C Sheet (Cont'd.)

Specimen Thermal History	Spec. Type	Test Temperature (°C)	Test Temperature (°F)	Yield Strength (MN/m²)	Yield Strength (ksi)	Ultimate Strength (MN/m²)	Ultimate Strength (ksi)	Total Elong. (%)
As-welded + 1000 hrs/ 1427°C (2600°F)	T	-46	-50	811	117.5	866	125.5	7.1
	T	RT	RT	723	104.8	771	111.7	7.7
	T	149	300	591	85.7	659	95.5	8.7
	T	204	400	538	78.0	581	84.2	7.3
	L	RT	RT	718	104.0	767	111.2	6.3
	L	52	125	682	98.9	759	110.0	11.2
	L	93	200	653	94.6	724	104.9	11.8
	L	149	300	590	85.5	677	98.1	16.2
PWA-1 hr/1649°C (3000°F) + 1000 hrs/ 1427°C (2600°F)	T	RT	RT	725	105.0	763	110.6	5.2
	T	93	200	651	94.3	712	103.2	9.4
	T	149	300	590	85.5	-	95.0	11.5
	L	-46	-50	820	118.8	656	121.0	3.0
	L	RT	RT	719	104.2	787	114.0	10.0
	L	66	150	680	98.6	754	109.3	16.1
	L	149	300	580	84.0	672	97.4	20.4
PWA-1 hr/1815°C (3300°F) + 1000 hrs/ 1427°C (2600°F)	T	RT	RT	721	104.5	737	106.8	1.9
	T	93	200	649	94.1	712	103.2	7.6
	T	149	300	580	84.1	649	94.0	8.9
	T	204	400	558	80.8	616	89.3	11.9
	L	RT	RT	723	104.8	768	111.3	6.6
	L	66	150	675	97.8	717	103.9	5.0
	L	93	200	460	66.6	727	105.3	14.9
	L	149	300	596	86.4	675	97.8	15.8
PWA-1 hr/1815°C (3000°F) + 1000 hrs/ 1427°C (2600°F)	T	RT	RT	727	105.4	749	108.5	2.8
	T	93	200	651	94.3	709	102.8	6.6
	T	149	300	587	85.1	650	94.2	9.5
	T	204	400	551	79.8	613	88.8	8.8
	L	149	300	575	83.3	620	89.8	3.6
	L	177	350	566	82.0	631	91.5	6.4
	L	204	400	539	78.1	620	89.9	13.8
	L	232	450	520	75.4	608	88.1	17.6

Strain Rate 0.05/min.
T = Transverse
L = Longitudinal

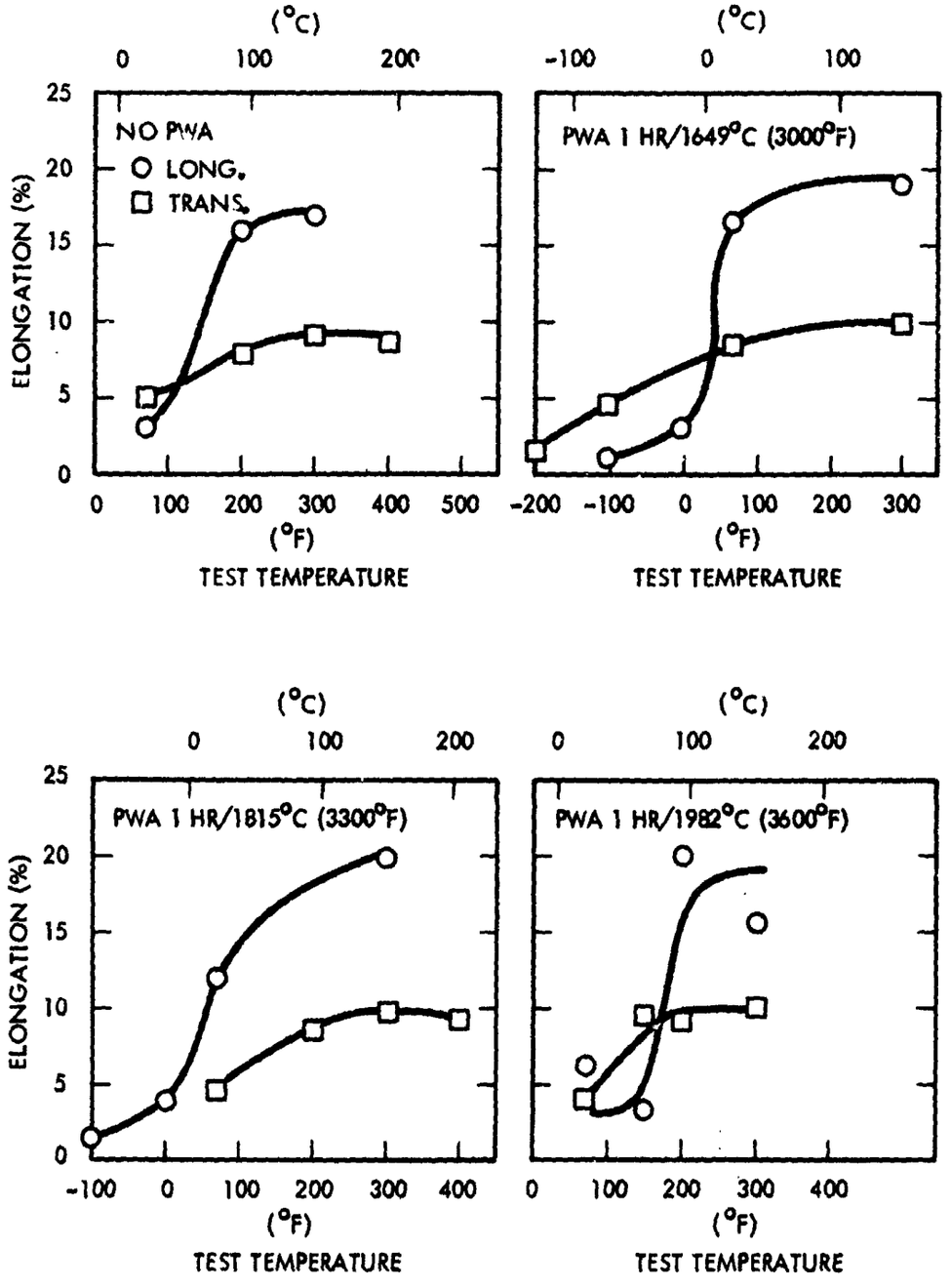

Figure 105. Tensile DBTT of GTA Welded ASTAR-1211C Sheet Thermally Aged 1000 Hrs./1149°C (2100°F)

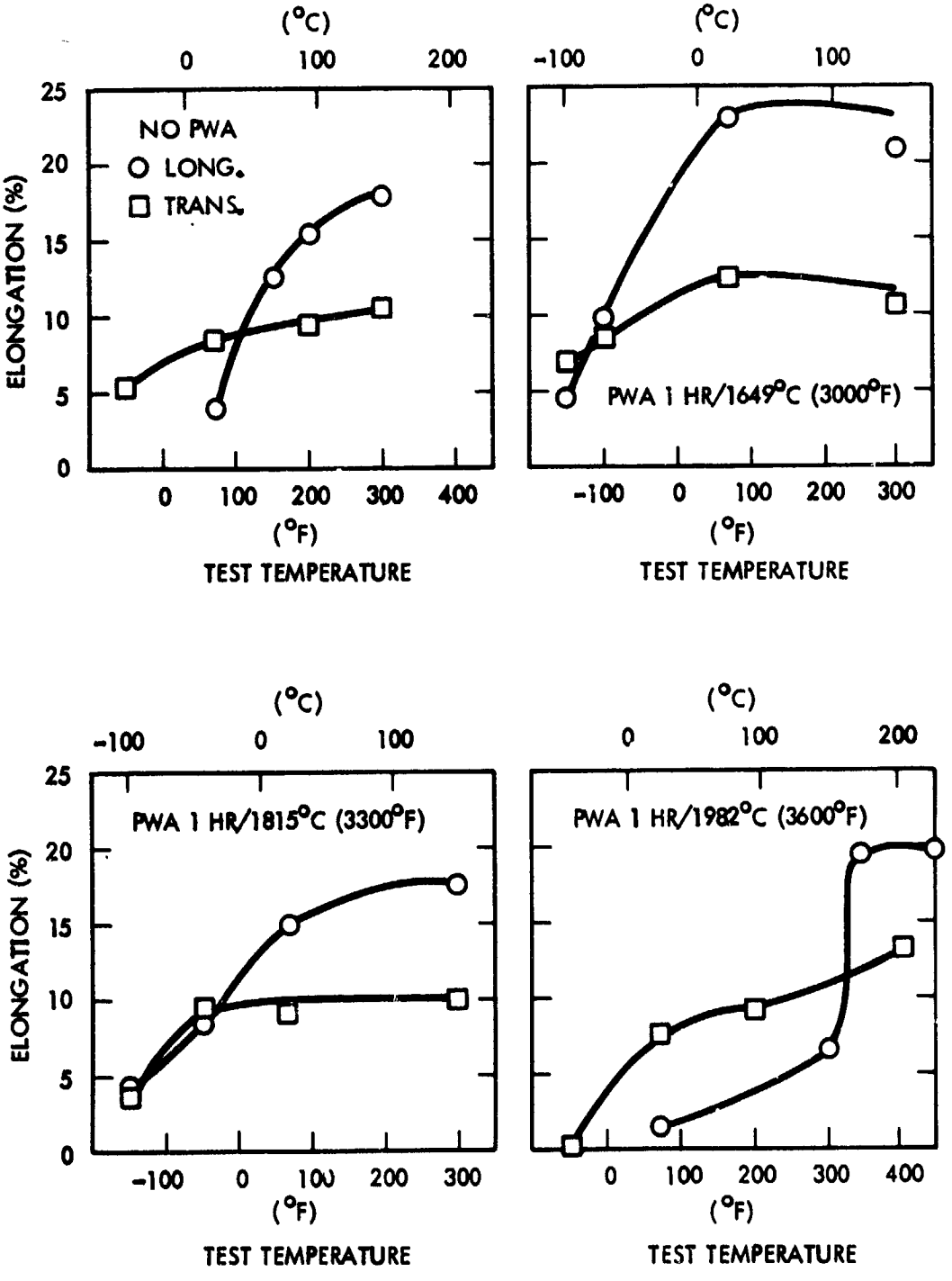

Figure 106. Tensile DBTT of GTA Welded ASTAR-1211C Sheet Thermally Aged 1000 Hrs./1316°C (2400°F)

and 107. Test data for both longitudinal and transverse orientations were included on the same plot. The longitudinal elongation values were generally higher than the transverse test values and exhibited classical ductile-to-brittle type behavior. The transverse data exhibited gradual changes in elongation with test temperature. The reason for the difference in behavior is shown in Figure 108. The tensile specimens were PWA 1 hour at 1649°C (3000°F) and aged at 1149°C (2100°F). The DBTT curves produced from test data of the pictured specimens are shown in Figure 105B. The longitudinal specimens showed evidence of ductile strain accommodation along the whole gage length at the higher test temperatures. The change in deformation mode as test temperature was reduced was also reflected in the fracture mode. At the lower test temperature, the fracture was essentially cleavage-type while ductile shear was evident at the higher temperatures. In the transverse tests, the strain was highly localized in the weld metal, producing lower overall elongation values. This behavior was particularly evident at temperatures above the DBTT. Thus, the curves produced by the transverse test data changed gradually with temperature rather than abruptly as was the case with the longitudinal test results. All transverse specimens, except two failed in the weld metal and in the gage section.

Ductile-brittle transition temperatures were taken from each curve and are summarized in Table 38. The DBTT was taken as the mid-point on the curve where the rate of changes of elongation with temperature was the greatest. The longitudinal values were readily obtained without much difficulty. The transverse values were more difficult to discern due to the shallow or small rate of change in elongation with temperature.

The DBTT are summarized in Figure 109. "As-welded" and unaged data were also included for comparison. In the longitudinal test mode, the "as-welded" material had a DBTT of 121°C (250°F). Post-weld anneals of 1 hour at 1649°C (3000°F), 1815°C (3300°F), and 1982°C (3600°F) reduced the DBTT to 24°C (75°F), 93°C (200°F), and 93°C (200°F), respectively.

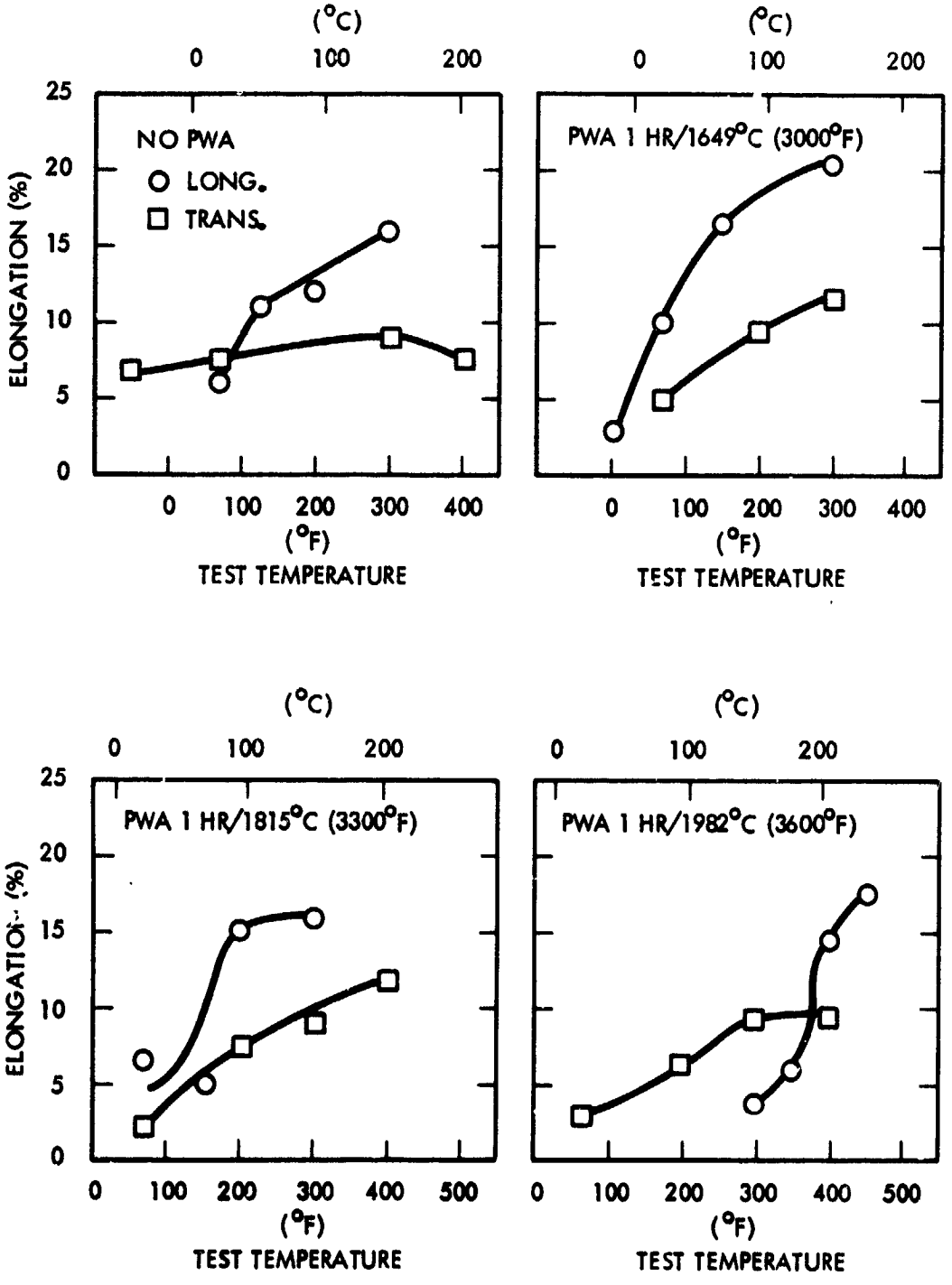

Figure 107. Tensile DBTT of GTA Welded ASTAR-1211C Sheet Thermally Aged 1000 Hrs./1427°C (2600°F)

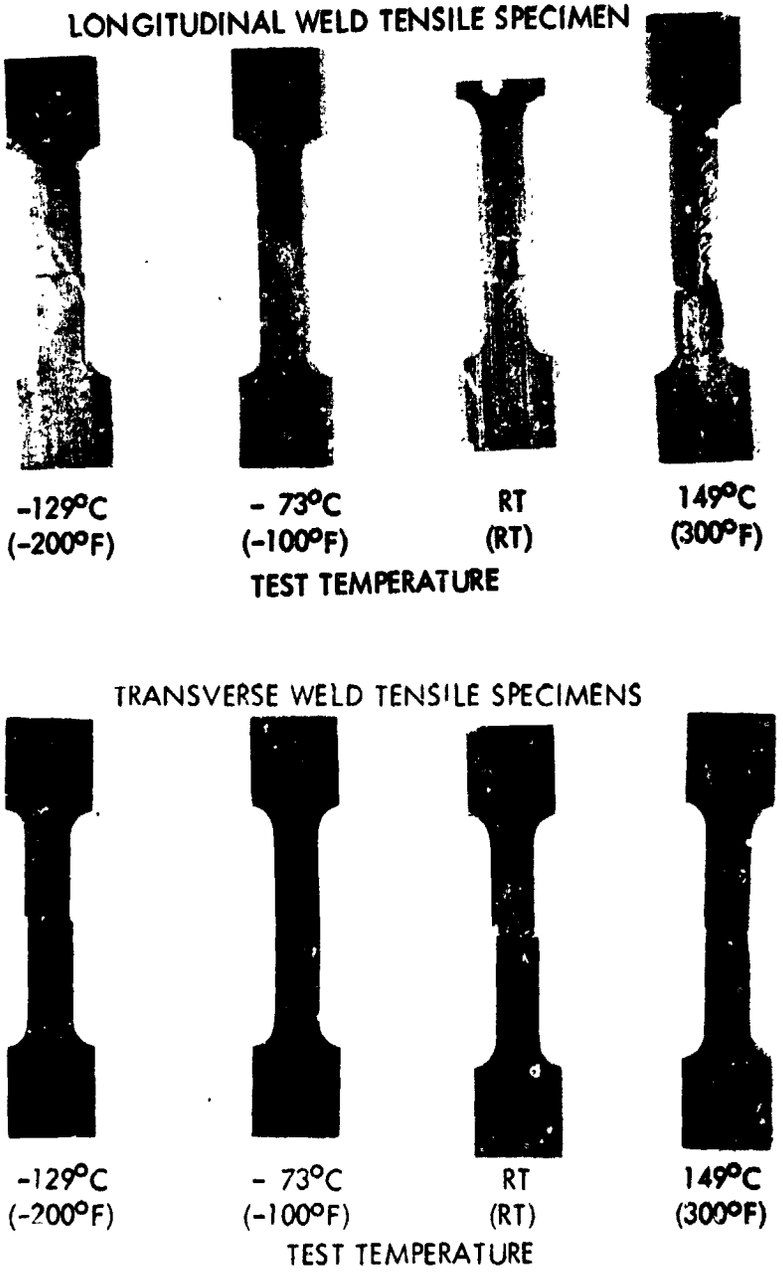

Figure 108. Typical Post-test Longitudinal and Transverse Tensile Specimens

Table 38. Summary of DBTT Test Results for GTA Welded, PWA, and Thermally Aged ASTAR-1211C Sheet

Specimen Thermal History				DBTT*			
PWA Temperature		Aging Temperature		Longitudinal		Transverse	
(°C)	(°F)	(°C)	(°F)	(°C)	(°F)	(°C)	(°F)
AW	AW	NA	NA	121	250	-18	0
1649	3000	NA	NA	24	75	52	125
1815	3300	NA	NA	93	200	66	150
1982	3600	NA	NA	93	200	38	100
AW	AW	1149	2100	66	150	93	200
1649	3000	1149	2100	10	50	-18	0
1815	3300	1149	2100	24	75	38	100
1982	3600	1149	2100	80	175	52	125
AW	AW	1316	2400	52	125	38	100
1649	3000	1316	2400	-46	-50	-46	-50
1815	3300	1316	2400	-18	0	-73	-100
1982	3600	1316	2400	163	325	24	75
AW	AW	1427	2600	66	150	66	150
1649	3000	1427	2600	38	100	66	150
1815	3300	1427	2600	66	150	93	200
1982	3600	1427	2600	191	375	107	225

NA = Not Aged

* Determine from transition curves, Figures 105, 106, and 107.

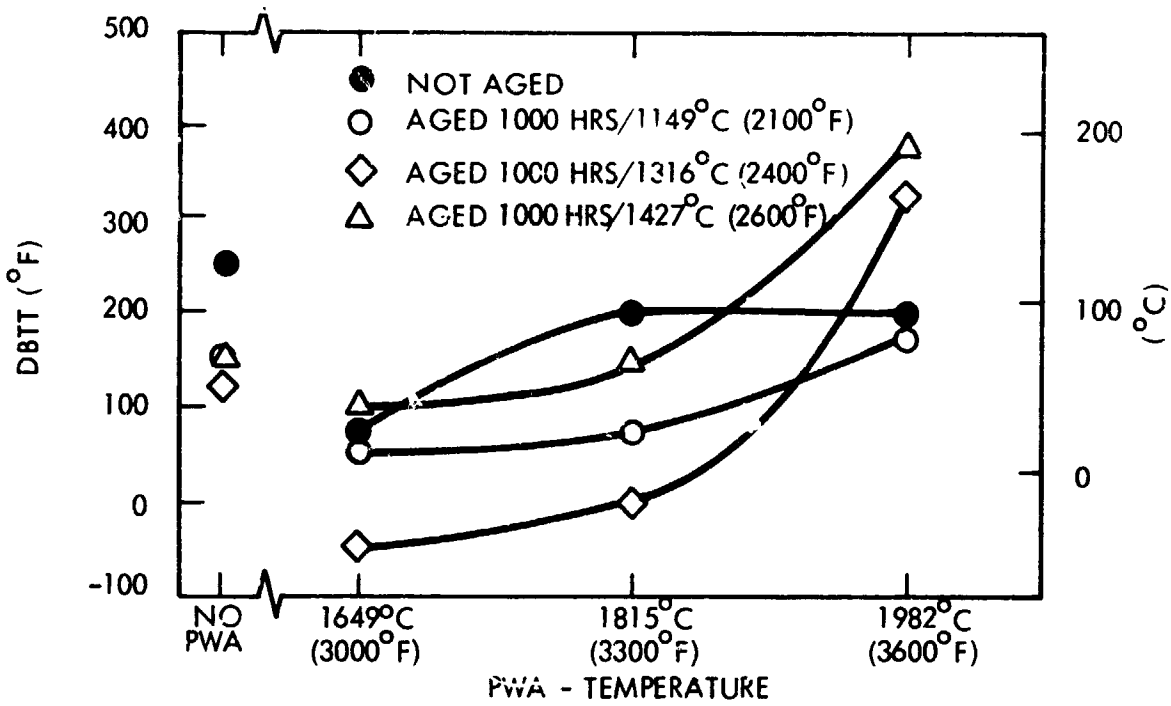

LONGITUDINAL TENSILE DBTT FOR ASTAR-1211C GTA WELDED SHEET

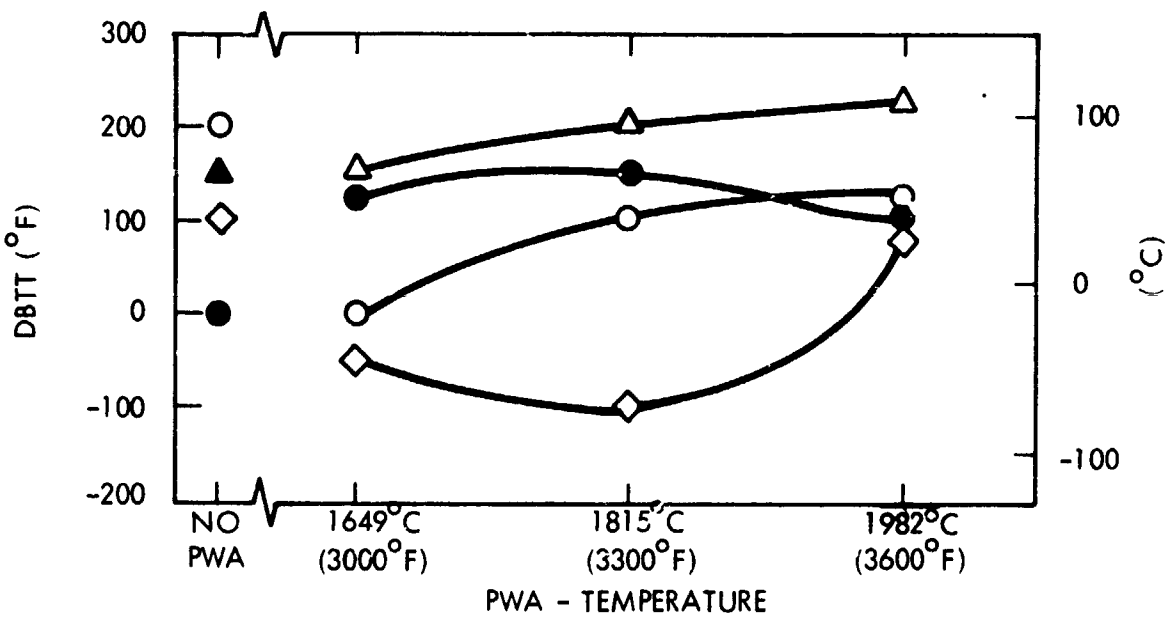

TRANSVERSE TENSILE DBTT FOR ASTAR-1211C GTA WELDED SHEET

Figure 109. Summary of DBTT Behavior of GTA Welded ASTAR-1211C Sheet

The effect of thermal aging on non-PWA and PWA material was quite pronounced. The transition temperatures of material not PWA but thermally aged were reduced to a temperature range of 52°C (125°F) to 66°C (150°F). The effect of PWA on the DBTT of thermally aged material was also significant. Material PWA at 1649°C (3000°F) exhibited the lowest transition temperatures observed in this study. The transition temperatures were equivalent to or lower than nonaged material with the same PWA. As the PWA temperature was increased, the transition temperatures for the aged material increased, but stayed below the value for non-aged material. At 1982°C (3600°F) transition temperatures for material aged at 1316°C (2400°F) and 1427°C (2600°F) increased above 149°C (300°F), while 1149°C (2100°F) annealed material remained comparable to nonaged material. Of the three PWA temperatures evaluated, the 1649°C (3000°F) anneal produced the most desirable results.

The results of the transverse tensile tests were less conclusive, as previously discussed. The DBTT was less sharply defined due to the nature of the transverse tensile test. In this evaluation, the as-welded material had a DBTT of -18°C (70°F) in contrast to the 1149°C (250°F) from the transverse case. The only clearly discernible trend was in regard to the effect of highest PWA temperature 1982°C (3600°F) on aged material. The increases were not as dramatic as in the case of the longitudinal test specimens. While the transverse tensile test condition did not provide conclusive results, no deleterious effects were noted for this mode of testing.

5.3.3.2 Hardness Evaluation of Aged GTA Welded ASTAR-1211C Sheet

Hardness traverses were conducted on specimens representing each of post-weld annealed and aged conditions. Measurements were made on base-metal, heat-affected zone (HAZ), and weld-metal regions of each using a 10 Kg load on a Vickers hardness tester. The results of the measurements are plotted in Figure 110. The hardness samples were taken from the head section of longitudinal room temperature tensile specimens, affording access to

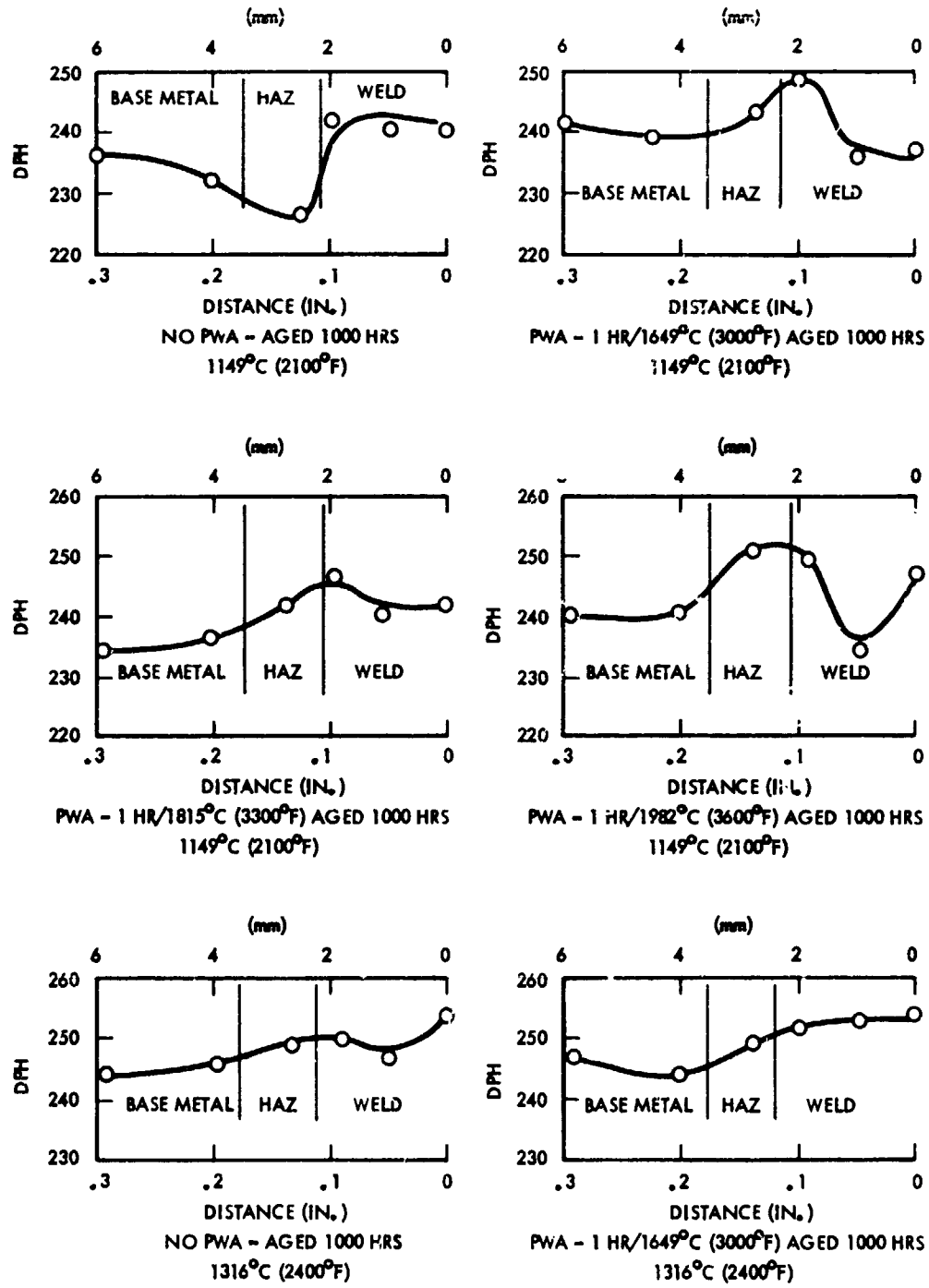

Figure 110. Hardness Traverses on GTA Welded and Aged ASTAR-1211C Sheet

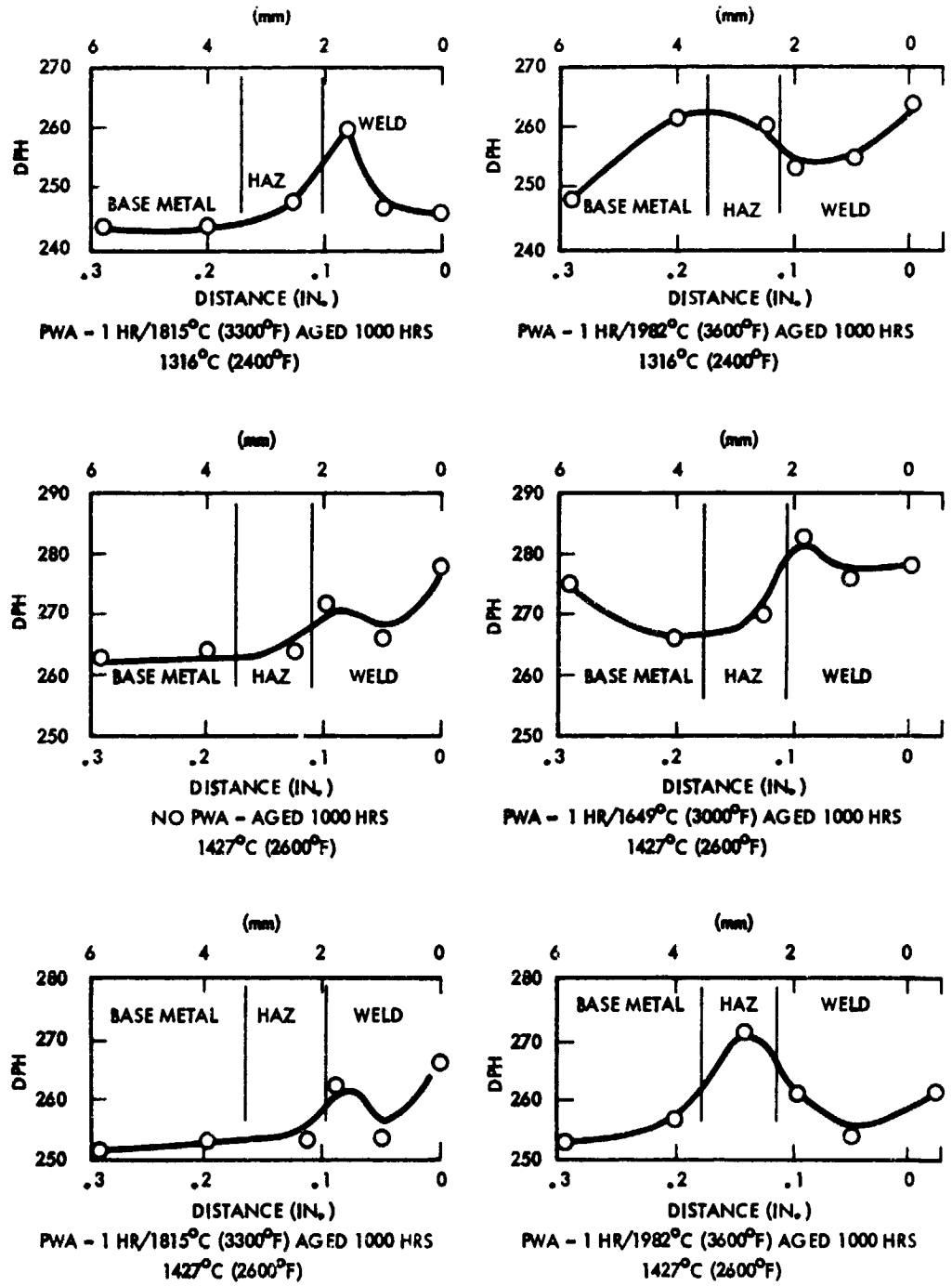

Figure 110. Hardness Traverses on GTA Weld and Aged ASTAR-1211C Sheet (Continued)

undisturbed base metal, HAZ, and weld metal. The aged ASTAR-1211C material produced the lowest hardness readings observed. The values ranged from 230 DPH for non-PWA material aged at 1149°C (2100°F) to 275 DPH for material PWA at 1982°C (3600°F) and aged at 1427°C (2600°F). The hardness values were constant in each specimen in that a variance of no greater than 15 DPH was noted in most cases for base metal, HAZ, and weld metal. Room temperature yield strength as indicated in Table 37, although lower than base metal properties, were not as low as would be indicated by room temperature hardness. This behavior has been observed in other alloys of similar composition.(2)

5.3.3.3 Metallographic Evaluation of Aged GTA Welded ASTAR-1211C Sheet

The microstructures of the post-weld annealed and thermally aged ASTAR-1211C GTA weld sheet are shown in Figures 111, 112, and 113. The micrograph includes weld metal, HAZ, and base metal. The microstructure for all the aged conditions appear quite similar. Large blocky precipitates are found at grain boundaries in all cases. This precipitate has been identified as Ta_2C by x-ray diffraction of extracted residues. The precipitate appears to be larger and more concentrated in the material thermally aged at 1149°C (2100°F). At the higher aging temperatures, the precipitates appear to be finer and more uniformly distributed on the grain boundaries. A second type precipitate was also evident within the interdendritic areas of the weld metal. The interdendritic precipitate appears to be stable and persists at the highest aging temperature. Material given a PWA at 1982°C (3600°F) has similar types of precipitates located within the grain matrix. This same type precipitate has been noted in unaged material annealed at 1982°C (3600°F). The fine precipitate has not been positively identified. One possibility, which has been postulated, suggested that the interdendritic phase is an intermetallic compound, W_2Hf[10]. The interdendritic zones are known to be high in hafnium due to solidification processes. Extraction techniques for successful removal of intermetallics from the base matrix are not known at this time.

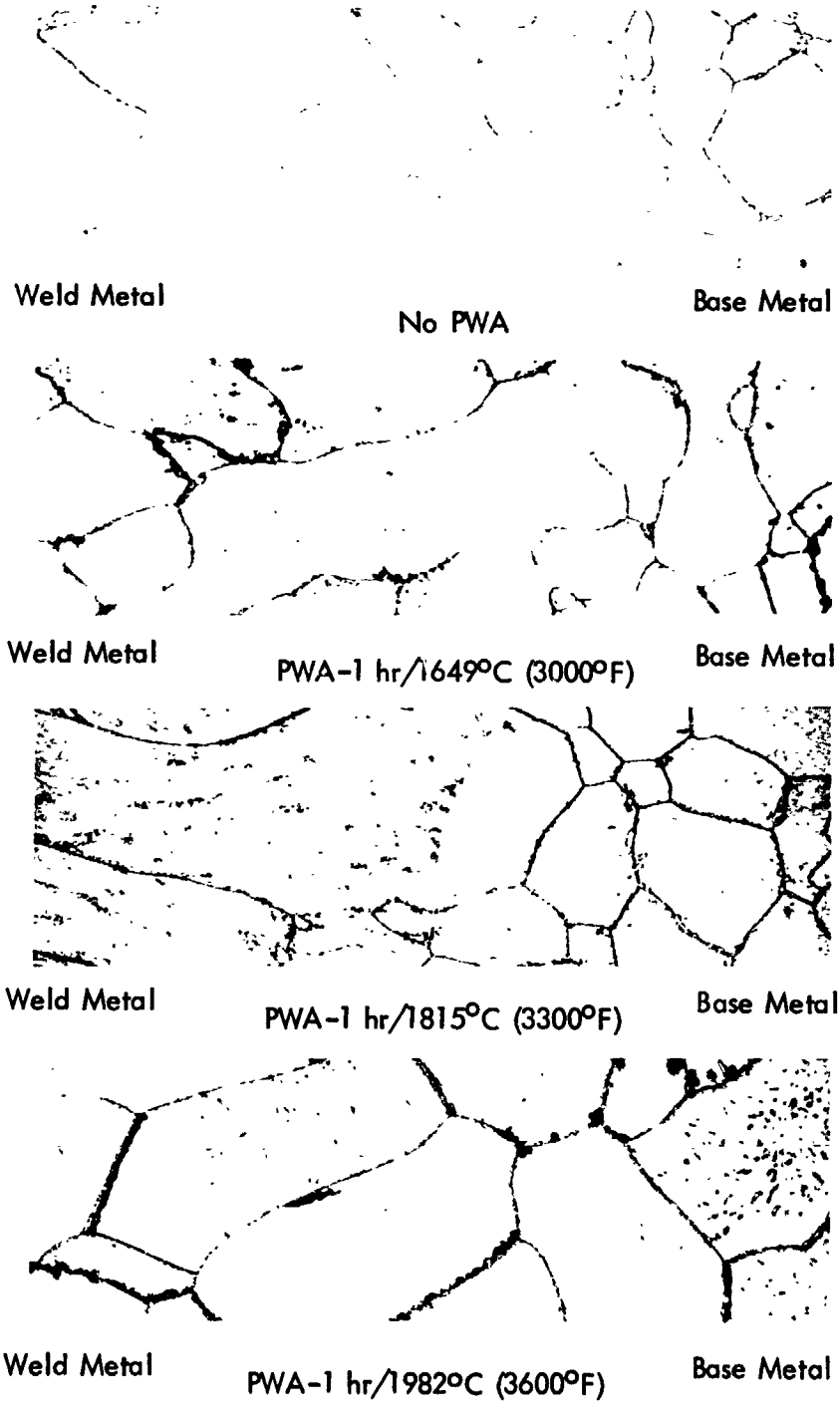

Figure 111. Microstructure of GTA Welded ASTAR1211C Sheet Aged at 1149°C (2100°F)

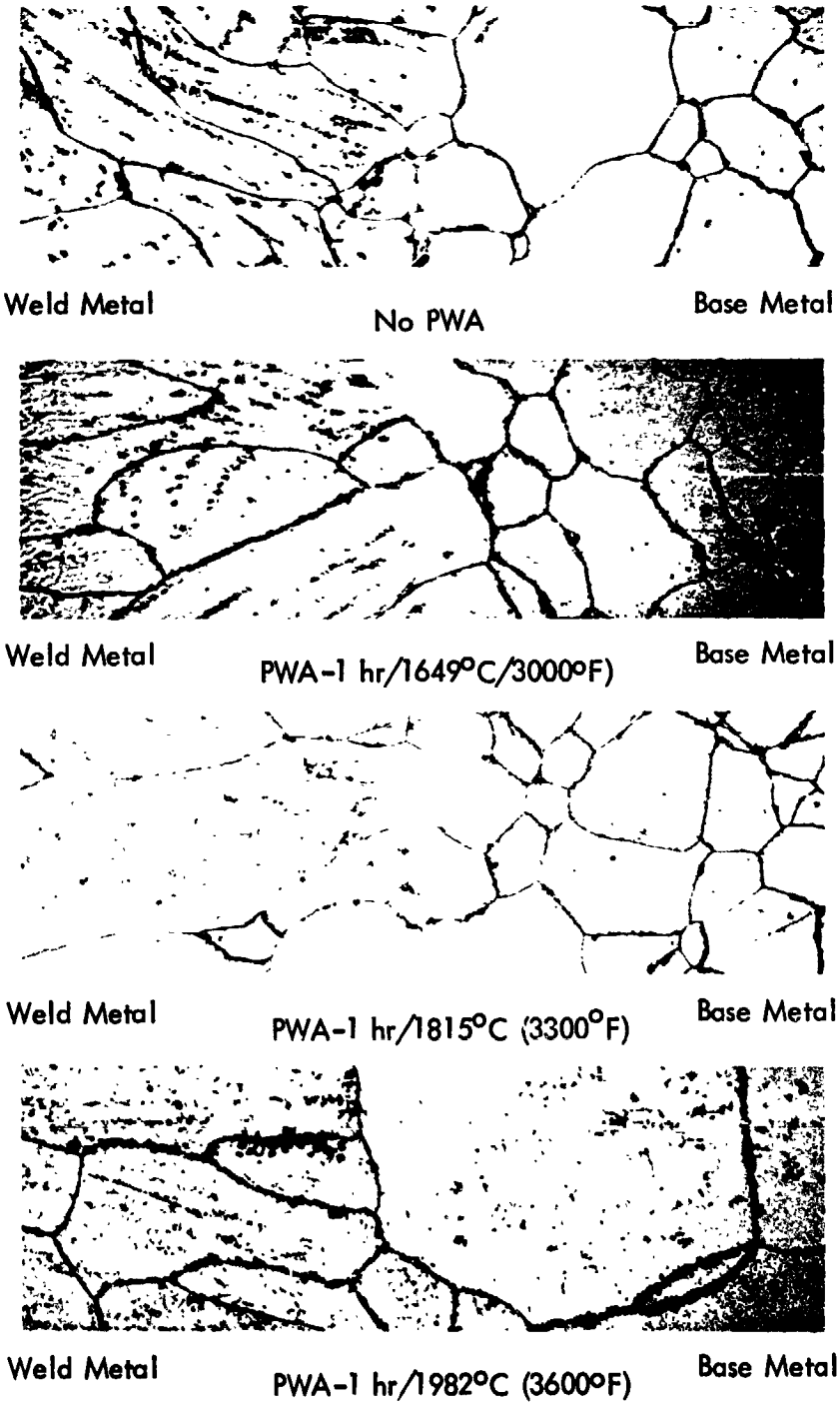

Figure 112. Microstructure of GTA Welded ASTAR-1211C Sheet Aged at 1316°C (2400°F)

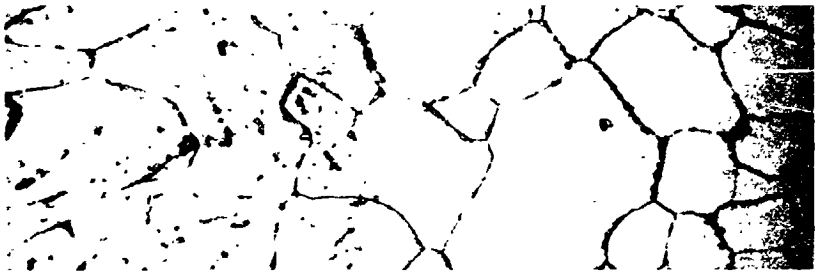

200X

Weld Metal — No PWA — Base Metal

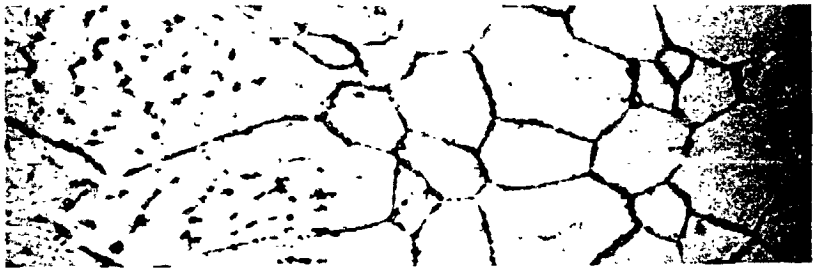

200X

Weld Metal — PWA-1 hr/1649°C (3000°F) — Base Metal

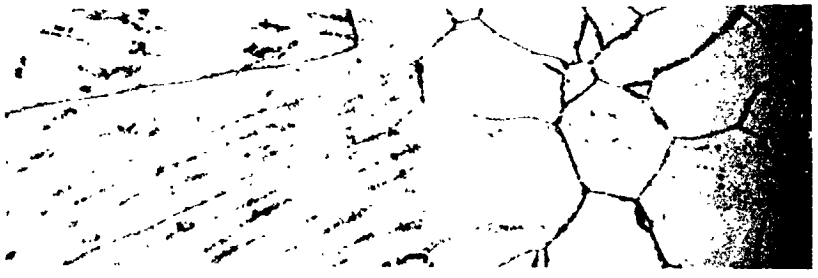

200X

Weld Metal — PWA-1 hr/1815°C (3300°F) — Base Metal

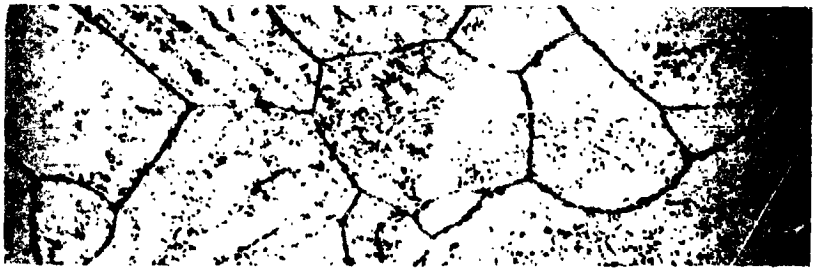

200X

Weld Metal — PWA-1 hr/1982°C (3600°F) — Base Metal

Figure 113. Microstructure of GTA Welded ASTAR-1211C Sheet Aged at 1427°C (2600°F)

The grain size of the heat affected zone increased significantly as PWA temperature increased. The grain size was increased to the extent that, in some cases, two grains composed the region between sheet surfaces in the HAZ. The ductile-brittle behavior of refractory alloys has been shown to be sensitive to grain size. Increasing grain size causes DBTT to increase.

5.3.3.4 Determination of Tensile DBTT of GTA Welded ASTAR-1511C Sheet

GTA welded, post-weld annealed, and thermally aged ASTAR-1511C sheet was also evaluated to determine tensile DBTT. ASTAR-1511C was only tested in the longitudinal configuration due to the limited supply of sheet material available. The same test procedures used for the ASTAR-1211C were used for ASTAR-1511C. Complete tensile data are given in Table 39. Elongation values as a function of test temperatures are given in Figures 114, 115, and 116. The ductile-brittle transition temperatures derived from the elongation-test temperature curves are summarized in Figure 117 and Table 40. The DBTT for ASTAR-1511C welded sheet was significantly higher than ASTAR-1211C. The additional tungsten, 3 percent, was responsible for the dramatic increase in DBTT. As in the case of ASTAR-1211C, the 1649°C (3000°F) PWA produced the lowest DBTT for each aging temperature. Tensile DBTT for "as welded" and PWA material but not aged were not obtained for comparison due to limited supply of sheet material. Increasing the PWA temperature to 1815°C (3300°F) and 1982°C (3600°F) caused only a moderate increase in the DBTT for material aged at 1149°C (2100°F) and 1316°C (2400°F). The material aged at 1427°C (2600°F), however, experienced a significant increase to above 260°C (300°F). From the data presented, it appears possible that a lower PWA temperature may exist.

5.3.3.5 Hardness Evaluation of Aged GTA Welded ASTAR-1511C Sheet

Hardness traverses were conducted on specimens representing each of the post-weld annealed and aged conditions. The specimens were taken from the head section of longitudinal room temperature tensile specimens. The results are presented in Figure 118. Base metal, HAZ

Table 39. Low Temperature Tensile Properties of GTA Welded, PWA, and Aged ASTAR-1511C Sheet

Specimen Thermal History	Spec. Type	Test Temperature (°C)	Test Temperature (°F)	Yield Strength (MN/m^2)	Yield Strength (ksi)	Ultimate Strength (MN/m^2)	Ultimate Strength (ksi)	Total Elong. (%)
As-welded	L	RT	RT	748	108.4	760	110.2	1.1
+ 1000 hrs/1149°C	L	149	300	606	87.9	680	98.5	5.0
(2100°F)	L	191	375	566	82.1	676	98.0	15.0
	L	232	450	533	77.2	649	94.0	16.8
PWA-1 hr/1649°C	L	RT	RT	704	102.0	749	108.5	2.7
(3000°F) + 1000 hrs/	L	93	200	652	94.5	727	105.3	7.7
1149°C (2100°F)	L	149	300	598	86.7	691	100.2	13.5
PWA-1 hr/1815°C	L	RT	RT	719	104.2	738	106.9	4.0
(3300°F) + 1000 hrs/	L	93	200	638	92.4	709	102.8	6.0
1149°C (2100°F)	L	149	300	591	85.6	679	98.4	8.9
	L	232	450	514	74.5	613	88.9	8.0
PWA-1 hr/1982°C	L	RT	RT	698	101.1	709	102.8	1.4
(3600°F) + 1000 hrs/	L	149	300	590	85.5	670	97.1	10.4
1149°C (2100°F)	L	191	375	559	81.0	649	94.1	9.6
	L	232	450	492	71.3	599	86.8	20.7
As-welded + 1000 hrs/	L	-46	-50	826	119.7	843	122.2	1.7
1316°C (2400°F)	L	RT	RT	730	105.8	794	115.1	6.6
	L	93	200	664	96.2	766	111.0	13.2
	L	149	300	618	89.6	711	103.1	12.8
PWA-1 hr/1649°C	L	-46	-50	834	120.8	860	124.6	2.7
(3000°F) + 1000 hrs/	L	RT	RT	740	107.2	800	116.0	6.1
1316°C (2400°F)	L	93	200	661	95.8	770	111.6	16.3
	L	149	300	606	87.8	690	100.0	17.8
PWA-1 hr/1815°C	L	RT	RT	736	106.7	773	112.0	4.5
(3300°F) + 1000 hrs/	L	93	200	664	96.2	683	99.0	2.4
1316°C (2400°F)	L	121	250	633	91.7	727	105.3	9.6
	L	149	300	611	88.5	704	102.0	11.7
PWA-1 hr/1982°C	L	RT	RT	731	106.0	735	106.5	.5
(3600°F) + 1000 hrs/	L	93	200	658	95.3	697	101.0	4.2
1316°C (2400°F)	L	149	300	576	83.5	666	96.5	10.3
As-welded + 1000 hrs/	L	RT	RT	697	101.0	828	120.0	6.1
1427°C (2600°F)	L	93	200	686	99.4	707	102.4	3.1
	L	121	250	692	100.3	774	112.2	12.3
	L	149	300	622	90.1	704	102.0	11.7
PWA-1 hr/1649°C	L	RT	RT	716	103.8	814	118.0	4.6
(3000°F) + 1000 hrs/	L	66	150	740	107.2	808	117.1	9.0
1427°C (2600°F)	L	93	200	707	102.5	791	114.7	14.0
	L	149	300	632	91.6	712	103.2	14.4
PWA-1 hr/1815°C	L	149	300	663	96.1	716	103.8	5.6
(3300°F) + 1000 hrs/	L	232	450	573	83.0	638	92.4	7.4
1427°C (2600°F)	L	274	525	522	75.7	572	82.9	4.8
	L	316	600	502	72.8	586	84.9	17.3
PWA-1 hr/1982°C	L	149	300	638	92.4	653	94.6	2.3
(3600°F) + 1000 hrs/	L	232	450	552	80.0	591	85.7	5.8
1427°C (2600°F)	L	274	525	513	74.4	578	83.7	6.5
	L	316	600	496	71.9	578	83.7	14.5

Strain Rate 0.05/min.
L = Longitudinal

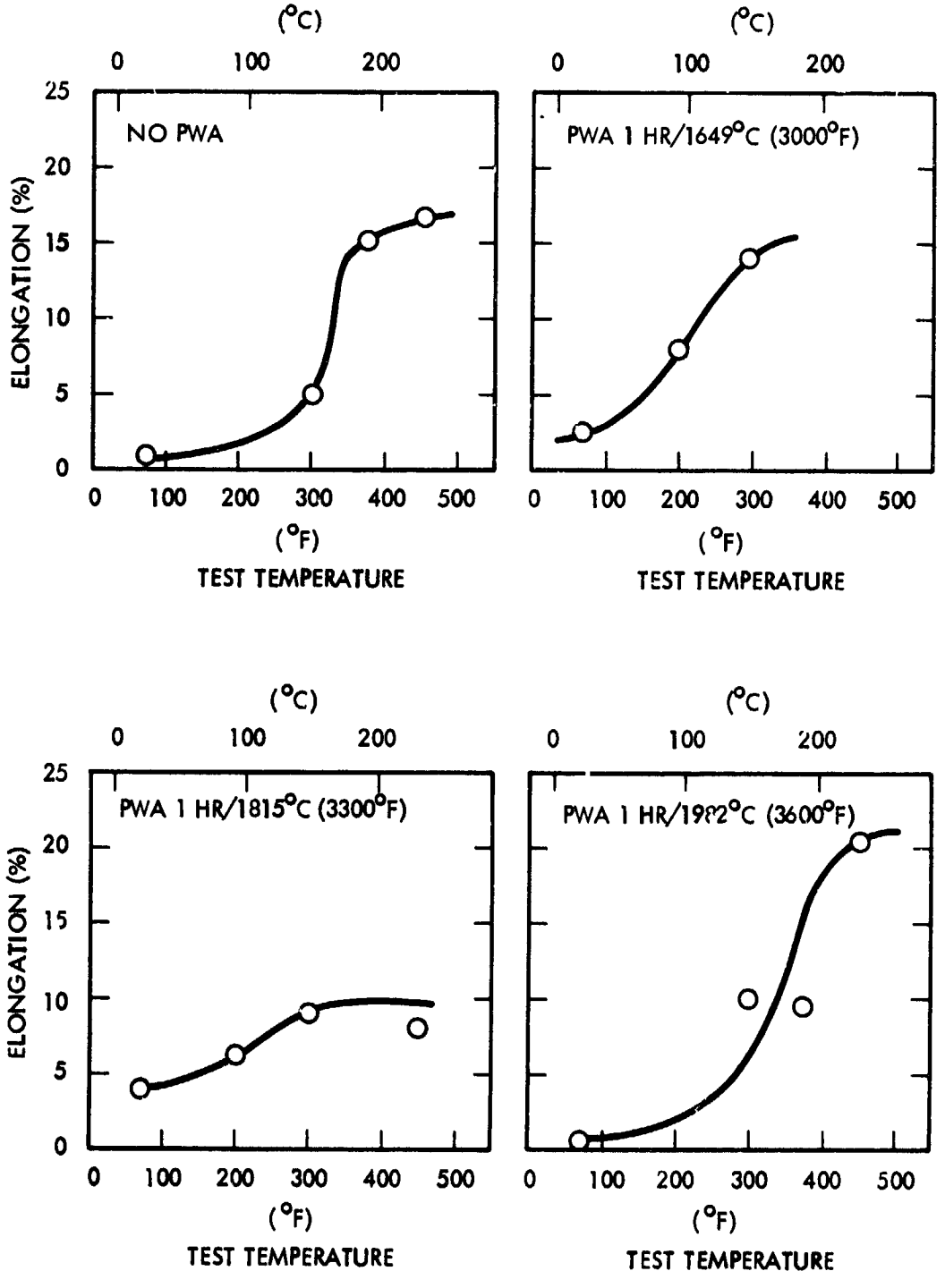

Figure 114. Tensile DBTT of GTA Welded ASTAR-1511C Sheet Thermally Aged 1000 Hrs./1149°C (2100°F)

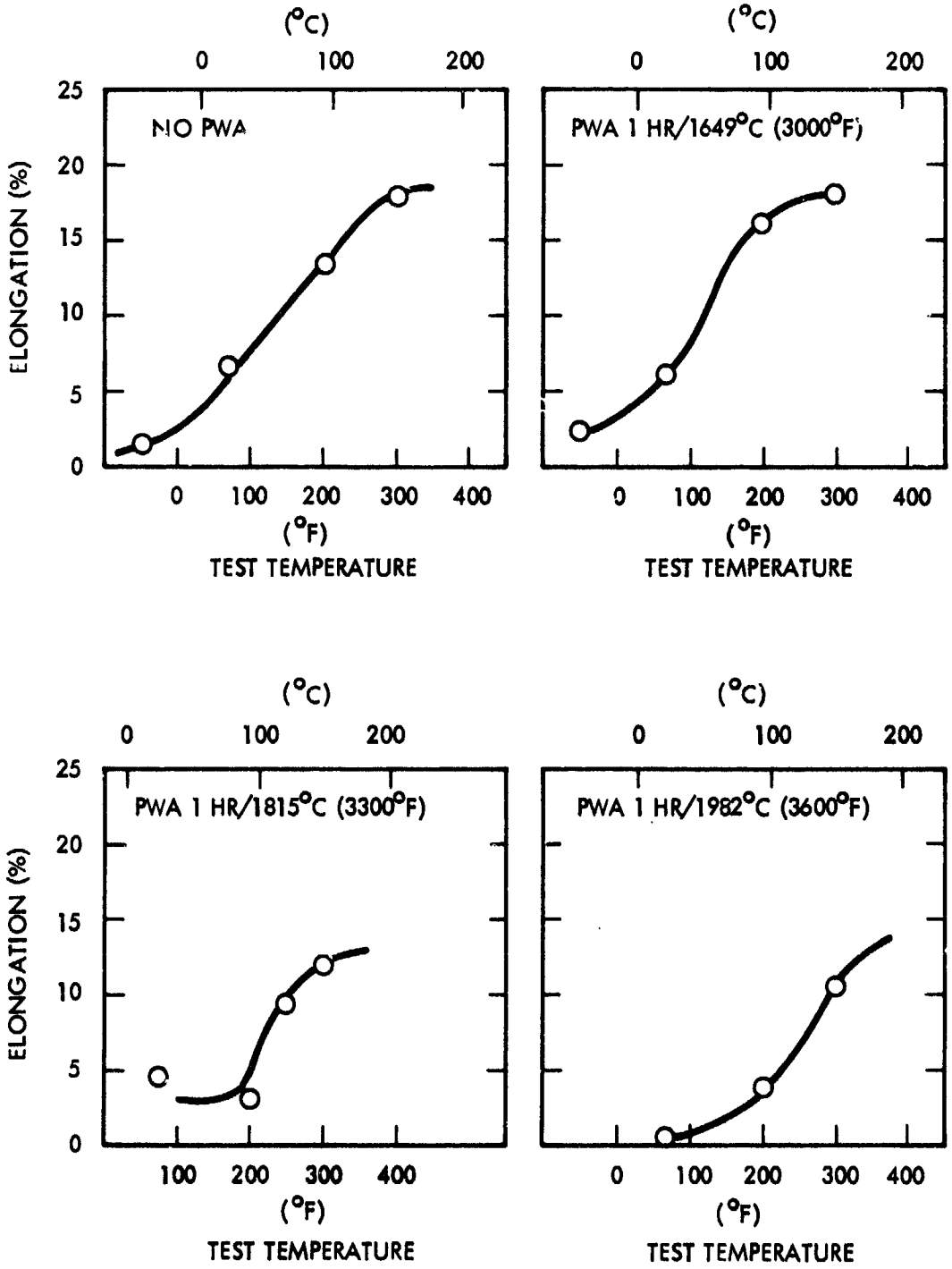

Figure 115. Tensile DBTT of GTA Welded ASTAR-1511C Sheet Thermally Aged 1000 Hrs./1316°C (2400°F)

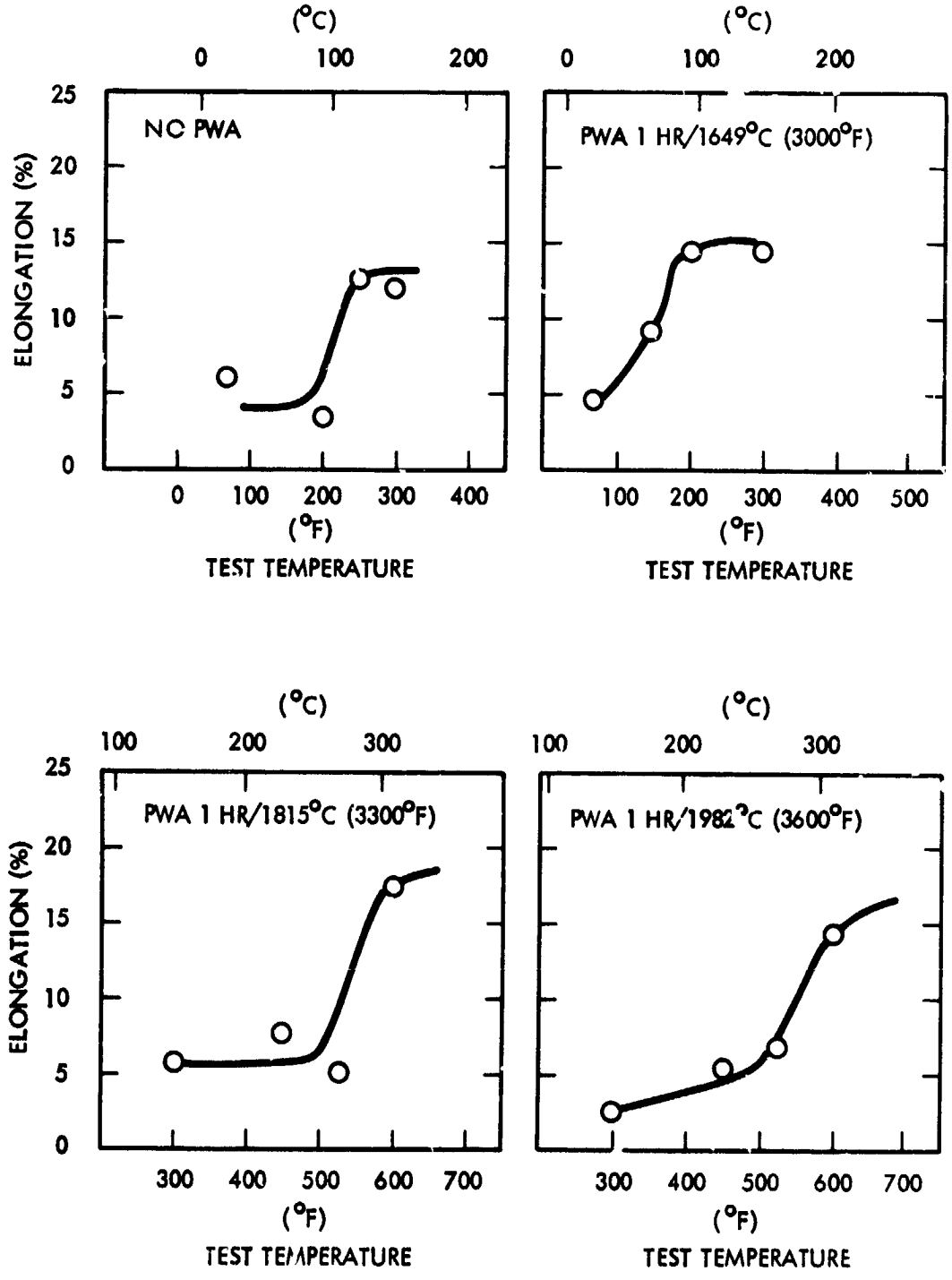

Figure 116. Tensile DBTT of GTA Welded ASTAR-1511C Sheet Thermally Aged 1000 Hrs./1427°C (2600°F)

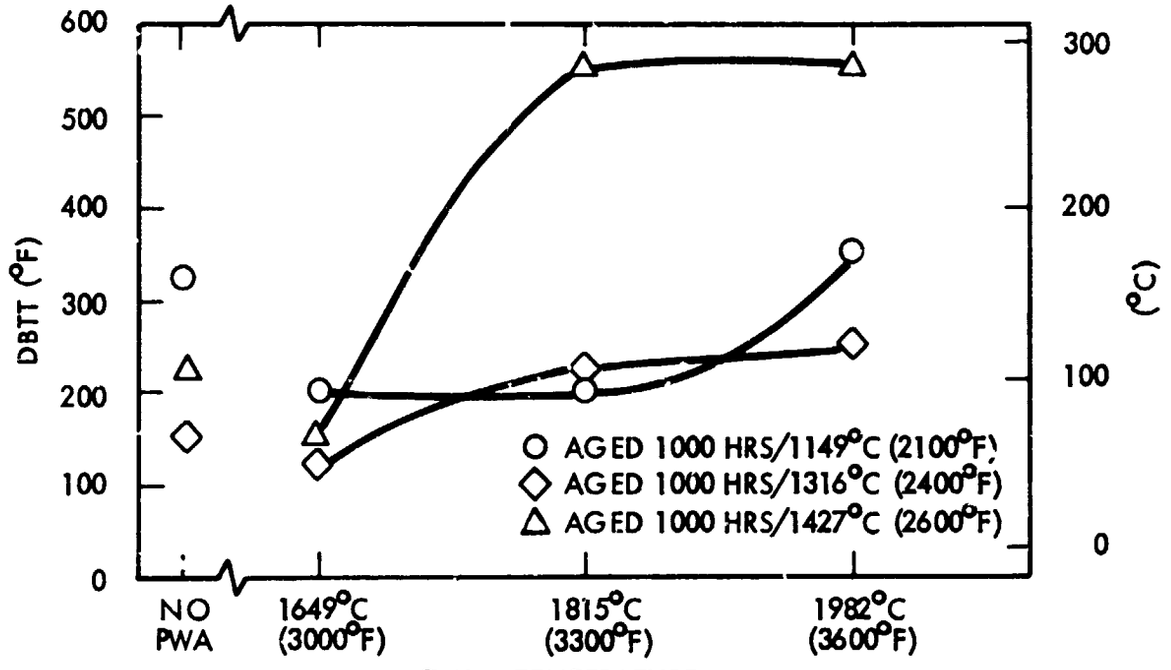

LONGITUDINAL TENSILE DBTT FOR ASTAR-1511C GTA WELDED SHEET

Figure 117. Summary of DBTT Behavior of GTA Welded ASTAR-1511C Sheet

Table 40. Summary of DBTT Test Results for GTA Welded, PWA, and Thermally Aged ASTAR-1511C Sheet

Specimen Thermal History				DBTT* Longitudinal	
PWA Temperature		Aging Temperature			
(°C)	(°F)	(°C)	(°F)	(°C)	(°F)
AW	AW	1149	2100	163	325
1649	3000	1149	2100	93	200
1815	3300	1149	2100	93	200
1982	3600	1149	2100	177	350
AW	AW	1316	2400	66	150
1649	3000	1316	2400	52	125
1815	3300	1316	2400	107	225
1982	3600	1316	2400	121	250
AW	AW	1427	2600	107	225
1649	3000	1427	2600	66	150
1815	3300	1427	2600	288	550
1982	3600	1427	2600	288	550

* Determined from transition curves, Figures 113, 114, and 115.

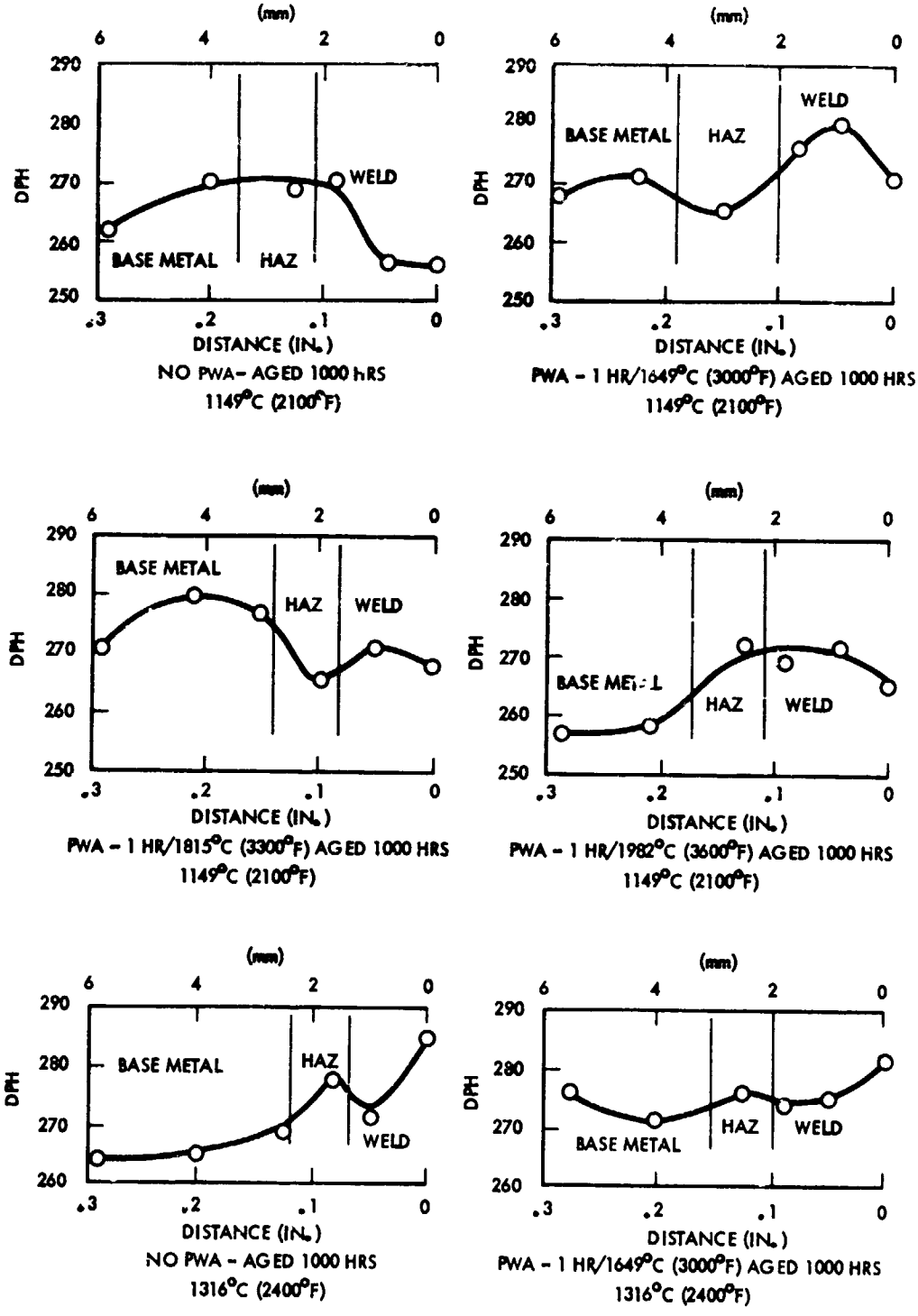

Figure 118. Hardness Traverses on GTA Welded and AGED ASTAR-1511C Sheet

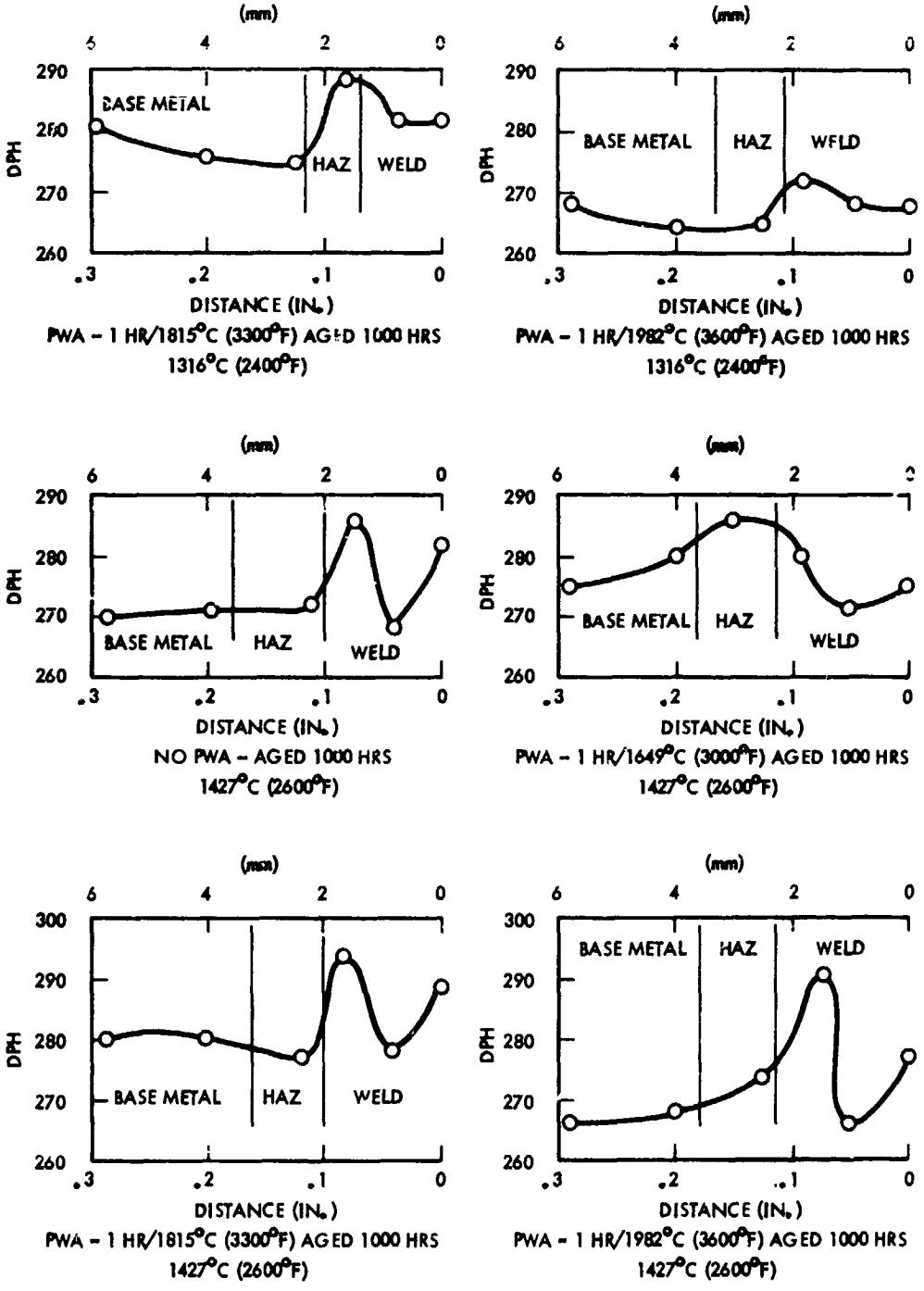

Figure 118. Hardness Traverses on GTA Welded and Aged ASTAR-1511C Sheet (Continued)

and weld metal hardnesses were measured for each condition. As was noted for ASTAR-1211C, the hardness values were unusually low. The hardness values for ASTAR-1511C were generally 30 to 40 DPH points higher than ASTAR-1211C for comparable thermal history. The same trends as noted for ASTAR-1211C were observed for ASTAR-1511C. The spread in hardness values for base metal, HAZ, and weld metal was 15 DPH points or less in most cases. The only explanation for the low hardness values is the complete precipitation of carbon from solution. Carbon has a significant effect on room temperature hardness. Room temperature tensile properties were lower than base metal data as was expected for welded tantalum alloy but not as much as indicated by hardness values.

5.3.3.6 Metallographic Evaluation of Aged GTA Welded ASTAR-1511C Sheet

The microstructure of base metal, HAZ, and weld metal of post-weld annealed and thermally aged ASTAR-1511C sheet are shown in Figures 119, 120, and 121. The observations, which were made for ASTAR-1211C, are also applicable for PWA and aged ASTAR-1511C. The higher the post-weld annealing temperature the larger the grain size in the HAZ. The second phase precipitate, Ta_2C, was found at the grain boundaries of all specimens examined. The Ta_2C phase was in evidence in the base metal, HAZ, and weld metal. An interdendritic phase was also present in the weld metal of most specimens, and its behavior was similar to that noted in ASTAR-1211C. The disposition of the second phases does not appear to play a significant role in the ductile-brittle behavior of these alloys.

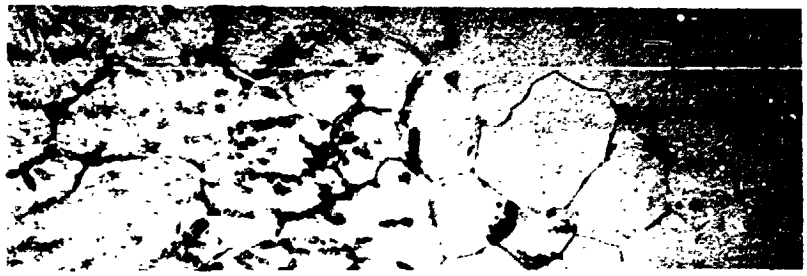

200X

Weld Metal — No PWA — Base Metal

200X

Weld Metal — PWA-1 hr/1649°C (3000°F) — Base Metal

200X

Weld Metal — PWA-1 hr/1815°C (3300°F) — Base Metal

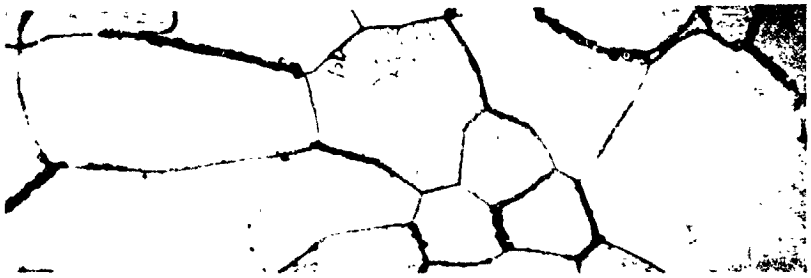

200X

Weld Metal — PWA-1 hr/1982°C (3600°F) — Base Metal

Figure 119. Structure of GTA Welded ASTAR-1511C Sheet Aged at 1149°C (2100°F)

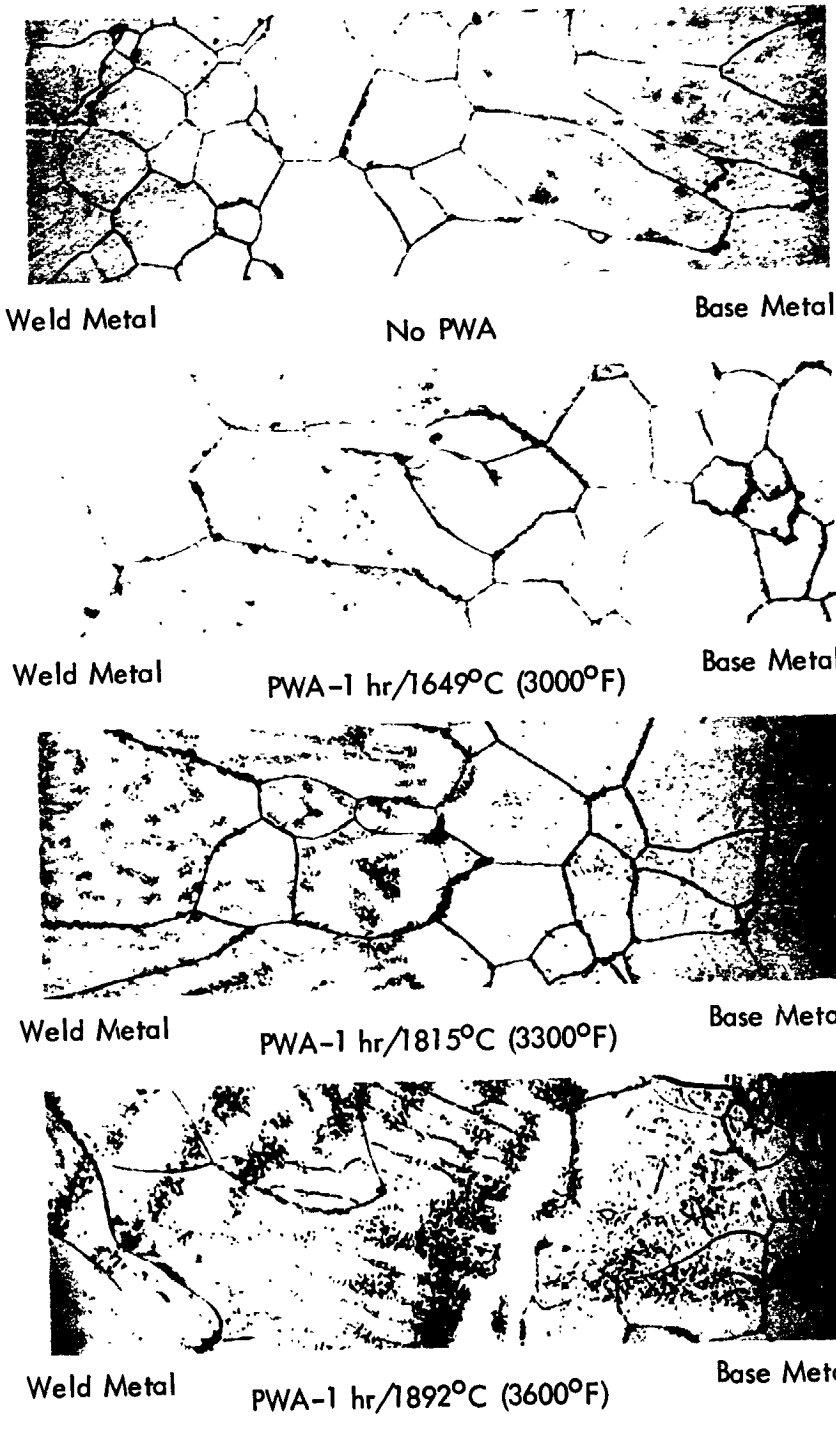

Figure 120. Microstructure of GTA Welded ASTAR-1511C Sheet Aged at 1316°C (2400°F)

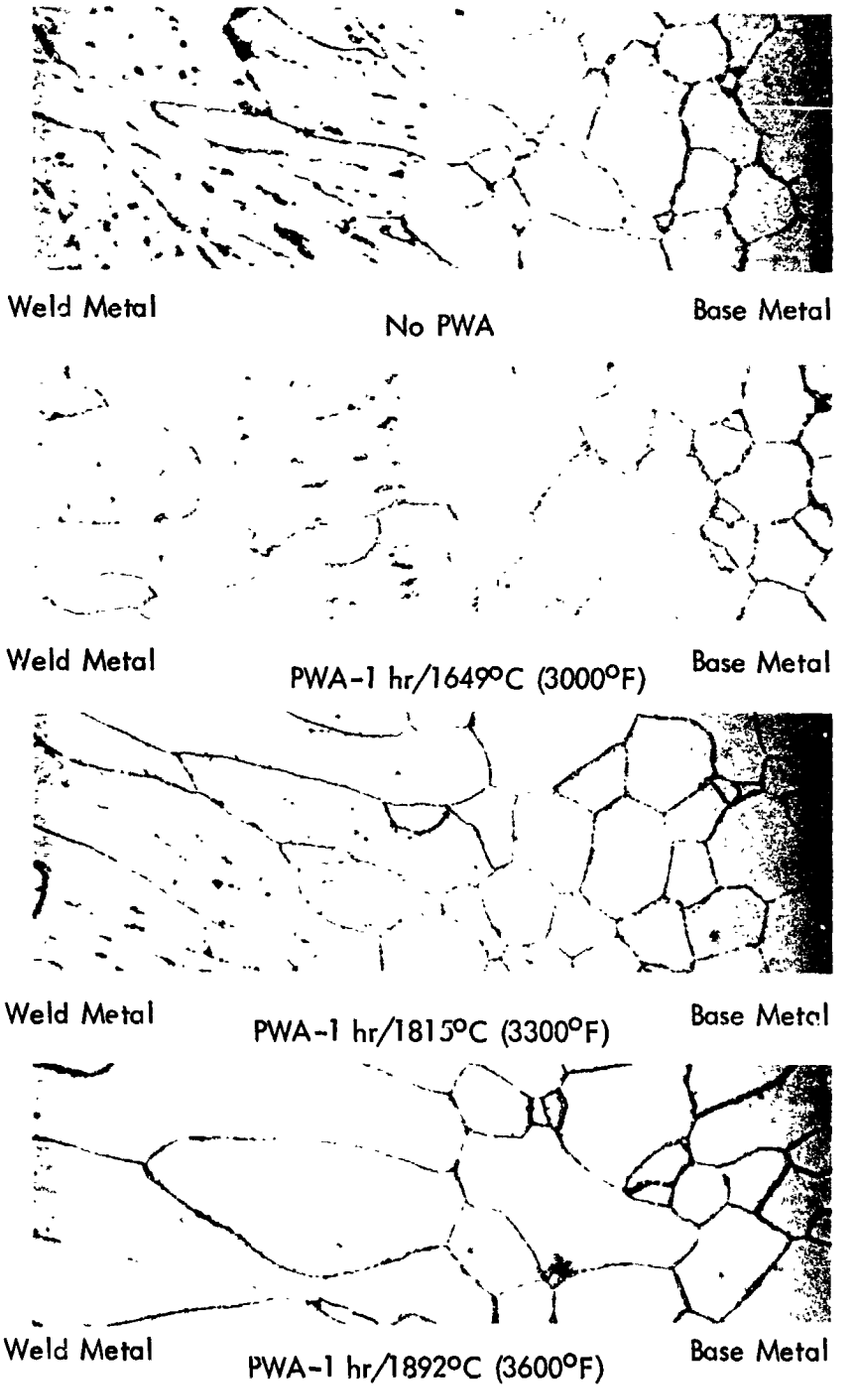

Figure 121. Microstructure of GTA Welded ASTAR-1511C Sheet Aged at 1427°C (2600°F)

6.0 PROCESSING AND EVALUATION OF TUBING

Since the alloys being investigated in this program were considered primarily as bar and forging material, the production of thin walled tubing was conducted as a feasibility study. The objective of this task was to make and evaluate 19.0 mm (0.750 inch) OD x 1.0 mm (0.040 inch) wall tubing. Two approaches for the fabrication of tubing are outlined in Figure 122. Two billets of each alloy composition were utilized. One billet was extruded to a solid round bar, then rifle drilled to produce a tube hollow for warm drawing. The second billet was drilled, then extruded over a mandrel to produce a tube hollow. The conditioned and annealed tube hollows were drawn over a mandrel at elevated temperature to the finished tube size. The drawing of the tube hollows was done at Superior Tube Company, Collegeville, Pa. In this approach, the tube rocking operation was bypassed since only a small quantity of finished tubing was required, and the drawability of the alloys was of primary concern. The extrusion and rifle drilling of a solid round bar appeared to be the most positive method for making redraw stock. The extrusion of the alloys over a mandrel was evaluated because the economic production of large quantities of tubing would require such a step.

In the event that finished tubing was produced, evaluation of the product was to be carried out according to the outline in Figure 123. Included in the evaluation was the determination of mechanical properties, uniaxial tensile, uniaxial and biaxial creep. Welded tubing in the "as-welded" and standard post-weld annealed conditions were scheduled for evaluation by determining uniaxial tensile DBTT, uniaxial tensile and elevated temperature tensile properties.

6.1 PROCESSING OF ASTAR-1211C AND ASTAR-1511C TUBING

6.1.1 Extrusion of ASTAR-1211C and 1511C Tube Hollows

Two billets of each composition were extruded as part of the processing evaluation for the production of tubing. One billet of each composition was encapsulated in a powder met molybdenum can as illustrated in Figure 23 and extruded to a solid round bar. A second

One 6.6 cm (2.6 in.) OD x 12.0 cm (4.75 in.) Long Annealed Billet Per Composition

↓

Clad in Powder Met Mo Can

↓

Extrude to 3.17 cm (1.25 in.) OD Solid Round Bar at 1649°C (3000°F) Reduction Ratio 6:1

↓

Reheat to 1371°C and Swaged Straighten as Required

↓

Declad, Inspect, and Machine to 2.9 cm (1.125 in.) OD - Cut to 25.4 cm (10 in.) Lengths

↓

Anneal - Temperature to be Determined

↓

Rifle Drill to 2.2 cm (0.875 in.) ID

↓

Hot Draw at 538°C (1000°F) to 1.9 cm (0.75 in.) OD x 1.0 mm (0.040 in.) Wall Tubing - Intermediate Anneals as Required

One 6.6 cm (2.6 in.) OD x 2.54 cm (1.0 in.) ID x 12 cm (4.75 in.) Long Annealed Billet per Composition

↓

Clad in Powder Met Mo Can

↓

Extrude over 1.78 cm (0.7 in.) Diameter Mandrel at 1649°C (3000°F) Reduction Ratio 6:1

↓

Reheat to 1371°C (2500°F) and Swage Straighten as Required

↓

Declad, Inspect, and Machine to 2.9 cm (1.125 in.) OD x 2.22 cm (0.875 in) ID Cut to 25.4 cm (10 in.) Lengths

↓

Anneal - Temperature to be Determined

↓

Hot Draw at 538°C (1000°F) to 1.9 cm (0.75 in.) OD x 1.0 mm (0.040 in.) Wall Tubing - Intermediate Anneals as Required

Figure 122. Processing Schedule for ASTAR-1211C and ASTAR-1511C Tubing

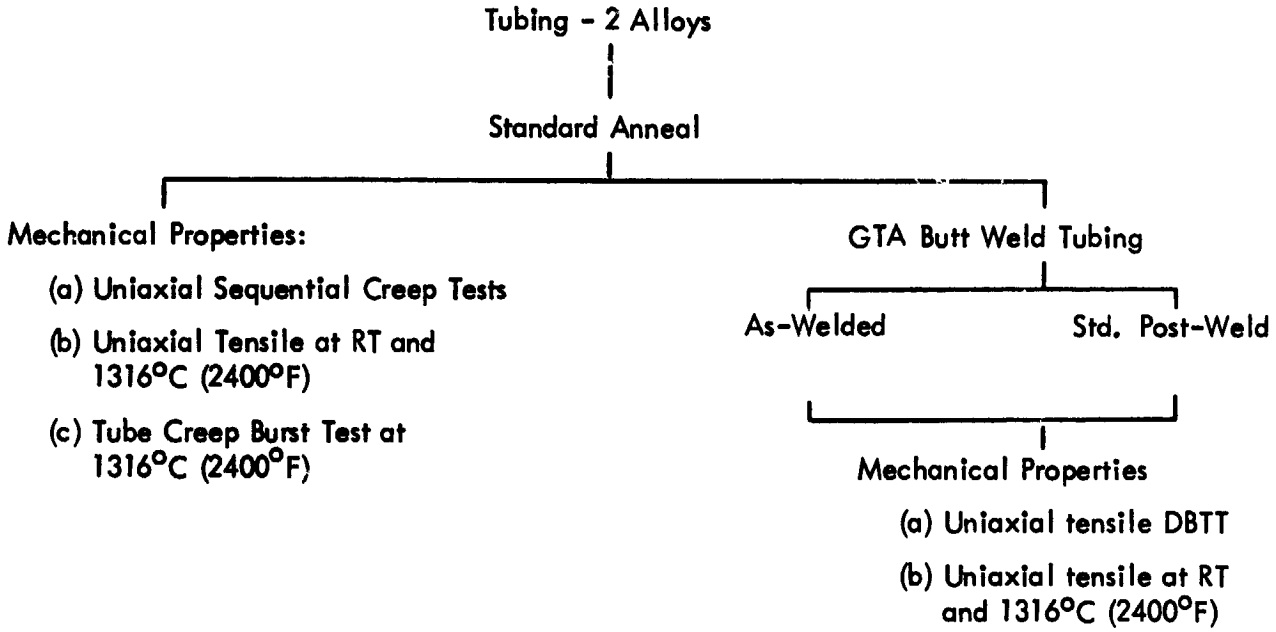

Figure 123. Evaluation Schedule for Tubing

billet of each composition was drilled and encapsulated as illustrated in Figure 124. The center hole was nominally 2.54 cm (1.0 inch) diameter. The billets were ultrasonically inspected according to MIL-STD-271D (Ships). A 0.8 mm (1/32 inch) diameter hole 1.25 cm (1/2 inch) deep drilled parallel to the billet axis midway between the OD and ID was used as a standard reference. Both billets were free of indications. The center hole was lined with a molybdenum tube with a 2.5 mm (0.1 inch) thick wall. The molybdenum can was braze-welded with vanadium as the filler metal. The drilled billets were extruded over a floating tapered tool steel mandrel which was coated with a 0.25 mm (0.01 inch) of zirconia. The extrusion data are listed in Table 41. In one case, the mandrel overheated and separated by tensile failure near the end of the extrusion and caused some loss of material. The solid round extrusions were reheated to 1371°C (2500°F) and swage straightened. The co-extruded molybdenum clad was retained in place to provide protection from atmospheric contamination during reheat and swaging. The extrusions were declad chemically and cut into sections 28 cm (11 inches) long. Sections of "as-extruded" tube hollows are shown in Figure 125, and a solid-round is shown in Figure 126. The tube hollows had an OD of 28.6 mm (1-1/8 inch) with an ID of 19.0 mm (3/4 inch). The solid round bars were approximately 2.5 cm (1.0 inch) in diameter. The solid round bars were sent to the vendor for deep hole drilling.

6.1.2 Tube Drawing

The extrusions were cut into segments approximately 28 cm (11 inches) long. The segments were slightly bowed, each having approximately a 1.6 mm (1/16 inch) gap between the chord and the tube hollow OD when placed on a flat surface. After discussions with the people at Superior Tube, it was decided that the first drawing pass would be used to straighten the tube hollows. The first drawing pass would be accomplished with the tube hollow ID and OD surfaces in the as-extruded condition. Conditioning and adjustment of wall thickness could be accomplished with less difficulty after the straightening operation.

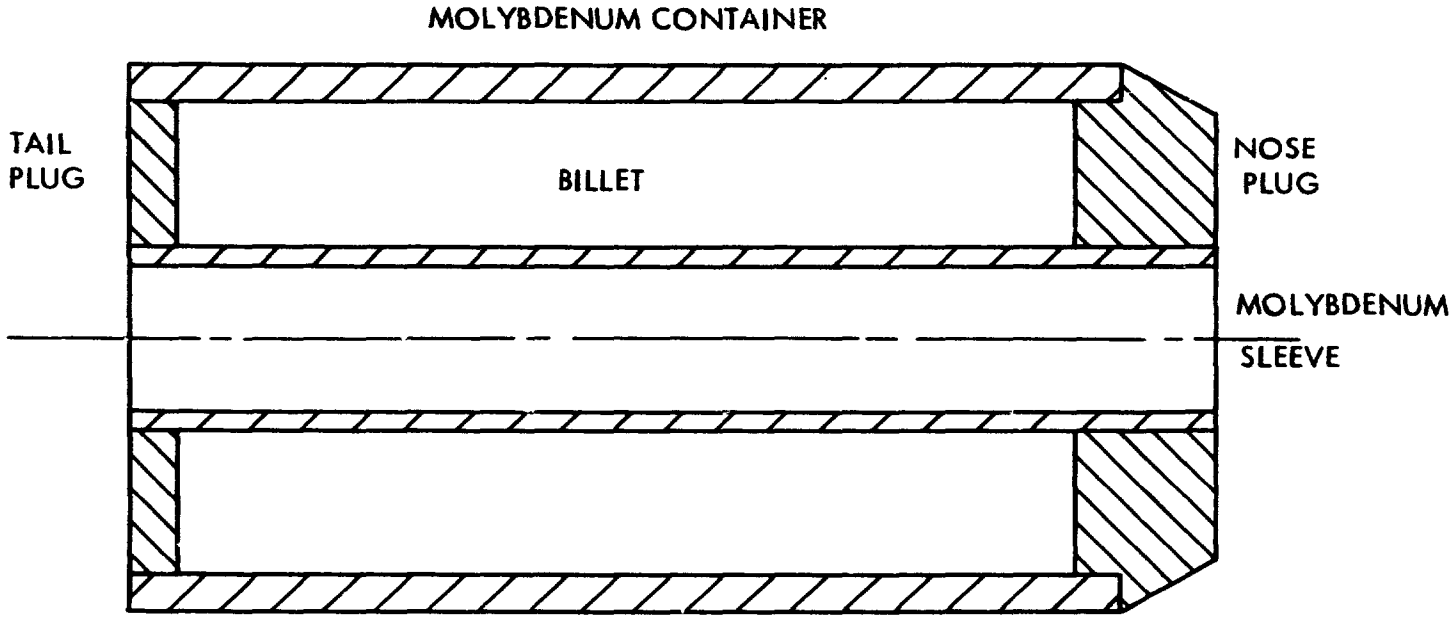

Figure 124. Cross Section of Canned Billet for Extrusion Over a Mandrel

Table 41. Extrusion Data for Tubing Study

Billet Identification	Extrusion Temperature		Reduction Ratio	Extrusion Constant Breakthrough		Extrusion Constant Running		Yield of Sound Material	
	(°C)	(°F)		(MN/m^2)	(ksi)	(MN/m^2)	(ksi)	(cm)	(in)
NASVF-1000-A-3	1538	2800	6:1*	563	81.5	521	75.5	61	24
NASVF-1000-A-4	1649	3000	6.3:1**	507	73.5	407	59.0	76	30
NASVF-2000-B-3	1649	3000	6.3:1**	597	86.5	518	75.0	66	26***
NASVF-2000-A-3	1649	000	6:1*	488	69.3	421	61.0	58	23

* Solid Round
** Extruded over a mandrel
***Mandrel broke during extrusion

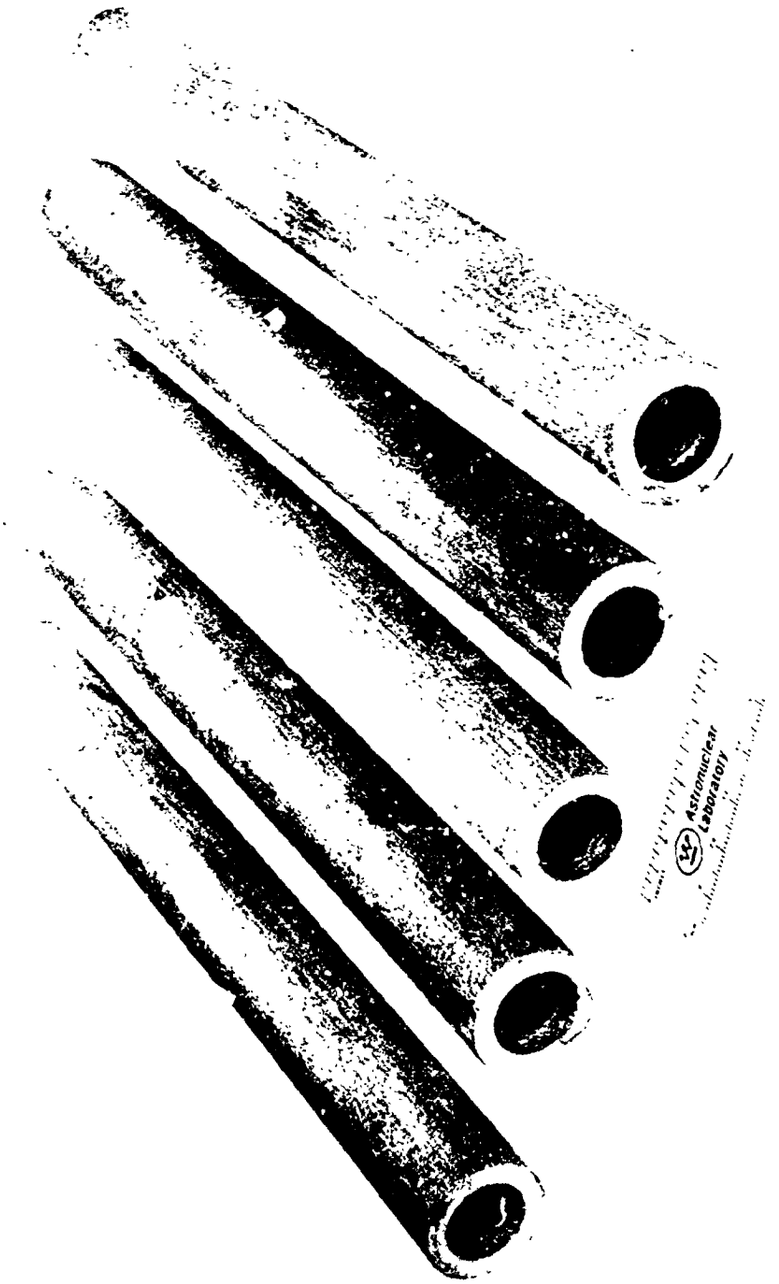

Figure 123. Extruded Tube Hollows of ASTAR-1211C and ASTAR-1511C

Figure 124. Extrusion of ASTAR-1211C, Billet NASVF-1000A-3, for Processing to Tubing

The tube hollows were given a duplex heat treatment - 1 hour at 1815°C (3300°F) followed by 1 hour at 1260°C (2300°F) - in preparation for tube drawing. The microstructure of the tube hollows after heat treatment are shown in Figure 127. The hardness values for the annealed material were 288 DPH for the ASTAR-1211C and 316 DPH for the ASTAR-1511C.

Prior to the drawing operation at Superior Tube, two experiments were conducted to provide guidance in selection of drawing parameters. A piece of annealed ASTAR-1211C sheet was given reductions of 10, 25, 50, and 75 percent by rolling to determine the work hardening rate. The hardness of ASTAR-1211C as a function of reduction by rolling is given in Figure 128. The thinness of the sheet reduced 75 percent made the hardness values uncertain. The greatest increase in hardness occurred at reduction in the 10 to 50 percent range. ASTAR-1511C would be expected to behave in a similar manner with the curve displaced upward to account for the higher hardness due to the higher alloy content. Reductions on the order of 10 to 20 percent between anneals were planned for both alloy compositions.

The second experiment consisted of an oxidation study to determine the maximum temperature which could be used in the drawing operation without severely contaminating the tube hollows.

Annealed tabs of ASTAR-1211C sheet 2.5 cm (1 inch) by 1.3 cm (1/2 inch) by 1.0 mm (0.040 inch) thick were exposed in still air at temperature for 24 hour periods. The samples were accurately weighed before and after the thermal exposure. The results of the experiment are given in Table 42. The calculated weight change values were based on uniform distribution of the contaminant throughout the sample, when in fact, the contaminant remains primarily at the surface. The 310°C (600°F) sample remained bright while the 427°C (800°F) and 538°C (1000°F) samples showed varying degrees of discoloration. The 649°C (1200°F) sample had a thicker surface film which spalled off in places during sample cooldown. Based on the experimental results, the drawing process was restricted to temperatures below 538°C (1000°F).

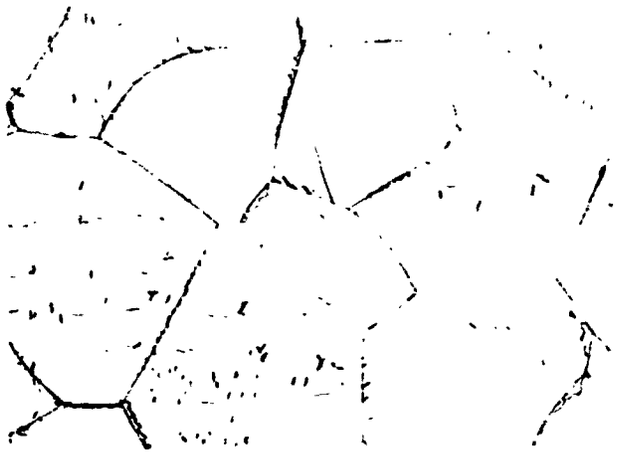

500X DPH 287

ASTAR-1211C

500X DPH 316

ASTAR-1511C

Figure 127. Microstructures of Heat Treated ASTAR 1211C and ASTAR 1511C Tube Hollows

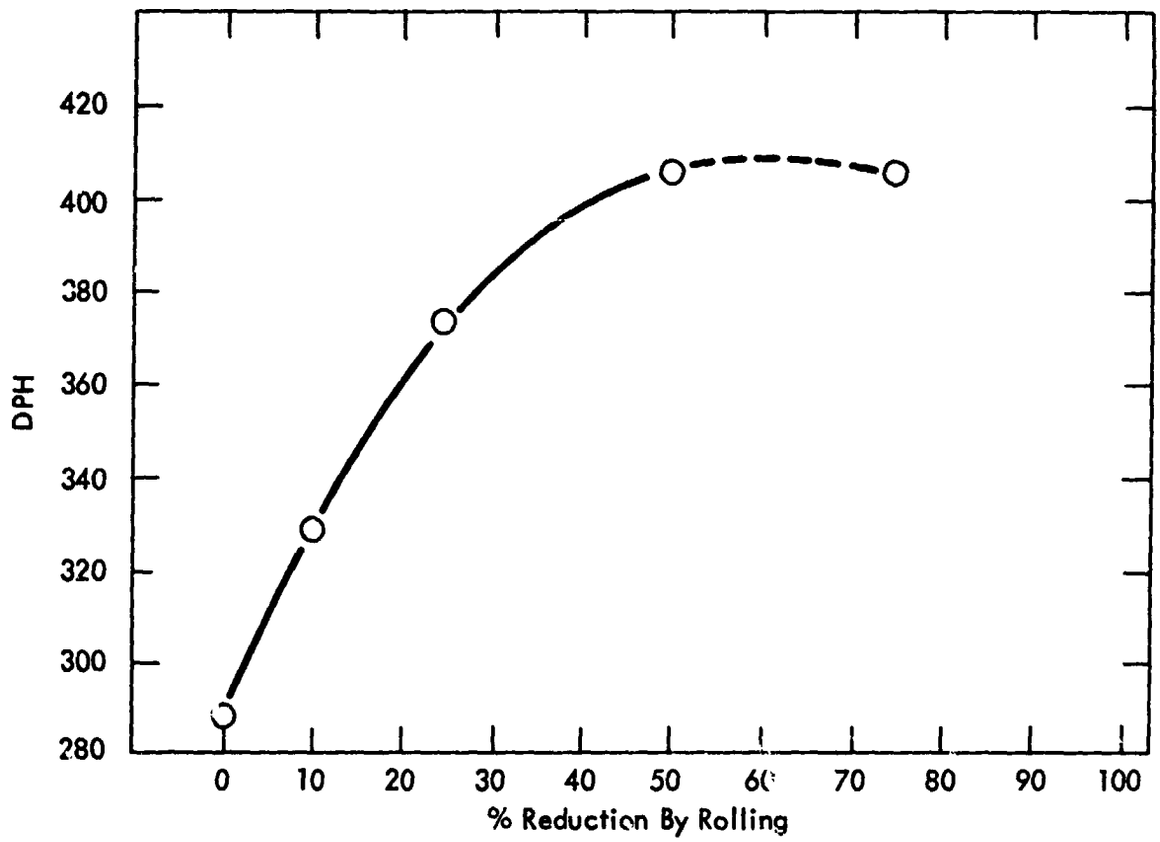

Figure 128. Room Temperature Hardness of ASTAR-1211C as a Function of Rolling Reduction

Table 42. Low Temperature Oxidation Study of ASTAR-1211C

Exposure Temperature		Sample Weight (g)	Weight Change After 24 hr. Exposure (g)	Weight Change Exposed as (ppm)*	Weight Change Per hr. (ppm/hr)
(°C)	(°F)				
316	600	5.5623	None	0	0
427	800	5.3396	+0.0003	56	2.3
538	1000	5.5766	+0.0006	107	4.5
649	1200	5.4184	+0.0063	1162	48.5

* Based on weight calculations

The tube drawing process used on this program utilized a hardened steel alloy mandrel to draw the tube hollow through the die. Under this arrangement, the OD and ID of the drawn tube can be carefully controlled. This procedure requires that the leading end of the tube be "tagged"; i.e., the OD and ID are reduced to provide a gripping area for the mandrel. In normally ductile material, a simple swaging reduction can serve to "tag" the tube hollow. Special hydraulic equipment specifically designed to handle more difficult experiments was also available.

For the initial drawing operation, four tube hollows, two of each composition, were sent to Superior Tube. Initial attempts to "tag" the ASTAR-1511C tube blanks were unsuccessful. Both ASTAR-1511C tubes developed longitudinal and transverse cracks as a result of the swaging process. Raising the swaging temperature to 316°C (600°F) to 427°C (800°F) was not effective in reducing the tendency to crack even at minimal reductions.

Two ASTAR-1211C tube hollows were successfully "tagged" with minor cracking. Both tube hollows were heated to 538°C (1000°F) and successfully drawn. The finished size was 25.9 mm (1.06 inch) OD x 17.9 mm (0.705 inch) ID for reduction of 10 percent based on change in cross sectional area. The "tagged" end of each tube hollow, which had been cracked, separated completely during the drawing operation. Removing the mandrel from the drawn tubing proved to be a difficult task. Normally, the tube walls are expanded away from the mandrel OD by a rolling operation. One tube hollow was broken during this operation. The successfully drawn tube hollows are shown in Figure 129. Examination of the tube blanks revealed circumferential cracks along the ID of both tubes. The cracks were attributed to the rolling operation used to remove the mandrel. After consultation with Superior Tube, the OD of all the ASTAR-1211C tube blanks and one ASTAR-1511C blank were machined to a nominal 25 cm (1 inch) diameter, and the ID was machined to give a 3.2 mm (1/8 inch) wall thickness. It was believed that the smaller wall thickness might be more amenable to swaging. The

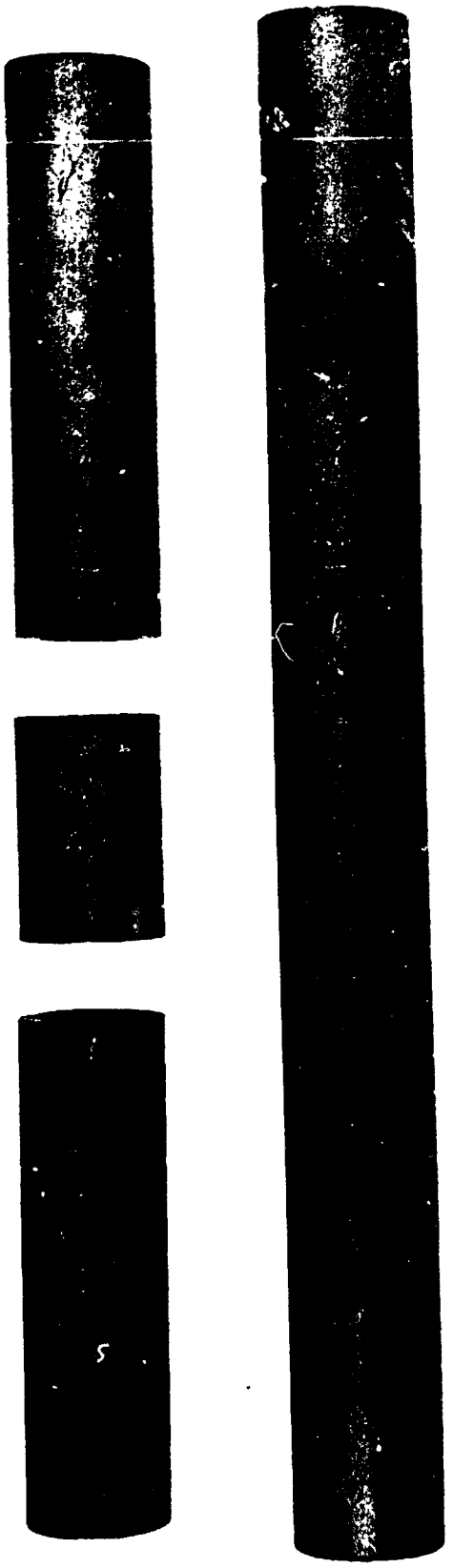

Figure 129. Successfully Drawn ASTAR-1211C Tube Hollows

ASTAR-1211C tube blanks were annealed 1 hour at 1649°C (3000°F) followed by 1 hour at 1260°C (2300°F). The results of an attempt to swage one of the shorter ASTAR-1211C tube blanks at 427°C (800°F) is shown in Figure 130. The failure was typical of the results of attempts to swage point ASTAR-1511C. It was concluded that "tagging" by swaging at temperatures in the range of 316°C (600°F) to 427°C (800°F) was unsatisfactory for these particular alloys.

Another approach, which offered possibilities of success, was hydrostatic extrusion. This process has been used successfully to deform brittle materials at ambient temperatures. Facilities for carrying out such an operation were available at the NASA-Lewis Research Center. It was decided that one small ASTAR-1211C tube hollow could be used to evaluate the hydrostatic deformation process as a means for "tagging" the tube blanks. The details of the operation of the NASA facility are given in a NASA Technical Note[11]. The tube blank was fitted with a mild steel mandrel to provide support at the tube blank ID and to provide a seal for retention of the working fluid. The objective was to push 1.3 cm (1/2 inch) to 1.9 cm (3/4 inch) of the tube blank into a conical shaped die. A die with a 40 degree included inlet angle was available and was used as a matter of convenience. The demonstration was quite successful and achieved what appeared to be a sufficient reduction in the first 1.3 cm (1/2 inch) of the tube. The remaining large ASTAR-1211C and the machined ASTAR-1511C were also processed in the same manner as the test piece. The results of the hydrostatic "tagging" operation are shown in Figure 131. The tube blanks were etched and dye penetrant inspected prior to shipment to Superior Tube for warm drawing. The dye penetrant inspection revealed that the ASTAR-1511C tube contained a circumferential crack just below the "tagged" or reduced end. The crack is not evident in the photograph of Figure 131. It was suspected that the crack may have formed during the etching process. There was no direct evidence to this effect, however. In light of this development, only the ASTAR-1211C tube blank was sent to Superior Tube for warm drawing.

Figure 130. ASTAR-1211C Tube Blank which Failed During Swaging

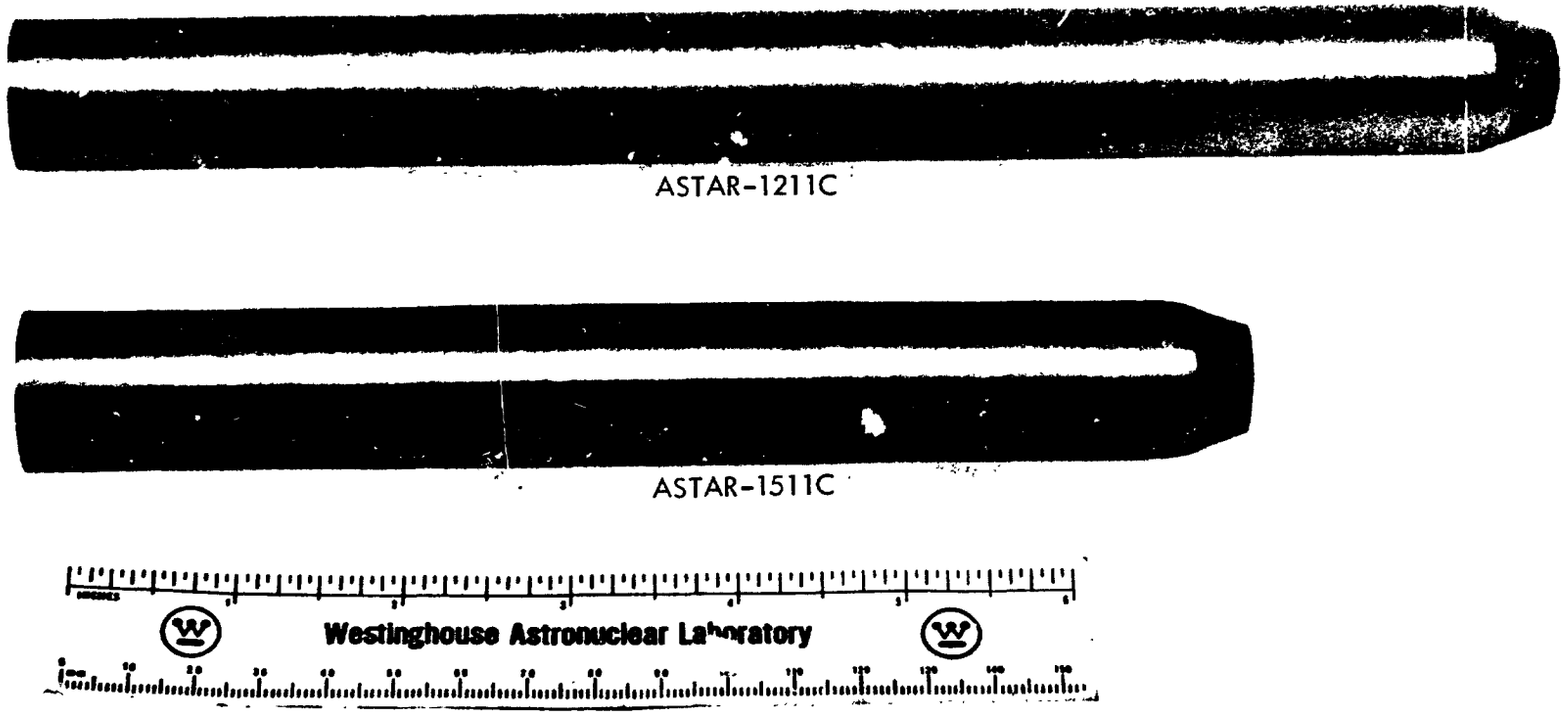

Figure 131. ASTAR-1211C and ASTAR-1511C Tube Blanks "Tagged" by Hydrostatic Extrusion

The tube blank was coated with a proprietary lubricant, heated to 316°C (600°F) and successfully drawn. The original tube blank was 20 cm (8 inches) long with a 24.4 mm (0.960 inch) OD and 3.1 mm (0.121 inch) wall. The drawing pass reduced the OD to 23.2 mm (0.914 inch) and the wall to 2.7 mm (0.107 inch), a reduction of 15.2 percent. Inspection of the tube blank after the drawing operation revealed a circumferential crack approximately 1/3 of the length back from the nose of the tube. The remainder of the tube blank was sound and possessed an excellent surface. Removal of the mandrel again caused difficulties. The mandrel removal procedure, which followed, consisted of heating the tube blank and mandrel to 482°C (900°F) for 10 minutes to allow the greater thermal expansivity of the Discalloy mandrel to expand the ASTAR-1211C tube blank. Then on cooling to ambient temperature the mandrel was moved approximately 1.3 cm (1/2 inch) with respect to the tube blank. An attempt to use the hydraulic draw bench to extract the mandrel the remainder of the distance was unsuccessful; the hydraulic system was stalled. A repeat of the thermal expansion of the tube blank using the procedure described above was again attempted without success. As a final attempt to remove the mandrel, it was decided that the tube might be expanded away from the mandrel by rapid heating of the tube OD. The mandrel and tube blank were allowed to cool to ambient temperature and then they were introduced into the 649°C (1200°F) zone of a multiple zone furnace for two minutes. The mandrel and tube blank were moved to a cooler part of the furnace in preparation for removal from the furnace. At that time, three audible "pings" were heard at one to two second intervals. The tube blank was removed from the furnace and examined. Three circumferential cracks were noted in the rear two-thirds of the tube blank. It was concluded that the cracks were most likely due to failure of the tube blank to accommodate the differential thermal expansion of the mandrel. It is not known what would cause the ASTAR-1211C, which has a tensile elongation of greater than 20 percent, to fail under the low imposed strain of thermal expansion.

The result of the drawing operation is shown in Figure 132. The end with the reduced OD, "tag", was pulled through the die first. The crack in the tag end occurred during the tagging process. The wide crack indicated by "A" occurred during the drawing process. The cracks indicated by "B", "C", and "D" occurred during the attempt to remove the mandrel. Micrographs of the cracked regions are shown in Figure 133. Figure 133A shows the crack which occurred during drawing. The crack in Figure 133B occurred during thermal cycling. Both cracks are primarily transgranular in nature, although some grain boundary separation can be noted. Hardness measurements taken adjacent to the cracked region ranged from 340 to 350 DPH which was typical for ASTAR-1211C which has been cold worked 13 to 15 percent. Check interstitial chemical analyses were conducted and revealed no significant change in bulk interstitial chemistry. Hydrogen level was 0.00008 percent, oxygen was 0.0004 percent, nitrogen was 0.0014 percent, and carbon was 0.0250 percent.

To check the possibility of an adverse reaction with the Superior Tube proprietary lubricant, three round bar tensile specimens were sent to Superior Tube for coating with the lubricant. On return to WANL, one specimen was thermally exposed at 316°C (600°F) for two hours. A second exposed at 482°C (900°F) and the third at 649°C (1200°F). After thermal exposure, the specimens were tested at room temperature along with an uncoated unexposed specimen. Tensile tests were carried out at a strain rate of 25.4 cm (10 inches) per minute. This speed approximated the tube drawing speed. Results of the tensile tests are given in Table 43.

Results for material tested at 0.05/min strain rate were also included to illustrate the effect of strain rate. The test results indicate that a significant reduction in total elongation occurred as the strain rate is increased. A corresponding increase in strength properties was also noted with the increased strain rate. The reduction in area, however, remained essentially the same. The specimens coated with Superior Tube lubricant and thermally aged show an effect due to the aging treatment. The specimen aged at 316°C (600°F) exhibits the lower elongation value while maintaining a comparable reduction in area. The specimens aged at 482°C

Astronuclear Laboratory

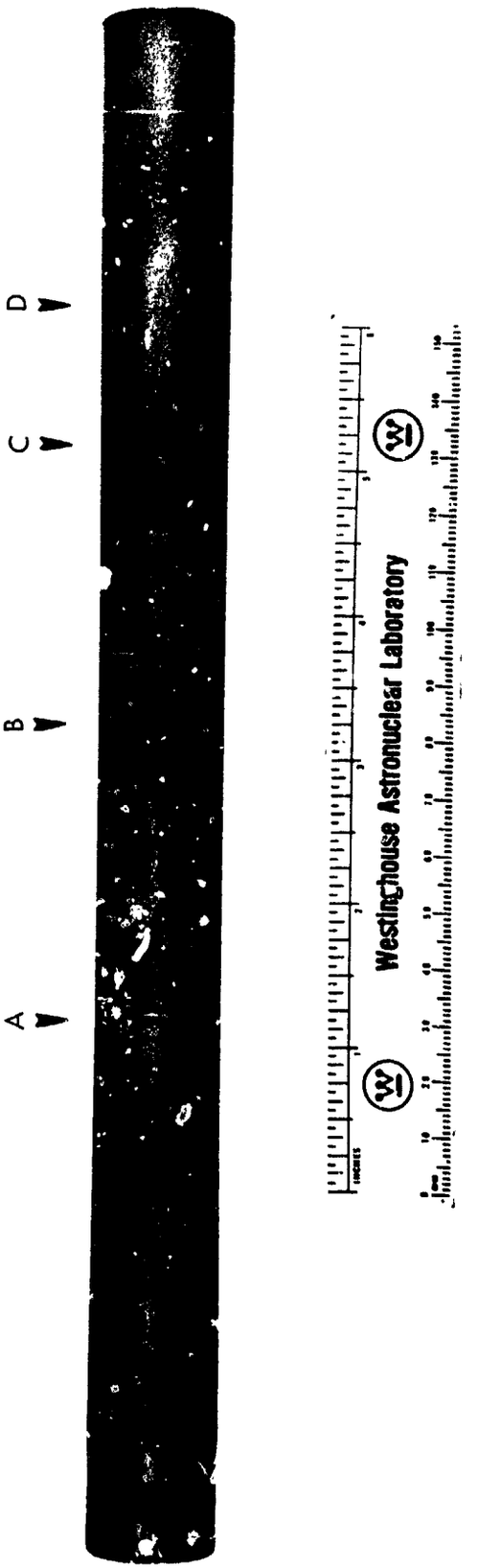

Figure 132. Failed ASTAR-1211C Tube Blank

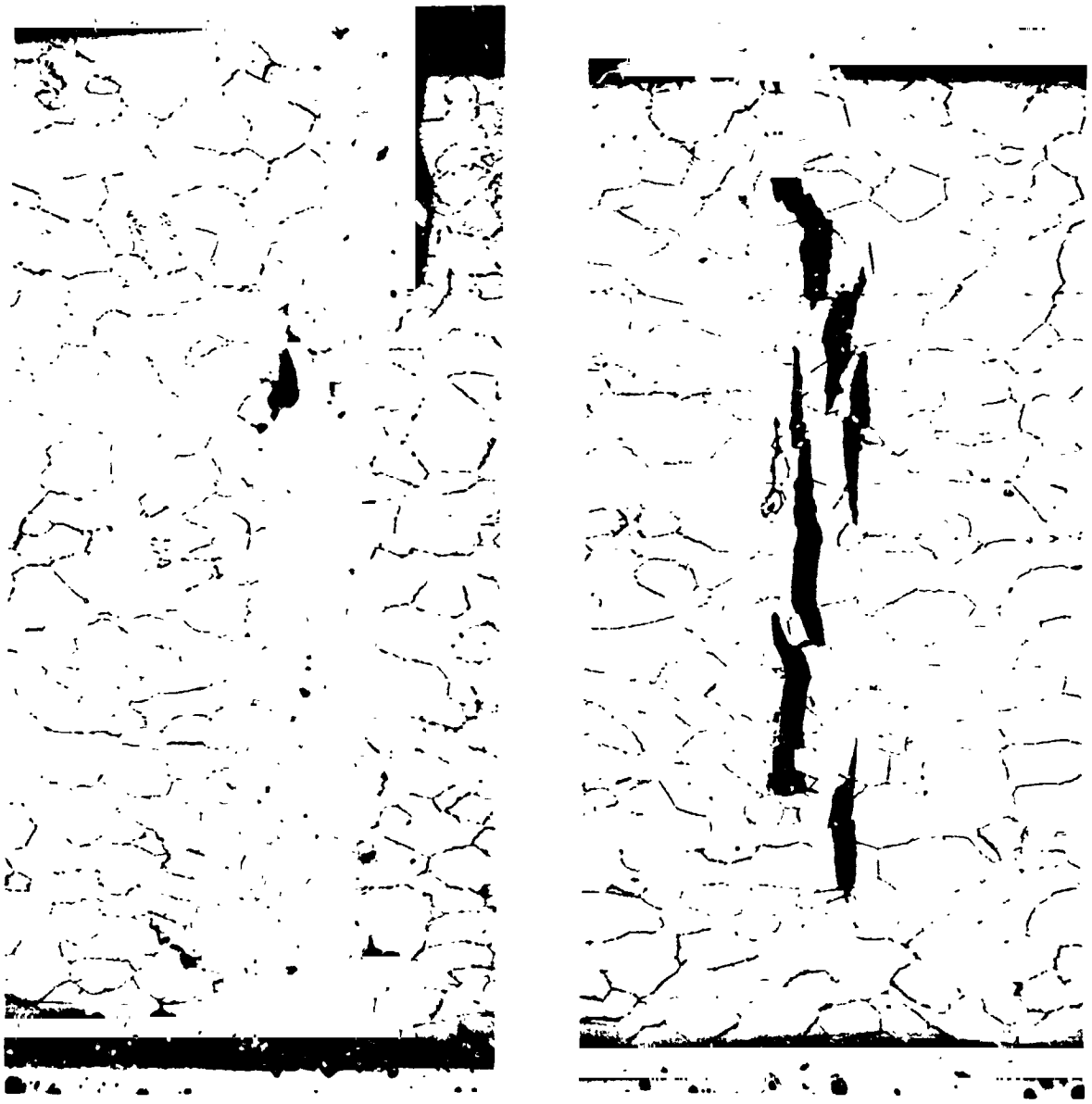

A B

Figure 133. Microstructure of Failed ASTAR-1211C Tube Blank

Table 43. Room Temperature Tensile Test Results for Lubricant Coated and Thermally Aged ASTAR-1211C Swaged Rod

Specimen Condition	Yield Strength		Ultimate Strength		Total Elongation (%)	Reduction in Area (%)
	(MN/m^2)	(ksi)	(MN/m^2)	(ksi)		
Uncoated Control*	1035	150	1035	150	1.7	56.3
Coated + 2 hrs. at 316°C (600°F)*	1082	157	1082	157	2.0	57.4
Coated + 2 hrs. at 482°C (900°F)*	--	--	1075	156	0.1	7.5
Coated + 2 hrs. at 649°C (1200°F)*	--	--	642	93	0.2	2.6
Uncoated**	764	110.6	918	133.0	23.6	47.6

* Strain Rate 10/min.
** Strain Rate 0.05/min.

(900°F) and 649°C (1200°F) exhibited both a drastic reduction in elongation as well as a significant reduction in area. It appeared that thermal aging above 316°C (600°F) produced a significant loss of ductility in ASTAR-1211C at the higher strain rate. It was not certain whether the loss in ductility was due to the thermal exposure along or was associated with the lubricant.

One last tube blank of ASTAR-1211C was processed at Superior Tube in an attempt to produce tubing. In light of the apparent strain rate sensitivity and the effect of temperature on the ductility of ASTAR-1211C, the processing schedule was changed. The drawing and "tagging" operations were carried out at 204°C (400°F) rather than 316°C (600°F) to 427°C (800°F). The drawing speed was reduced from well over 76.2 cm (30 inches) a minute to 25.4 cm (10 inches) a minute. The lubricant was switched from one Superior Tube proprietary lubricant, which contained a glass frit for elevated temperature, to one more suitable for the revised 204°C (400°F) drawing temperature. The tube blank, which was approximately 23.9 cm (9 inches) long and had an OD of 2.5 cm (0.980 inch) with a 2.9 mm (0.114 inch) wall thickness. The tube blank was successfully "tagged" without cracking. This was done in small 2.6 mm (1/8 inch) incremental steps. The tube blank was successfully drawn at 232°C (450°F) at a reduction of 12 percent. The finished length was approximately 25.4 cm (10 inches) long. The finished OD was 2.31 cm (0.910 inch) giving a final wall thickness of approximately 2.5 mm (0.100 inch). The blank was heat treated 1 hour at 1316°C (2400°F) and returned to Superior Tube for second drawing operation. The parameters for the second draw were the same as for the first.

The resulting tube from the second drawing pass was crack free. The tube was removed from the mandrel by passing the tube through a bar rolling mill. In this operation, the tube was worked slightly in the same direction as the drawing operation. The resulting tube OD was 2.2 cm (0.864 inch) with a 2.4 mm (0.096 inch) wall thickness for a total reduction of

11.8 percent. A third successful tube reduction step was also carried out using the same procedure. The resulting crack-free tube, shown in Figure 134, had a final OD of 2.1 cm (0.830 inch) with a 2.2 mm (0.087 inch) wall thickness. The reduction was on the order of 12.3 percent.

At this point, the feasibility study was concluded. Although the objective of producing 1.9 cm (0.750 inch) by 1.0 mm (0.040 inch) wall tubing was not achieved, it was concluded that the final process that was investigated demonstrated that ASTAR-1211C tubing of the target dimensions could indeed be produced.

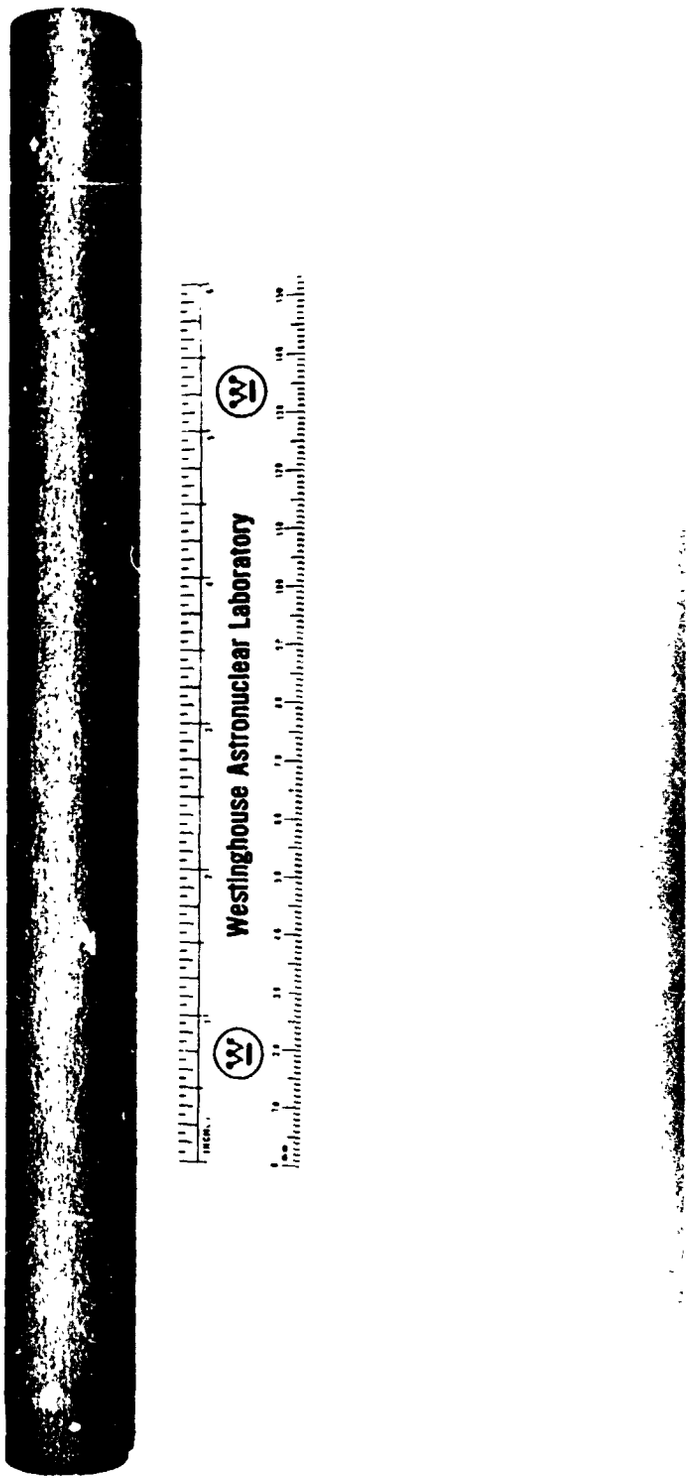

Figure 134. Successfully Drawn ASTAR-1211C Tubing.

7.0 PROCESSING AND EVALUATION OF FORGED ASTAR-1211C AND ASTAR-1511C DISCS

The objective of this task was to evaluate the forgeability and obtain the mechanical properties of ASTAR-1211C and ASTAR-1511C. Three billets of each composition were upset forged to round discs. Creep and tensile specimens cut parallel to the radii of the discs were tested. The processing and evaluation schedule is given in Figure 135.

7.1 PROCESSING OF FORGED DISCS

The billets, which were annealed 1 hour at 1815°C (3300°F), were encapsulated in powder met molybdenum cans as shown in Figure 136. The billets were surrounded with approximately 1.3 cm (1/2 inch) thick molybdenum clad at the OD. To protect the billet ends, molybdenum sheet 0.5 mm (0.020 inch) thick was weld brazed in place using vanadium as a filler braze material. The billets were heated to 1538°C (2800°F) in an inert atmosphere induction heating furnace. The billets were then upset forged with one blow in a Dynapak high-energy-rate forming machine. The forging details are given in Table 44.

Forged discs of ASTAR-1211C are shown in Figure 137. Despite the high reductions, 60 to 73 percent, little or no checking or cracking was observed. The constraint provided by the thick molybdenum can during the forging process apparently was helpful in reducing the tendency for cracking at the OD of the discs. The 0.5 mm (0.020 inch) sheet at the billet end reduced the tendency for dishing out at the center of the discs. Thickness of the declad discs were very uniform from edge to center.

7.2 EVALUATION OF FORGED ASTAR-1211C AND ASTAR-1511C DISCS

The evaluation of the forged discs consisted of macroscopic examination, determination of recrystallization behavior, and mechanical property testing. Included in the mechanical

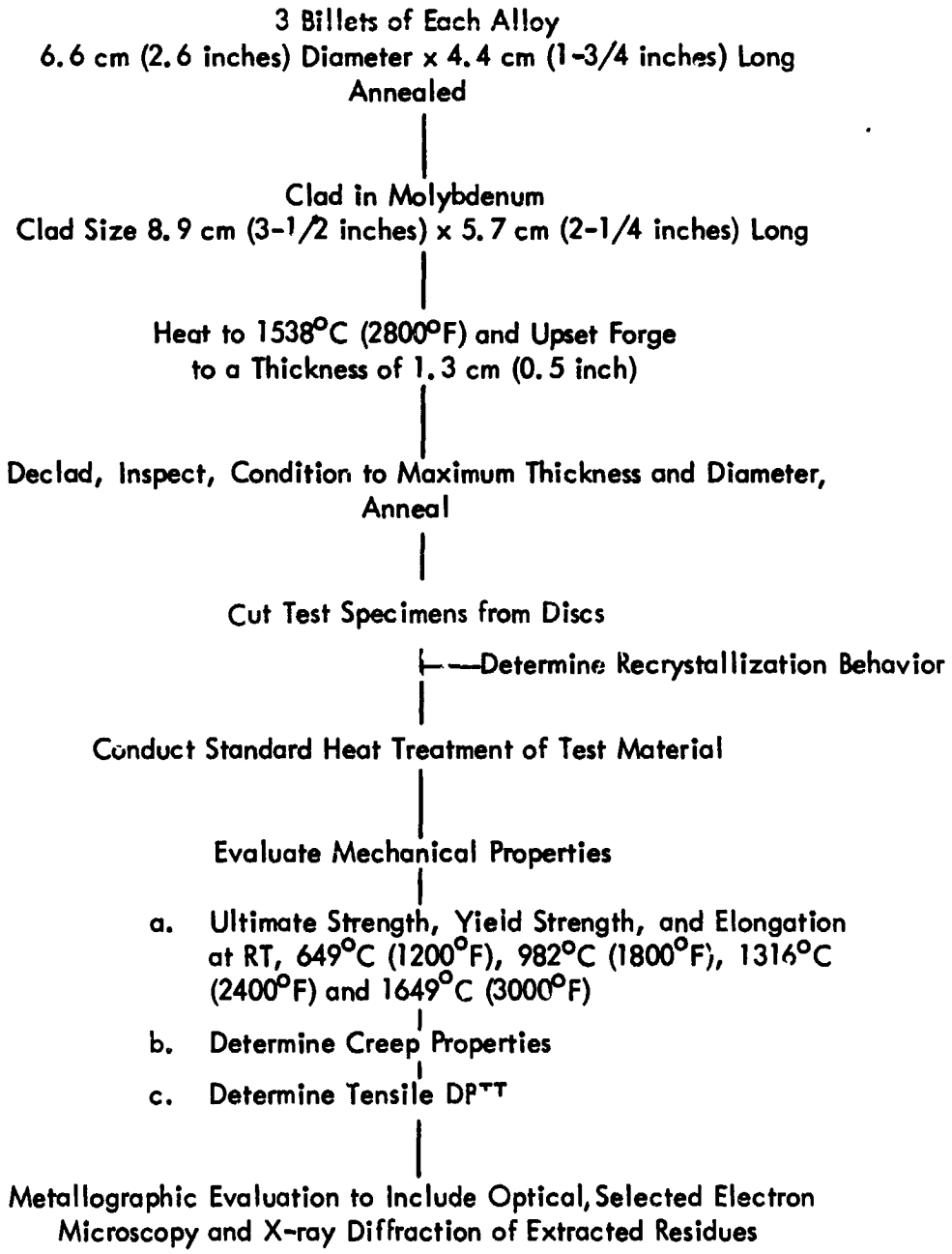

Figure 135. Schedule for Processing and Evaluation of Forged ASTAR-1211C and ASTAR-1511C Discs

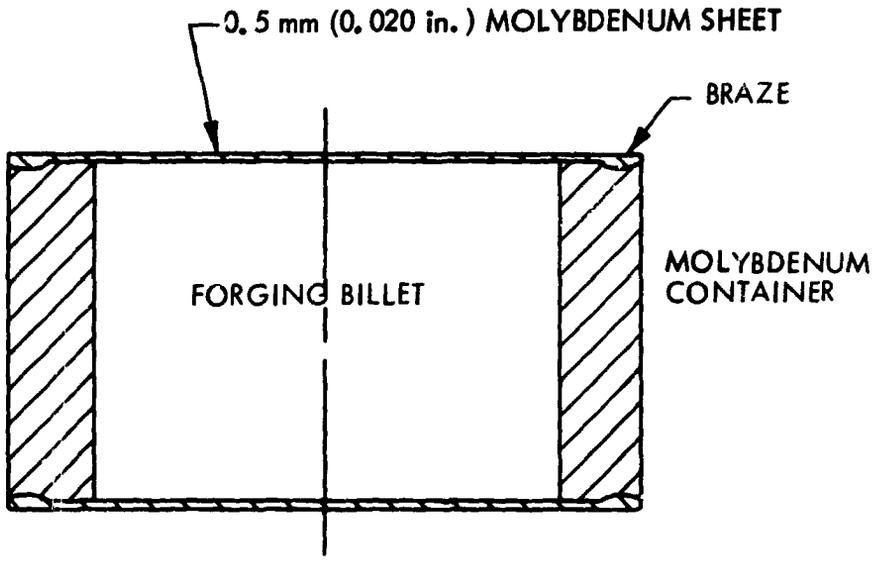

Figure 136. Encapsulation of Billets for Forging

Table 44. Forging Data for ASTAR-1211C and ASTAR-1511C Discs

Billet Designation	Diameter		Height		Weight		Final Thickness		Upset Ratio	Upset* Constant (K_u)	
	(cm)	(in)	(cm)	(in)	(kg)	(lbs)	(mm)	(in)		(MN/m^2)	(ksi)
NASVF-1000-B4	6.61	2.60	4.44	1.75	2.7	6.0	16.0	.631	2.8	980	142
1000-B5	6.73	2.65	4.29	1.69	2.6	5.8	12.3	.485	3.5	911	132
1000-B6	7.01	2.76	4.29	1.69	2.7	6.1	11.5	.455	3.7	897	130
2000-A4	6.34	2.50	4.44	1.75	2.4	5.4	12.7	.500	3.5	1090	158
2000-A6	6.73	2.65	4.44	1.75	2.7	6.0	13.9	.545	3.2	1123	163
2000-B5	6.86	2.70	4.44	1.75	2.9	6.3	13.3	.525	3.3	1180	171

* Based on a calculated K_u for Mo of 558 MN/m^2 (81.0 ksi)

Figure 137. Forged Discs of ASTAR-1211C

property testing were the determination of tensile DBTT, notched-unnotched strength ratio, and elevated temperature tensile and creep behavior.

7.2.1 Recrystallization Behavior

Two discs of ASTAR-1211C were cut through the diameter and the surfaces through forging were examined macroscopically. The macrograph of the etched surfaces are shown in Figure 138. No distinct flow pattern was evident in the macrostructure. The material appears to have deformed in a more or less idealized manner. No "dog bone" shaped pattern, which characterizes forging with inadequate lubrication, was evident. Only a very faint indication of the prior extrusion direction was discernible.

Samples were cut from the forging and annealed for 1 hour at 1093°C (2000°F), 1260°C (2300°F), 1371°C (2500°F), 1482°C (2700°F), 1649°C (3000°F), 1815°C (3300°F), and 1982°C (3600°F). The microstructures of the forged and heated samples of ASTAR-1211C and ASTAR-1511C are shown in Figures 139 and 140, respectively. The "as-forged" microstructure of each alloy shows the deformed grain structure produced by the forging reduction. The billets were annealed for 1 hour at 1815°C (3300°F) prior to forging, producing the large grain size evident in the micrographs. The response of both alloys to the heat treatments were similar. In the temperature range 1093°C (2000°F) to 1482°C (2700°F), no evidence of recrystallization was detected. Precipitation of Ta_2C at grain boundaries was noted particularly in the temperature range 1093°C (3000°F) to 1260°C (2300°F). X-ray diffraction analysis of extracted residues identified Ta_2C as the only precipitate present. As the heat treating temperature increased, the quantity of grain boundary precipitate decreased. Evidence of a fine general precipitate which occurred during cooldown was present in the microstructure of material annealed at the highest temperature.

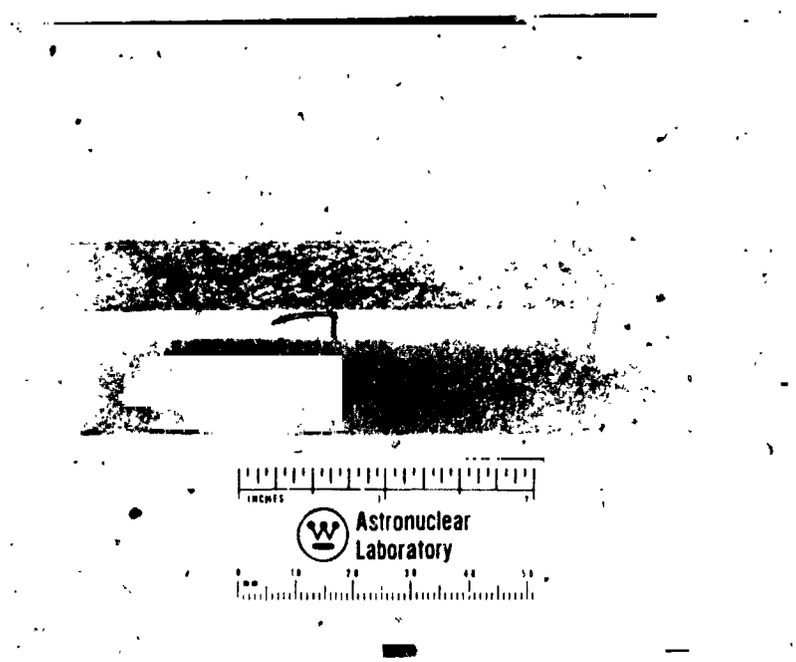

Figure 138. Macrostructure of "As-forged" ASTAR-1211C Discs

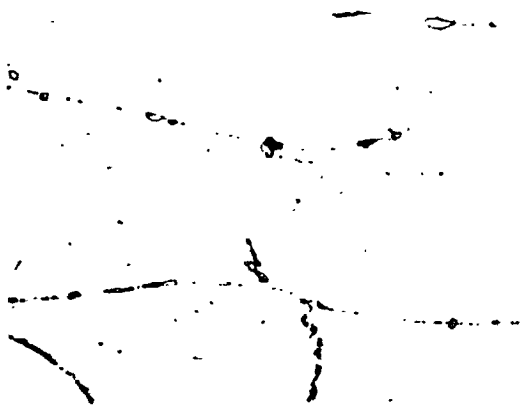

500X DPH 366

A. As Forged

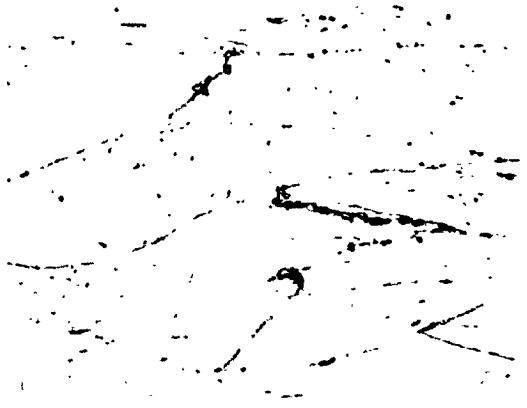

500X DPH 342

B. Forged + 1 hr/1093°C (2000°F)

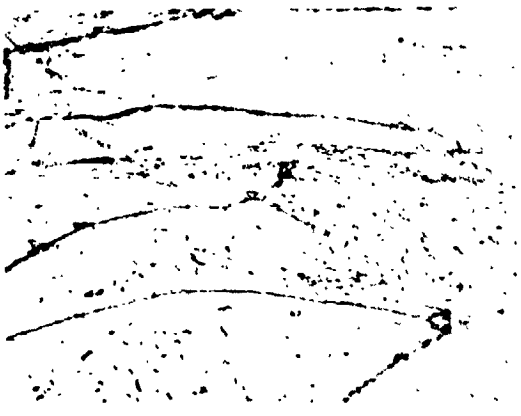

500X DPH 332

C. Forged + 1 hr/1260°C(2300°F)

500X DPH 327

D. Forged + 1 hr/1371°C(2500°F)

Figure 139. Microstructure of Forged and Heat Treated ASTAR 1211C

500X DPH 321

E. Forged + 1 hr/1482°C (2700°F)

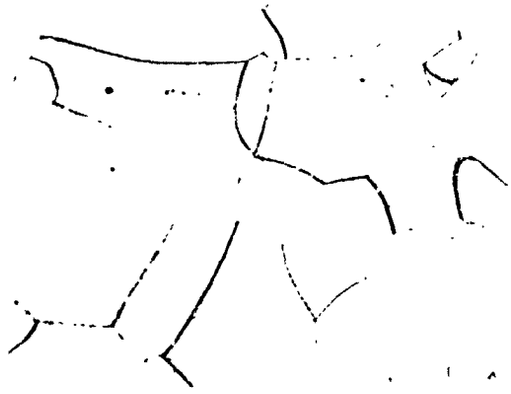

500X DPH 306

F. Forged + 1 hr/1649°C (3000°F)

500X DPH 302

G. Forged + 1 hr/1815°C (3300°F)

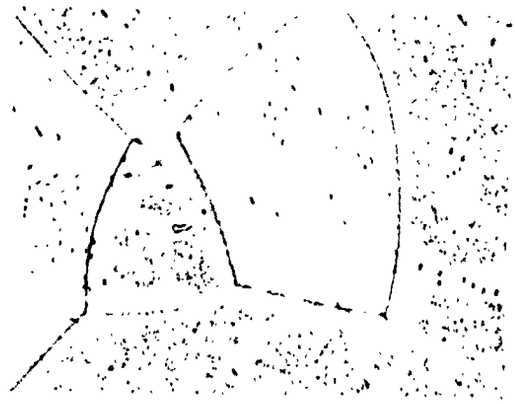

500X DPH 295

H. Forged + 1 Hr/1982°C (3600°F)

Figure 139. Microstructure of Forged and Heat Treated ASTAR 1211 C (Continued)

500X DPH 385

A. As Forged

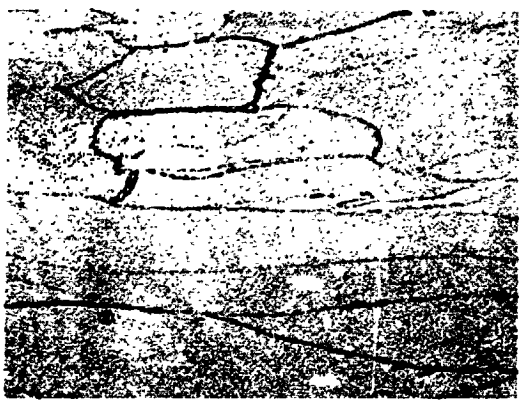

500X DPH 367

B. Forged + 1 hr/1093°C (2000°F)

500X DPH 357

C. Forged + 1 hr/1260°C(2300°F)

500X DPH 343

D. Forged + 1 hr/1371°C (2500°F)

Figure 140. Microstructure of Forged and Heat Treated ASTAR 1511C

C-4

Astronuclear Laboratory

500X DPH 344

E. Forged + 1 hr/1482°C (2700°F)

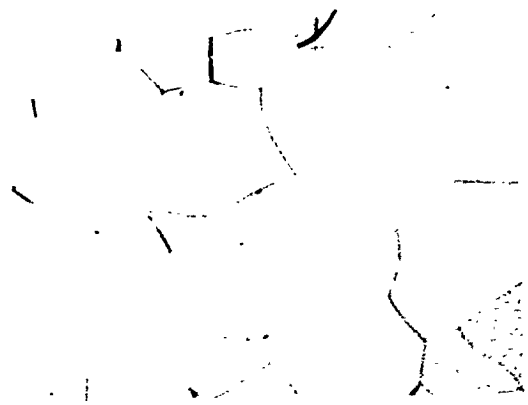

500X DPH 354

F. Forged + 1 hr/1649°C (3000°F)

500X DPH 336

G. Forged + 1 hr/1815°C (3300°F)

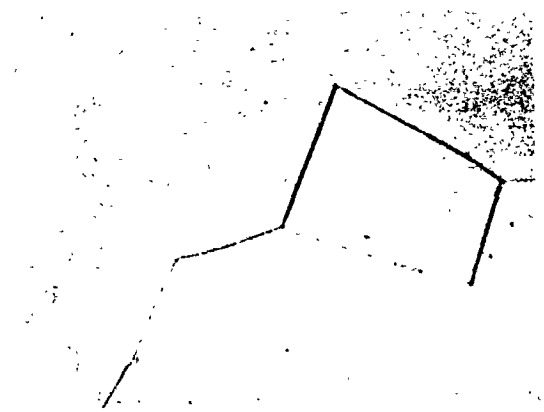

500 DPH 332

H. Forged + 1 hr/1982°C (3600°F)

Figure 140. Microstructure of Forged and Heat Treated ASTAR 1511C (Continued)

Hardness data for the forged and annealed materials are shown in Figure 141. Recrystallization did not occur in either alloy until the annealing temperature reached 1649°C (3000°F). The amount of reduction, which ranged from 64 to 73 percent, and the forging temperature 1538°C (2800°F), produced the higher recrystcllization temperature. The hardness data reflected the normal behavior expected of tantalum-base alloy, recovery as indicated by the reduction in hardness prior to achieving recrystallization as annealing temperature increased. The ASTAR-1511C under went hardness increase at 1649°C (3000°F) while no such peak occurred for ASTAR-1211C. Both hardness responses have been observed for similar conditions.

7.2.2 Tensile DBTT and Elevated Temperature Properties

Tensile specimen blanks were cut from the forged discs. The specimen blanks were cut parallel to the discs' radii to insure uniformity in microstructure from specimen to specimen. The machined tensile specimens were given the standard heat treatment, 1 hour at 1649°C (3000°F). The low temperature tensile properties of ASTAR-1211C and ASTAR-1511C are given in Table 45 along with tensile strength data for motched specimens. The tensile elongation values are plotted in Figure 142. The DBTT for the forged ASTAR-1211C was approximately -115°C (-175°F). The value for ASTAR-1511C was near room temperature. The DBTT for the forged material was higher for both alloys than swaged rod with comparable final heat treatment.

The notched-unnotched strength ratios are given in Table 46. The same pattern noted for swaged rod was also noted for forged material. The ASTAR-1211C exhibited a notched-unnotched strength ratio of 1.59 at room temperature. The ratio decreased as the test temperature decreased, but remained above 1.0. The ASTAR-1511C exhibited similar behavior, however, the ratio dropped below 1.0 at -129°C (200°F) test temperature. This behavior plus the fact that the stress concentration factor (K_t) for ASTAR-1511C was 3.0 opposed to 4.2 for ASTAR-1211C indicate that the forged ASTAR-1511C was more notch sensitive.

The elevated temperature properties for forged ASTAR-1211C and ASTAR-1511C are listed in Table 47. Test specimens were heat treated for 1 hour at 1649°C (3000°F) prior to testing

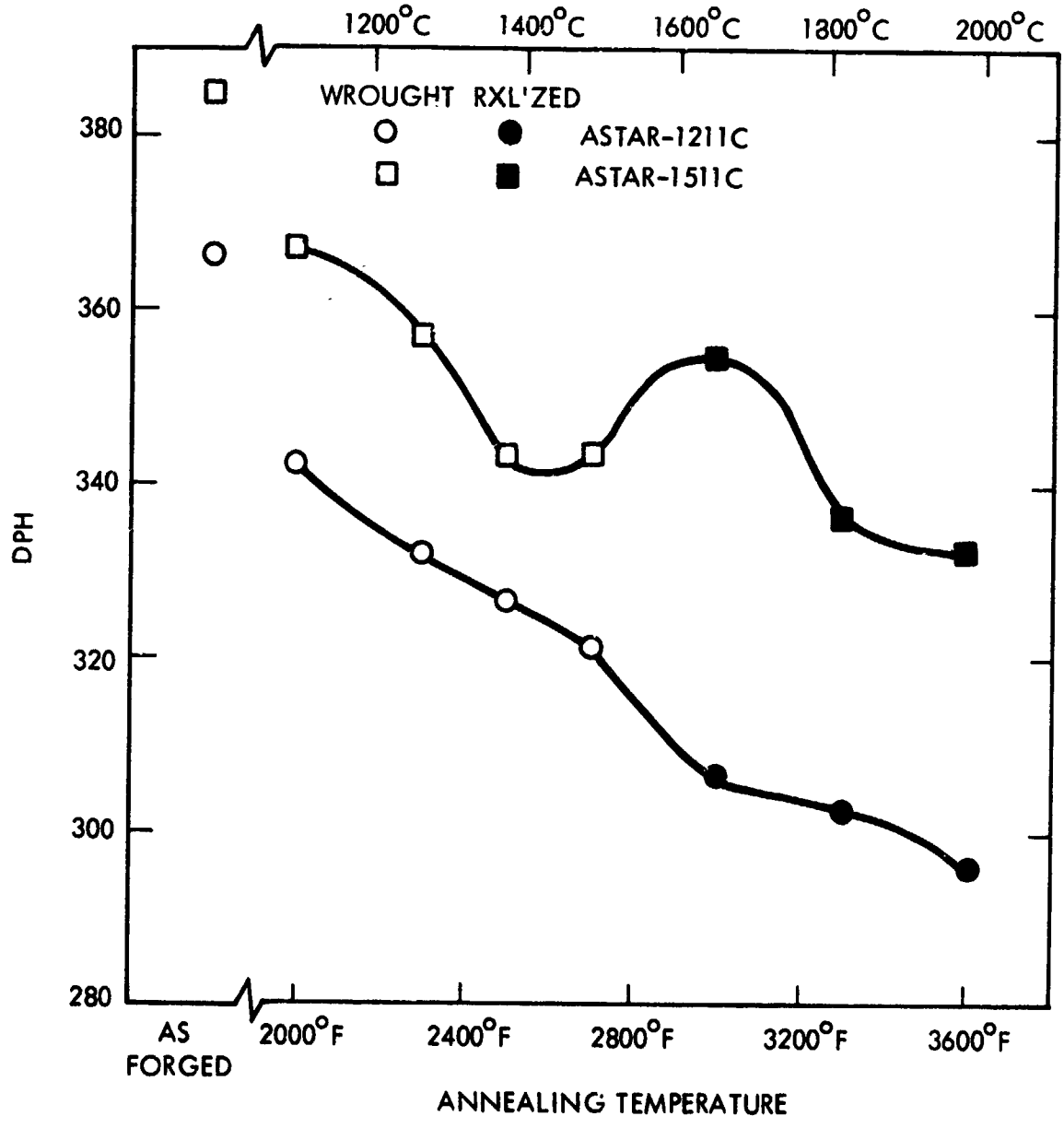

Figure 141. Hardness of Forged and Heat Treated ASTAR-1211C and ASTAR-1511C

Table 45. Low Temperature Tensile Properties of Forged ASTAR-1211C and ASTAR-1511C

Test Temperature		Yield Strength		Ultimate Strength		Elongation		Reduction in Area (%)
(°C)	(°F)	(MN/m^2)	(ksi)	(MN/m^2)	(ksi)	Uniform (%)	Total (%)	
				ASTAR-1211C				
RT	RT	792	114.8	907	131.4	12.7	22.1	53.2
RT*	RT*		-	1440	208.7	-	-	-
- 73	-100	941	136.3	1045	151.5	12.4	17.9	31.1
- 73	-100*		-	1465	212.2	-	-	-
-129	-200	993	143.9	1142	165.5	9.8	9.8	9.6
-129	-200*		-	1480	214.4	-	-	-
-157	-250	1124	162.9	1170	169.5	3.4	3.4	4.1
-157	-250*		-	1600	232.1	-	-	-
-196	-320	1253	182.0	1310	189.8	1.5	1.5	2.4
-196	-320*		-	1620	234.5	-	-	-
				ASTAR-1511C				
RT	RT	928	134.6	963	139.3	9.1	11.1	20.0
RT*	RT*		-	1388	201.0	-	-	-
- 73	-100	1088	157.6	1095	158.7	1.3	1.3	2.6
- 73	-100*		-	1161	168.1	-	-	-
-101	-150	1170	169.3	1190	172.5	1.0	1.0	2.1
-101	-150*		-	640	92.7	-	-	-
-101	-150*		-	1410	204.1	-	-	-
-129	-200	1174	171.5	1195	173.1	0.7	0.7	0.6
-129	-200*		-	1115	161.4	-	-	-

Strain Rate 0.05/min.

* Notched

$K_t = 4.2$ - ASTAR-1211C

$K_t = 3.0$ - ASTAR-1511C

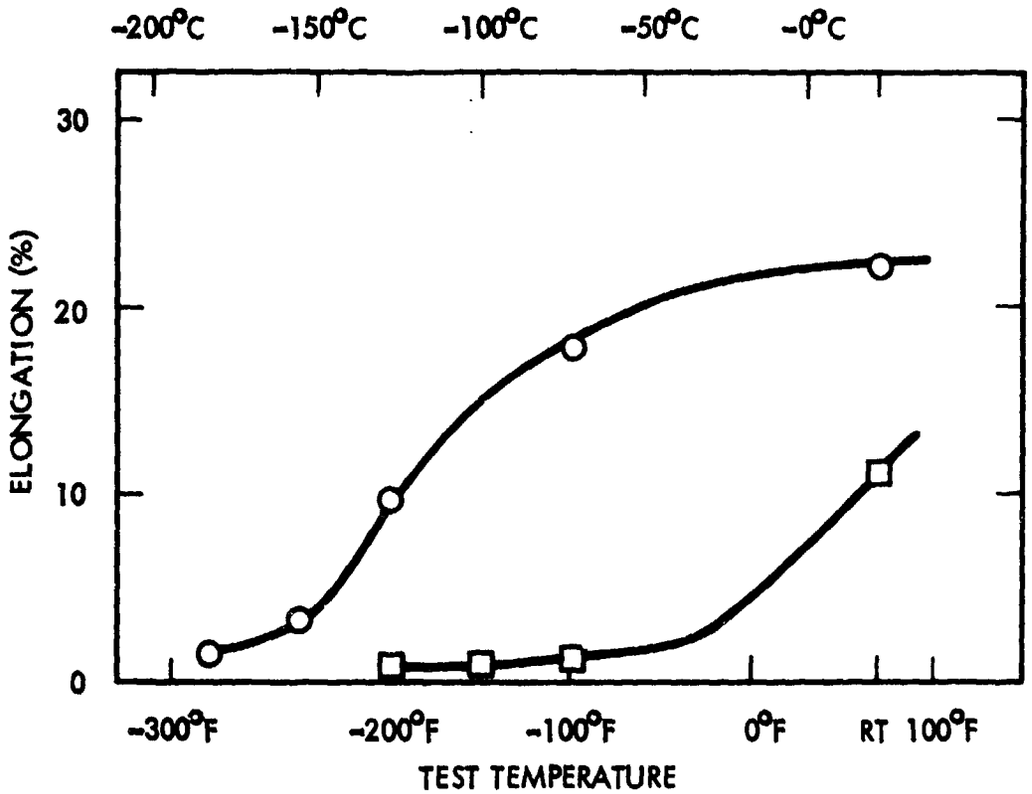

Figure 142. Tensile DBTT for Forged ASTAR-1211C and ASTAR-1511C

Table 46. The Notched-Unnotched Strength Ratio of Forged ASTAR-1211C and ASTAR-1511C as a Function of Test Temperature

Test Temperature		Notched Strength Ratio	
(°C)	(°F)	ASTAR-1211C	ASTAR-1511C
RT	RT	1.59	1.44
- 73	-100	1.40	1.06
-101	-150	-	1.18
-129	-200	1.30	0.93
-157	-250	1.37	-
-196	-320	1.24	-

K_t for ASTAR-1211C - 4.2

K_t for ASTAR-1511C - 3.0

The strength properties are plotted as a function of test temperature in Figure 143. The significance of the tensile properties was the extraordinary properties of ASTAR-1511C. The yield and ultimate strength values were greater than those of swaged material, particularly at temperatures of 1316°C (2400°F) and above.

7.2.3 Creep Properties

Creep test specimens were annealed 1 hour at 1649°C (3000°F) prior to testing. Creep data are presented in Table 48. Larson-Miller parameters for 1 percent creep strain are plotted in Figure 144 along with data for swaged rod. Data for T-111 and ASTAR-811C were included for reference. The creep results for ASTAR-1211C were quite consistent. The creep data for ASTAR-1211C were generated from four test specimens, although some load and temperature changes were required during testing to produce discernible creep rates. The creep properties of the forged ASTAR-1211C were comparable or slightly better than those of swaged rod.

The data for ASTAR-1511C were not consistent. Three test specimens were used to generate the data points on the Larson-Miller parameter plot for ASTAR-1511C. The slope of the curve for forged ASTAR-1511C diverged significantly from the data for swaged rod, particularly at the lower stress levels where test temperature was 1316°C (2400°F). The continuity of the curve suggests that the anomalous creep behavior was likely characteristic of the materials rather than due to a hidden flaw in the specimen. The low stress data for forged ASTAR-1511C indicated lower creep resistance than ASTAR-811C. This creep behavior was inconsistent from a composition standpoint; ASTAR-1511C has 7 percent higher tungsten content than ASTAR-811C and, therefore, would be expected to possess greater high temperature creep resistance. The anomalous creep behavior of ASTAR-1511C could have been caused by a number of factors. Incomplete recrystallization is known to have a significant deleterious affect on creep properties of tantalum alloys. Additional testing of material from a different forging were precluded due to lack of time.

Table 47. Elevated Temperature Tensile Properties of ASTAR-1211C and ASTAR-1511C

Test Temperature		Yield Strength		Ultimate Strength		Elongation		Reduction in Area (%)
(°C)	(°F)	(MN/m^2)	(ksi)	(MN/m^2)	(ksi)	Uniform (%)	Total (%)	
				ASTAR-1211C				
649	1200	437	63.4	715	103.6	9.9	13.8	63.7
982	1800	354	51.3	698	101.1	13.8	18.9	57.7
1316	2400	268	38.9	358	51.8	7.4	25.6	63.8
1649	3000	214	31.0	217	31.4	0.7	23.1	38.2
				ASTAR-1511C				
649	1200	635	92.0	736	106.8	5.7	11.4	57.5
982	1800	594	86.0	728	105.6	6.2	10.5	51.8
1316	2400	530	76.7	552	79.9	1.6	8.7	41.3
1649	3000	258	37.4	305	44.2	3.7	31.9	48.1

Strain Rate 0.05/min.

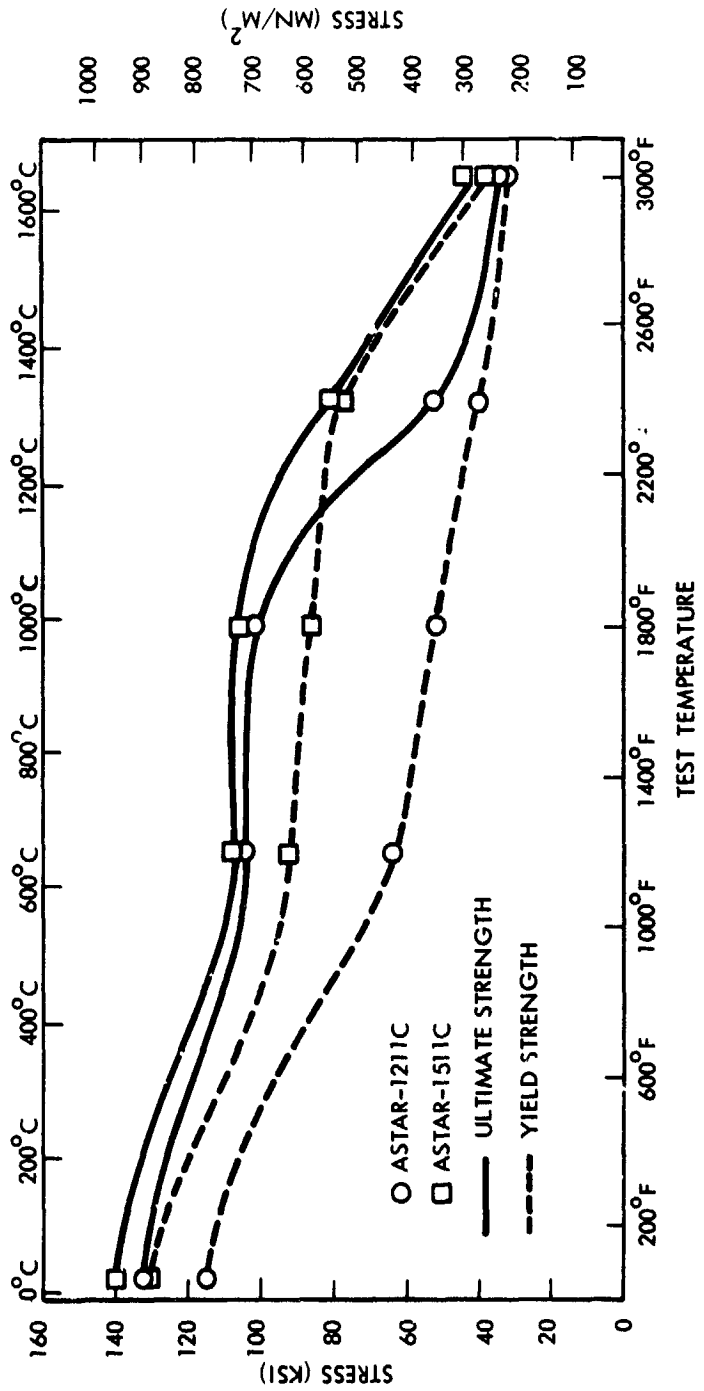

Figure 143. Elevated Temperature Tensile Properties of Forged ASTAR-1211C and ASTAR-1511C

Table 48. Creep Data for Forged ASTAR-1211C and ASTAR-1511C

Load		Test Temperature		Strain on Loading (%)	Secondary Creep Strain (%)	Secondary Creep Time (hrs.)	Creep Rate (%/hr.)	Time to 1% Strain (hrs.)	P **
(MN/m^2)	(ksi)	(°C)	(°F)						
					ASTAR-1211C				
276	40	1093	2000	0.25	2.65**	830**	**	360	43.2
207	30	1149	2100	0.15	0.45	1001	0.00045	2250	46.9
138	20	1204	2200	0.04	***	502	***	-	-
138	20	1260	2300	-	***	167	***	-	-
138	20	1316	2400	-	1.09	209	0.00522	192	49.5
103	15	1260	2300	0.07	***	432	***	-	-
103	15	1316	2400	-	***	163	***	-	-
103	15	1371	2500	-	0.30	210	0.00143	700	52.8
					ASTAR-1511C				
276	40	1093	2000	0.09	0.15	378	0.00040	2500	45.3
207	30	1204	2200	0.15	1.24	264	0.00480	213	46.1
173	25	1204	2200	-	.86	330	0.00260	384	46.8
138	20	1204	2200	-	.35	319	0.00110	912	47.8
103	15	1316	2400	.08	1.71	233	0.00784	136	49.0
69	10	1316	2400	-	.82	346	0.00237	422	50.4

* $P = T_R^{\circ} (15 + \log t) \times 10^{-3}$

** No secondary creep rate established - time to 1 percent strain taken from creep curve.

*** No detectable strain - temperature was increased.

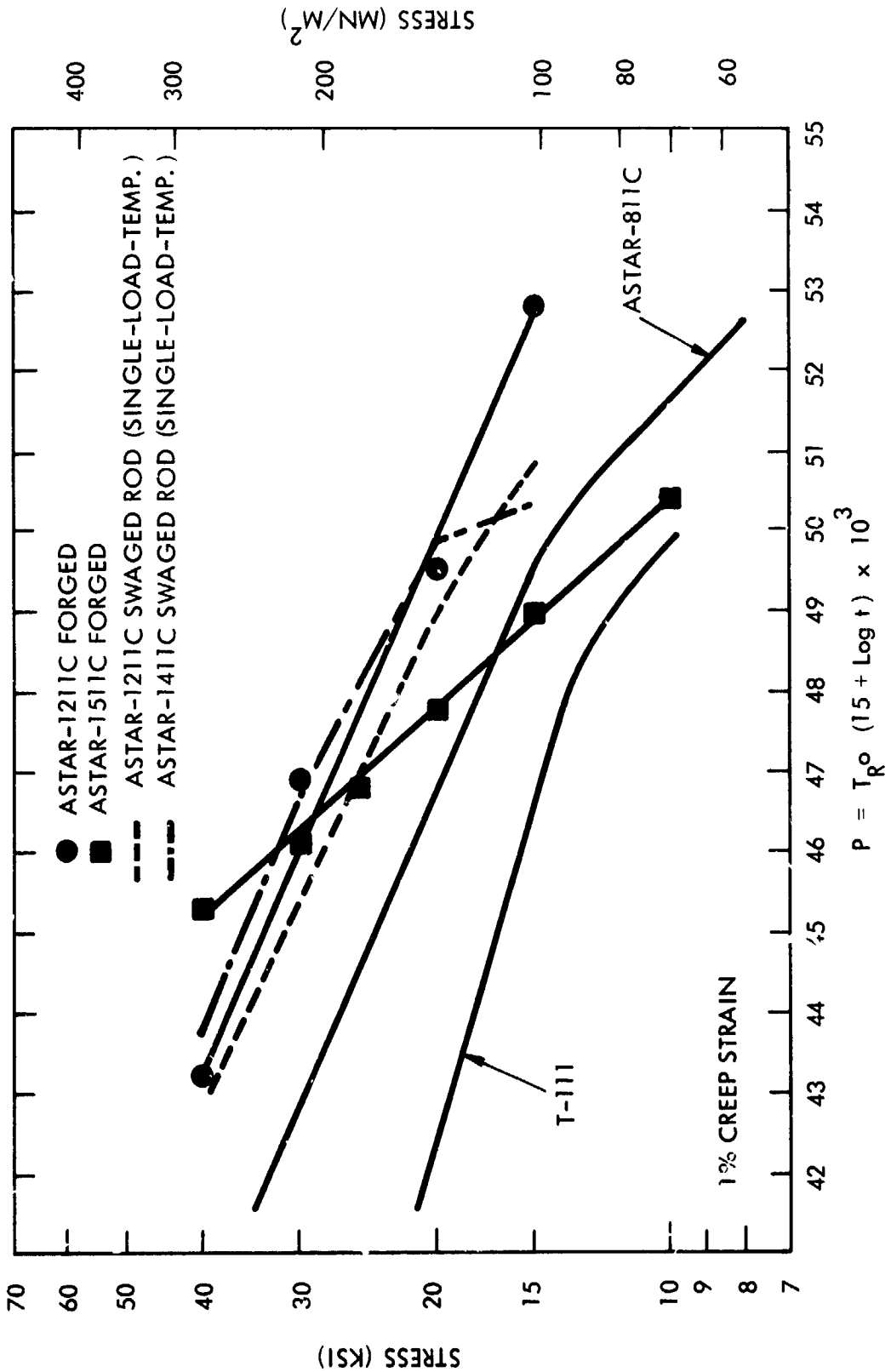

Figure 144. Creep Data for Forged ASTAR-1211C and ASTAR-1511C

8.0 CONCLUSIONS

8.1 PROCESSING OF STARTING MATERIAL

Both alloy compositions ASTAR-1211C and ASTAR-1511C were successfully produced as 12.6 cm (5.0 inch) diameter ingots by double vacuum arc melting. Target alloy levels were achieved within the tolerances set forth in the program plan. Initial melting of elemental electrodes was carried out using AC power on a routine basis. Final DC melting was accomplished with minor difficulty traced to a nonvariable power stirring coil. (The over powered stirring coil caused the arc to ratate rapidly at the mid-point of the coil and thus raised the power required to melt the electrode. Proper control of stirring coil power during DC arc melting will minimize arc rotation.) No evidence of segregation was detected in all the processing and evaluation tasks of this program. The experience with 12.6 cm (5.0 inch) diameter ingots indicates that larger, homogeneous billets of both alloy compositions can be produced without major difficulty.

8.2 PROCESSING AND EVALUATION OF SWAGED ROD

8.2.1 Process Evaluation

Both alloys were successfully converted to small diameter 1 cm (0.4 inch) rod by double extrusion to nominal 2.5 cm (1 inch) diameter bar with molybdenum clad in place and swaging to size at 1371°C (2500°F) and 1649°C (3000°F). Evaluation of processing temperatures and final annealing temperatures with respect to low temperature ductility, elevated temperature tensile strength, and creep properties of both alloys revealed the following:

- The tensile ductile-to-brittle-transition-temperatures for both alloys were more sensitive to final annealing temperature than processing temperature. Final annealing temperatures of 1649°C (3000°F) and below produced tensile DBTTs well below room temperature < -157°C (-250°F). As final annealing temperatures increased, the tensile DBTTs also increased but remained below room temperature for both alloy compositions.

- For recrystallized material, processing temperature and final annealing temperatures, appeared to have little affect on room temperature and 1316°C (2400°F) tensile properties of ASTAR-1211C. The elevated temperature tensile properties of ASTAR-1511C exhibited some degree of sensitivity to processing temperature. The material swaged at 1649°C (3000°F) had tensile strength properties which averaged 69 MN/m^2 (10 ksi) higher than material swaged at 1371°C (2500°F).
- The creep behavior of both alloys were similar. Material of both alloy compositions processed at 1649°C (3000°F) had greater creep resistance than material processed at the lower temperature. The disparity in creep resistance was greatest for final annealing temperatures below 1649°C (3000°F). In general, the higher the final annealing temperature, the better the creep properties for both alloy and both processing temperatures.
- Based on the results of the low temperature ductility behavior, 1316°C (2400°F) tensile properties, and creep properties, a standard final annealing temperature of 1 hour at 1649°C (3000°F) was selected for both alloys. This final annealing temperature provides the best compromise between low temperature ductility and elevated temperature strength properties.

Extended evaluation of standard annealed swaged rod produced the following conclusions:

- The higher solute content of ASTAR-1511C was evident in all of the alloy properties evaluated.
- ASTAR-1211C and ASTAR-1511C had tensile strength properties at room temperature and at 1316°C (2400°F) that were significantly higher than ASTAR-811C.
- At 1649°C (3000°F), ASTAR-1511C had an ultimate strength of 244 MN/m^2 (35.4 ksi) compared to 204 MN/m^2 (29.5 ksi) for ASTAR-1211C.
- Young's modulus for ASTAR-1511C was slightly higher than ASTAR-1211C, 199.1 GN/m^2 (28.8 x 10^6 psi) versus 196.1 GN/m^2 (28.4 x 10^6 psi) at at room temperature.
- Shear modulus for ASTAR-1511C was 76.8 GN/m^2 (11.3 x 10^6 psi) and 74.7 GN/m^2 (10.8 x 10^6 psi) for ASTAR-1211C.
- Poisson's Ratio for ASTAR-1211C was 0.32 and 0.30 for ASTAR-1511C. Both values remained constant up to 871°C (1600°F).

- Under impact loading, ASTAR-1211C exhibited indications of a transition from brittle-to-ductile behavior as temperature increased to 538°C (1000°F) while ASTAR-1511C exhibited completely brittle behavior up to the same temperature.
- The tensile DBTT for swaged rod annealed 1 hour at 1649°C (3000°F) was < -157°C (-250°F) for ASTAR-1211C and approximately -129°C (-200°F) for ASTAR-1511C.
- The creep properties of ASTAR-1511C were slightly better than ASTAR-1211C. The stress required to produce 1 percent creep strain in 1000 hours at 1204°C (2000°F) was 176 MN/m^2 (25.5 ksi) for ASTAR-1511C compared to 155 MN/m^2 (22.5 ksi) for ASTAR-1211C. These values were a significant improvement over ASTAR-811C, 124 MN/m^2 (18 ksi) and 93 MN/m^2 (13.5 ksi) for T-111 under the same test conditions.
- Duplex annealing, 1 hour at 1649°C(3000°F) followed by 1 hour at 1260°C (2300°F), was found to reduce room temperature tensile strength approximately 10 percent without adversely affecting room temperature ductility. Although 1316°C (2400°F) tensile strength properties were reduced about 10 percent by the duplex heat treatment, creep properties were unaffected.

8.3 PROCESSING AND EVALUATION OF SHEET

- Both ASTAR-1211C and ASTAR-1511C can be converted to sheet using fairly routine conversion practice. Once material has been converted to a thickness suitable for rolling, both alloys can be rolled at a nominal temperature of 204°C (400°F) to 316°C (600°F) at 10 percent reductions per rolling pass. ASTAR-1211C requires an intermediate anneal after a total reduction of 60 percent and ASTAR-1511C requires an anneal after 40 percent reduction.
- Tensile and creep properties of ASTAR-1211C and ASTAR-1511C sheet given the standard final anneal, 1 hour at 1649°C (3000°F) are comparable to swaged rod properties.
- The longitudinal GTA bend DBTT for ASTAR-1211C sheet in the "as-welded" condition is 121°C (250°F) compared to 10°C (50°F) for base metal. A post-weld anneal of 1 hour at 1649°C (3000°F) reduces the weld bend DBTT to 38°C (100°F).

- The "as-welded" bend DBTT for longitudinal EB welded ASTAR-1211C sheet is 24°C (75°F). A post-weld anneal of 1 hour at 1815°C (3300°F) produces an increase in the DBTT to 38°C (100°F).
- Longitudinally GTA welded ASTAR-1511C has a weld bend DBTT above 316°C (600°F) for "as welded" sheet. A post-weld-anneal of 1 hour reduces the DBTT to 149°C (3000°F).
- Longitudinally EB welded ASTAR-1511C has a bend DBTT of 107°C (225°F) in the "as-welded" condition which is reduced to 93°C (200°F) by a post-weld-anneal of 1 hour at 1649°C (3000°F).
- The tensile DBTTs for GTA welded nonpost-weld-annealed ASTAR-1211C sheet aged for 1000 hours at 1149°C (2100°F), 1316°C (2400°F), and 1427°C (2600°F) fell into the temperature range 52°C (125°F) to 66°C (150°F) compared to 121°C (250°F) for nonaged "as-welded" condition.
- A post-weld-anneal of 1 hour at 1649°C (3000°F) reduced the tensile DBTT of GTA welded ASTAR-1211C sheet to 24°C (75°F) for nonaged material. Thermal aging at 1149°C (2100°F), 1316°C (2400°F), and 1427°C (2600°F) for 1000 hours had no adverse affect on the DBTTs. Material aged at 1316°C (2400°F) displayed a DBTT of -46°C (-50°F). Material given a post-weld-anneal of 1 hour at 1815°C (3300°F) exhibited a DBTT of 97°C (200°F) for the nonaged -18°C (0°F) to 66°C (150°F). The DBTTs of material given a post-weld-anneal of 1 hour at 1982°C (3600°F) were affected by thermal aging. Material post-weld-annealed at 1982°C (3600°F) but not aged and material post-weld-annealed and aged at 1149°C (2100°F) had essentially the same DBTT, 97°C (200°F) while material aged at 1316°C (2400°F) and 1427°C (2600°F) exhibited a marked increase to 163°C (325°F) and 191°C (375°F), respectively.
- The tensile DBTT behavior of GTA welded ASTAR-1511C sheet was similar to that of ASTAR-1211C. Material post-weld-annealed at 1649°C (3000°F) followed by thermal aging at 1149°C (2100°F), 1316°C (2400°F), and 1427°C (2600°F) exhibited DBTTs which ranged from 52°C (125°F) to 93°C (200°F). These values were the lowest for all conditions evaluated. Material thermally aged but not post-weld-annealed had DBTTs which ranged from 66°C (150°F) to 163°C (325°F). Material post-weld-annealed at 1815°C (3300°F) and 1983°C (3600°F) exhibited DBTTs which ranged from 93°C (200°F) to 288°C (550°F).

- Both ASTAR-1211C and ASTAR-1511C are amenable to welding by the GTA and EB techniques; however, the DBTTs, which are slightly higher than room temperature in the optimum condition, must be carefully considered in weld joint design.

8.4 PROCESSING AND EVALUATION OF TUBING

- ASTAR-1211C can be fabricated to tubing. Tube hollows suitable for tube drawing can be produced by extrusion of drilled billets over a mandrel. The resulting tube hollows 2.7 cm (1.1 inch) OD by 2.3 cm (0.9 inch) ID can be reduced to 1.9 cm (0.75 inch) OD by 1.0 mm (0.040 inch) wall tubing by drawing over a mandrel in the temperature range 204°C (400°F) to 316°C (600°F). Reductions of 10 to 12 percent are possible with frequent intermediate stress relief anneals.
- The feasibility of producing ASTAR-1211C tubing has been demonstrated. The processing, however, requires development to optimize reduction and heat treatment schedules.
- The feasibility of producing ASTAR-1511C is marginal. The higher strength and lower ductility of ASTAR-1511C make tubing production more difficult.

8.5 PROCESSING AND EVALUATION OF FORGED DISCS

- Both ASTAR-1211C and ASTAR-1511C are forgeable when properly protected during heatup and actual forging. Simple shapes such as discs can be upset forged at upset ratios of 3.7:1 or possibly higher.
- Mechanical properties of forged material of both alloys were comparable to swaged rod and sheet given the same standard final annealing treatment.

8.6 GENERAL OBSERVATIONS

The objectives of the program were achieved in all respects.

- The ASTAR-1211C alloy composition selection demonstrated that superior high temperature strength could be achieved by trading off low temperature ductility particularly in the welded condition. The ASTAR-1211C alloy was readily processed to small diameter swaged rod, rolled to sheet, fabricated to tubing, and upset forged without requiring special or unique handling. Mechanical properties of all mill shapes were consistent.

- The ASTAR-1511C alloy composition confirmed the trade-off premise by illustrating the fact that even higher strength properties could be produced at the sacrifice of low temperature ductility. ASTAR-1511C was readily not swaged and forged to desired shapes; however, rolled sheet was more difficult to produce than ASTAR-1211C requiring less reduction and more frequent intermediate anneals. ASTAR-1511C tubing could not be fabricated.

- ASTAR-1211C and ASTAR-1511C exhibited, respectively, a 52% and a 67% higher tensile strength than T-111 at 1649°C (3000°F). ASTAR-811C by comparison exhibited only a 21% improvement in tensile strength over T-111 at the same temperature.

- In creep, ASTAR-1211C and ASTAR-1511C displayed improvements of 67% and 89%, respectively, over T-111 at 1204°C (2200°F). ASTAR-811C by comparison exhibited a 33% improvement in creep strength over T-111 at the same temperature.

- The creep strength of ASTAR-1511C is equivalent to TZM up to 1260°C (2300°F). At temperatures above 1260°C (2300°F), ASTAR-1511C becomes competitive and exceeds the creep strength of TZM on a strength-density basis with increasing temperature.

9.0 REFERENCES

1. R. W. Buckman, Jr. and R. C. Goodspeed, "Development of Precipitation Strengthened Tantalum Base Alloys", Final Technical Report, WANL-PR-Q-017, Westinghouse Astronuclear Laboratory.

2. R. W. Buckman, Jr., "Development of Advanced High Strength Tantalum Base Alloys", Part I - Scale Up Investigation", NASA-CR-120818, December 1971, Westinghouse Astronuclear Laboratory (WANL-PR-71-001).

3. R. W. Buckman, Jr, and J. A. Heatherington, "An Apparatus for Determining Creep Behavior Under Conditions of Ultra-High Vacuum", Review of Scientific Instruments, Vol. 37, No. 8 August 1966.

4. B. Avitzer, "Analysis of Central Burst Defects in Extrusion and Wire Drawing", Transactions of the ASME, Journal of Engineering for Industry, Vol. 90, Series B No. 1, February 1968.

5. L. L. Seigel and C. D. Dickinson, "Effects of Mechanical and Structural Variables on the Ductile-Brittle Transition in Refractory Metals", Refractory Metals and Alloys, Metallurgical Society Conference, April 1962.

6. R. L. Ammon and R. T. Begley, "Pilot Production and Evaluation of Tantalum Alloy Sheet", Summary Phase Report, Contract Nou-62-0656-d, June 15, 1963 (WANL-RR-M-004).

7. K. A. Fowler, "Elastic Moduli of Thin Filaments and Fibers by Thin Line Ultrasonics", Technical Memorandum No. 2, Nondestructive Testing and Measurements Dept., Panametrics, Inc., November 1969.

8. R. L. Ammon, R. W. Buckman, Jr., and D. L. Harrod, "Development of Advanced High Strength Tantalum Base Alloys, Part III - Influence of Metallurgical Condition on the Mechanical Properties of ASTAR-811C Sheet", NASA-CR-121096, December 1972, Westinghouse Astronuclear Laboratory (WANL-M-FR-72-009.

9. R. E. Gold and G. G. Lessmann, "Influence of Restraint and Thermal Exposure on Welds in T-111 and ASTAR-811C", NASA-CR-72858, March 1971, Westinghouse Astronuclear Laboratory, (WANL-PR(VVV)-001).

10. G. G. Lessmann, "The Weldability of Refractory Metal Alloys- Part I of Determination of Weldability and Elevated Temperature Stability of Refractory Metal Alloys", NASA-CR-1607, August 1970.

11. C. P. Blankenship, "Some Effects of Cold Working By Hydrostatic Extrusion on Mechanical Properties of High-Strength Steels", NASA-TN-D 6186, February 1971.